For Reference

NOT TO BE TAKEN FROM THIS ROOM

For Reference

NOT TO BE TAKEN FROM THIS ROOM

Ex libris
Universitatis
Albertaensis

UNIVERSITY OF ALBERTA
QUAECUMQUE VERA

University of Alberta
Printing Department

Digitized by the Internet Archive
in 2018 with funding from
University of Alberta Libraries

https://archive.org/details/cocurrentstratif00mich

Thesis
1963(F)
#5D

THE UNIVERSITY OF ALBERTA

THE CO-CURRENT STRATIFIED FLOW OF TWO IMMISCIBLE LIQUIDS IN A RECTANGULAR CONDUIT

by

M.E. Charles

A THESIS

SUBMITTED TO THE FACULTY OF GRADUATE STUDIES

IN PARTIAL FULFILMENT OF THE REQUIREMENTS FOR THE DEGREE

OF DOCTOR OF PHILOSOPHY

DEPARTMENT OF CHEMICAL AND PETROLEUM ENGINEERING

EDMONTON, ALBERTA

SEPTEMBER, 1963

ABSTRACT

Open form expressions for the velocity distribution and volumetric flow rates were derived for the co-current stratified fully developed laminar flow of two immiscible liquids in a rectangular conduit. The effect of the presence of the less viscous layer was to reduce the pressure gradient necessary for the transport of the more viscous phase at a given rate by a factor which was a function of the input ratio, the viscosity ratio and the conduit aspect ratio. Pressure gradient reduction factors and holdup ratios were evaluated with the aid of an IBM 1620 computer for viscosity ratios from 1 to 1000 and aspect ratios from 7.896:1 to 1:3. The pressure gradient reduction factor increased concomitantly with viscosity ratio and aspect ratio. For a viscosity ratio of 1000 the maximum pressure gradient reduction factor was 3.38 for an aspect ratio of 7.896:1 and only 1.13 for an aspect ratio of 1:3.

Experiments were performed with oil and water having a viscosity ratio of 5.326 and a rectangular conduit having an aspect ratio of 7.95:1 and an overall length of 37.5 feet. For given input conditions measurements were obtained of the insitu ratio, the pressure gradient and the interface velocity.

In the laminar-laminar regime no waves were present at the interface and reasonably good agreement with the theory was obtained. Coincident with the transition to turbulence in the less viscous water phase the interface became disturbed by small two-dimensional waves, the velocities of which were essentially the same as the actual average water velocities. These waves appeared to have their origin in the pressure fluctuations in the water phase. At high water-to-oil input ratios large two-dimensional and roll waves were observed which were relatively slow moving and were apparently caused by an instability of the mean flow. Wavelengths and amplitudes of these waves were estimated using a stereophotogrammetric technique. In the laminar-turbulent regime pronounced deviations from the laminar-laminar theory were evident; in particular, the pressure gradient reduction factors were always much less than the corresponding laminar-laminar values. Lockhart-Martinelli type parameters were found useful in correlating the pressure gradient data in the laminar-turbulent regime. The transition to turbulence in the oil phase caused the two-dimensional characteristics of the interfacial waves to be destroyed and at high flow rates of both phases three-dimensional waves were observed.

TO BARBARA

without whose patience and encouragement this thesis would not have been written.

ACKNOWLEDGEMENTS

The author is indebted to Dr. Lembit U. Lilleleht for many helpful discussions during the course of the project.

Thanks are due to the National Research Council for financial aid, Messrs. U.V. Helava and M.C.Van Wijk, Photogrammetric Research, Division of Applied Physics, National Research Council for much helpful advice on the stereophotogrammetric aspects of the study, the Director, Federal Department of Mines and Technical Surveys, Ottawa, for the loan of cameras, Photographic Services, University of Alberta, for the photographs of the dye traces and the qualitative photographs of the interfacial waves, and the staff of the department workshop for their ready help in constructing and modifying the equipment.

The author also thanks his wife, Barbara, for much help with the preparation of the manuscript, Mr. Frank Copeland, for his care and precision in preparing the figures and Mrs. Georgina Smith for her patience in typing the final copy of the manuscript.

TABLE OF CONTENTS

Page

List of Tables ix

List of Figures x

INTRODUCTION 1

A The Concepts of Laminar, Turbulent and Transitional Flow 3

B The Generation of Water Waves by Wind 8

1. Pressure fluctuation theories 10

2. Instability of mean flow theories 11

C The Stratified Flow of Miscible Fluids 14

D Co-current Two-Phase Flow Through Closed, Horizontal Conduits 19

1. The flow of gas and liquid through circular pipes 19

2. The flow of gas and liquid through rectangular conduits 25

3. The flow of two immiscible liquids through circular pipes 30

E The Effect of Additives on the Stability of a Fluid-Fluid Interface 39

F Formulation of the Present Investigation 41

Page

THEORY 44

A Single-Phase Flow Through a Rectangular Conduit 44

B Laminar Stratified Flow of Two Immiscible Liquids in a Rectangular Conduit 48

1. Expressions for velocity distribution and flow rates 48

2. Computation 60

3. Results 62

(i) velocity distributions 62

(ii) pressure gradient reduction factors 67

(iii) holdup ratios 75

4. Analogues of stratified flow 82

EQUIPMENT 85

A Fluids 85

B Rectangular Conduit 87

C Auxiliary Equipment 94

EXPERIMENTAL TECHNIQUES AND PROCEDURE 101

A Techniques 101

1. Flow conditions 101

2. Insitu ratios 102

Page

3. Pressure gradients 103
4. Local velocities 108
5. Wave characteristics 111

B Procedure 115

RESULTS AND DISCUSSION 118

A Single-Phase Flow 118

B Two-Phase Flow 122

1. Flow regimes and interfacial structure 122
2. Laminar-laminar regime 141
3. Laminar-turbulent regime 151
   (i) insitu ratios 151
   (ii) interface velocities 154
   (iii) pressure gradients 157
   (iv) wave properties 162
4. Turbulent-turbulent regime 170

CONCLUSIONS 173

NOMENCLATURE 176

BIBLIOGRAPHY 182

Page

APPENDICES 190

Appendix A - Numerical Data Evaluated from Laminar Stratified Flow Theory 191

Appendix B - Physical Properties of Oil and Water 210

Appendix C - Calibration of Rotameters 213

Appendix D - Theoretical Analysis of the Motion of a Spherical Particle Rising Through a Parabolic Velocity Distribution 218

Appendix E - Application of Stereophotogrammetry to the Measurement of Wavelength and Amplitude 228

1. Determination of wavelength 228

2. Determination of amplitude 229

i) Theory 229

ii) Calibration procedure 239

Appendix F - Experimental Data 245

LIST OF TABLES

		Page
I	Variation of Holdup Ratio with Aspect Ratio for a Viscosity Ratio of 100	82
II	Physical Properties of Liquids	87
III	Data for Large Two-Dimensional and Roll Waves	169
A1	Theoretical Velocity Data	192
A2	Theoretical Pressure Gradient Reduction Factors and Holdup Ratios for Viscosity Ratios from 1 to 1000 and Aspect Ratios from 7.896:1 to 1:3	194
A3	Theoretical Data for a Viscosity Ratio of 5.326 and an Aspect Ratio of 7.95:1	210
F1	Data for the Flow of Oil Alone	246
F2	Data for the Flow of Water Alone	248
F3	Two-Phase Data	251

LIST OF FIGURES

Figure Number		Page
1	Comparison of Theoretical and Experimental Pressure Gradients for Oil-Water Laminar Stratified Flow in a Circular Pipe	36
2	Comparison of Theoretical and Experimental Pressure Gradients for Air-Water Laminar Stratified Flow in a Circular Pipe	38
3	Model of Stratified Flow	50
4	Vertical Velocity Profiles	64
5	Interfacial Velocity Profiles	66
6	Pressure Gradient Reduction Factors for an Aspect Ratio of 7.896:1	68
7	Pressure Gradient Reduction Factors for an Aspect Ratio of 3:1	70
8	Pressure Gradient Reduction Factors for an Aspect Ratio of 1:1	71
9	Pressure Gradient Reduction Factors for an Aspect Ratio of 1:3	72
10	Maximum Pressure Gradient Reduction Factors for Various Conduits	74
11	Maximum Pressure Gradient Reduction Factors for Various Viscosity Ratios	76
12	Holdup Ratios for an Aspect Ratio of 7:896:1	77
13	Holdup Ratios for an Aspect Ratio of 3:1	79
14	Holdup Ratios for an Aspect Ratio of 1:1	80
15	Holdup Ratios for an Aspect Ratio of 1:3	81

Figure Number		Page
16	Experimental Equipment	86
17	Rectangular Conduit	88
18	Cross-Section Through Rectangular Conduit	90
19	Entry Section	91
20	Photographic Section and Cameras	95
21	Oil-Water Separator	97
22	Micromanometer	105
23	Friction Factor - Reynolds Number Relationship for Single-Phase Flow	120
24	Flow Regimes and Interfacial Structure	123
25	Dye Traces	125
26	Small Two-Dimensional Waves	131
27	Large Two-Dimensional Waves	133
28	Roll Waves	134
29	Three-Dimensional Waves	136
30	Pressure Gradients at a Constant Oil Reynolds Number	137
31	Pressure Gradients at a Constant Water Reynolds Number	138
32	Comparison of Experimental and Theoretical Laminar-Laminar Interface Velocities	142
33	Comparison of Experimental and Theoretical Laminar-Laminar Insitu Ratios	143

Figure Number		Page
34	Comparison of Experimental and Theoretical Laminar-Laminar Pressure Gradient Reduction Factors	144
35	Laminar-Turbulent Insitu Ratios	153
36	Laminar-Turbulent Interface Velocities	155
37	Laminar-Turbulent Pressure Gradient Reduction Factors	158
38	Correlation of Laminar-Turbulent Pressure Gradient Data	160
39	Laminar-Turbulent Wave Velocities	163
40	Stereophotographs of Large Two-Dimensional Waves	166
41	Stereophotographs of Roll Waves	167
42	Turbulent-Turbulent Pressure Gradient Reduction Factors	171
43	Oil Viscosity and Viscosity Ratio as a Function of Temperature	212
44	Calibration Curves for Water Rotameters	216
45	Calibration Curves for Oil Rotameters	217
46	Difference Between Fluid and Particle Velocities as a Function of y	224
47	Comparison of Fluid and Bubble Velocities	226
48	Horizontal Scale Factor	230
49	Idealized Stereo-Model	231

Figure Number | | Page

50 Elevation Adjustment for Actual System 235

51 Refraction Adjustment Coefficients 242

52 Comparison of Computed and Actual Elevations 244

I INTRODUCTION

One of the more interesting and potentially useful phenomena associated with the simultaneous, horizontal pipeline flow of two incompressible fluids is the fact that the pressure gradient and power requirement necessary for the flow of the more viscous phase at a given rate may be substantially reduced by the presence of the less viscous phase. The most common practical example in which this effect is evident is the pipeline flow of petroleum and water.

The advantage to be derived by adding water to petroleum flowing in a pipeline was first suggested by Isaacs and Speed in a patent(47) obtained in 1904. However, it is only in recent years that theoretical and experimental studies have been undertaken with the objectives of obtaining fundamental information concerning the mechanics of this two-phase system and quantitative predictions of the extent to which the pressure gradient may be reduced.

One important result of these studies which will be subsequently discussed in detail is that concentric flow, in which the less viscous liquid completely surrounds the more viscous liquid, is much more effective in reducing the pressure gradient than stratified flow. Concentric flow can be established

if the liquids are introduced concentrically into the pipeline and the density differential between the liquids is almost non-existent. However, in the presence of even a slight density differential the liquids tend to stratify and, unless the pipe is strongly wet by the less viscous phase, stratified flow results with part of the pipe surface wet by the more viscous phase. The fact that, in general, pairs of immiscible liquids have different densities makes stratified flow the much more widespread and, therefore, important configuration.

Studies of the stratified flow of two incompressible fluids between infinitely wide parallel plates and in circular pipes have contributed to the knowledge of this flow system but have, at the same time, exposed the extremely complex nature of the interaction between the phases, especially when waves are present at the interface.

This introduction consists basically of a critical review of the literature which is relevant to the co-current horizontal, stratified flow of two immiscible, incompressible fluids with a view to establishing the objectives of the present investigation. Certain concepts and characteristics of single phase flow will be discussed before considering two-phase systems.

A. THE CONCEPTS OF LAMINAR, TURBULENT AND TRANSITIONAL FLOW

The concepts of laminar, transitional and turbulent fluid flow are basic to any theoretical or experimental study in fluid mechanics. Consider, as an example, the flow of a fluid through a straight circular pipe with smooth walls and constant cross section. At low flow rates every fluid particle moves with uniform velocity parallel to the pipe boundary. Viscous forces slow down the particles near the wall relative to those in the central core. This well-ordered type of flow is termed laminar or viscous flow. However, at higher flow rates laminar flow ceases to exist and a mixing of the particles occurs, for superimposed on the axial motion are subsidiary motions normal to it. Such fluid motion is described as turbulent and has been defined by Hinze(42) as "...an irregular condition of flow in which the various quantities show a random variation with time and space co-ordinates, so that statistically distinct average values can be discerned".

The two types of flow were first observed by Reynolds(74) who injected a thin filament of dye into the flowing stream. Under laminar conditions the dye filament maintained its identity, but under turbulent conditions eddies caused the filament to diffuse throughout the fluid. Reynolds found

that the quantity $\frac{\rho VD}{\mu}$, now known as the Reynolds number, in which ρ is the density of the fluid, V is the average flow velocity, D is the pipe diameter and μ is the viscosity of the fluid, is important in determining the conditions under which the laminar motion is unstable and becomes turbulent. The Reynolds number may be shown(81) to represent the ratio of inertia forces to viscous forces. Inertia forces tend to promote instability while viscous forces tend to damp out disturbances and maintain laminar flow. The critical value of the Reynolds number, i.e. the value at which the transition from laminar to turbulent flow occurs, was determined by Reynolds to be about 2300. It is now established, as was suspected by Reynolds, that the numerical value of the critical Reynolds number depends upon the size of disturbances in the entrance to the pipe. This has been demonstrated by Ekman(27) who maintained laminar flow up to a Reynolds number of 40,000 by the use of an inlet section exceptionally free from disturbances. More recently Leite(57), who also used a specially designed entrance section to stabilize the flow, found laminar flow to be stable up to a Reynolds number of 20,000. In addition he artificially created disturbances of known amplitude and found that the transition to turbulent flow occurred when the amplitude of the disturbance exceeded a threshold

value. The value of the threshold amplitude decreased with an increase of Reynolds number.

While there is doubt about the upper value of the critical Reynolds number, little doubt remains that below a Reynolds number of approximately 2000 laminar flow is stable despite the presence of large disturbances.

The transition to turbulent flow causes profound changes in the velocity distribution and the law of resistance. Whereas in laminar pipe flow the velocity distribution is parabolic, in turbulent flow the higher lateral transport of momentum causes the velocity distribution to be much more uniform. Under laminar flow conditions the pressure gradient required to maintain the flow is directly proportional to the average flow velocity, while in the turbulent regime the pressure gradient is proportional the average velocity raised to about the 1.75 power, reflecting the additional energy losses associated with the eddies.

The transition from laminar to turbulent flow in pipes has been described by Schlichting(81) who used the recent experimental work of Rotta(76) as a basis for his discussion. In the region of the critical Reynolds number the flow becomes intermittent in that it alternates in time between the laminar and turbulent states. In particular, the velocity distribution

alternates between a laminar distribution and a corresponding turbulent distribution. The nature of the flow can be described by an intermittency factor, γ, which is defined as that fraction of time during which the flow at a given position remains turbulent. For continuous turbulent flow $\gamma = 1$ and for continuous laminar flow $\gamma = 0$. Rotta found that the transition was completed in the range of Reynolds number from 2300 to 2600, γ showing a steady increase with Reynolds number through this range. The intermittency factor was a function of the axial distance from the entry section and increased with the distance, indicating that the length of the turbulent patches increased as the fluid flowed along the pipe.

Much effort, especially in recent years, has been devoted to the theoretical prediction of the critical Reynolds number for various flow geometries. The basic principles of stability theory have been reviewed by Lin(60) and Schlichting(81). Briefly, the theory involves the superposition of a small disturbance on the basic flow under investigation. Solution of the differential equation of the disturbance, an Orr-Sommerfeld type of equation, with the appropriate boundary conditions indicates whether the initial disturbance is amplified, in which case the flow is unstable, or whether the disturbance is damped out and the flow is stable. The mathematics is always

exceedingly complex.

The theory has been successful in predicting boundary layer instabilities for flow over a flat plate which agree well with experimental observations(81) but as far as fully developed flows are concerned contradictions exist. Several theoretical studies, notably those of Wasow(93), Zondek and Thomas(97), Gallagher and Mercer(34) and Deardorff(21), all based on small disturbance principles, appear to indicate that plane Couette flow, where the velocity distribution is linear, is always stable. However, turbulent plane Couette flow has been observed by Robertson(75) at high Reynolds numbers. Lin(60) reports that flow between infinite parallel plates or plane Poiseulle flow has been shown to be both stable and unstable and suggests that the confusion may have resulted from the exceedingly complex role played by viscosity. Viscous forces can serve as a source of instability by creating stresses which transfer energy from the basic motion into the disturbance. No evidence of the instability of fully developed flow in a circular pipe has been found theoretically(81) while, of course, turbulent flow is observed experimentally. Lin has suggested that the origin of turbulence for flow in a circular pipe may be in the entry section where a boundary layer exists close to the pipe surface and the flow is essentially uniform in the region of the pipe axis.

It would appear, therefore, that fully developed laminar flows, except perhaps plane Poiseuille flow, are stable as far as very small disturbances are concerned. Observed turbulence would appear to originate either from boundary layer instabilities in the entrance section or from disturbances in the main flow which have a sufficiently large amplitude, as demonstrated by Leite(57).

Recently Benjamin(5) investigated theoretically the effect of a flexible boundary on the stability of boundary layer flow and found that, under certain conditions, the flexible nature of the boundary could tend to stabilize the flow.

B. THE GENERATION OF WATER WAVES BY WIND

The generation of waves by wind blowing over a water surface has intrigued philosophers for many years. As Ursell(89) has pointed out the problem is merely one of mathematics provided it is accepted that the fluid motions are subject to the laws of classical mechanics with the appropriate boundary conditions. Unfortunately the resources of mathematics are insufficient for a complete solution, although progress can be made when suitable physical assumptions are made. The real problem is to determine the proper assumptions, and this can only be done through a combination of theory and experiment.

Scott Russell's(77) observations of the initiation of waves on water have been quoted by Lamb(55). Scott Russell observed that the water surface was perfectly smooth and reflected the image of surrounding objects up to a wind velocity of about 0.5 miles/hr. At a velocity of about 1 mile/hr. the water no longer gave a clear reflection due to the presence of minute capillary waves. These waves ceased almost simultaneously with a lull in the wind and were incapable of travelling any distance in the absence of the wind. On a further increase in wind velocity to about 2 miles/hr. small gravity waves arose uniformly over the whole water surface, while the capillary waves remained superimposed upon them.

Similarly, Benjamin(4) observed the flow of air over thin layers of water and highly viscous syrup. In the case of water, initially some apparently random agitation of the water surface was observed, while long-crested, slow moving waves subsequently appeared. In the case of the highly viscous liquid the random disturbances were not visible but long-crested waves appeared which were very similar to those on the water surface.

Benjamin suggested, therefore, that waves can be initiated in two basic ways. The random, small disturbances initially observed on the water surface are presumably caused by turbulent

pressure fluctuations in the air stream, while the regular long-crested waves would appear to have their origin in the instability of the mean flows of air and water adjacent to the interface. Two entirely different theoretical approaches are therefore possible - the first concerned with the generation of waves by random, turbulent pressure fluctuations and the second based on small disturbance theory, similar in principle to that already outlined for the prediction of instability of single phase laminar flow. The theory which would apply in a given naturally occurring or experimental system would depend on the nature of the observed waves.

1. Pressure fluctuation theories

The generation of waves by random fluctuations of pressure in the turbulent air stream has been investigated by Eckart(25) and Phillips(73). Eckart assumed a random distribution of normal pressure acted over a circular region of the ocean which was assumed to be an inviscid fluid and incorporated the ideas of statistical correlation analysis. No account was taken of the differences in pressure between the wind-ward and lee-ward slopes of the waves, nor the tangential wind stress. In these respects his approach is unrealistic, and, in fact, the heights of predicted waves are less than those observed.

Phillips's theory is concerned with the resonance effect of pressure fluctuations in the turbulent air stream on an initially calm water surface. Agreement of the theory with observations is good and Phillips suggested that the pressure resonance mechanism may well be the principal means by which energy is transferred to waves.

2. Instability of mean flow theories

The Kelvin-Helmholtz theory(56) is based on the simplest possible model in which uniform flow is assumed in each phase, the velocity distribution being discontinuous at the interface. Viscosity is neglected so that the motion arising at the interface from a small arbitrary disturbance can be described by a velocity potential. The motion is controlled by gravity and surface tension. The critical wind velocity, i.e. the velocity for which the disturbance will neither grow nor decay, is predicted to be about 650 cm/sec. (15 miles/hr.), whereas in nature waves are observed at wind velocities very much below this value.

Lock(61) and Wuest(94) have extended the Kelvin-Helmholtz model to take viscosity into account i.e. boundary layers are formed on both sides of the interface. Outside the boundary layers the air moves with uniform velocity and the water is at rest. Lock considered a velocity profile calculated from a

particular point upstream, while Wuest arbitrarily chose approximations to actual boundary layer profiles. Ursell(89) remarks that, although the numerical calculations based on Lock's theory are far from complete, the theory seems to indicate that a wind velocity of 100 cm/sec. (2.5 miles/hr) is capable of raising waves, and that it appears that Wuest's calculations may contain some errors.

Feldman(32) considered the stability of a horizontal liquid film in contact with a semi-infinite air stream. He assumed parallel laminar flow with a linear velocity distribution in both phases, a discontinuity in slope existing at the interface. The critical velocity by Feldman's analysis is an order of magnitude greater than the experimental velocity observed by Knuth(54) for annular flow of air and water in a circular pipe. Feldman suggested the discrepancy could be due to the relative stability of the plane Couette flow assumed in his theory compared with flows having curved velocity profiles.

The foregoing instability theories have assumed laminar flow in both phases. Turbulence has been taken into account by Jeffreys(48), Miles(68) and Benjamin(4), but only to the extent that it determines the relevant properties of the mean flow. Jeffreys made use of the principle that a wave will

grow in amplitude if the wind supplies energy to it at a greater rate than that of viscous dissipation in the water. He neglected inertial effects and tangential stress due to the wind and considered only the pressure difference on the windward and leeward sides of the waves caused by separation of the air stream on the leeward side. To express the magnitude of the pressure difference Jeffreys introduced a sheltering coefficient, S, the numerical value of which he calculated from experimental observation of the critical wind velocity.

Jeffreys's criterion for the generation of waves is:

$$\frac{1}{V'_{ac}} \left[\frac{\nu_w g \ \Delta\rho_{aw}}{\rho_a} \right]^{1/3} = 0.215 \qquad (1)$$

where ρ_a = density of the air

$\Delta\rho_{aw}$ = density difference between air and water

g = gravitational acceleration

ν_w = kinematic viscosity of water

V'_{ac} = critical air velocity

However, experimental measurements of S using fixed wave models have shown it to be an order of magnitude smaller than that postulated by Jeffreys, and Ursell(89) drew the conclusion that the sheltering theory in its simplest form is insufficient to explain the growth of waves. However, Miles(68) has removed the doubt concerning the value of S by showing

theoretically that for a moving wave system a sufficiently large value of S may be attained even in the absence of flow separation. Miles concludes that his model is an important adjunct to Phillips's theory. Benjamin(4) calculated the normal and tangential stresses on a wavy surface caused by the turbulent flow of air and showed that they are distributed in much the same way as if the leeward slopes of the waves were sheltered.

Whatever mechanism is responsible for the initiation of water waves, once the waves are formed energy is transferred to the waves by several mechanisms and any simplified theory is unlikely to predict exactly the characteristics of the waves observed in nature.

C. THE STRATIFIED FLOW OF MISCIBLE FLUIDS

In addition to the case of wind blowing over water other naturally occurring stratified systems are important in meteorology and oceanography. These may be divided into two groups, depending on whether the stratification is due to a continuous variation in density or whether it is caused by fluid layers of essentially different density. An example of the former type is an atmosphere in which the density decreases continuously with height, and an example of the second type is

found in river estuaries when the river efflux tends to flow over the salt water of the ocean. In all these naturally occurring phenomena the flow of the different layers may be co-current or counter-current. In the case of a river estuary, for example, flow will tend to be co-current while the tide is ebbing and counter-current while the tide is rising.

The important difference between these stratified systems and the air-water system is that, whereas air and water are immiscible, the layers in the stratified systems cited above are miscible with each other. Thus, while at low differential velocities the layers remain distinct, at higher velocities the interface becomes unstable and waves develop in much the same way as for the air-water system with the subsequent diffusion of one layer into the other.

Motions in a continuously stratified fluid have been investigated theoretically by Taylor(86), Yih(95,96), Drazin and Howard(22), and Eliassen et al(28) and both theoretically and experimentally by Long(64).

Counter-current flow of distinct layers has been studied by Graebel(39), Mittendorf(69) and Macagno and Rouse(67) and is relatively unstable because of the inflexion point which occurs in the velocity profile at, or near, the interface. The co-current flow of two or more fluid layers over an obstacle,

representing a mountain barrier to the movement of air currents, has been studied both theoretically and experimentally by Long(65,66). The motion of two liquid layers towards an orifice, as could be encountered in the withdrawal of water from the ocean, has been investigated theoretically by Craya(18) and experimentally by Gariel(35). Esch(30,31) considered the stability of a shear layer between unbounded parallel streams, and the flow of a liquid with a free surface over a slightly heavier liquid. He found theoretically, using small disturbance principles, that the former case is always potentially unstable and the latter may be stable, depending primarily upon the depth and velocity of the upper fluid. Presumably the presence of the free surface has a stabilizing effect.

Investigations of essentially co-current flow which are of particular relevance in the present study are those of Taylor(87), Keulegan(51) and Ippen and Harleman(46). All were concerned with the development of interfacial instability and the subsequent mixing in systems in which one fluid flowed past a second layer of miscible fluid, which was stationary except for the movement caused by the drag of the moving phase. Lofquist(63) has recently extended Keulegan's work, but without further clarification of the criterion for interfacial instability.

Taylor observed the flow of fresh water over a layer of brine in a closed rectangular conduit and described how initially the interface was smooth and subsequently, with increase of the water flow rate, wave motions and mixing developed at the interface. Taylor did not report quantitatively the conditions under which the instability occurred.

Keulegan performed experiments similar to those of Taylor in conduits having cross sections of 2 by 4 cms., 4 by 8 cms. and 11.3 by 28.5 cms., the greater dimension being vertical in each case. The fluids used were water and sugar solution and the depths of the two layers were approximately equal. Experiments were conducted in each of the three conduits to determine the effect of the Reynolds number of the flowing water layer on the instability of the interface, while tests were conducted in the medium sized conduit to determine the effect of the viscosity of the lower or sugar solution layer on the instability. He recorded the maximum velocity of the water layer, calculated by dividing the volumetric flow of water by the area of cross-section of the water layer, at which the interface was smooth and the velocity at which the first signs of mixing appeared. The mean of these two velocities was defined as the critical velocity, V'_{wc}.

Keulegan derived a criterion for instability of the interface as:

$$\frac{1}{V'_{wc}} \left[\frac{\nu_s \; g \; \Delta\rho_{ws}}{\rho_w} \right]^{1/3} = \Theta \quad \text{(a constant)} \qquad (2)$$

where ρ_w = density of the upper water layer

$\Delta\rho_{ws}$ = difference in density of the two liquids

ν_s = kinematic viscosity of the lower sugar solution layer

g = acceleration of gravity

Experiments in the medium sized conduit confirmed the criterion to the extent that V'_{wc} was approximately proportional to $(\nu_s)^{1/3}$. Experiments in the three conduits enabled the value of Θ to be determined for both laminar and turbulent flow of the upper fluid. For turbulent flow $\Theta = 0.178$ and for laminar flow $\Theta = 0.127$.

Keulegan pointed out that his criterion has the same form as that of Jeffreys(48) and, further, the value of Θ determined from Jeffreys's observations of the initiation of waves on a water surface is 0.215 - not very different in magnitude from Keulegan's turbulent value of 0.178.

Ippen and Harleman performed similar experiments to those of Keulegan, except brine underflowed a layer of fresh

water. They measured the critical velocity for conditions in which the brine was in laminar flow at Reynolds numbers less than those in Keulegan's experiments. For this regime they found, as they predicted theoretically, that Θ was a linear function of the reciprocal of the Reynolds number and not a constant as Keulegan had predicted. However, Keulegan obtained few experimental data in the laminar regime and these do agree closely with the results of Ippen and Harleman. Most of Keulegan's data were obtained for the transition and turbulent regimes and there is little doubt that in the turbulent regime the constancy of Θ was verified.

Since both Keulegan, and Ippen and Harleman, observed waves when both phases were in laminar motion, it would appear that the waves must have been caused by a fundamental instability of the mean flow and not by turbulent pressure fluctuations in one of the phases.

D. CO-CURRENT TWO-PHASE FLOW THROUGH CLOSED, HORIZONTAL CONDUITS

1. The flow of gas and liquid through circular pipes

The flow of two phases through closed, horizontal conduits is encountered in many engineering situations, such as pipeline transportation, tubular reactors, and film coolers. In this section attention is focused on gas-liquid flow through circular, horizontal pipes.

Little doubt remains concerning the nature of the flow patterns which occur in co-current gas-liquid horizontal pipeline flow. Govier and Omer(38) and Hoogendoorn(44) have covered wide ranges of individual flow rates and input ratios. Govier and Omer observed the flow patterns established by air and water flowing in a 1-inch pipe, while Hoogendoorn was concerned with air and water, and air and oil, flowing in pipes with diameters ranging from 1 to 5.5 inches. At low flow rates of both phases stratified flow with a smooth interface takes place. If the flow of liquid is maintained constant and the gas flow rate increased the interface becomes unstable and waves develop. Further increase in the gas flow rate causes the liquid to climb up the pipe wall and eventually "annular flow" is established when a liquid annulus adheres to the pipe wall and completely surrounds the gas core.

If a low gas flow rate is initially combined with a relatively large liquid flow rate then "bubble flow" - in which bubbles of gas move along the top of the pipe - occurs. Subsequent increase in the gas flow rate does not establish stratified flow - but rather "plug flow" wherein larger gas bubbles or plugs move along the upper part of the pipe and subsequently "slug flow" in which splashes or slugs of liquid occasionally pass through the pipe with a higher velocity

than the bulk of the liquid. Slug flow may be considered as an extension of stratified flow in which the waves have become very large compared with the pipe diameter and liquid is torn from the crests.

Stratified flow, with or without waves, is, therefore, but one of the flow patterns encountered in the simultaneous flow of gas and liquid through a circular pipe. Since the gas is compressible its density must decrease as the pressure decreases along the pipeline. The consequent acceleration of the gas causes an increasing drag upon the liquid surface and the liquid also accelerates. This manifests itself, for constant gas and liquid mass rates of flow, in an interfacial gradient and unequal pressure gradients in the gas and liquid phases. No analytical solution exists for the stratified flow of two fluids when one of them is compressible.

Govier and Omer(38) in reviewing the literature on the flow of gas-liquid mixtures through pipes concluded that the nature of the flow pattern greatly influences the pressure gradient. They suggested, therefore, that either a separate correlation is required for each flow pattern or in the case of an overall correlation, such a correlation must include all the variables which determine the flow pattern. They also noted that, while the effects of the individual flow rates on

the flow pattern are reasonably well known, the effects of the densities and viscosities of the fluids and the pipe diameter are not.

Lockhart and Martinelli(62) proposed an overall correlation, with complete disregard for the flow patterns, in terms of two parameters

$$\phi_1^2 = \left(\frac{\partial p}{\partial z}\right)_{tp} \Big/ \left(\frac{\partial p}{\partial z}\right)_1 \quad (3)$$

and

$$X^2 = \left(\frac{\partial p}{\partial z}\right)_1 \Big/ \left(\frac{\partial p}{\partial z}\right)_g \quad (4)$$

where $\left(\frac{\partial p}{\partial z}\right)_{tp}$ = two phase pressure gradient

$\left(\frac{\partial p}{\partial z}\right)_g$ = pressure gradient for gas flowing alone

$\left(\frac{\partial p}{\partial z}\right)_1$ = pressure gradient for liquid flowing alone

and the four flow regimes: turbulent-turbulent, turbulent-laminar, laminar-turbulent, and laminar-laminar. A phase was assumed to be in turbulent flow if the superficial Reynolds number for the phase exceeded 2000 and to be in laminar flow if the Reynolds number was less than 1000. Four curves were established, one for each regime, with which their experimental two-phase pressure gradients agreed to within about ± 55 percent. It has since been found by Gazley(36), Hoogendoorn(44) and

Govier and Omer(38) that the Lockhart-Martinelli correlation considerably and consistently over-estimates the two phase pressure gradient for stratified and wave flow in all four regimes. A basic assumption made by Lockhart and Martinelli was that the pressure gradients in both phases were equal. That this is definitely not so for stratified flow has given some investigators, for instance, Gazley(36) a ready explanation for the discrepancy. However it would appear that the basic assumption of equality of pressure gradients in the two phases is unlikely to hold for any of the flow patterns and that the real reason for the discrepancy is that the correlation is inadequate to cover the different flow patterns. This has been strikingly demonstrated by Hoogendoorn(44) who was able, by making suitable modifications to the entry section, to obtain either stratified flow with waves or slug flow, other conditions being the same. Pressure gradients for slug flow were approximately twice those for the corresponding wave flow.

Gazley(36) investigated the co-current, stratified flow of air and water in a horizontal 2-inch diameter, 22-foot long pipe. No part of the pipe was transparent and the details of the flow patterns could not be observed. The water phase was allowed to fall freely from the end of the pipe and because of this the interfacial and pressure gradients reported,

especially at low flow rates, cannot be considered to be representative of those to be expected in a long pipeline. Nevertheless, certain qualitative effects are of definite interest.

Gazley found by measuring pressure gradients that the presence of a moving layer of water delayed the transition to turbulence in the gas phase. Whereas for the flow of air alone the transition from laminar to turbulent flow occurred over the range of air Reynolds number 2000 to 4000, for the two phase system the transition took place in the range of superficial air Reynolds number 3000 to 5000. Conversely Gazley found that the presence of a turbulent air layer caused the transition to turbulence in the water phase to occur at slightly lower Reynolds numbers than for single phase flow of water.

The point at which the interface became wavy for a constant liquid flow rate was detected by the presence of a change in slope in the curve representing the relationship between the two-phase pressure gradient and superficial air velocity. While the slope was 1.8 with both phases in turbulent motion and no interfacial waves, the slope increased to 2.75 when waves were present. It was found that the onset of a wavy interface did not occur at a definite air Reynolds

number and depended on the water flow rate. The higher the water flow rate, the lower the air Reynolds number at which the waves first appeared. However, the air was always either in transitional or turbulent flow when waves were detected.

Mologin(70) determined the boundaries of the wave flow pattern for the flow of air and water in pipes ranging in diameter from 1 to 4 inches. He determined the period and amplitude of the waves with the aid of a motion picture camera and presented empirical formulae for these quantities. No pressure gradients were reported, nor were the transitions from laminar to turbulent flow in each phase indicated.

2. The flow of gas and liquid through rectangular conduits

Theoretical and experimental studies of the stratified, co-current flow of gas and liquid in a rectangular conduit have been undertaken to determine the basic nature of the interaction between the phases. Stratified flow in a rectangular conduit is a simpler situation than stratified flow in a circular pipe. In a rectangular conduit the depths of both phases are constant across the width of the conduit and, provided the ratio of width to depth is large, the velocity distribution is two-dimensional in the central region of the conduit.

Keulegan(52) and Johnson and Rice(49) investigated the flow of air over a "stationary" body of water, simulating wind

blowing over the ocean. Keulegan was interested in the interfacial gradients developed and Johnson and Rice measured wave characteristics at various points along the conduit. The significant heights and periods were related to the air velocity and fetch.

Hanratty and Engen(40) studied the interaction between a turbulent air stream and a water layer flowing co-currently in a 12-inch by 1-inch rectangular conduit. Five flow patterns were observed: smooth interface, two-dimensional waves, squall surface or three-dimensional waves, roll waves, and dispersed flow. Initially at low flow rates of both phases the interface was smooth and no disturbances were visible to the naked eye. If the liquid flow rate was maintained constant and the gas flow steadily increased a series of transitions took place. Two-dimensional waves first appeared which were long-crested and had a wavelength of approximately 1 cm., followed by three-dimensional waves in which the lengths of the wave crests were approximately the same as the wavelengths. Three-dimensional waves gave way to roll waves, which had irregular shaped crests running across the width of the conduit. In this flow pattern part of the liquid was picked up and carried over the liquid surface. Finally dispersed flow, in which droplets of liquid were removed from the liquid phase

and carried in the gas stream, was observed. As would be expected these flow patterns are similar to those observed in pipe flow when the liquid flow rate is relatively small.

Hanratty and Engen made several significant observations. They found that the transition from a smooth interface to one with two-dimensional waves did not necessarily coincide with the transition from laminar to turbulent flow in the gas phase. In fact they noted that at low liquid flow rates a smooth interface coexisted with a turbulent gas phase and, at high liquid flow rates two-dimensional waves were formed in the presence of a laminar gas phase. Thin liquid layers were therefore more stable than thick ones. This was found to be so for all the transitions in surface structure. Further, they found the presence of the interfacial waves distorted the gas phase velocity profile in that the maximum in the profile was moved away from the interface. This effect, which was negligibly small for two-dimensional waves, increased with increasing roughness of the interface. The position of the maximum in the velocity profile, together with the depth of the water layer and the pressure gradient enabled the interfacial shear stress to be evaluated.

Ellis and Gay(29) performed similar experiments to Hanratty and Engen and determined the interfacial shear stress from a knowledge of the gas phase velocity profile and the liquid depth only. Ellis and Gay compared their results with those of Hanratty and Engen and found good agreement.

Hanratty and Hershman(41) derived a criterion for the initiation of roll waves on a liquid layer flowing co-currently with gas in a closed rectangular conduit by extending Jeffreys's theory(48). Excellent agreement between theory and experiment was obtained in that the theory correctly predicted both the trend and numerical values of the gas phase Reynolds number at which roll waves first appeared for air and water flowing in a 12-inch by 1-inch conduit. If the effect of surface tension is neglected, then as the liquid phase Reynolds number becomes very small, their criterion becomes:

$$V'_{gc} = \left[\frac{2\ \Gamma_g\ b\ g}{R}\right]^{1/2} \tag{5}$$

where V'_{gc} = actual time average velocity in gas phase

Γ_g = gas velocity profile factor determined from experimental measurements

$2b$ = depth of the conduit

R = density ratio (gas/liquid)

Lilleleht and Hanratty(58,59) developed an experimental technique, based on the partial absorption of a light beam by a dye dissolved in the water phase, to determine wave characteristics during the co-current flow of air and water in a rectangular conduit. At a constant liquid Reynolds number the root mean square wave height was found to increase rapidly with increasing gas phase Reynolds number for two-dimensional waves and then pass through a maximum for three-dimensional waves. The three-dimensional waves were explored in greater detail and it was found that a Gaussian model approximately described the wave structure. The interfacial shear stress was correlated with the root mean square wave height.

Van Rossum(91) observed the flow of air over a thin layer of water in a 6-inch square duct. He was interested in the transition from a smooth interface to one with waves and from a wavy interface to dispersed flow. The critical air velocity necessary to produce waves decreased with increasing film thickness, confirming the observations of Hanratty and Engen(40) and Gazley(36), and tended to a constant value for thick water layers. This constant value was about twice the value predicted by Jeffreys's theory(48). The average thickness of the water layer with waves present at the interface was

found to be only about 50 percent of the thickness predicted by laminar flow theory assuming a smooth interface.

The fact that the initiation of interfacial waves during the flow of air and water through rectangular channels does not coincide with the transition to turbulent flow in the gas phase leads to the same conclusion drawn from the results of experiments with miscible liquids, i.e. the waves are caused by a fundamental instability of the mean flow.

3. The flow of two immiscible liquids through circular pipes

It has previously been mentioned that the pressure gradient and power requirement necessary for the flow of a viscous liquid at a given flow rate in a horizontal, circular pipe may be substantially reduced by the presence of a less viscous liquid. In order to estimate the effectiveness of different flow configurations Russell and Charles(78) analysed theoretically the laminar flow of two incompressible fluids flowing stratified between infinitely wide parallel plates and concentrically in a circular pipe. It was apparent that concentric flow, in which the less viscous fluid occupies the region of high shear rate next to the pipe wall, is much more effective in reducing the pressure gradient than stratified flow where the less viscous liquid is in contact with only

part of the conduit boundary. For both flow patterns the pressure gradient reduction factor - defined as the ratio of the pressure gradient for the flow of the more viscous fluid at a given flow rate to the pressure gradient for the two phase system with the more viscous fluid flowing at the same rate - was found to be a function of only the viscosity ratio and the input ratio.

For concentric flow Russell and Charles found that the maximum pressure gradient reduction factor was proportional to the viscosity ratio at high viscosity ratios. At a viscosity ratio of 1000 the maximum pressure gradient reduction factor was predicted to be 500. Charles, Govier and Hodgson (12) reported the results of an experimental investigation of the co-current pipeline flow of two liquids, oil and water, having the same densities. The liquids were introduced concentrically into the pipe and concentric flow, with the oil flowing inside the water, was found to be stable over a wide range of flow rates. Three oils having viscosities of 6.29, 16.8 and 65 centipoise were used in the experiments. For each oil the maximum pressure gradient reduction factor observed was somewhat less than that predicted by theory because concentric flow was not stable at the input ratio predicted by theory to give the maximum beneficiation, the oil forming slugs moving

in a continuous water phase. Nevertheless the experimentally determined maximum pressure gradient reduction factors were considerable - being 1.7 for the 6.29 centipoise oil, 6.0 for the 16.8 centipoise oil and 10.0 for the 65 centipoise oil. The commercial application of the concentric configuration to reduce pressure gradients during the pipeline transportation has been outlined in patents by Isaacs and Speed(47), Clark and Shapiro(16) and Chilton and Handley(14). However, it is unlikely that this extremely desirable configuration will find widespread use because, in the presence of even a small density differential, the fluids tend to stratify.

The results obtained by Russell and Charles for stratified flow between parallel plates indicated that the maximum pressure gradient reduction factor was not proportional to the viscosity ratio at high viscosity ratios as for concentric flow but appeared to approach a constant value at high viscosity ratios. At a viscosity ratio of 1000 the maximum pressure gradient reduction factor was predicted to be approximately 3.7, compared with 500 for concentric flow.

The laminar, stratified flow of two incompressible fluids in a circular pipe has since been treated numerically by Charles and Redberger(13) and by Gemmell and Epstein(37) using slightly different numerical methods. The analytical solution

has now also been obtained by Bentwich(6) but his solution has not yet been evaluated and compared with the numerical results.

The numerical results of Charles and Redberger, and Gemmell and Epstein agree well with each other in that the pressure gradient reduction factors predicted by the two methods agree within about 7 percent, those of Gemmell and Epstein being consistently greater than those of Charles and Redberger. It is doubtful which results are more accurate; Charles and Redberger used considerably smaller distance increments in the finite difference approximation to the basic differential equation, while Gemmell and Epstein used somewhat better finite difference approximations to the boundary conditions. As for stratified flow between parallel plates, the pressure gradient reduction factor is a function of the viscosity ratio and input ratio only and the maximum pressure gradient reduction factor tends to a constant value at high viscosity ratios. At a viscosity ratio of 1000 Charles and Redberger predicted a maximum pressure gradient reduction factor of 1.31 and Gemmell and Epstein a value of 1.41. Stratified flow in a circular pipe is, therefore, the least attractive configuration from the point of view of pressure gradient reduction. This is a direct consequence of the proportion of the conduit boundary which is wet by the less

viscous fluid. The addition of a small amount of the less viscous fluid wets the complete boundary in concentric flow, half the boundary for stratified flow between parallel plates and only a small proportion of the boundary for stratified flow in a circular pipe.

In the above theoretical studies the fluids were assumed to be incompressible and have Newtonian characteristics. The motion was assumed to be laminar with a smooth interface. Integration to obtain the velocity distribution and volumetric flow rates was carried out using the appropriate boundary conditions, which were

(1) the velocity of the more viscous liquid in contact with the boundary was zero

(2) the velocity of the less viscous liquid in contact with the boundary was zero

(3) the velocities of both phases were equal at the interface, i.e. there was no slip between the phases

(4) shear stress was continuous across the interface

These conditions would appear to be quite adequate although any effects due to the meniscus at the pipe wall in stratified flow and anomalous interfacial viscosity, were neglected.

Several experimental investigations have produced data which may be compared with the numerical results obtained for stratified flow in a circular pipe. Russell, Hodgson and Govier(79) reported pressure gradients for the co-current flow of an oil having a viscosity of 18 centipoise and water in a 1-inch diameter pipe. At high input ratios of water to oil the oil formed itself into bubbles which flowed along the top of the pipe in a continuous water phase. Decrease in the water to oil input ratio resulted in stratified flow with a smooth interface. At higher flow rates the interface became wavy, and subsequently a mixed type of flow was observed. No attempt was made to describe in detail the characteristics of the wavy interface. The pressure gradient reduction factors computed from their pressure gradient measurements for conditions under which the flow was stratified with a smooth interface are plotted in Figure 1, along with the predicted curves of Charles and Redberger, and Gemmell and Epstein. The experimental data scatter approximately ± 30 percent about the predicted curves and in addition, while theory predicts that for a given viscosity ratio the pressure gradient reduction factor is a function of the input ratio or input oil fraction only, the experimental data appear to be a function of the water Reynolds number as well. Further, at input fractions

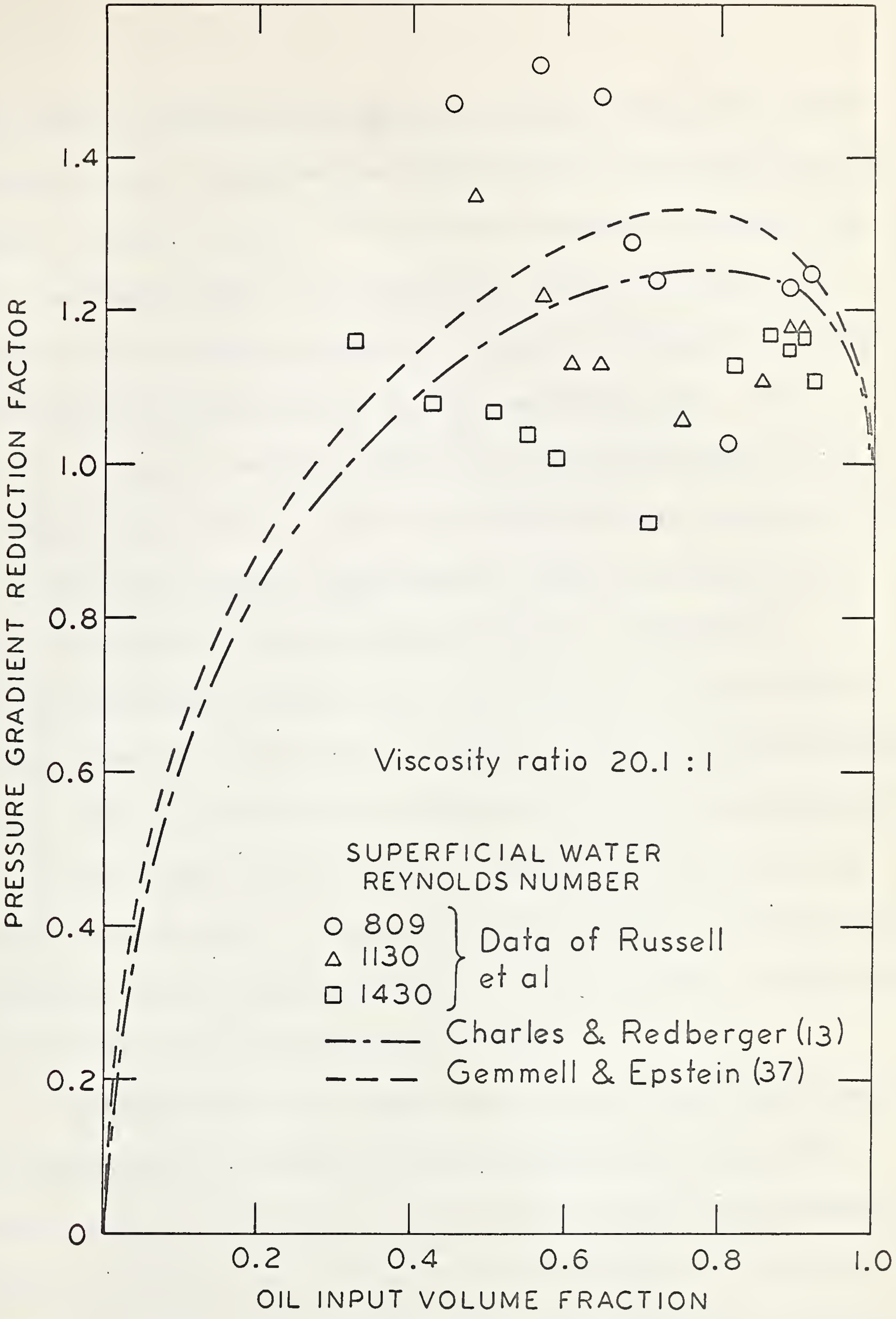

FIGURE 1 - COMPARISON OF THEORETICAL AND EXPERIMENTAL PRESSURE GRADIENTS FOR OIL-WATER LAMINAR STRATIFIED FLOW IN A CIRCULAR PIPE.

where theory predicts the pressure gradient reduction factor to pass through a maximum the experimental data show distinct minima. Govier and Omer(38) measured pressure gradients for the stratified flow of air and water. Data for which both phases were in laminar motion are plotted in Figure 2, along with the curve predicted by Charles and Redberger. Under the low pressure gradients prevailing when both phases were in laminar flow the air can be considered to be incompressible. It is apparent that the experimental reduction factors are about 50 percent of the predicted values. Charles(11) reported pressure gradient reduction factors for the flow of viscous crude oil with water in both 1- and 2-$^1/_2$-inch diameter pipes. While a significant density differential existed between the oil and water and the flow was assumed to be stratified, it was not possible to observe the flow pattern. The measured pressure gradient reduction factors were an order of magnitude greater than those predicted by theory.

Assuming that the experimental flows were fully developed, the descrepancies between the experimental and theoretical results may be attributed to the fact that the actual experimental situations were not exact reproductions of the theoretical model. In the 1-inch diameter pipes used by Russell, Hodgson and Govier, and Govier and Omer the meniscus effect at the pipe

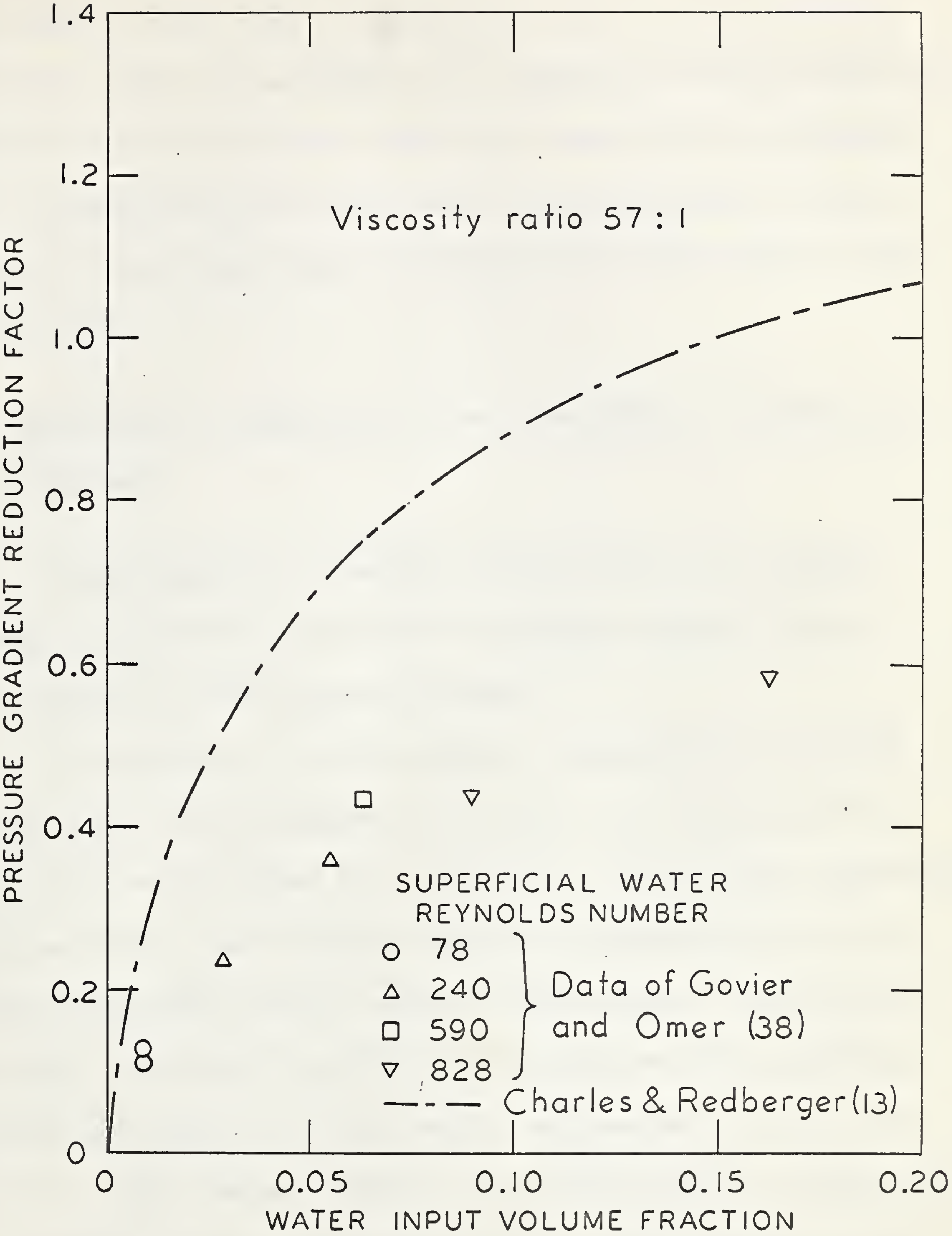

FIGURE 2 - COMPARISON OF THEORETICAL AND EXPERIMENTAL PRESSURE GRADIENTS FOR AIR-WATER LAMINAR STRATIFIED FLOW IN A CIRCULAR PIPE.

wall may well have had a significant effect on the pressure gradient, while the extremely high pressure gradient reduction factors obtained by Charles with the crude oil-water system may be explained by the fact that a certain amount of water adhered to the upper part of the pipe wall and aided the flow of the oil.

E. THE EFFECT OF ADDITIVES ON THE STABILITY OF A FLUID-FLUID INTERFACE

The presence of a surface active agent or a solute soluble in both fluids may have a profound effect on the stability of a fluid-fluid interface.

The effect of the presence of a monolayer of surface active agent on the appearance of water waves generated by wind has been discussed by Davies(19). The monolayer effectively eliminates the small ripples which are superimposed on the longer wavelength gravity waves. This causes a reduction in the drag exerted by the wind and, at the same time, greatly reduces the amount of energy which is dissipated in the wave motions. The combined effect is that more energy is converted into kinetic energy associated with the bulk movement of the water. That this is so was strikingly demonstrated by Davies when a slick of hexadeconal was found to accelerate across a

lake under the action of the wind.

Hanratty and Hershman(41) found that the addition of less than 0.01 percent of sodium lauryl sulphate suppressed the two- and three-dimensional waves normally observed in the flow of air and water in a rectangular conduit, but did not affect the transition to roll waves.

One effect of the presence of surface active agent is to reduce the surface tension. Such an effect would decrease the stability of the interface. The experimental observations are contrary to this and other properties of surface films, e.g. anomalous surface viscosity effects, must be important.

The presence of a soluble solute in, and hence mass transfer between, two liquid phases causes local variations in solute concentration and, therefore, interfacial tension. These local variations cause agitation of the interface. This effect, known as the Marangoni effect, has been studied from the hydrodynamical point of view by Sternling and Scriven(85) and its effect on mass transfer has recently been reported by Sawistowski and Goltz(80).

F. FORMULATION OF THE PRESENT INVESTIGATION

The following conclusions were drawn from the literature survey:

(1) The nature of laminar, transitional and turbulent flow of a single phase is reasonably well understood. It appears that fully developed laminar flows, except perhaps plane Poiseuille flow, are stable for infinitesimal disturbances. Contemporary theory is, therefore, inadequate to predict the transition from laminar to turbulent flow. Observed turbulence probably originates either in the boundary layer present in the entry section to a conduit or from disturbances of the fully developed flow which have amplitudes greater than a threshold value. In a two-phase system the effect that the moving fluid-fluid interface has on the transition from laminar to turbulent flow in the phases is not known.

(2) There are two basic approaches to the prediction of instability at a fluid-fluid interface. One is based on the effect of turbulent pressure fluctuations in one of the phases and the other is concerned with instability of the mean flow, whether or not one of the phases is turbulent. Both methods have been applied with some success to the air-water system. However, instability analyses are exceedingly complex

and have led to results which are not in complete agreement. This disagreement is a consequence of the fact that it has not yet been possible to include all mechanisms of energy transfer in a single theory.

(3) The fact that instability of the interface in the stratified flow of two miscible liquids has been observed while both phases are in laminar flow substantiates the hypothesis that interfacial instability is not necessarily caused by turbulent fluctuations and may be caused by instability of the mean flow.

(4) The experimental investigation of co-current gas-liquid flow in circular pipes, and in rectangular conduits where attention has been focussed on the stratified flow pattern, is reasonably well advanced. On the other hand the experimental investigation of co-current liquid-liquid systems is not far advanced despite the possible importance of such systems in pipeline transportation, tubular reactors, and liquid-liquid extraction processes. Further, the few available data for laminar-laminar stratified flow of two immiscible liquids in a circular pipe by no means verify theoretical predictions.

(5) The profound effects that the presence of dissolved solutes and surface active agents may have on the stability of a fluid-fluid interface show that the presence of such

substances should be very carefully controlled in any study of the hydrodynamics of two-phase systems.

It was decided, therefore, to carry out an experimental investigation of a co-current liquid-liquid system, and to compare theoretical and experimental results for the case when both fluids were in laminar flow. A rectangular conduit of large aspect ratio was selected as being most suitable for the experiments because it would result in the depths of the two phases being constant across the width of the conduit, the velocity distribution in the central part of the conduit being approximately two-dimensional and, lastly, meniscus effects at the sides of the conduit having a relatively small effect on the flow.

II THEORY

A. SINGLE-PHASE FLOW THROUGH A RECTANGULAR CONDUIT

In the most general case of fluid flow the variables velocity, temperature, pressure and physical properties of the fluid are functions of the space co-ordinates x, y and z and the time t. The basic differential equations of fluid flow are the continuity equation which is based on the law of conservation of mass, the momentum equation which is based on Newton's second law of motion, and the energy equation which is based on the law of conservation of energy. In addition, two other relationships are usually available - the equation of state of the fluid and, in the case of Newtonian fluids, the relation between shear stress and shear rate or velocity gradient. For non-Newtonian fluids the shear stress-shear rate relationship can usually be approximated by a mathematical model, at least over a limited range of shear rate. The most general forms of these equations have been discussed and summarized by Knudsen and Katz(53).

When the fluid is incompressible and Newtonian and the flow is horizontal, steady, and fully developed in a conduit of constant cross-sectional area then, in the absence of heat

interchange with the surroundings and body forces other than gravity, the energy equation reduces to the statement that the pressure loss along the conduit is completely accounted for by viscous energy dissipation effects within the fluid. Since the amount of heat generated in this way is usually exceedingly small the fluid can be assumed to have uniform temperature and, therefore, constant physical properties.

With the additional assumption that the flow is laminar then the continuity and momentum equations are also greatly simplified. With an x, y, z Cartesian co-ordinate system positioned so that the direction of flow coincides with the z-axis then, if the velocity in the z-direction is denoted by w, the pressure by p and the viscosity of the fluid by μ, the continuity equation reduces to

$$\frac{\partial w}{\partial z} = 0 \tag{6}$$

which, when substituted in the momentum equation, together with the conditions stated above gives

$$\text{x-direction:} \quad \frac{\partial p}{\partial x} = 0 \tag{7}$$

$$\text{y-direction:} \quad \frac{\partial p}{\partial y} = 0 \tag{8}$$

$$\text{z-direction:} \quad \frac{\partial^2 w}{\partial x^2} + \frac{\partial^2 w}{\partial y^2} = \frac{g_c}{\mu}\frac{\partial p}{\partial z} \tag{9}$$

where g_c is the dimension conversion factor. Equations (7) and (8) simply indicate that the pressure is constant in the x-y plane for any value of z.

The velocity distribution and flow rate for laminar flow in a rectangular conduit were obtained theoretically by Cornish(17). He integrated equation (9) with the boundary condition that the fluid at the conduit surface had zero velocity. Cornish considered a conduit of width 2a and depth 2b and located the origin of his co-ordinates at the axis of the conduit. With the x-axis horizontal, the y-axis vertical and flow in the z-direction Cornish obtained

$$w = - \frac{16\, b^2\, g_c}{\pi^3 \mu} \frac{\partial p}{\partial z} \sum_{n=1,3..} \left[\frac{(-1)^{\frac{n-1}{2}}}{n^3} \frac{\cosh \frac{n\pi x}{2b}}{\cosh \frac{n\pi a}{2b}} \cos \frac{n\pi y}{2b} \right] - \frac{g_c}{2\mu} \frac{\partial p}{\partial z} (b^2 - y^2) \qquad (10)$$

for the velocity distribution, and

$$Q = - \frac{4\, a\, b^3}{3\mu} \frac{\partial p}{\partial z} \left[1 - \frac{192\, b}{\pi^5\, a} \sum_{n=1,3..} \left[\frac{1}{n^3} \tanh \frac{n\pi a}{2b} \right] \right] \qquad (11)$$

for the volumetric flow rate.

It is interesting to note that as $\frac{a}{b} \rightarrow \infty$, i.e. the conduit becomes infinitely wide, both equations (10) and (11) reduce to the corresponding expressions for flow between infinitely wide parallel plates.

Cornish performed experiments with water in a rectangular conduit with an aspect ratio, $\frac{a}{b}$ of 2.92 and verified equation (11). Equation (11) may be rearranged to

$$f = \frac{3}{2}\left(\frac{De}{b}\right)^2 \frac{1}{Re'} \Bigg/ \left[1 - \frac{192\ b}{\pi^5\ a} \sum_{n=1,3..} \left[\frac{1}{n^3} \tanh \frac{n\pi a}{2b}\right]\right] \tag{12}$$

where f and Re'are the Fanning friction factor and Reynolds number respectively and are defined by

$$f = -\frac{1}{2}\frac{\partial p}{\partial z}\frac{g_c\ D_e}{\rho\ V^2} \tag{13}$$

$$\text{and} \quad Re' = \frac{\rho V\ De}{\mu} \tag{14}$$

in which V is the average fluid velocity computed by dividing the volumetric flow rate by the cross-sectional area of the conduit, ρ is the fluid density and D_e is the equivalent diameter of the conduit defined by four times the cross-sectional area divided by the wetted perimeter.

Hence

$$D_e = \frac{4\ a\ b}{a + b} \tag{15}$$

The relationship between the friction factor and the Reynolds number for laminar flow in a rectangular conduit is therefore not unique but depends on the aspect ratio. As $\frac{a}{b} \rightarrow \infty$ equation (12) reduces to

$$f = \frac{24}{Re'} \tag{16}$$

which is the relationship for infinitely wide parallel plates.

No extensive results for the turbulent velocity distribution in rectangular conduits have been reported$^{(53)}$. However, Nikuradse$^{(72)}$ did measure point velocities in non-circular ducts, including rectangular conduits, and found that secondary motions of the fluid particles into the corners and away from the walls were superimposed upon the longitudinal motion.

Claibourne$^{(15)}$ in a review of pressure gradient data obtained by many investigators for turbulent flow in smooth non-circular conduits concluded that the results could be correlated by means of the Blasius equation

$$f = 0.0792\ (Re')^{-1/4} \tag{17}$$

The conduits had annular, triangular and rectangular cross sections and the scatter of the data was ± 15 percent for $Re > 5000$ and ± 35 percent for $2100 < Re < 5000$.

B. LAMINAR STRATIFIED FLOW OF TWO IMMISCIBLE LIQUIDS IN A RECTANGULAR CONDUIT

1. Expressions for velocity distribution and flow rates

The development of the velocity distribution and flow rate expressions for the co-current laminar stratified flow of two immiscible, Newtonian incompressible fluids in a

rectangular conduit is now undertaken. The flow is assumed to be fully developed and the interface between the fluid layers is assumed to be smooth and horizontal. The flow model is depicted in Figure 3. The conduit is represented by ABCD and the interface by EF. Liquid 2 flows above liquid 1, the depths being b_2 and b_1 respectively. The width of the conduit is 2a. The x, y, z co-ordinate system has the origin at 0 with the x-axis co-incident with the interface and flow in the z-direction.

The basic differential equation governing the flow of both fluids is equation (9) which may be written for each phase as

$$\frac{\partial^2 w_j}{\partial x^2} + \frac{\partial^2 w_j}{\partial y^2} = \frac{g_c}{\mu_j}\frac{\partial p}{\partial z} \quad j = 1,2 \tag{18}$$

w is the point velocity which is a function of both x and y. The boundary conditions are:

$$w_1 = 0 \quad \text{when} \quad x = \pm a,\ -b_1 \leqslant y \leqslant 0 \tag{19}$$

$$w_1 = 0 \quad \text{when} \quad -a \leqslant x \leqslant a,\ y = -b_1 \tag{20}$$

$$w_2 = 0 \quad \text{when} \quad x = \pm a,\ 0 \leqslant y \leqslant b_2 \tag{21}$$

$$w_2 = 0 \quad \text{when} \quad -a \leqslant x \leqslant a,\ y = b_2 \tag{22}$$

$$\left.\begin{aligned} & w_1 = w_2 & (23)\\ & \mu_1 \frac{\partial w_1}{\partial y} = \mu_2 \frac{\partial w_2}{\partial y} & (24)\end{aligned}\right\} \quad \text{when } -a \leqslant x \leqslant a,\ y = 0$$

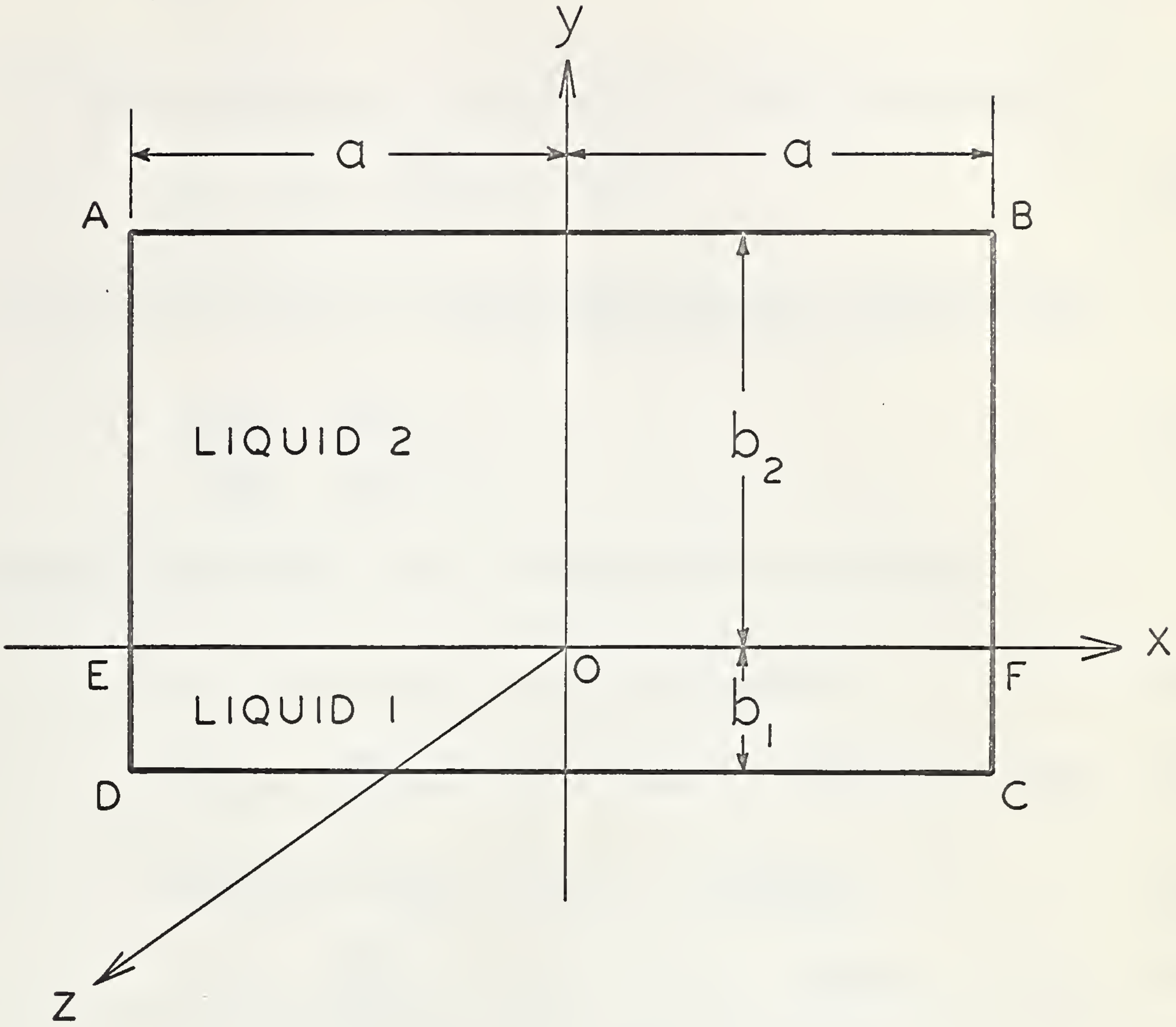

FIGURE 3 - MODEL OF STRATIFIED FLOW.

Let
$$k_j = \frac{g_c}{\mu_j} \frac{\partial p}{\partial z} \tag{25}$$

and
$$m = \frac{\mu_2}{\mu_1} \tag{26}$$

If the variable W_j is defined by the relationship

$$w_j = W_j + \frac{k_j}{2} (x^2 - a^2) \tag{27}$$

then substitution for w_j in the differential equation (18) gives

$$\frac{\partial^2 W_j}{\partial x^2} + \frac{\partial^2 W_j}{\partial y^2} = 0 \tag{28}$$

The boundary conditions (19) through (24) now become

$$W_1 = 0 \quad \text{when} \quad x = \pm a, \ -b_1 \leqslant y \leqslant 0 \tag{29}$$

$$W_1 = -\frac{k_1}{2} (x^2 - a^2) \quad \text{when} \quad -a \leqslant x \leqslant a, \ y = -b_1 \tag{30}$$

$$W_2 = 0 \quad \text{when} \quad x = \pm a \qquad 0 \leqslant y \leqslant b_2 \tag{31}$$

$$W_2 = -\frac{k_2}{2} (x^2 - a^2) \quad \text{when} \quad -a \leqslant x \leqslant a, \ y = b_2 \tag{32}$$

$$\left.\begin{aligned} & W_2 - W_1 = \frac{1}{2}(k_1 - k_2)(x^2 - a^2) \qquad (33) \\ & \frac{\partial W_1}{\partial y} - m \frac{\partial W_2}{\partial y} = 0 \qquad (34) \end{aligned}\right\} \text{when } -a \leqslant x \leqslant a, \ y = 0$$

Boundary conditions (29) and (31) give $W_j = 0$ when $x = \pm a$ and are staisfied by terms of the form

$$Y_j \cos \frac{(2i + 1)\pi}{2a} x \tag{35}$$

where Y_j is a function of y only and i is an integer.

Let $$n = \frac{(2i + 1)\ \pi}{2a} \tag{36}$$

and substitute
$$W_j = Y_j \cos nx \tag{37}$$

in equation (28)

i.e. $$\frac{\partial^2 Y_j}{\partial y^2} - n^2\ Y_j = 0 \tag{38}$$

from which it follows that

$$Y_j = A_j(n)\ \sinh ny + B_j(n)\ \cosh ny \tag{39}$$

in which $A_j(n)$ and $B_j(n)$ are functions of n and, therefore, of i but not of x and y. The solution may therefore be written in the form

$$W_j = \sum_{i=0}^{\infty} \left[A_j(n) \sinh ny + B_j(n)\ \cosh ny \right] \cos nx \tag{40}$$

which may be considered as a cosine Fourier series, the term coefficients being functions of y. Two of the six boundary conditions have been used. Four remain, therefore, for the evaluation of $A_j(n)$ and $B_j(n)$, $j = 1,2$.

Substitution of boundary condition (30) into equation (40) gives

$$- \frac{k_1}{2}(x^2-a^2) = \sum_{i=0}^{\infty} \left[A_1(n)\ \sinh\ (-nb_1) + B_1(n) \cosh(-nb_1) \right] \cos nx \tag{41}$$

Multiplication of both sides of equation (41) by cos n'x where n' is any one of the possible values of n and integration with respect x between the limits -a and +a gives

$$\int_{-a}^{+a} -\frac{k_1}{2}(x^2-a^2)\cos n'x\,dx =$$

$$\int_{-a}^{+a} \sum_{i=0}^{\infty} \Big[A_1(n)\sinh(-nb_1) + + B_1(n)\cosh(-nb_1)\Big] \cos nx \cos n'x\,dx \qquad (42)$$

$$\text{Since} \quad \int_{-a}^{+a} \cos nx \cos n'x = 0 \quad \text{for} \quad n \neq n' \qquad (43)$$

equation (42) becomes

$$\int_{-a}^{+a} -\frac{k_1}{2}(x^2-a^2)\cos nx\,dx =$$

$$= \Big[A_1(n)\sinh(-nb_1) + B_1(n)\ \cosh nb_1 \Big] \int_{-a}^{+a} \cos^2 nx\,dx \qquad (44)$$

from which

$$-\ A_1(n)\sinh nb_1 + B_1(n)\cosh nb_1 = \frac{2k_1(-1)^i}{a\ n^3} \qquad (45)$$

By substituting boundary condition (32) into equation (40) and following a procedure similar to that used for deriving equation (45) it follows that

$$A_2(n)\sinh nb_2 + B_2(n)\cosh nb_2 = \frac{2k_2\,(-1)^i}{a\ n^3} \qquad (46)$$

Substitution of boundary condition (33) in equation (40) gives

$$\Big[B_2(n) - B_1(n)\Big] \int_{-a}^{+a} \cos^2 nx\,dx = \frac{1}{2} \int_{-a}^{+a} (k_1-k_2)\,(x^2-a^2)\cos nx\,dx \qquad (47)$$

from which

$$B_2(n) - B_1(n) = \frac{2(k_1-k_2)(-1)^{i+1}}{a\ n^3} \tag{48}$$

By differentiating equation (40) with respect to y and using boundary condition (34) it follows that

$$A_1(n) = m\ A_2(n) \tag{49}$$

Equations (45), (46), (48) and (49) may be solved simultaneously for the coefficients $A_1(n)$, $A_2(n)$, $B_1(n)$, $B_2(n)$.

Thus

$$A_1(n) = \frac{\frac{2m(-1)^i}{a\ n^3}\left[k_2 \cosh nb_1 - k_1 \cosh nb_2 + (k_1-k_2)\cosh nb_1\ \cosh nb_2\right]}{\cosh nb_1\ \sinh nb_2 + m\ \sinh nb_1\ \cosh nb_2} \tag{50}$$

$$A_2(n) = \frac{\frac{2(-1)^i}{a\ n^3}\left[k_2 \cosh nb_1 - k_1 \cosh nb_2 + (k_1-k_2)\cosh nb_1\ \cosh nb_2\right]}{\cosh nb_1\ \sinh nb_2 + m\ \sinh nb_1\ \cosh nb_2} \tag{51}$$

$$B_1(n) = \frac{\frac{2(-1)^i}{a\ n^3}\left[k_1 \sinh nb_2 + mk_2 \sinh nb_1 + m(k_1-k_2)\sinh nb_1\ \cosh nb_2\right]}{\cosh nb_1\ \sinh nb_2 + m\ \sinh nb_1\ \cosh nb_2} \tag{52}$$

$$B_2(n) = \frac{\frac{2(-1)^i}{a\ n^3}\left[mk_2 \sinh nb_1 + k_1 \sinh nb_2 - (k_1-k_2)\sinh nb_2\ \cosh nb_1\right]}{\cosh nb_1 \sinh nb_2 + m\ \sinh nb_1\ \cosh nb_2} \tag{53}$$

The desired solution for the velocity distribution is

$$w_1 = \sum_{i=0}^{\infty}\left[A_1(n)\sinh ny + B_1(n)\cosh ny\right]\cos nx + \frac{k_1}{2}(x^2-a^2) \tag{54}$$

with $A_1(n)$ and $B_1(n)$ given by equations (50) and (52) respectively and

$$w_2 = \sum_{i=0}^{\infty} \left[A_2(n) \sinh ny + B_2(n) \cosh ny\right] \cos nx + \frac{k_2}{2} (x^2-a^2) \quad (55)$$

with $A_2(n)$ and $B_2(n)$ given by equations (51) and (53).

Immediate checks on the velocity distribution expressions were obtained in two ways:

(i) If $m = 1$ and, therefore, $k_1 = k_2$ then fluids 1 and 2 are identical as far as this problem is concerned. If, in addition, $b_1 = b_2 = b$ then the x-axis lies equidistant between the top and bottom of the conduit. With these substitutions both equations (54) and (55) reduce to the expression derived by Cornish for the velocity distribution in single-phase flow, equation (10).

(ii) If $y = 0$ and $b_1 = b_2 = b$ then both equations (54) and (55) reduce to the equation

$$w = \frac{(x^2-a^2)(k_1+mk_2)}{2(1+m)} + \sum_{i=0}^{\infty} \frac{2(-1)^i (k_1+mk_2)}{a\, n^3 (1+m) \cosh nb} \cos nx \quad (56)$$

which has been obtained by Dumitrescu and Staniscu(24) for the interfacial velocity distribution for the special case when the depths of the fluid layers are equal.

Since it was desired to evaluate the velocity distribution by automatic digital computation, equations (54) and (55) were rearranged into more convenient forms as follows

$$w_1 = \frac{8a^2}{\pi^3} \sum_{i=0}^{\infty} \frac{(-1)^i}{(2i+1)^3} \left[\left(B_1'(n) + m\ A_1'(n) \right) e^{ny} + \left(B_1'(n) - m\ A_1'(n) \right) e^{-ny} \right] + \\ + \frac{k_1}{2} (x^2 - a^2) \qquad (57)$$

and

$$w_2 = \frac{8a^2}{\pi^3} \sum_{i=0}^{\infty} \frac{(-1)^i}{(2i+1)^3} \left[\left(B_2'(n) + A_2'(n) \right) e^{ny} + \left(B_2'(n) - A_2'(n) \right) e^{-ny} \right] + \\ + \frac{k_2}{2} (x^2 - a^2) \qquad (58)$$

in which

$$A_1'(n) = A_2'(n) = \\ = \frac{k_2 \cosh nb_1 - k_1 \cosh nb_2 + (k_1 - k_2) \cosh nb_1 \cosh nb_2}{\cosh nb_1 \sinh nb_2 + m \sinh nb_1 \cosh nb_2} \qquad (59)$$

$$B_1'(n) = \frac{k_1 \sinh nb_2 + mk_2 \sinh nb_1 + m(k_1 - k_2) \sinh nb_1 \cosh nb_2}{\cosh nb_1 \sinh nb_2 + m \sinh nb_1 \cosh nb_2} \qquad (60)$$

$$B_2'(n) = \frac{mk_2 \sinh nb_1 + k_1 \sinh nb_2 - (k_1 - k_2) \sinh nb_2 \cosh nb_1}{\cosh nb_1 \sinh nb_2 + m \sinh nb_1 \cosh nb_2} \qquad (61)$$

The volumetric flow rates Q_1 and Q_2 are obtained by evaluating the integrals

$$Q_1 = \int_{-b_1}^{0} \int_{-a}^{+a} w_1 \, dx \, dy \qquad (62)$$

and

$$Q_2 = \int_{0}^{b_2} \int_{-a}^{+a} w_2 \, dx \, dy \tag{63}$$

Substitution for w_1 and w_2 from equations (54) and (55) gives finally

$$Q_1 = \sum_{i=0}^{\infty} \frac{2(-1)^i}{n^2} \Big[A_1(n)(1 - \cosh nb_1) + B_1(n) \sinh nb_1 \Big] - - \frac{2}{3} k_1 a^3 b_1 \tag{64}$$

and

$$Q_2 = \sum_{i=0}^{\infty} \frac{2(-1)^i}{n^2} \Big[A_2(n)(\cosh nb_2 - 1) + B_2(n) \sinh nb \Big] - - \frac{2}{3} k_2 a^3 b_2 \tag{65}$$

with $A_1(n)$, $A_2(n)$, $B_1(n)$ and $B_2(n)$ given by equations (50) through (53).

Alternatively equations (64) and (65) may be written in the form

$$Q_1 = \frac{128a^4}{\pi^5} \sum_{i=0}^{\infty} \frac{1}{(2i+1)^5} \Big[mA_1'(n)(1-\cosh nb_1) + B_1'(n) \sinh nb_1 \Big] - - \frac{2}{3} k_1 a^3 b_1 \tag{66}$$

and

$$Q_2 = \frac{128a^4}{\pi^5} \sum_{i=0}^{\infty} \frac{1}{(2i+1)^5} \Big[A_2'(n)(\cosh nb_2 - 1) + B_2'(n) \sinh nb_2 \Big] - - \frac{2}{3} k_2 a^3 b_2 \tag{67}$$

with $A_1'(n)$, $A_2'(n)$, $B_1'(n)$ and $B_2'(n)$ given by equations (59) through (61).

The following check was obtained for the flow rate expressions. If $b_1 = b_2 = b$ and $m = 1$ then fluids 1 and 2 are identical and $Q_1 = Q_2$. The sum of Q_1 and Q_2 should be identical with the flow rate expression derived by Cornish, equation (11) for single phase flow. This is, in fact, so.

Expressions have been derived in open form for the velocity distribution and volumetric flow rates for the stratified, laminar flow of two fluids in a closed rectangular conduit. The velocity distribution and flow rates can, therefore, be calculated from a knowledge of the physical dimensions of the conduit, the fluid properties, the pressure gradient and the position of the interface.

It is now convenient to define several terms which will be useful in the presentation of the theoretical results. Reference was made in the introduction to the pressure gradient reduction factor for the simultaneous flow of two fluids through closed conduits. The pressure gradient reduction factor is defined as the ratio of the pressure gradient for the flow of the more viscous phase alone to the pressure gradient for the flow of the two-phase system, the flow rate of the more viscous phase being the same in each case. In presenting the results of the present investigation it will be assumed that the viscosity of the upper liquid 2 is equal to or greater than the viscosity

of the lower liquid 1 i.e. $m > 1$.

Hence

$$\text{pressure gradient reduction factor} = \frac{\left(\frac{\partial p}{\partial z}\right)_2}{\left(\frac{\partial p}{\partial z}\right)_{tp}} \quad \text{for same } Q_2 \qquad (68)$$

Now, since for a given interface position flow rate and pressure gradient are directly proportional to each other the pressure gradient reduction factor may also be written in the form

$$\text{pressure gradient reduction factor} = \frac{(Q_2)_{tp}}{Q_2} \text{ for same } \frac{\partial p}{\partial z} \qquad (69)$$

$$= \frac{\text{equation (67)}}{\text{equation (11) written for liquid 2}}$$

$$\text{for same } \frac{\partial p}{\partial z} \qquad (70)$$

By dividing equation (67) by equation (11) it is possible to show that the pressure gradient reduction factor is a function of the interface position, the viscosity ratio and the conduit aspect ratio only. Hence for different aspect ratios it is possible to represent the pressure gradient reduction factor as a function of the interface position and viscosity ratio.

The position of the interface will be defined by

$$\text{relative interface position} = \frac{b_2}{b_1 + b_2} \qquad (71)$$

The relative interface position varies from 0 when liquid 1 flows alone to 1.0 when liquid 2 flows alone.

In general, a characteristic of two-phase flow is that the average velocities of the two phases in the conduit are not equal. This causes the insitu ratio of the phases to be different from the input ratio or flow rate ratio.

If

$$\text{input ratio} = \frac{Q_1}{Q_2} \tag{72}$$

and

$$\text{insitu ratio} = \frac{b_1}{b_2} \tag{73}$$

then the holdup ratio is defined by

$$\text{holdup ratio} = \frac{\text{input ratio}}{\text{insitu ratio}} \tag{74}$$

2. Computation

Representative velocity profiles were evaluated using equations (57) and (58) to illustrate the effects of interface position and aspect ratio on the velocity distribution. Pressure gradient reduction factors and holdup ratios were evaluated from equations (11), (66) and (67) for the entire range of interface position for viscosity ratios from 1 to 1000 and aspect ratios from 8:1 to 1:3. Equation (11) was evaluated with the aid of a desk calculator and the other equations with the aid of the University of Alberta IBM 1620 computer having punched card input and output. Programs were written in

Fortran II.

All of the equations evaluated consist of two parts - one in open form and the other in closed form. In each case the sum of the open form expression was obtained until the value of the next term was less than 0.01 percent of the sum already accummulated. That this was a reliable procedure leading to negligible error was confirmed in two ways:

(i) Interfacial velocities evaluated from equations (57) and (58) always agreed to within approximately 1 percent. Usually between four and ten terms were required in the infinite series to give the stated tolerance. The series in the flow rate expressions converged faster than the series in the velocity expressions showing that the error introduced by neglecting terms in the flow rate expressions having a magnitude less than 0.01 percent of the sum would cause even less error than in the velocity expressions.

(ii) The sum of the flow rates calculated from equations (66) and (67) for any interface position and a viscosity ratio of unity agreed to within approximately 0.5 percent with the flow rate for single-phase flow evaluated from equation (11).

It is worthwhile to consider the convergence of the series in more detail. Consider, for example, equation (67)

which is the flow rate expression for liquid 2. The series converges because as n increases the two terms $A'_2(n)(\cosh nb_2 - 1)$ and $B'_2(n)\sinh nb_2$ become more nearly equal in magnitude and opposite in sign. Further, for a given value of n, the values of $\cosh nb_2$ and $\sinh nb_2$ become very large for large values of b_2/a, i.e. for small aspect ratios. Consequently it would be expected that machine round-off error would be more troublesome for computations involving small aspect ratios. This was, in fact, found to be so. Whereas ordinary precision floating point arithmetic in which 8 figures were carried was sufficient for an aspect ratio of 8:1 extended precision floating point arithmetic in which 28 figures were carried was necessary for an aspect ratio of 1:3. Round-off error manifested itself in extremely "wild" results being obtained which disappeared when sufficient figures were carried.

3. Results

(i) Velocity distributions

The evaluation of complete velocity distributions for wide ranges of interface position, viscosity ratio and aspect ratio was not warranted in the present study. Rather, representative profiles were calculated to illustrate

(1) the effect on the profile of different interface positions for given viscosity and aspect ratios and

(2) the effect on the profile of different aspect ratios for a given interface position and viscosity ratio.

The effect of interface position is illustrated in Figure 4 in which velocity profiles on the y-axis are shown for a viscosity ratio of 5.326 and an aspect ratio of 7.95:1. The velocities are represented by the dimensionless ratio w/V_{pp} where w is the local velocity calculated for a given pressure gradient and V_{pp} is the average velocity for flow of the more viscous phase under the same pressure gradient between parallel plates $(b_1 + b_2)$ apart. In this way the results are independent of the pressure gradient. The relative interface position is shown for each profile. A relative position of 0 corresponds to the flow of the less viscous phase alone and a relative position of 1 corresponds to the flow of the more viscous phase alone.

It is apparent that the addition of the less viscous phase extends the profile within the more viscous phase. In doing so the maximum in the profile always occurs at a point below the mid-point between the top and bottom of the conduit. For relative interface positions less than 0.7 approximately the maximum occurs in the less viscous phase; for relative positions greater than approximately 0.7 the maximum occurs

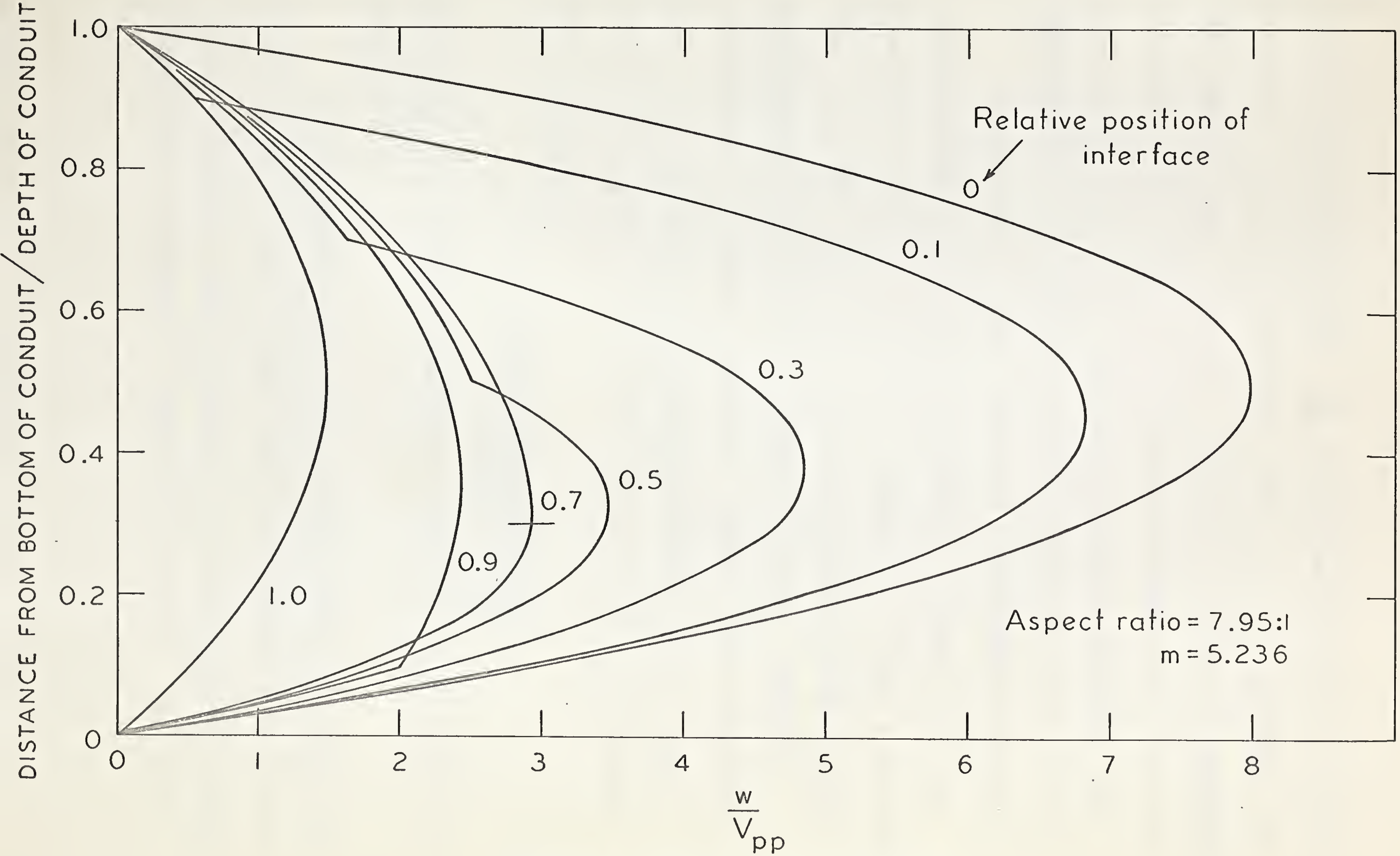

FIGURE 4 - VERTICAL VELOCITY PROFILES

in the more viscous phase. At a relative position of approximately 0.7 the maximum velocity occurs at the interface. It also appears from the figure, although it cannot be considered as proven, that for a given pressure gradient and this particular aspect ratio the interface velocity is greatest when the maximum in the complete profile occurs at the interface.

The effect of aspect ratio is illustrated in Figure 5 in which interfacial velocity profiles, i.e. at y = 0, are shown for a relative interface position of 0.9 and a viscosity ratio of 5.326. The velocities are represented by the same dimensionless ratio used in Figure 4 and are, therefore, independent of pressure gradient. Aspect ratios range from ∞:1, i.e. infinitely wide parallel plates, to 1:3. The interface velocity for an aspect ratio of ∞:1 was computed from the equation

$$w_i = -\frac{g_c}{2}\frac{\partial p}{\partial z}\frac{(b_1 + b_2)\,b_1\,b_2}{(b_2\,\mu_1 + b_1\,\mu_2)} \qquad (75)$$

which may be obtained by extending the analysis of Russell and Charles(78).

It is apparent that for an aspect ratio of 7.95:1 the velocity profile for x/a less than 0.5 is coincident for all practical purposes with the profile for flow between parallel plates and is, therefore, a function of y only. For such an

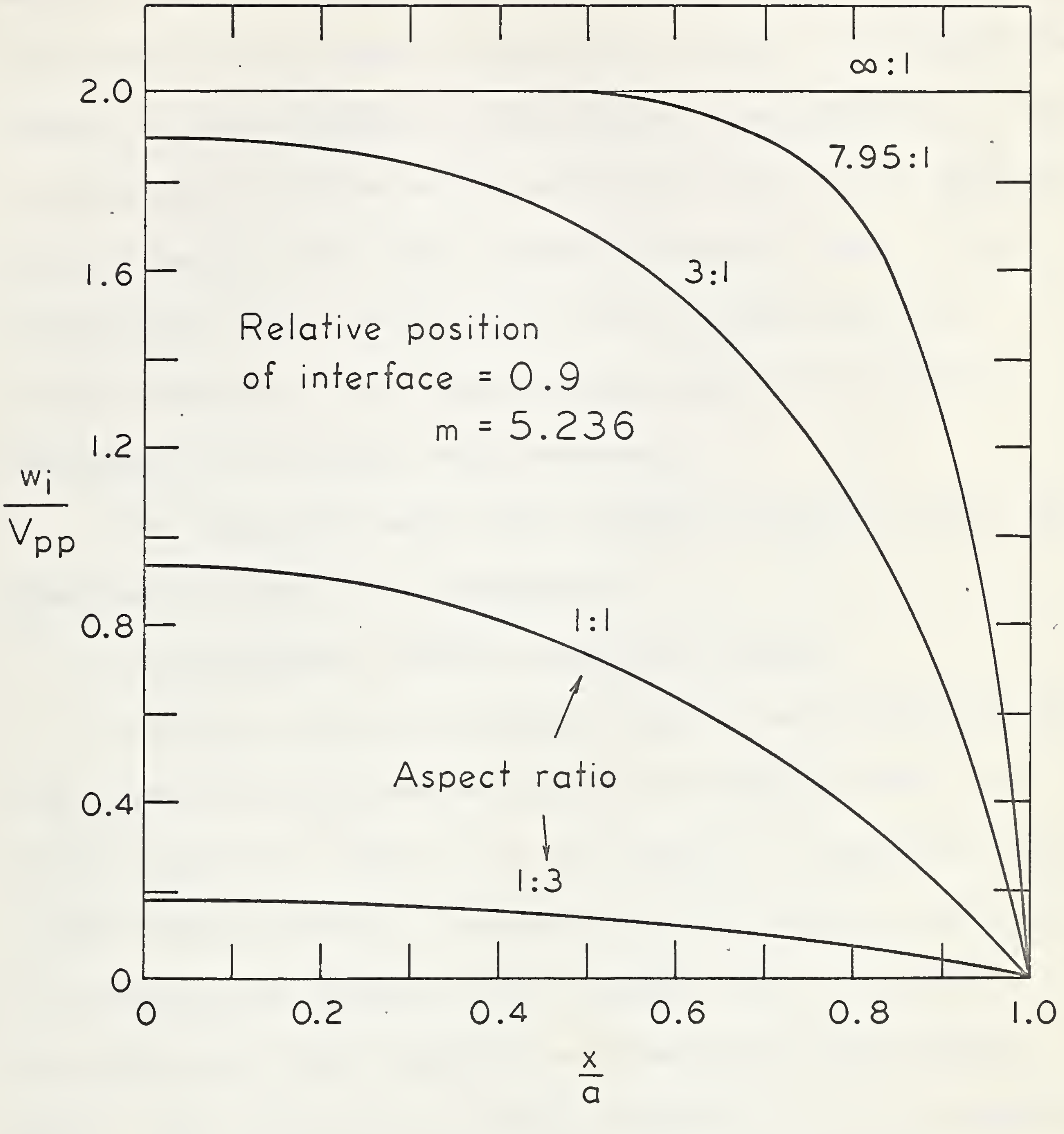

FIGURE 5 - INTERFACIAL VELOCITY PROFILES

aspect ratio the effect of the sides of the conduit are only apparent for x/a greater than 0.5. For an aspect ratio of 3:1 the effect of the sides is transmitted across the width of the conduit so that no part of the profile is two-dimensional and, in addition, the value of the velocity at x/a = 0 is approximately 5 percent less than the parallel plate value. The profiles for aspect ratios of 1:1 and 1:3 show that, as would be expected, the effect of the sides of the conduit increases as the aspect ratio decreases.

The numerical data used to prepare Figures 4 and 5 are tabulated in Table A1 of Appendix A.

(ii) Pressure gradient reduction factors

Pressure gradient reduction factors were evaluated over wide ranges of interface position and viscosity ratio for aspect ratios of 7.896:1, 3:1, 1:1 and 1:3. Viscosity ratios ranged from 1 to 1000. Pressure gradient reduction factors are presented in Figure 6 for an aspect ratio of 7.896:1. The curves for each viscosity ratio have the same general shape. For a relative interface position of 1.0 the interface is at the bottom of the conduit, the more viscous phase flows alone and the pressure gradient reduction factor is unity. With increasing amounts of the less viscous phase the pressure

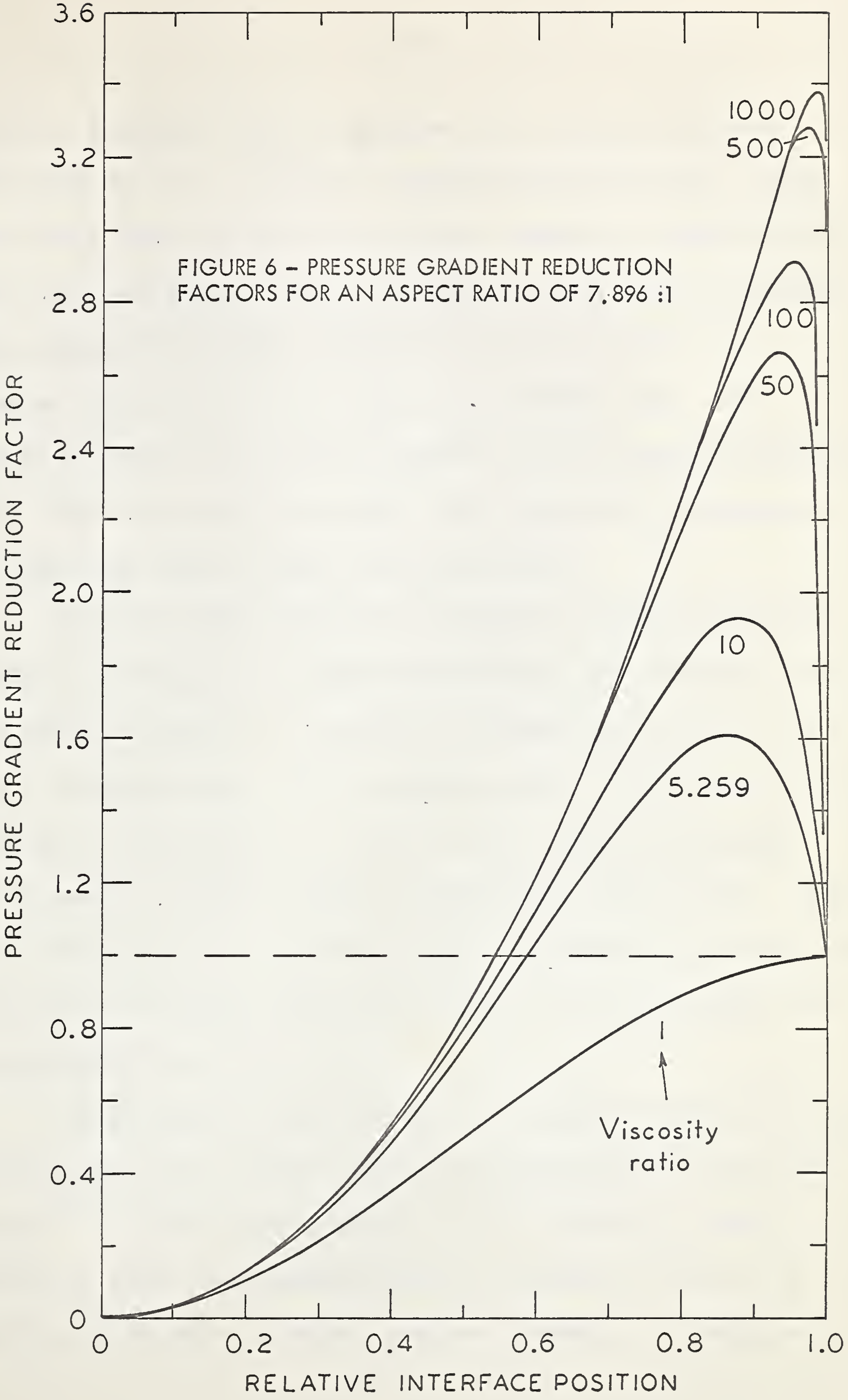

FIGURE 6 – PRESSURE GRADIENT REDUCTION FACTORS FOR AN ASPECT RATIO OF 7.896 :1

gradient reduction factor increases to a maximum and then decreases to 0 at a relative interface position of 0. Under conditions when the pressure gradient reduction factor exceeds unity the two-phase pressure gradient is less than the single-phase pressure gradient, despite the fact that the more viscous phase flows at the same rate in both cases. The factor by which the pressure gradient can be reduced increases with viscosity ratio but becomes less sensitive to variation in viscosity ratio at high viscosity ratios.

Similar plots showing the pressure gradient reduction factor as a function of interface position and viscosity ratio are shown in Figures 7, 8 and 9 for aspect ratios of 3:1, 1:1 and 1:3 respectively. It is apparent that as the aspect ratio decreases the addition of a less viscous phase to decrease the pressure gradient becomes increasingly unattractive. Thus for a viscosity ratio of 1000, while the maximum reduction factor is 3.38 for an aspect ratio of 7.896:1, it is only about 1.13 for an aspect ratio of 1:3.

Superimposed on the curves for a square conduit in Figure 8 are curves for a circular pipe obtained by Charles and Redberger(13). It is immediately apparent that for a given viscosity ratio the maximum reduction factor is less for a circular pipe than it is for a square conduit. In addition,

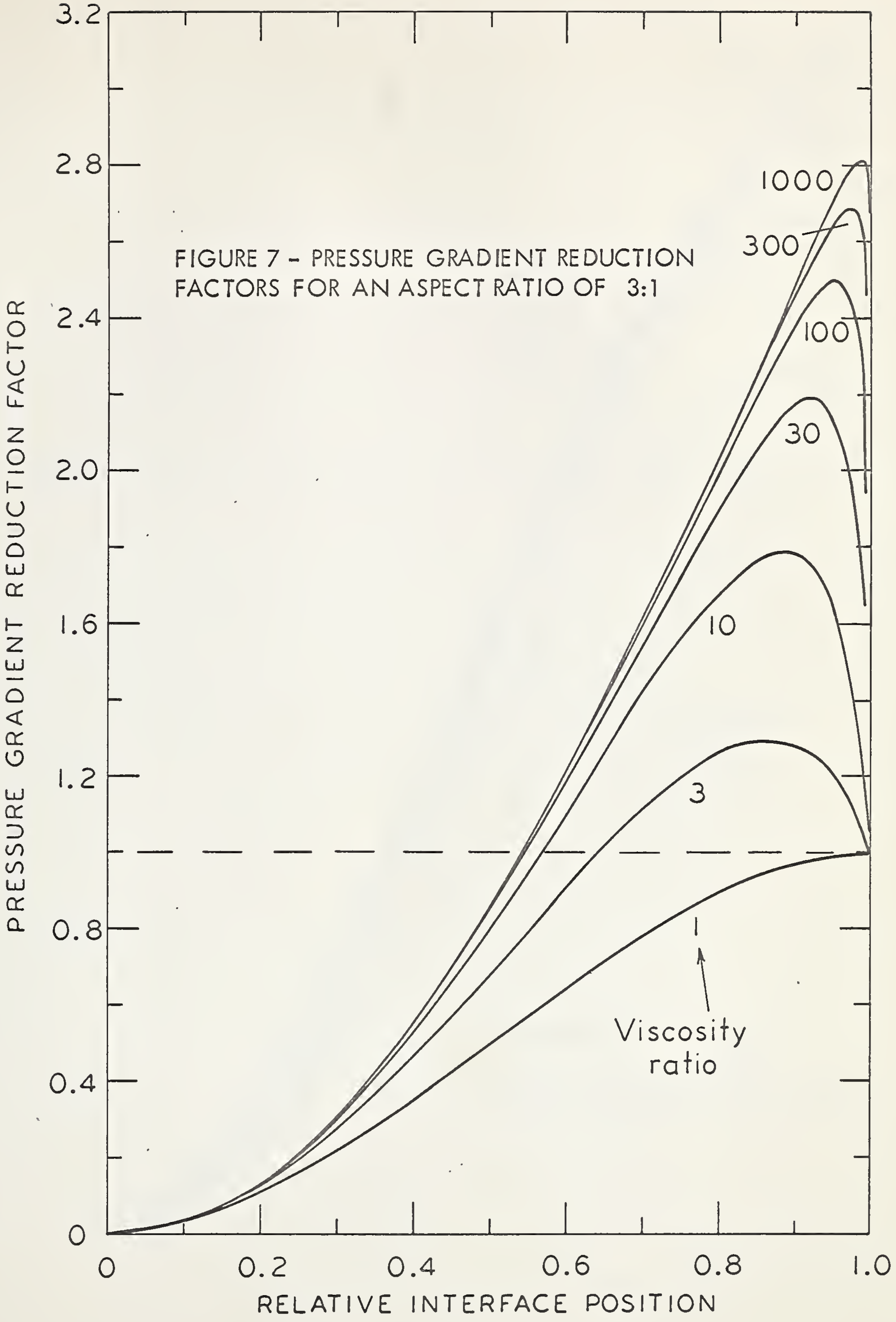

FIGURE 7 - PRESSURE GRADIENT REDUCTION FACTORS FOR AN ASPECT RATIO OF 3:1

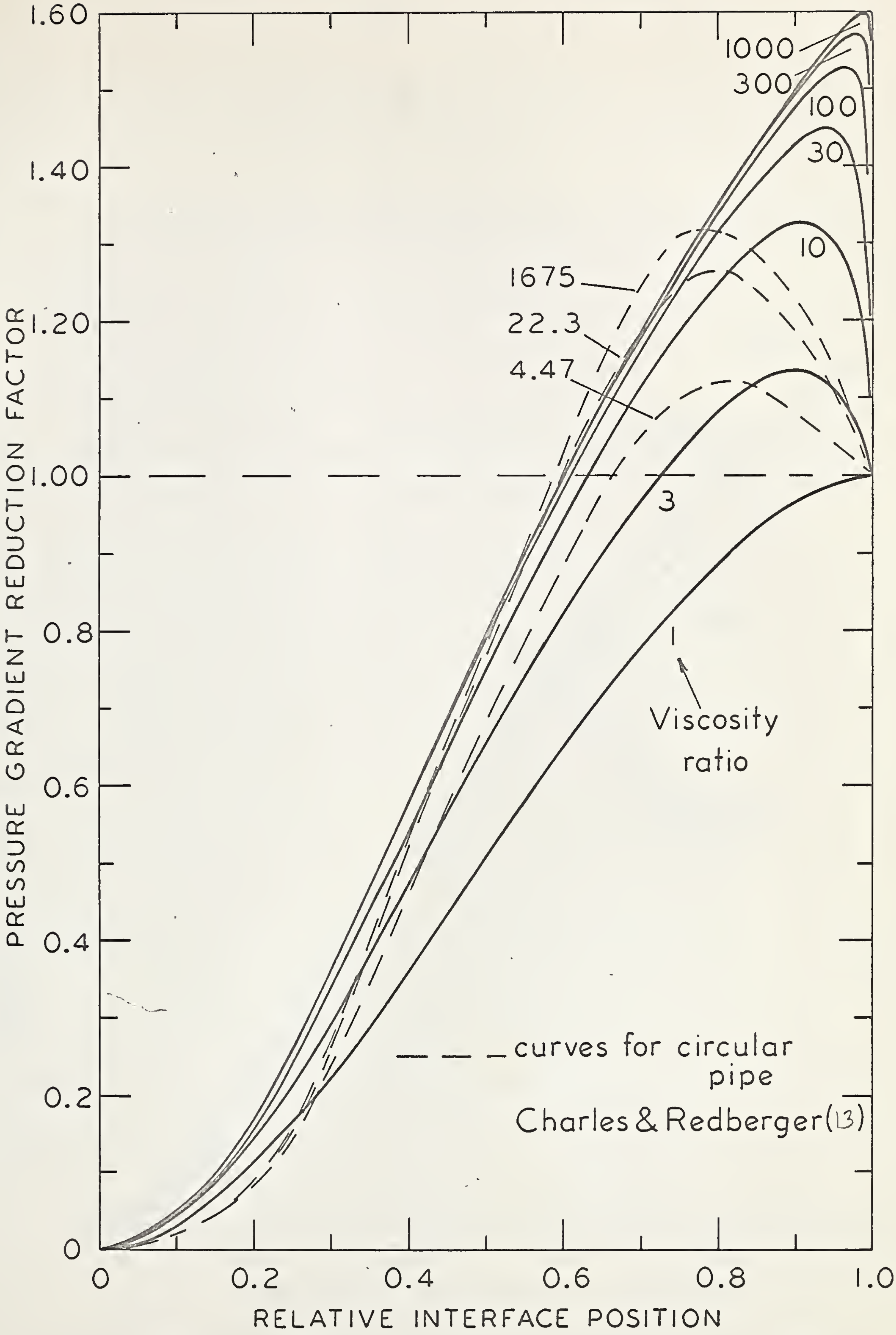

FIGURE 8 - PRESSURE GRADIENT REDUCTION FACTORS FOR AN ASPECT RATIO OF 1:1

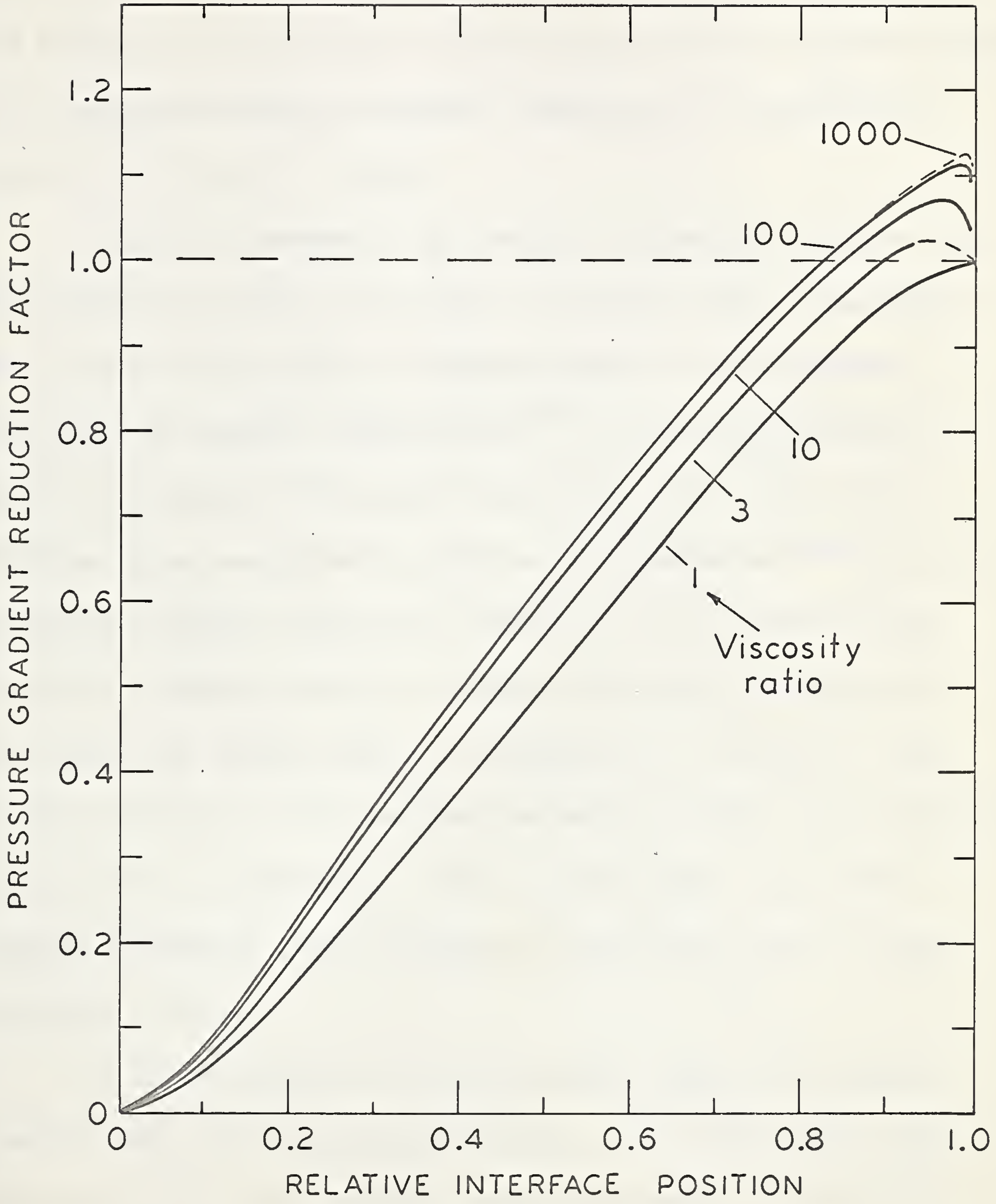

FIGURE 9 - PRESSURE GRADIENT REDUCTION FACTORS FOR AN ASPECT RATIO OF 1:3

the depth of the less viscous phase required to produce the maximum value of the reduction factor is considerably greater for the pipe than for the square conduit. As a consequence the proportion of the less viscous phase in the flowing stream for a maximum pressure gradient reduction is considerably greater for flow in a pipe.

Figure 10 compares the maximum reduction factors for the different aspect ratios and a circular pipe. Included in this figure is the curve evaluated from the expressions developed by Russell and Charles(78) for stratified flow between infinitely wide parallel plates, the curve for a circular pipe evaluated by Charles and Redberger(13) and the curves for aspect ratios of 7.896:1, 3:1, 1:1 and 1:3 for which the maximum pressure gradient reduction factors were read from the curves shown in Figures 6, 7, 8 and 9. The steady decrease in the maximum reduction ractor with decreasing aspect ratio is apparent. For a given aspect ratio the maximum reduction factor tends to a constant value at high viscosity ratios.

It is worthwhile to consider the cases of a square conduit and a circular pipe further. At a viscosity ratio of 1000 not only is the maximum reduction factor 1.595 for a square conduit and 1.31 for a circular pipe but the greater

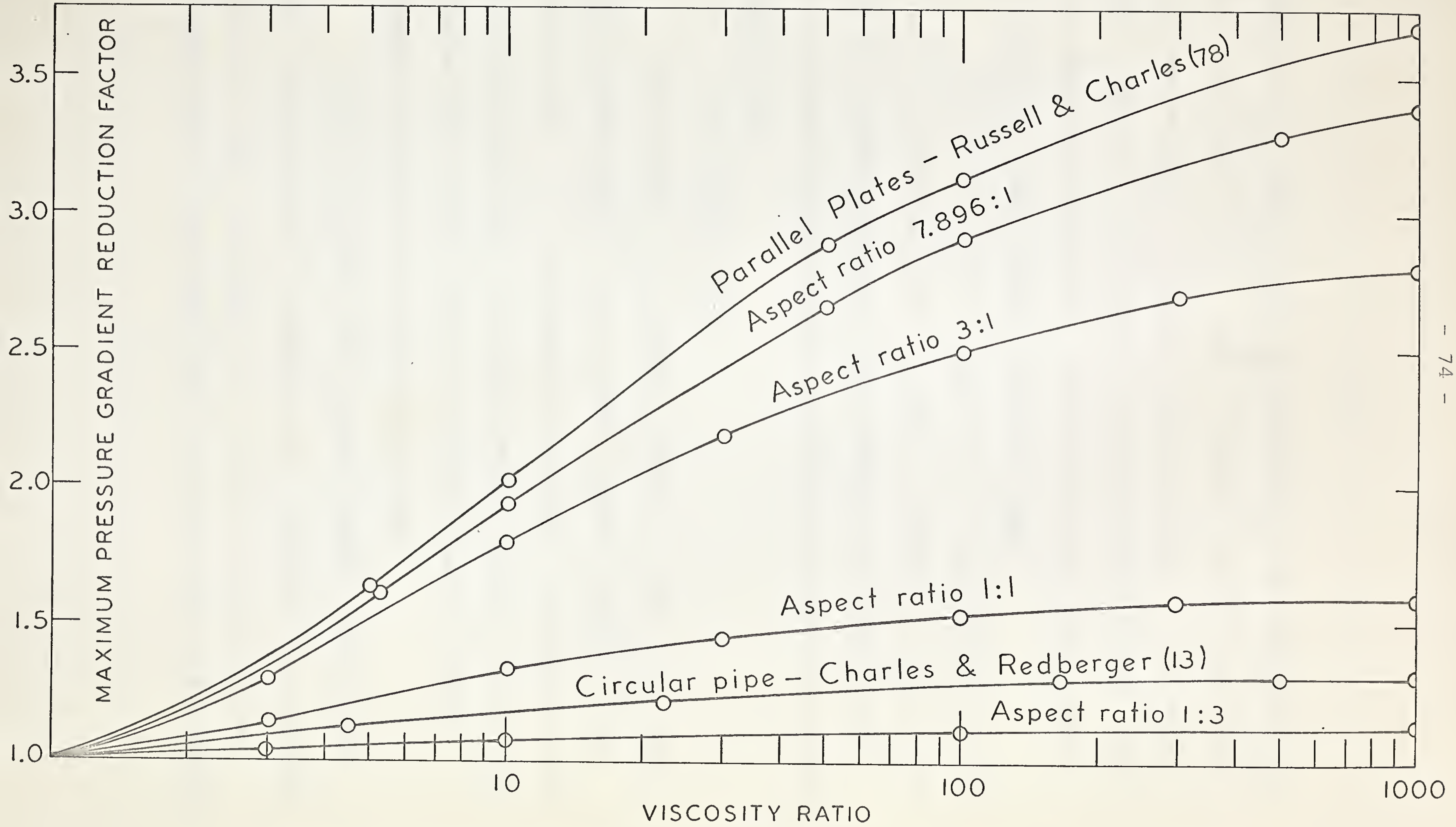

FIGURE 10 - MAXIMUM PRESSURE GRADIENT REDUCTION FACTORS FOR VARIOUS CONDUITS

reduction is achieved with a considerably less proportion of the less viscous phase - only 1.5 percent of the total flow in a square conduit compared with 90 percent in a circular pipe. This is a consequence of the relatively higher interface position in pipe flow allowing the less viscous phase a relatively easy passage through the pipe.

The curves shown in Figure 10 for the different aspect ratios are cross plotted in Figure 11 showing in more detail how the maximum reduction factor varies with aspect ratio. Also included are the maximum reduction factors for an infinite aspect ratio.

(iii) Holdup ratios

The holdup ratio has been defined as the input ratio (less viscous phase to more viscous phase) divided by the insitu ratio. As a consequence, a holdup ratio greater than unity indicates that the actual average velocity of the less viscous phase in the conduit is greater than the actual average velocity of the more viscous phase.

Curves of holdup ratio plotted against insitu ratio with viscosity ratio as parameter are presented for an aspect ratio of 7.896:1 in Figure 12. As would be expected the holdup ratio is unity when both the insitu ratio and viscosity

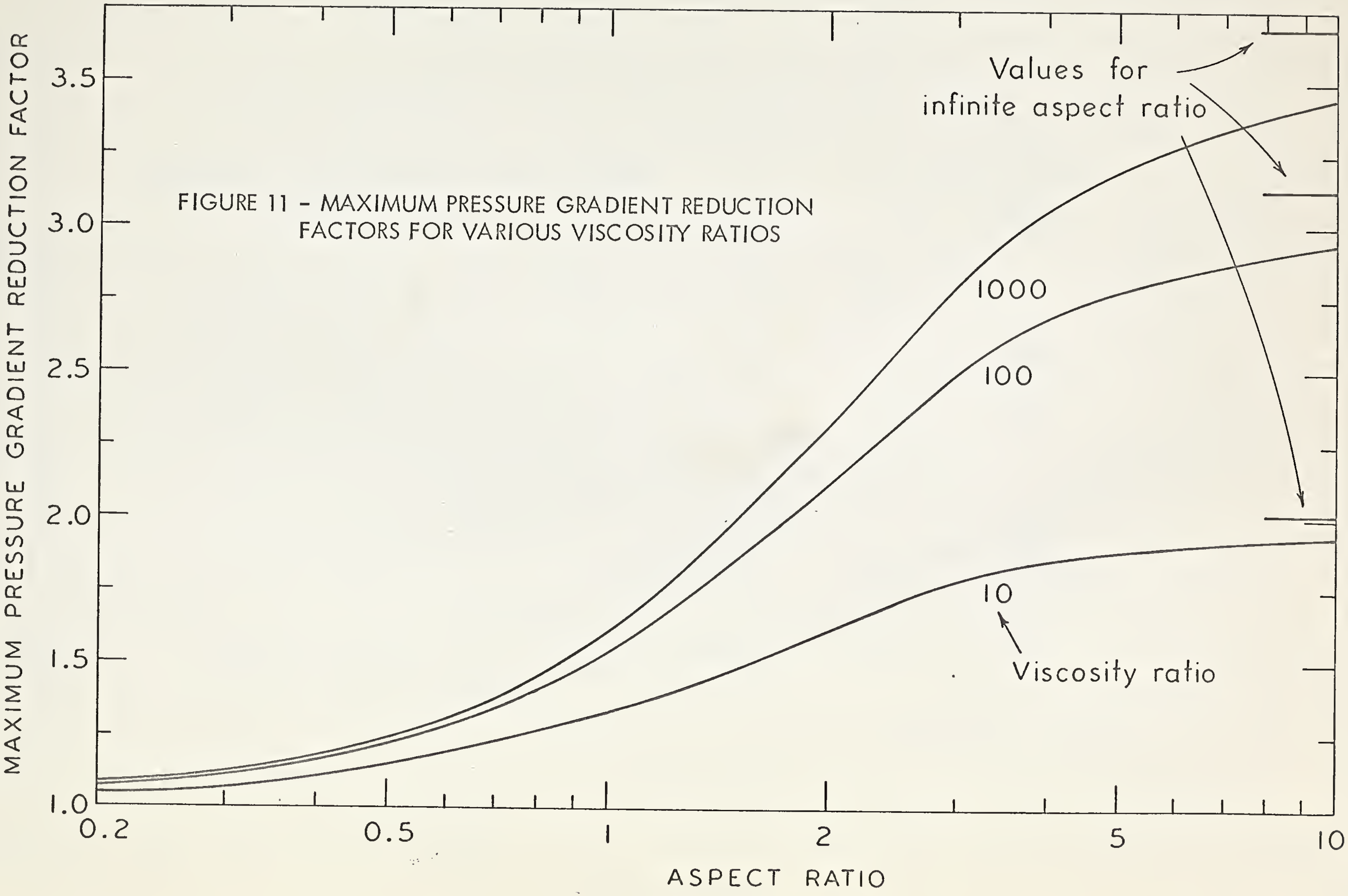

FIGURE 11 - MAXIMUM PRESSURE GRADIENT REDUCTION FACTORS FOR VARIOUS VISCOSITY RATIOS

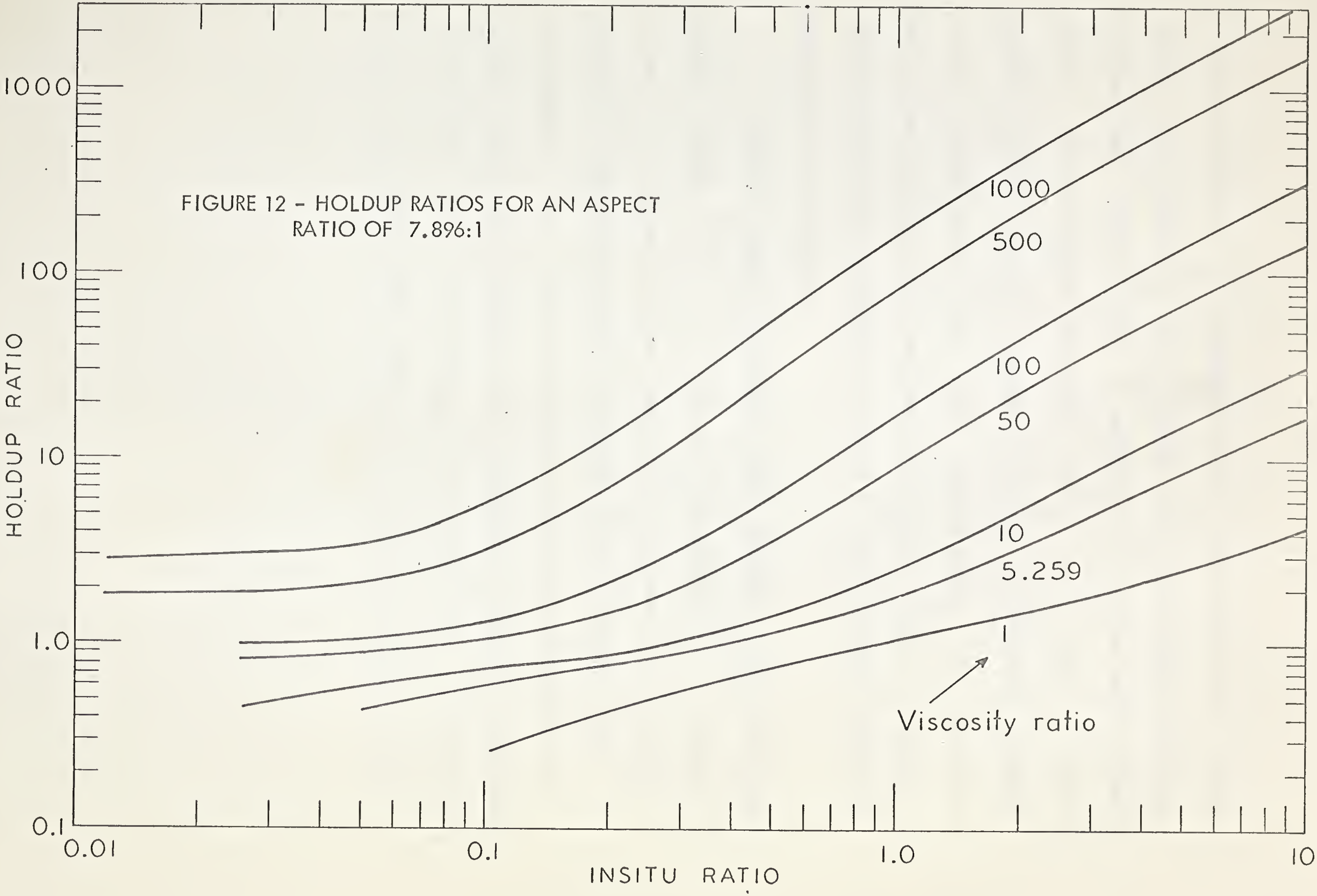

FIGURE 12 - HOLDUP RATIOS FOR AN ASPECT RATIO OF 7.896:1

ratio are unity. It is apparent that the higher the viscosity ratio, the greater is the tendency for the average velocity of the less viscous phase to exceed that of the more viscous phase. At the higher viscosity ratios it is only at very low insitu ratios that the average velocity of the more viscous phase exceeds that of the less viscous phase. The manner in which the holdup ratio varies with insitu ratio is readily appreciated when reference is made to the velocity profiles presented in Figure 4.

Similar plots of holdup ratio against insitu ratio for aspect ratios of 3:1, 1:1 and 1:3 are presented in Figures 13, 14 and 15. While all the families of curves are basically similar a definite trend is evident as the aspect ratio decreases: for a given viscosity ratio, at relatively low insitu ratios the holdup ratio increases, while at relatively high insitu ratios the holdup ratio decreases. The following table illustrates this trend for a viscosity ratio of 100.

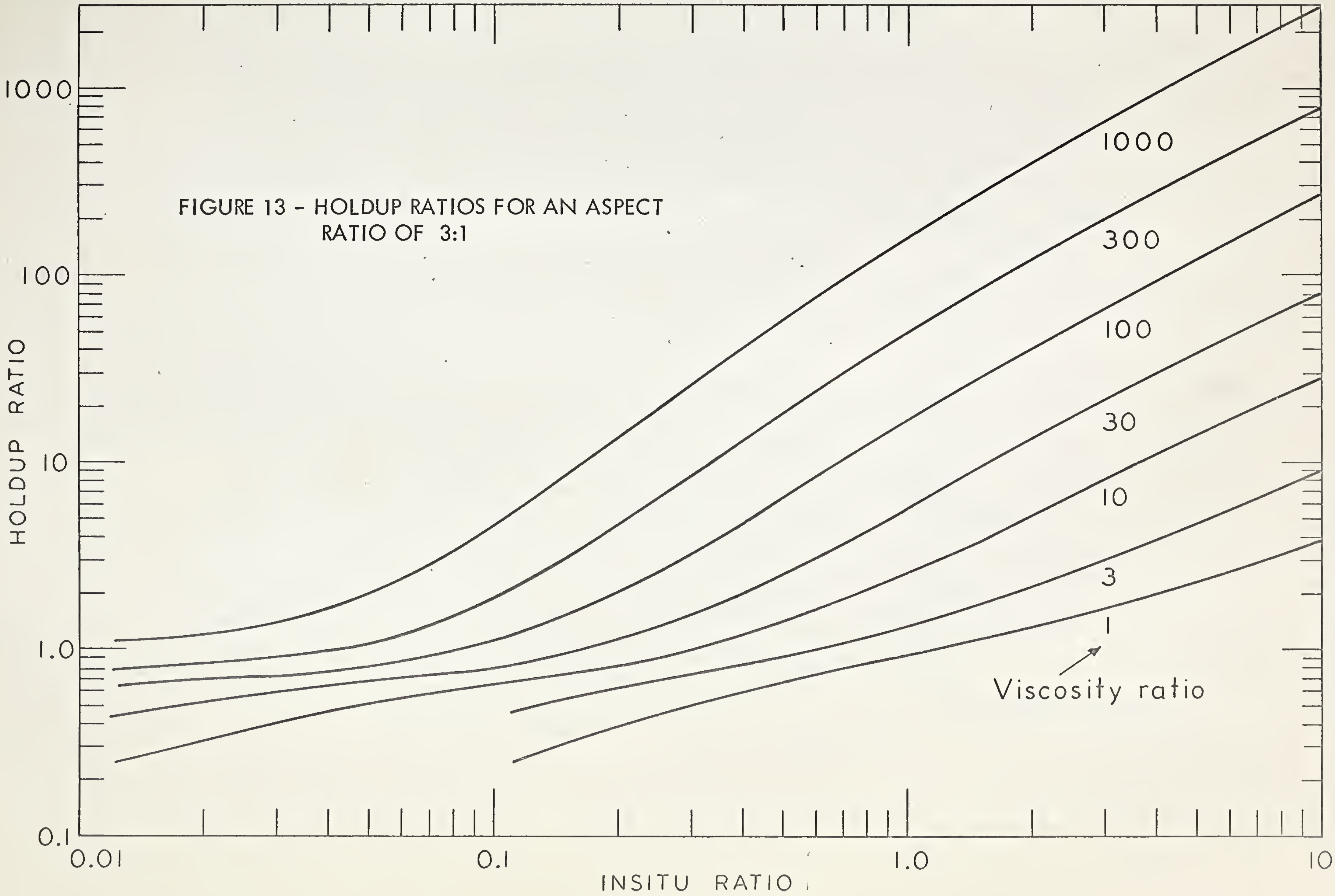
FIGURE 13 - HOLDUP RATIOS FOR AN ASPECT RATIO OF 3:1

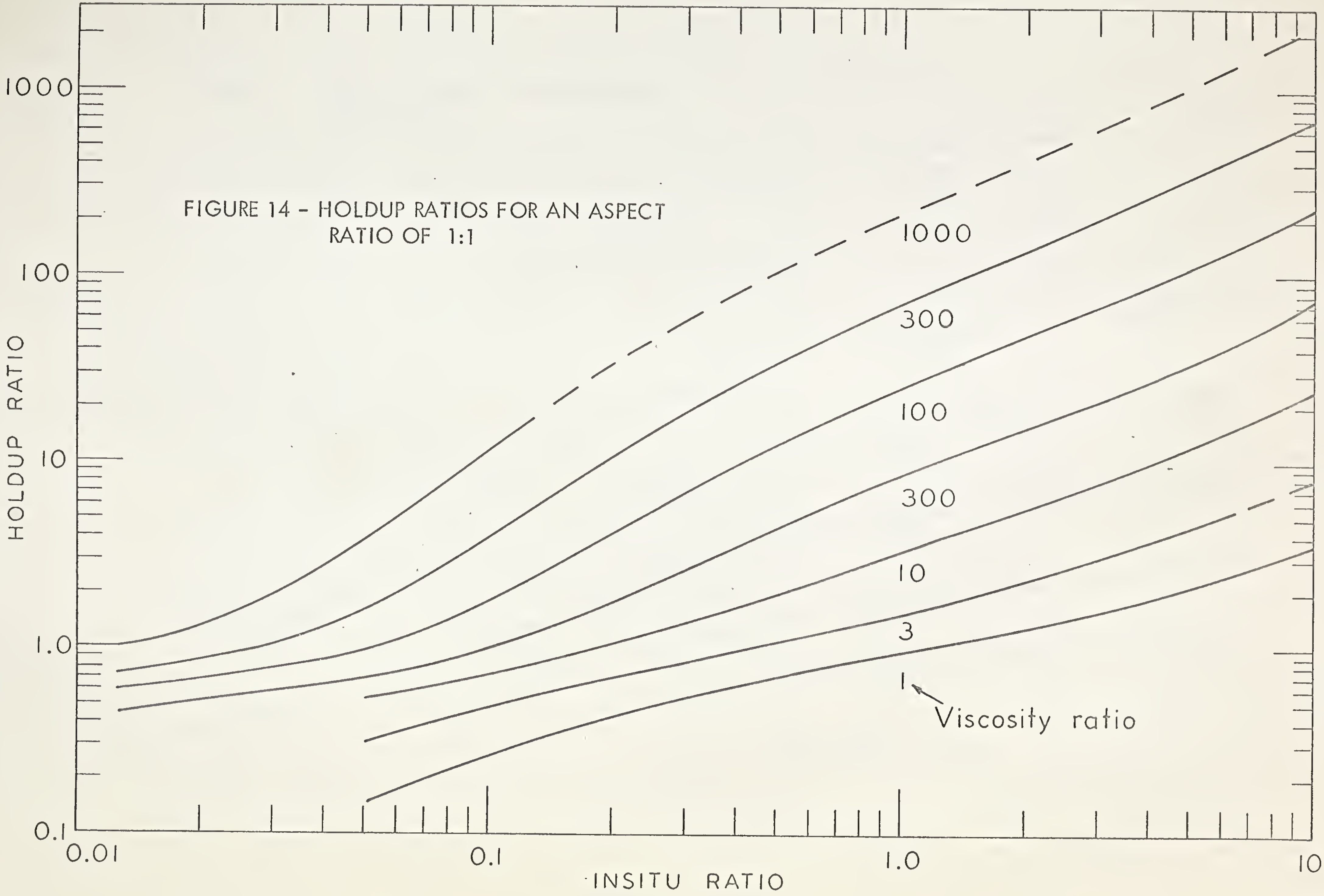

FIGURE 14 - HOLDUP RATIOS FOR AN ASPECT RATIO OF 1:1

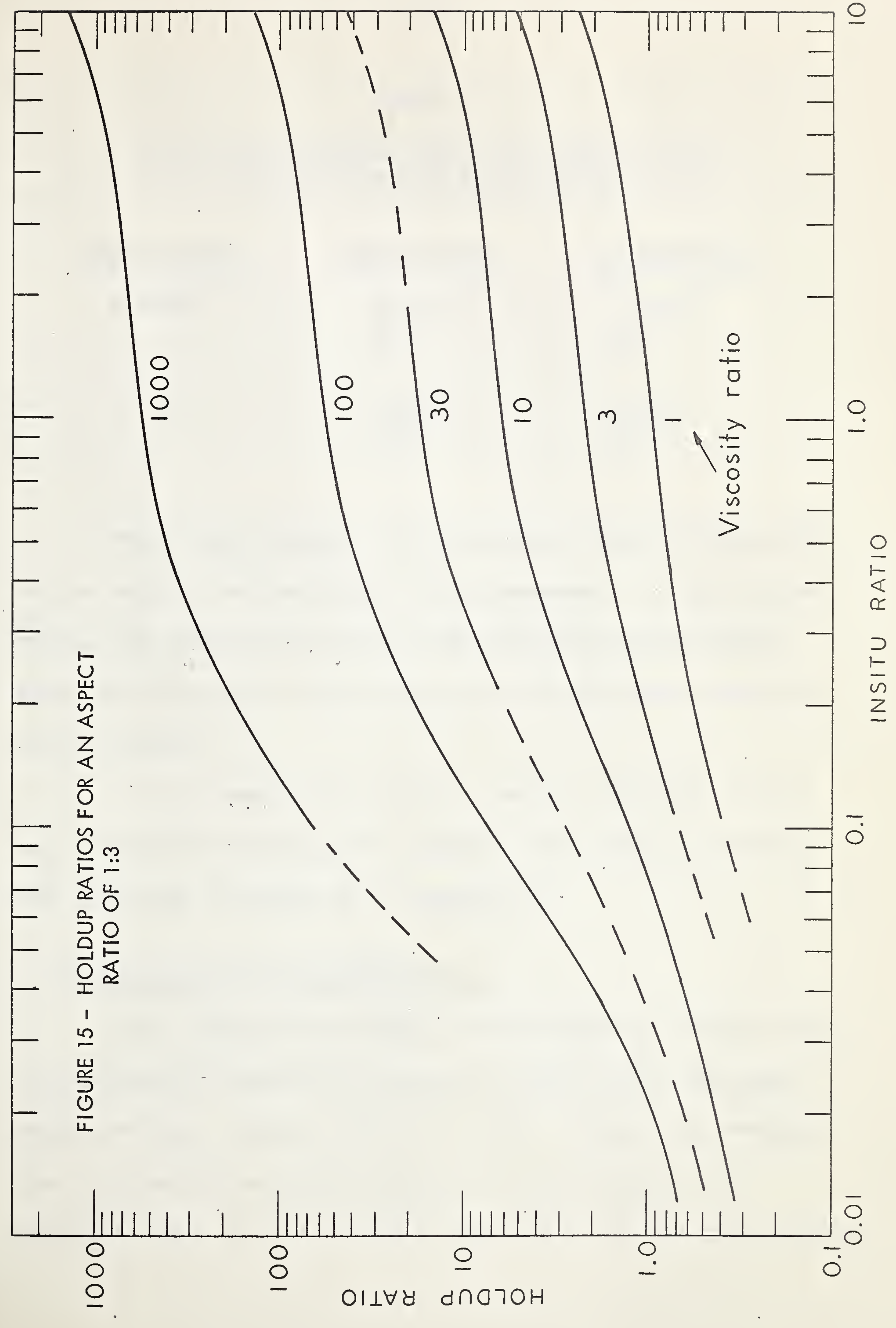

FIGURE 15 - HOLDUP RATIOS FOR AN ASPECT RATIO OF 1:3

TABLE I

Variation of Holdup Ratio with Aspect Ratio for a Viscosity Ratio of 100

Aspect Ratio	Insitu Ratio	Holdup Ratio
7.896:1	0.30	3.20
	10.0	300
1:3	0.30	29.0
	10.0	115

The trend reflects the increasing effect of the sides of the conduit as the aspect ratio decreases. At low insitu ratios the sides tend to hold back the more viscous phase, while at high insitu ratios they tend to hold back the less viscous phase.

All the numerical pressure gradient reduction factor and holdup ratio data used to prepare the foregoing figures are tabulated in Table A2 of Appendix A.

4. Analogues of stratified flow

Other physical processes are governed by the same form of differential equation as governs steady fully developed unidirectional, laminar flow of a fluid. Thus, for example, the differential equations for the stress distribution resulting from the torsion of a long solid bar and the tempera-

ture distribution created by uniform heat generation within a long bar have the same form as equation (9). The latter example is of more interest in chemical engineering and will be considered in some detail.

If heat is generated uniformly in a long solid bar of constant cross-sectional area by, for instance, ionizing radiation at the rate of q BTU/unit volume/unit time then the differential equation governing the steady state temperature distribution is

$$\frac{\partial^2 T}{\partial x^2} + \frac{\partial^2 T}{\partial y^2} = \frac{1}{k} q \qquad (76)$$

where T is temperature and k is the thermal conductivity. Consequently the thermal conductivity and rate of heat generation are equivalent to viscosity and pressure gradient respectively.

Consider, now, a long composite bar of rectangular cross section consisting of two materials of different thermal conductivity joined together such that no temperature difference exists across the interface and no heat is generated or removed in the interface itself. If the outside of the bar is maintained at some reference temperature then the solution of the differential equation (76) is identical in form to the solution of the laminar, stratified flow problem.

The velocity profiles already presented are, therefore, representative of the corresponding temperature profiles of the analogue. Further, the pressure gradient reduction factor is representative of the ratio of the amount of heat stored in the material having the higher thermal conductivity in the composite bar to the amount which would be stored in a bar having the same outside dimensions as the composite bar but composed only of the material having the higher thermal conductivity. Finally, the holdup ratio is representative of a ratio which would indicate which part of the bar contained the more heat, provided, of course, the specific heats of the two materials were the same.

III EQUIPMENT

Equipment was designed and constructed so that two immiscible liquids could be pumped simultaneously through a rectangular conduit of large aspect ratio. In this section the selection of the fluids and the design of the rectangular conduit and auxiliary equipment will be discussed. The arrangement of the experimental equipment is illustrated diagrammatically in Figure 16.

A. FLUIDS

The liquids were selected with the following three factors in mind:

(1) the liquids should have a sufficient viscosity differential for the laminar-turbulent regime to cover wide ranges of individual flow rates,

(2) the liquids should separate readily under the action of gravity and

(3) both liquids should be colourless so that the interfacial structure would not be obscured.

Water and a refined mineral oil with a viscosity of approximately five centipoise were chosen. The oil was a 5:1 blend of Mentor 29 and Bayol 35, both supplied by Imperial Oil Ltd.

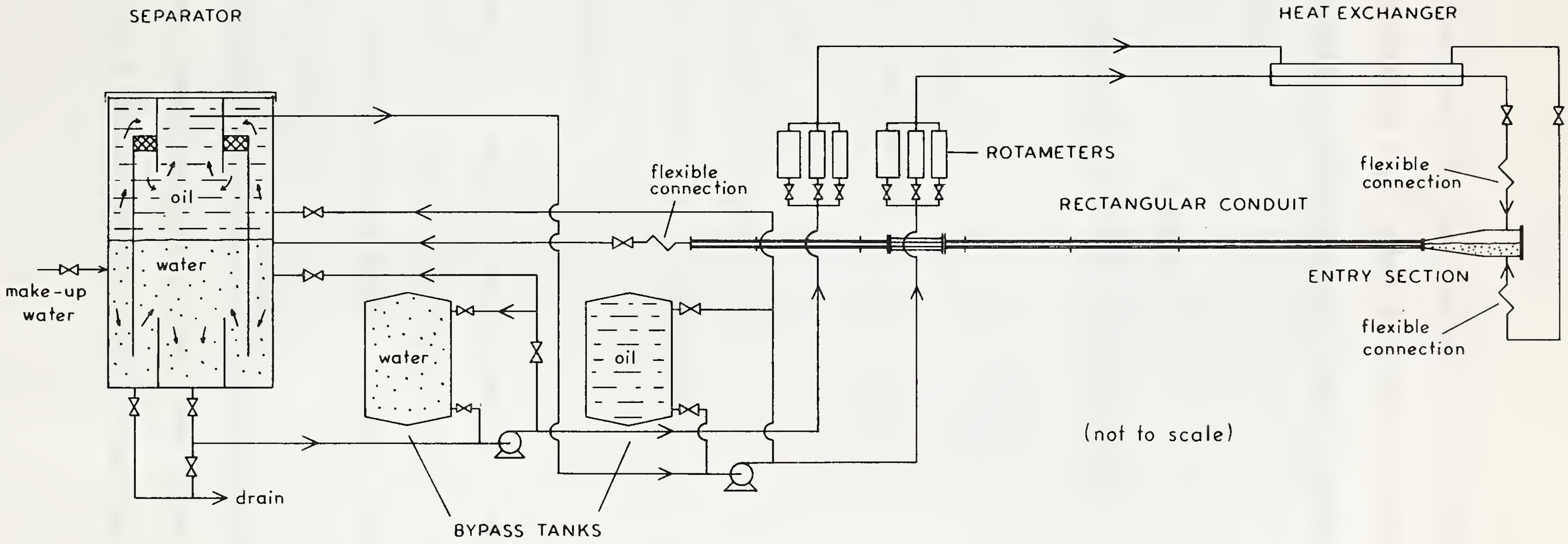

FIGURE 16 - EXPERIMENTAL EQUIPMENT

The physical properties of the liquids at the average temperature of the experiments are given in Table II and an account of their determination and variation with temperature is given in Appendix B.

Table II

Physical Properties of Liquids

	Oil	Water
Specific gravity	0.818	0.997
Viscosity (centipoise)	4.82	0.905

Density ratio = 0.821

Viscosity ratio = 5.326

Interfacial tension = 42 dynes/cm.

B. RECTANGULAR CONDUIT

The rectangular conduit had an overall length, including the entry, calming, test and discharge sections, of 37 feet and a nominal 1-inch by 8-inch cross section. Figure 17 is a photograph of the conduit.

The top and bottom plates of the conduit were 1/2-inch thick transparent Plexiglas plastic and the sides were 3/4-inch thick. Except for a photographic section the top, bottom and

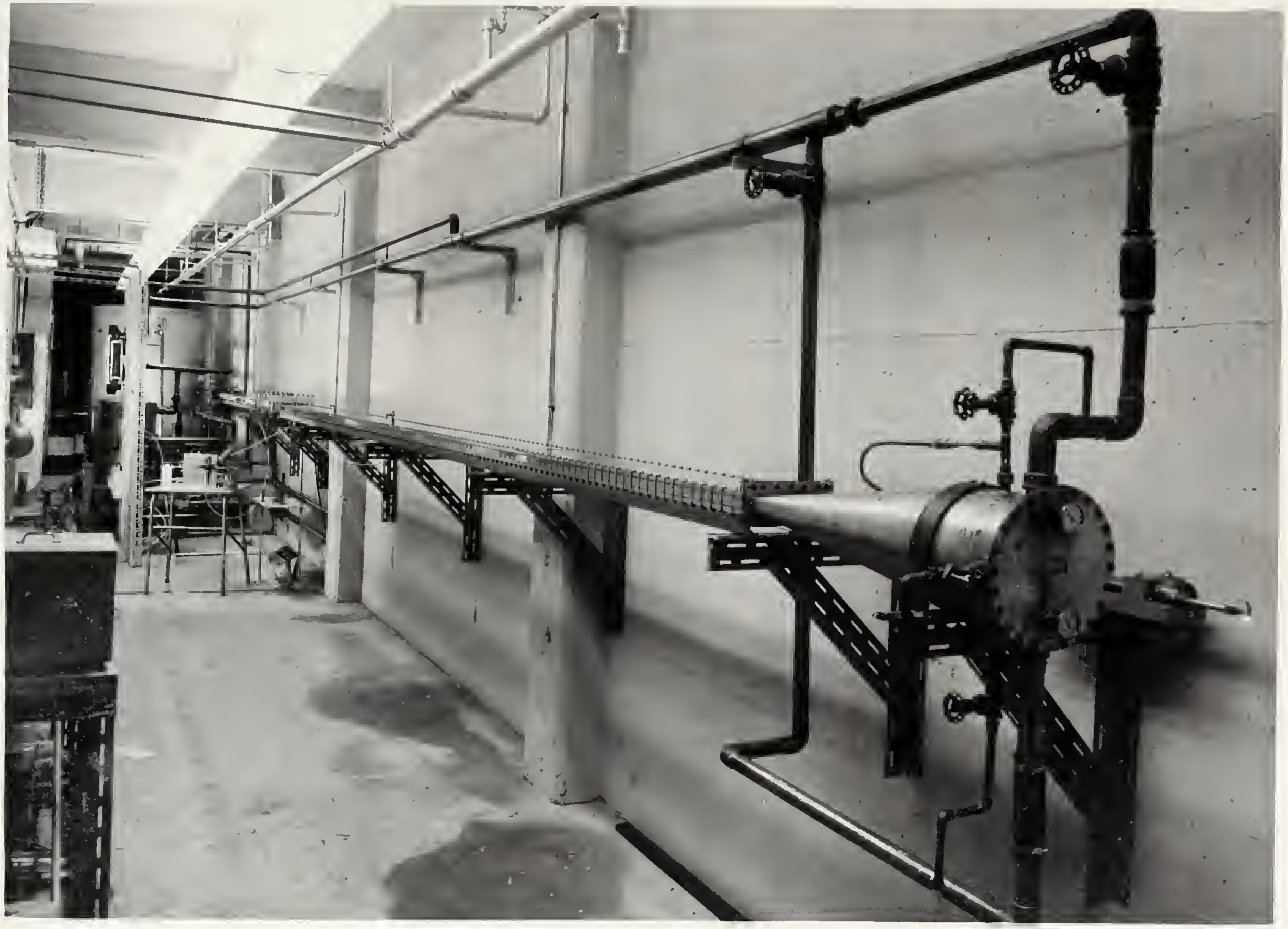

FIGURE 17 - RECTANGULAR CONDUIT

sides of the channel were continuous and formed by joining 6-foot lengths with a cement consisting of plastic chips dissolved in ethylene dichloride. The faces to be joined were milled to a 45° slope to give the joints greater strength. The manner in which the top, bottom and sides of the conduit were assembled together is shown in Figure 18. The 1/4-inch diameter bolts were spaced every two inches along the entire length of the conduit and electrical insulation tape was a satisfactory gasket material.

The conduit, except for the photographic section, rested freely upon two 2-inch x 1-inch channel iron runners which were bolted to supports attached rigidly to the wall. The conduit was thus free to expand and contract under the influence of changes in ambient temperature since all connections to the conduit contained flexible linkages. The conduit was levelled to within 0.02 inches over its entire length and was completely free from external vibrations.

The sheet metal entry section was designed to bring the two phases into contact across a horizontal interface with as little turbulence as possible and was similar to the one used by Gazley(36) to introduce air and water to a circular pipe. The section is illustrated in Figure 19 and was found to be completely satisfactory over the entire range of input

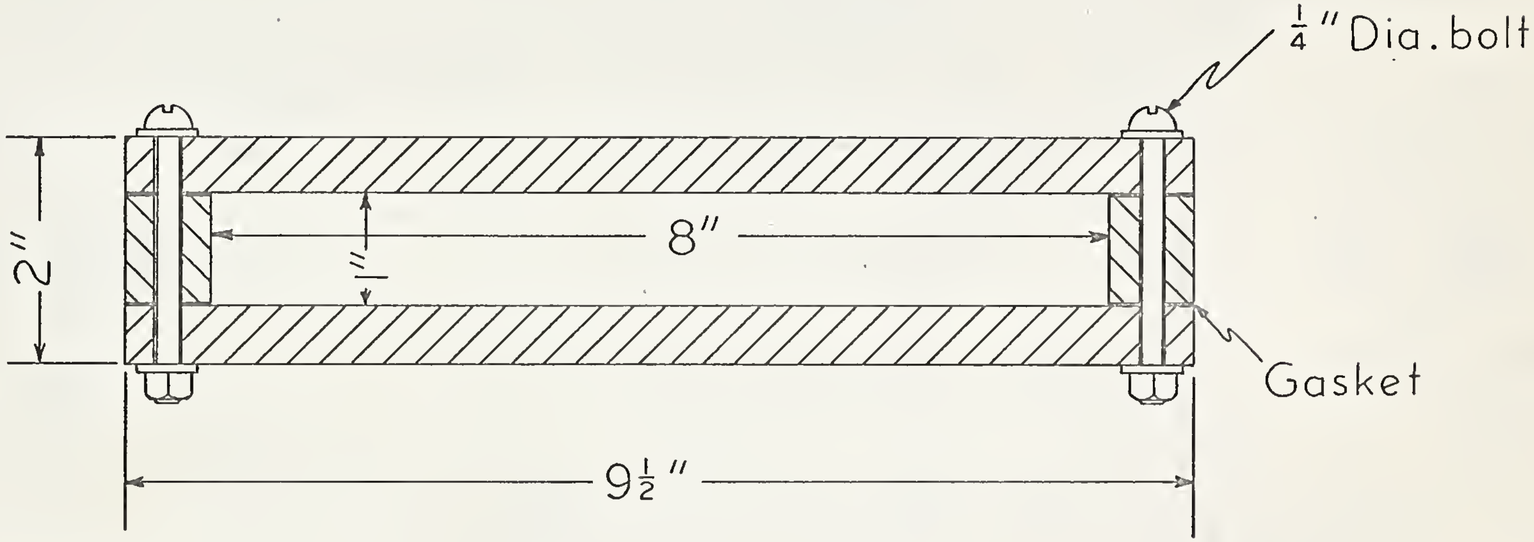

Approx. scale: half full size

FIGURE 18 – CROSS SECTION THROUGH RECTANGULAR CONDUIT

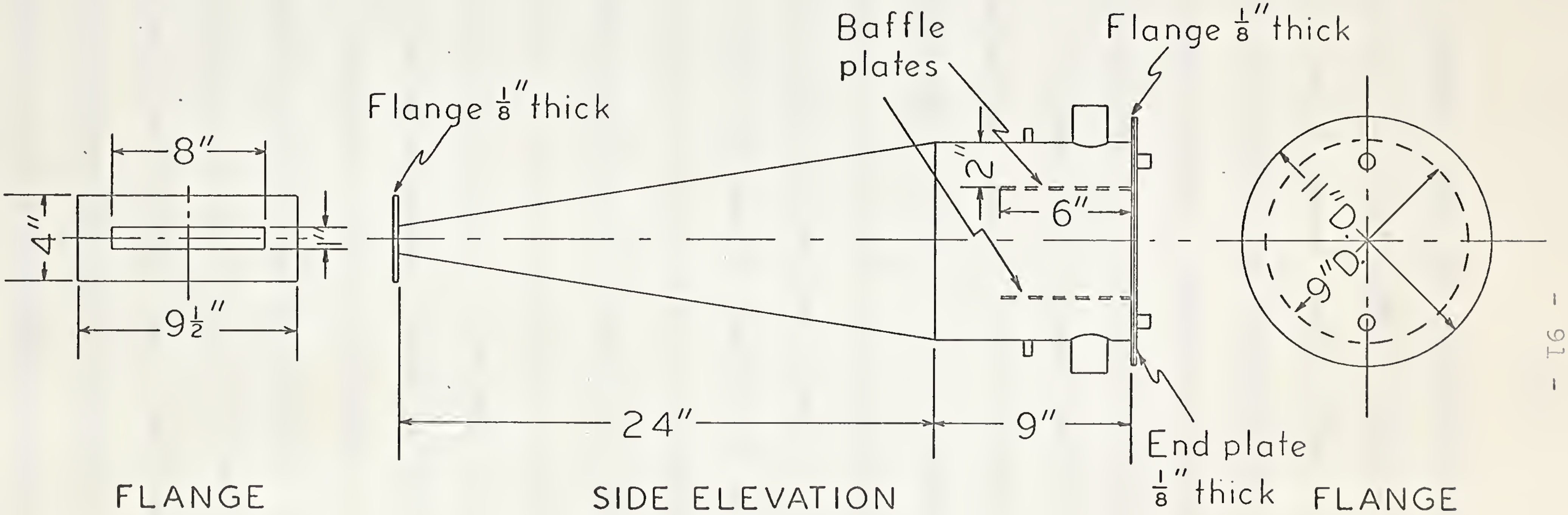
Baffle plates
Flange $\frac{1}{8}''$ thick
Flange $\frac{1}{8}''$ thick
8″
4″
1″
9½″
2″
6″
11″D.
9″D.
24″
9″
End plate $\frac{1}{8}''$ thick
FLANGE
SIDE ELEVATION
FLANGE

Material: 20 gauge galvanized iron
Approx. scale : 1 cm. = 3 inches

FIGURE 19 - ENTRY SECTION

water-oil ratios. The two liquids entered the section at the top and bottom of a horizontal cylinder which was 9 inches in diameter and 9 inches long. Interior baffle plates prevented the phases from impinging directly upon each other. The circular cross section gradually changed to the rectangular cross-section over a distance of two feet. A removable, circular end plate held in position by twenty four 1/4-inch bolts enabled the section to be cleaned periodically. Dial thermometers were inserted through openings in this end plate and, therefore, indicated the temperatures of both phases at the inlet to the rectangular conduit. The entry section was joined to the rectangular conduit by a flange containing fourteen 1/4-inch bolts and was provided with a vent and drain.

The calming section was 12.5 feet or 84 equivalent diameters long. This length was considered to be sufficient for the velocity profile to become fully developed after a study of the experimental results obtained by Eckert and Irvine(26) who measured local pressure gradients along both a rectangular and triangular conduit. The rectangular conduit had an aspect ratio of 3:1 and pressure gradients were measured with both abrupt and rounded entrance sections. With the abrupt entrance pressure gradients measured for the flow of air alone in the rectangular conduit at Reynolds numbers

ranging from 300 to 11,600 indicated that the calming length amounted to no more than 40 equivalent diameters. With the rounded entrance pressure gradients measured for Reynolds numbers ranging from 6,000 to 10,000 indicated that the calming length was no greater than 70 equivalent diameters. Since the entry section used in the present study could be considered intermediate between the abrupt and rounded entrances used by Eckert and Irvine, 84 equivalent diameters were judged to be entirely sufficient for the establishment of fully developed flow.

The test section was 20 feet or 135 equivalent diameters long and the discharge section was 2 feet or 13.5 equivalent diameters long. Pressure taps, formed by drilling 1/16-inch diameter holes through the bottom plate along the centre line of the conduit, were situated every five feet along the test section.

The 18-inch photographic section was carefully constructed so that its internal dimensions matched those of the parts of the conduit to which it was joined to within 0.001 inches. It was necessary to have a removable photographic section so that it could be readily cleaned. To ensure dimensional stability the top and bottom plates of the photographic section were made from 1-inch thick plastic. Flanged connections

each with twelve 1/4-inch diameter bolts and locating pins, joined the removable section to the upstream and downstream portions of the conduit. A photograph of the removable section in position is shown in the upper part of Figure 20.

C. AUXILLIARY EQUIPMENT

Previous experimental studies (79,12) of the pipeline flow of oil-water systems involved a separation procedure requiring intermittent operation. In the present study more convenient continuous operation was achieved by using a combined storage and separator tank. The two phases were withdrawn individually from the separator by positive displacement pumps and rotameters indicated the flow of the two phases to the test section. The unwanted portions of the total pump discharges were either returned to the separator tank or circulated through bypass tanks. Upon leaving the rotameters the liquids passed through a concentric tube heat exchanger, which promoted thermal equilibrium between them, and subsequently were admitted to the rectangular conduit. After flowing through the conduit the oil and water discharged tangentially into the separator where they settled under the action of gravity to form two distinct layers. Copper pipe was used throughout so that corrosion would be kept to a minimum. Figure 16 shows

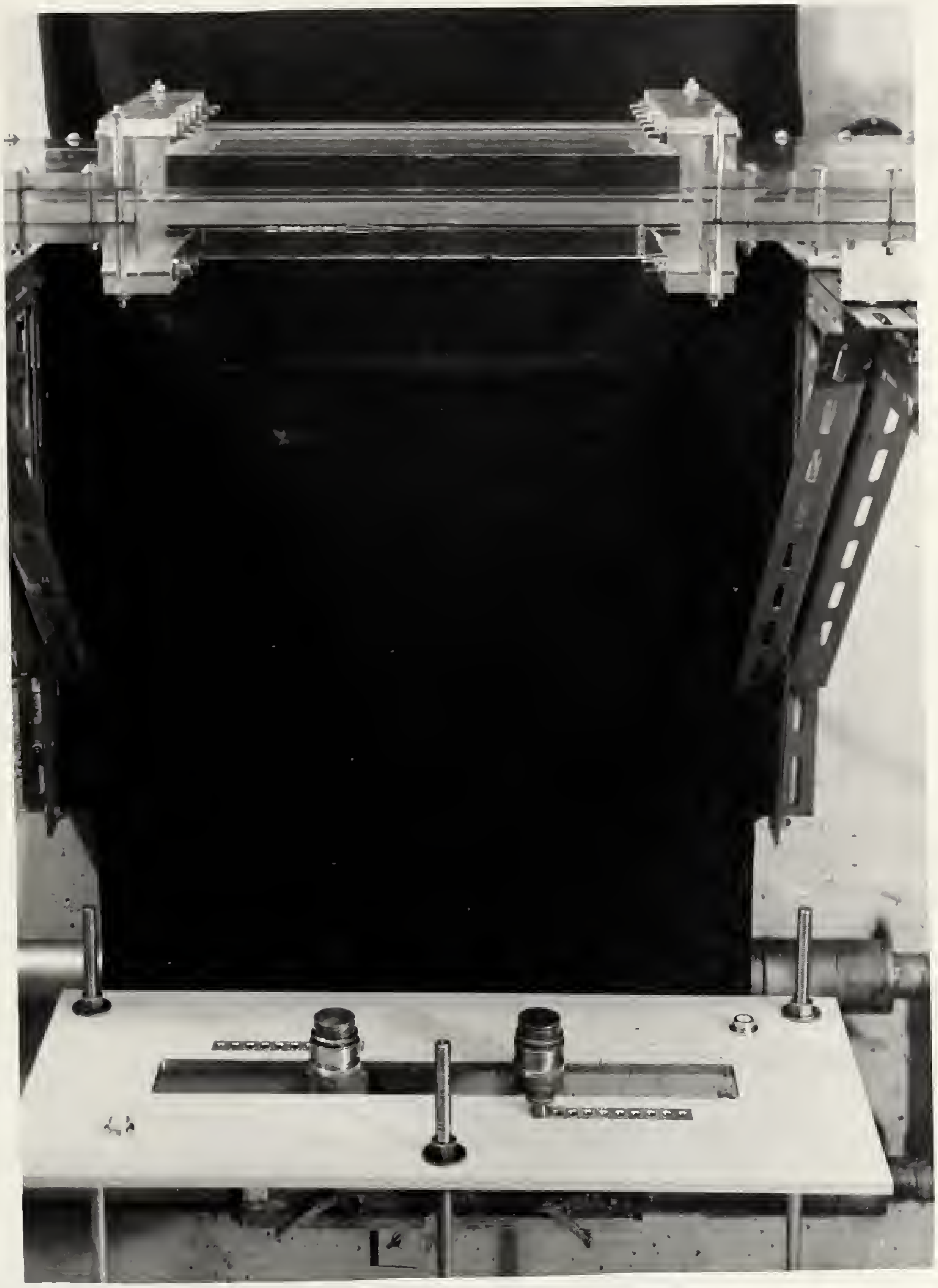

FIGURE 20 - PHOTOGRAPHIC SECTION AND CAMERAS

the relative positions of the different items of the equipment.

The separator consisted of a 52-inch diameter, 75-inch high cylindrical tank with a flat bottom and removable cover. The inside of the tank was baffled in order to aid the separation process. A sectional elevation and a plan view of the separator are given in Figure 21. The baffles were cylindrical, the outer one being 42 inches in diameter and 52 inches high and the inner ones being 27 inches in diameter and 26 inches high. The two-phase mixture entered the separator tangentially at the mid-point of the vertical side through a 3-inch diameter line. The tangential entry minimized the turbulence and consequent emulsion formation which would have resulted had the entry been normal to the periphery of the tank. The separation of the oil and water took place in the annular space between the outer baffle and the tank wall. The oil then overflowed, and the water underflowed, the outer baffle into the relatively undisturbed region inside the outer baffle. It was found that the oil tended to carry minute droplets of water over the outer baffle and these were removed by a bed of coarse sodium chloride supported on a perforated tray between the outer and inner baffles.

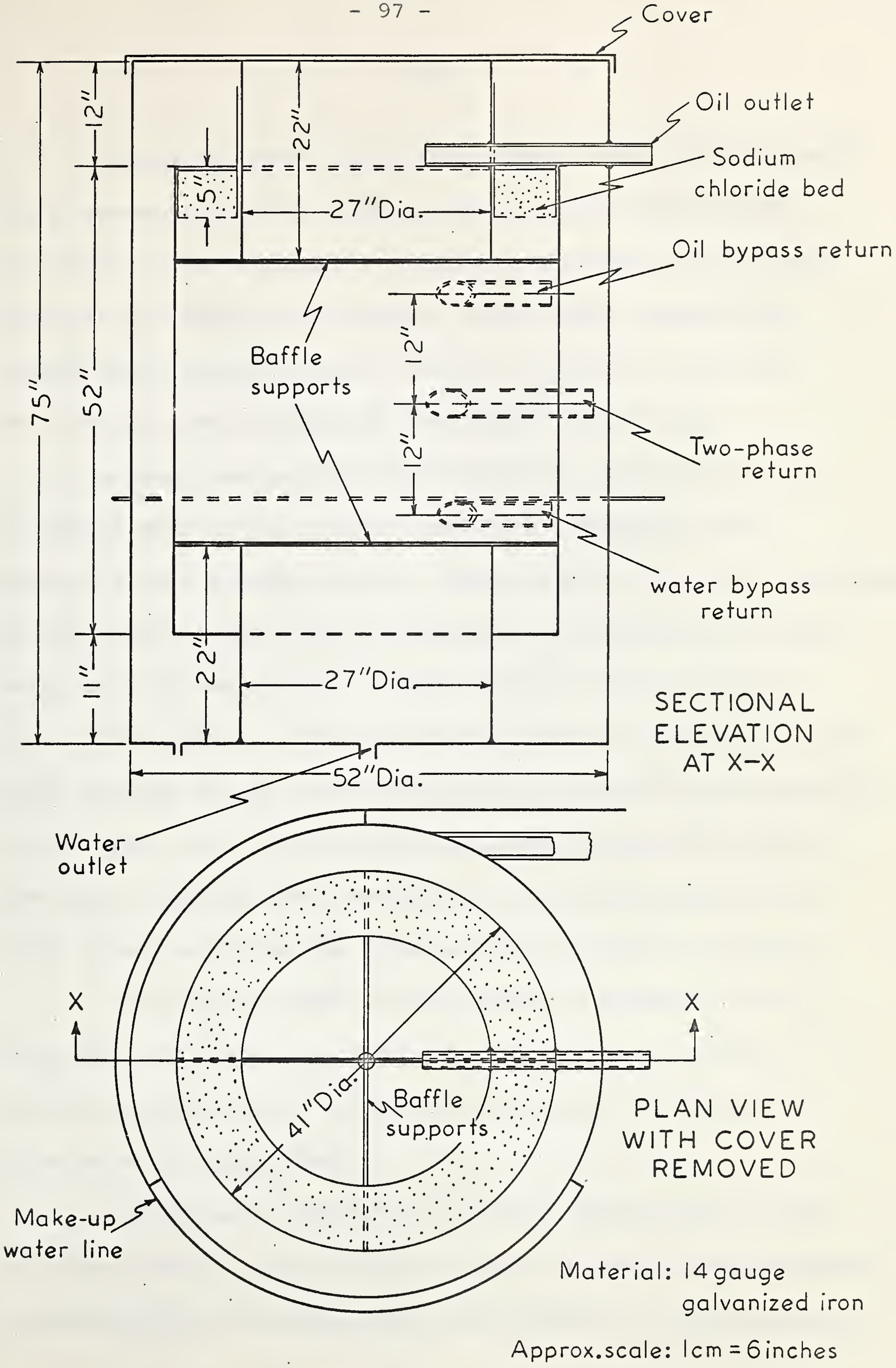

FIGURE 21 - OIL-WATER SEPARATOR

Inside the outer baffle the phases first flowed towards their common interface and then subsequently away from the interface to the respective outlets - the outlet for the oil being at the centre of the upper inner baffle, about five inches below the oil surface and the outlet for the water being at the centre point of the bottom of the tank.

Bypass flows entered the separator tank tangentially, 12 inches above and 12 inches below the two-phase entry, through 2-inch diameter lines. These bypass lines were positioned so that both liquids could be completely circulated to ensure uniformity of temperature without passing them through the rectangular conduit. Fresh make-up water was admitted through three equally spaced 1/2-inch diameter openings on the periphery of the tank. Dial thermometers inserted through the side of the tank indicated the temperatures of the two phases and a sight glass indicated the level of the oil-water interface.

The separator tank was manufactured completely from 14 gauge galvanised iron sheet, contained about 300 U.S. gallons of each phase, and was positioned on a wooden platform about 18 inches high.

A sheet metal adapter was used to convert the 1-inch x 8-inch conduit cross-section into the 3-inch diameter circular cross-section of the pipe which ran directly to the separator.

This pipe contained a 3-inch A.C.F. ball valve. This valve, when fully open, provided a smooth passage for the oil and water leaving the conduit. A valve of the gate or globe type would have created turbulence tending to emulsify the oil and water together.

Two bypass tanks, one for each phase, were installed to allow the unwanted portions of the total flow from each pump to be circulated without returning the flows to the separator. High bypass flows returned directly to the separator tended to hinder the separation process. The tanks were identical with capacities of approximately 50 U.S. gallons and had cylindrical bodies, 35 inches high and 22 inches diameter, and ends coned outwards. Tanks with substantial capacities, rather than just pipe connections, were installed so that the rise in temperature of the liquids on continued recirculation through the pumps would be kept to a minimum.

Both pumps were of the positive displacement gear type. The oil pump, model K30 manufactured by G.D. Roper Corporation, had a capacity of 36 U.S. gallons per minute at 1750 R.P.M. and the water pump, model FL manufactured by Jabsco Pump Co., had a capacity of 30 U.S. gallons per minute at 1750 R.P.M. Both pumps were driven by 3-phase, two-horse power electric motors running at 1750 R.P.M.

Rotameter type flow meters had been found to be entirely satisfactory in previous investigations(79,12) and similar instruments were used in the present study. Oil flow rates in the range 0.3 to 36 U.S. gallons per minute were covered by three rotameters in which the floats were of the sharp edged type to provide immunity to slight viscosity variations. Water flow rates from 0.3 to 30 U.S. gallons per minute were also covered by three rotameters. Since the temperature coefficient for the viscosity of water is relatively small, sharp edged floats were not used in the water rotameters and consequently use could be made of smaller sized rotameters. Details of the rotameters and their calibration are given in Appendix C.

IV EXPERIMENTAL TECHNIQUES AND PROCEDURE

The independent variables in the experimental investigation were the flow rates of the two phases which were indicated by the rotameters described in the previous section and Appendix C. For a given combination of flow rates the input water-oil volume ratio was, of course, also fixed. Under each set of input conditions it was desired to determine the following dependent variables

(1) the flow condition, i.e. laminar, transitional or turbulent in each phase,
(2) the insitu water-oil volume ratio,
(3) the pressure gradient,
(4) local velocities, and
(5) wave velocity, wavelength and wave amplitude for conditions under which interfacial waves were present.

A. TECHNIQUES

1. Flow conditions

Flow conditions were determined by injecting soluble dyes into the flowing fluids by means of extremely small

diameter hypodermic needles inserted through the top and bottom of the conduit at the upstream end of the photographic section. Under laminar conditions the dye filaments retained their identity, while in turbulent flow the eddies caused the filaments to break up and the dye diffuse throughout the fluid. In general, the dye traces were observed visually although a few representative traces were recorded photographically.

2. Insitu ratios

Insitu ratios were determined from measurements of the depth of the oil phase. Relatively large oil depths were measured with the aid of a scale, which was read to 0.005 inches, attached to the outside of the conduit. Small depths were recorded by means of a pointer gauge which consisted of a hypodermic needle attached to the shaft of a micrometer. The micrometer was adjusted until the tip of the needle just touched the interface and was read to 0.001 inches.

For conditions when no waves were present at the interface, or waves of very small amplitude, it was possible to obtain the oil depth under flowing conditions. However, when pronounced waves were present, the oil depth was recorded immediately after the flows of both phases were stopped simul-

taneously and the A.C.F. valve between the test section and the separator closed. In this way the oil depth was measured after the waves had disappeared but before any imperfections in the levelling of the conduit caused the level of the interface to change.

3. Pressure gradients

Pressure drops in earlier studies(79,12) of the horizontal pipeline flow of oil-water mixtures were measured by means of a manometer system in which the pressure in the pipeline was transmitted to the manometer by air adjusted to the correct pressure by pressure reduction valves. Such a system prevented oil-water mixture being present in the manometer lines, which would have caused erroneous results. The method was, however, cumbersome in operation since it required an operator to be present at each pressure tap.

Since the present study was restricted to an investigation of stratified flow it was not necessary to adopt the method used previously. Pressure taps located in the bottom of the conduit allowed water to be used as the fluid transmitting pressure to the manometers with no danger of the oil entering the manometer lines.

Pressure drops over the 20-foot test section ranged from about 0.1 inches of water at low flow rates to about 4 inches of water at high flow rates. Pressure drops up to about one inch of water were measured by the use of a specially constructed micromanometer, while greater pressure drops were measured by means of an inclined manometer.

Single phase pressure drops were recorded by the use of the micromanometer and inclined manometer in the case of the flow of water, and by the use of an inclined manometer only in the case of the flow of oil.

The micromanometer is shown diagrammatically in Figure 22 and was based on an instrument marketed by Flow Corporation, Massachusetts, which was designed to measure pressure drops in gas flow. The design was modified so that it could be used as a two-liquid manometer - the liquids being carbon tetrachloride and water. The instrument consisted basically of a U-tube, one side of which was a 4-inch diameter reservoir and the other a 4mm-diameter glass tube inclined at 30° to the horizontal. A flexible, 1mm inside diameter, polyethylene tube joined the reservoir to the inclined tube, which itself was held in a brass slide raised and lowered by adjustment of the micrometer.

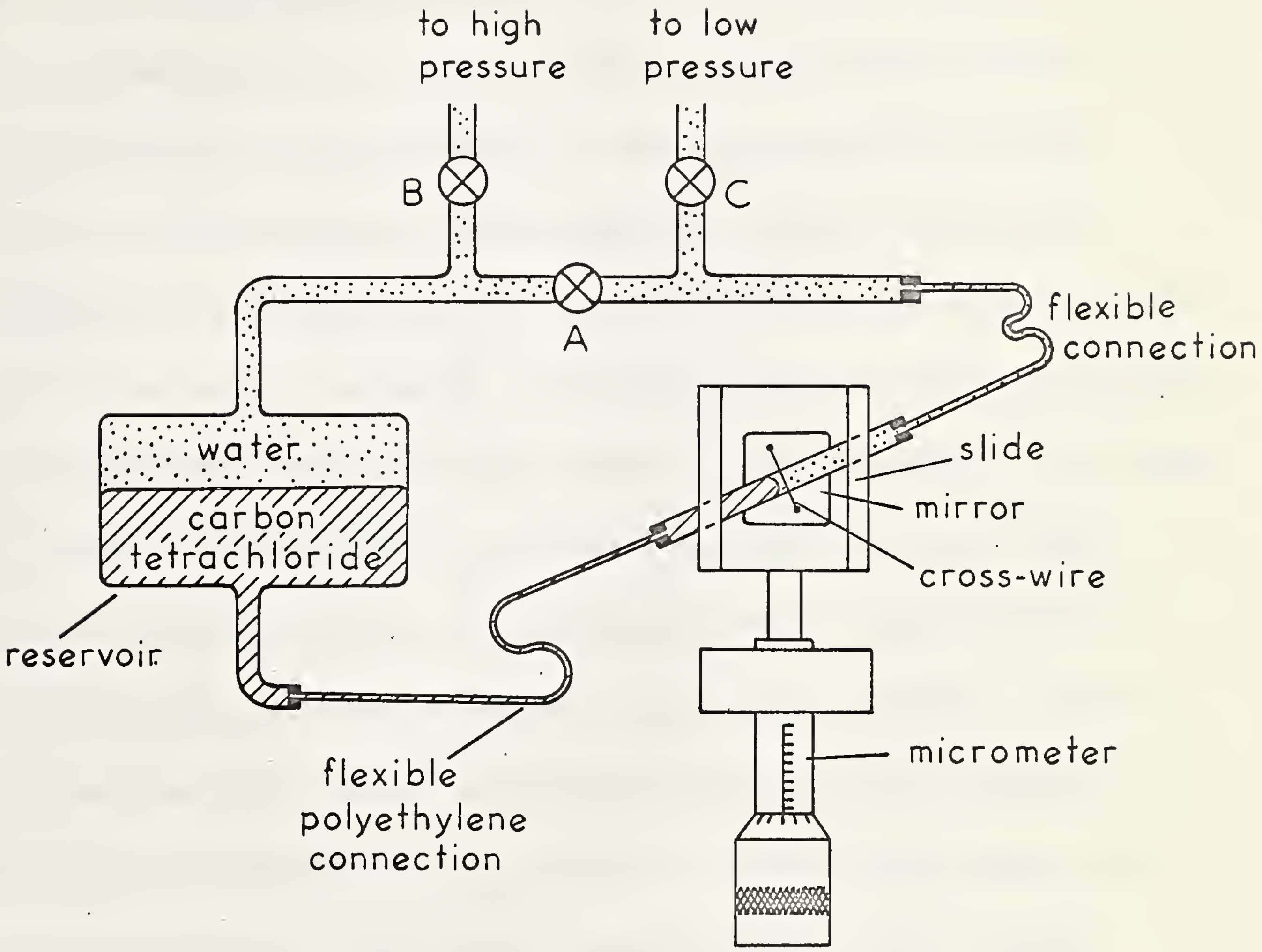

FIGURE 22 - MICROMANOMETER

Pressure drops were obtained in the following manner. Initially, a "zero" reading was obtained by adjusting the micrometer so that the meniscus in the inclined tube just touched the cross-wire with tap A open and taps B and C closed. Subsequently, with tap A closed and taps B and C open the meniscus was returned to the cross-wire by again adjusting the micrometer. The pressure drop was therefore represented by a column of fluid having a density equal to the density differential between the carbon tetrachloride and water, and a height equal to the difference of the micrometer readings.

Since the meniscus was always returned to the same position in the inclined tube no errors were introduced by local variations in tube diameter. The only possible error arose from the very small change in volume of the flexible tube joining the reservoir with the inclined tube during the vertical movement of the tube. However, the large cross-sectional area of the reservoir caused any variation in the volume of the flexible tube to be entirely negligible. The micromanometer was found to be sensitive to a change in pressure corresponding to 0.001 inches of water.

The successful operation of the instrument depended primarily on the inside of the inclined tube being perfectly

clean, otherwise the meniscus would not move freely and erroneous readings were obtained.

Pressure drops were also obtained with the micromanometer modified to the form of a water-air inverted manometer. Although somewhat less sensitive, this arrangement was found to be less troublesome in operation than the two-liquid arrangement.

The inclined manometer used for measuring pressure drops in excess of one inch of water was of the inverted form and had a 1 in 4 slope. Air separated the liquid in the two legs of the manometer. In experiments with water flowing alone and with the two-phase system water was admitted to the manometer from the test section, while in experiments with oil flowing alone oil was admitted to the manometer.

The pressure transmission lines consisted of semi-transparent, flexible polyethylene tubing. Such tubing readily allowed any air bubbles to be observed and removed. Polyethylene tubing was found to be preferable to vinyl tubing, supplied by Fisher Scientific Co., the position of which was found to affect the pressure differential indicated by the oil-air manometer. The cause of this interaction between the vinyl tubing and the oil was not determined.

4. Local Velocities

Plans were originally made to determine the complete velocity profile on the vertical centre line of the conduit. For laminar conditions in both phases the experimental velocity profiles could then be compared with profiles similar to those shown in Figure 3. With one, or both, of the phases in turbulent flow the experimental measurements would yield information concerning the nature of the interaction between the phases. The use of pitot tubes was rejected on the basis that the velocity heads under laminar conditions would be of the order of 0.01 inches of water and therefore too small to be measured accurately without extremely elaborate pressure measuring equipment. A flow visualization technique appeared, therefore, to be most suitable.

Flow visualization techniques have been discussed by Hyzer(45) and Hinze(42). Measurement of the velocity of particles carried in a flowing fluid to determine velocity profiles has been used by Van Driest(90), who was concerned with turbulent diffusion in open channels, Gaffyn and Underwood(33), who were interested in velocity profiles for liquid flow in pipes, and Nedderman(71) who measured velocities in the wall region for turbulent liquid flow in pipes. All these investigators used particles which did not drift signi-

ficantly under the action of gravity, i.e. the particle and fluid densities were either equal or the particle was so small that its drift velocity was negligible.

In the present investigation it was proposed to use a modified flow visualization method in which a small air bubble, injected through the bottom of the conduit, would rise through the flowing liquids under the action of gravity. At the same time, however, the bubble would be carried horizontally by the moving fluid. Stroboscopic illumination of the air bubble would allow the complete trajectory of the bubble, viewed from the side of the conduit, to be recorded on a single sheet of photographic film. Subsequent analysis of the trajectory would yield information concerning the local horizontal velocity at each vertical elevation.

A theoretical prediction of the trajectory of a small air bubble having a diameter of 0.5 mm rising through a parabolic velocity field indicated that inertia effects of the bubble and its associated fluid would be negligible for liquids having viscosities in excess of about 5 centipoise. On the other hand, the inertia effect for the bubble rising through water would not be insignificant. The theoretical analysis and the predicted bubble velocities are presented in Appendix D.

In addition to the doubt raised about the suitability of the method by the theoretical analysis experimental difficulties were experienced in obtaining suitable photographs. While reasonably good photographs were obtained with an air bubble rising through a clear single phase, it was found that in the two-phase system the two liquids contaminated each other slightly and neither was perfectly clear. Consequently the definition of the photographic image was extremely poor. Further, in the two phase system, the air bubble was found to be held at the interface by interfacial tension, thus preventing the photographing of the trajectory within the upper phase.

It was concluded that the method would be very suitable for single phase flow of a liquid with a viscosity greater than about 5 centipoise but as far as the present project was concerned the method was felt to be unsuitable.

Velocity measurements were, therefore, restricted to measurements of the interface velocity. Very fine aluminium powder, supplied by Fisher Scientific Co., was introduced through the top of the conduit and allowed to settle to the interface. Measurement of the time required for the powder to travel a known distance enabled the interface velocity to be calculated. These rather limited velocity measurements did, however, present a very clear picture of the nature of the

interaction between the phases and they could, of course, be compared with the theoretical values when both phases were in laminar flow.

5. Wave Characteristics

Wave velocities were obtained simply by timing the movement of a particular wave over a distance of three feet. Measurements of wavelength and amplitude were not so easily performed.

Several experimental investigations have been reported in which film thicknesses or wave profiles were measured. Amongst these, Bunt(9) measured film thickness using fluorescence, Dukler and Bergelin(23) used a capacitometer in conjunction with an oscillograph to determine wave forms on liquids flowing down inclined plates and Lilleleht and Hanratty(58) used a light absorption technique to determine wave profiles at the interface for the co-current flow of air and water in a rectangular conduit. The use of stereophotogrammetry in contouring ocean waves has been discussed by Schumacher(82) and Brobikov(8).

It was decided to investigate the use of stereophotogrammetry to obtain wavelengths and amplitudes on the relatively small laboratory scale. The method has the advantage that

no probes of any kind interfere with the flow of the fluids and the disadvantage that only a relatively small part of the interface can be analysed. The only requirement of the method is that the interface must be visible to the cameras.

The two cameras were identical small field cameras manufactured by Instruments Ltd., Ottawa. The focal lengths of the lenses were 112 mm and in order that the cameras could be focused on the interface special brass adapters were manufactured to extend the lens to photographic plate distance. The holders took either 3 $^1/4$-inch x 4$^1/4$-inch sheet film or glass plates. Fiducial marks within the cameras appeared on the exposed film.

The cameras were arranged as shown in Figure 20 so that photographs could be taken from beneath the conduit. They were rigidly attached to a 1/2-inch thick brass plate by means of 90° brackets and thumb screws, so that the photographic planes were parallel to the plate. The horizontal distance between the cameras could be varied in 1/2-inch intervals. The brass plate was supported by three vertical rods, the upper ends of which were threaded. Nuts on the threaded parts beneath the plate allowed the vertical position of the plate, and hence the cameras, to be adjusted. Initially the plate was approximately levelled using the circular levels

attached to the upper surface of the plate. The final levelling was performed with the aid of a level sensitive to 0.001 inches over a distance of one foot.

The positions of the cameras relative to each other and to the interface are important in that they affect the parallax readings which are used in the calculation of the elevation of different points on the interface. For a given elevation difference, parallax difference is greater when the cameras are further apart and closer to the interface. However, under such conditions the overlapping field of view is relatively small. Consequently it is necessary to compromise accuracy and field of view. In order to obtain an overlapping field of view amounting to about six inches in the direction of flow, the cameras were positioned approximately 27 inches below the conduit and with about 6.5 inches between the optical axes. With this arrangement it was found that only the wavelength and amplitude of waves having relatively large amplitudes could be obtained accurately. Had cameras been available with wider fields of view then a higher degree of accuracy could have been obtained by positioning the cameras further apart and closer to the interface. Nevertheless, valuable information concerning the larger amplitude waves was obtained.

Photographs were obtained on Kodak Tri-X glass plates which are extremely insensitive to ambient temperature and humidity changes$^{(1)}$. Ordinary flexible sheet film was found to be completely inadequate owing to its dimensional instability and to the fact that it would not lie perfectly flat in the holders. The interface was made visible by injecting aluminium powder into the oil phase such that it settled to the interface before reaching the photographic section. Simultaneous photographs were obtained by using an electronic flash with 1/1200 seconds duration and 200 watt-secs power and by having the camera shutters open and the laboratory in otherwise total darkness. The camera aperture setting was f/16.

The stereo pairs of negatives were placed on a light table and viewed under a Wild ST3 mirror stereoscope. Parallax differences were obtained by the use of a parallax bar.

Complete details of the theory of the method and the calibration procedure are given in Appendix E.

B. PROCEDURE

The conduit was periodically cleaned by closing the valves at both ends of the conduit, removing the photographic section and the end plate of the entry section, and pushing absorbant material through the conduit on the end of a 12-foot rod. No detergent was used in the cleaning operation because of the profound effects which the presence of even a very small amount of surface active agent may have on the stability of a fluid-fluid interface.

After replacing the removable section and the end plate on the entry section adjustment of the amount of water in the separator enabled the level of the oil surface in the separator to be positioned approximately five inches above the oil outlet and the level of the oil-water interface to be positioned level with the mid-point of the conduit. This was done in order to provide a sufficient head above the oil outlet so that air would not be withdrawn with the oil and also so that approximately a constant back-pressure would be maintained on the conduit during the experiments.

In the case of single-phase experiments the particular liquid was pumped slowly into the conduit with the A.C.F. valve between the conduit and the separator closed and the

vent on the entry section open. When the conduit was full the vent was closed and the A.C.F. valve opened. The flow rate was then adjusted to the desired value by manipulating the rotameter and bypass valves. Such a procedure prevented the other phase from entering the conduit and adhering to the conduit walls.

A similar procedure was followed in the case of two-phase experiments. Water was pumped into the conduit first, and when the water completely covered the bottom of the conduit oil was pumped in until it made contact with the top of the conduit. The vent was then closed, the A.C.F. valve opened and the flow rates adjusted to the desired valves. A final adjustment was made to the level of the oil-water interface in the separator so that it coincided as nearly as possible with the level of the interface in the conduit.

At start-up the oil and water had approximately the same temperature as the laboratory which was usually very close to 76°F. With continuous circulation of the liquids through the pumps their temperature rose slightly, the temperature of the oil phase being about 0.5°F higher than that of the water phase.

After visual observation and the measurement of the pressure gradient indicated that conditions had become steady, the pressure gradient was recorded over the 20-foot test section, the oil depth was measured at the mid-point of the test section (no evidence of an interfacial gradient was found outside the initial part of the calming section) and the interface velocity in the central region of the conduit was measured by timing the movement of the aluminium dust over an 8-foot length in the downstream half of the test section. When waves were present at the interface their velocity was obtained by timing their movement over a 3-foot section and, in certain cases, stereo-pairs of photographs were made of the interfacial structure.

V RESULTS AND DISCUSSION

A. SINGLE-PHASE FLOW

The rectangular conduit was constructed using a wooden, internal spacer block 8 inches wide and 1 inch deep. Subsequent physical measurements of the width of the conduit gave an average value of 8.01 inches. Direct physical measurements of the exact depth of the conduit could, however, not be made. Although the sides of the conduit were exactly 1 inch deep, the gasket material contributed an unknown amount to the conduit depth. Further, it was found that the top and bottom of the conduit warped slightly, possibly due to stresses caused by the tightening of the bolts or ambient temperature changes. In addition, the depth varied slightly with the internal pressure. On applying the normal operating pressure of approximately three feet of water the top and bottom moved apart by about 0.01 inches. In view of the fact that the depth of the conduit was a very important variable, the pressure gradient being proportional to the cube of the depth in single-phase flow, it was decided to determine the average depth over the twenty-foot test section under operating conditions by measuring pressure drops for the

laminar flow of oil alone since theoretical expressions for single-phase laminar flow in non-circular ducts have been verified by Cornish(17) and Sparrow(83).

Pressure drops were recorded using the inclined manometer for oil Reynolds numbers in the range 1250 to 2300, for which dye injection showed the oil to be in laminar flow, and were reproducible to within 0.5 percent. Two sets of data are given in Table 1F of Appendix F. Flow rate was carefully plotted against pressure gradient on logarithmic paper and a straight line of unit slope drawn through the data. Equation (11), verified by Cornish(17), represented the line and thus enabled the depth of the conduit to be calculated as 1.007 inches. The aspect ratio and equivalent diameter of the conduit were, therefore, 7.95 and 1.786 inches respectively.

Substitution of the physical dimensions of the conduit into equation (12) gave the friction factor-Reynolds number relationship as

$$f = \frac{20.5}{Re'} \tag{77}$$

This relationship is shown in Figure 23 along with the data for the oil in laminar flow. Both sets of data are included but only at a Reynolds number of 3240 is there a sufficient

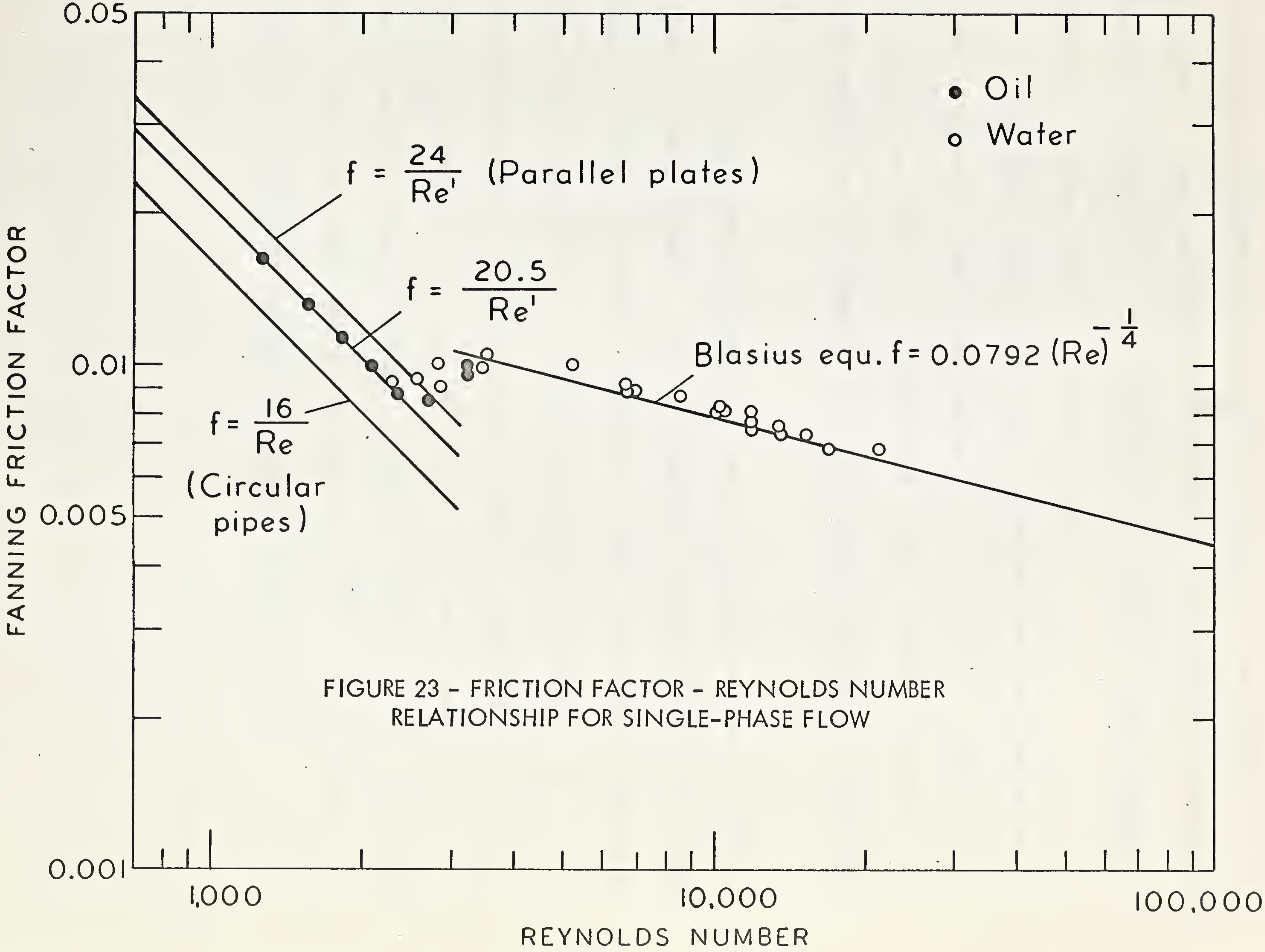

FIGURE 23 - FRICTION FACTOR - REYNOLDS NUMBER RELATIONSHIP FOR SINGLE-PHASE FLOW

difference between the friction factors for two points to be plotted. Also included in the figure for comparison purposes are the theoretical relationships for laminar flow between parallel plates and in circular pipes.

Pressure drops were also recorded for the turbulent flow of water at Reynolds numbers up to 20,000. The data, tabulated in Table 2F, Appendix F, and plotted in Figure 23, show excellent agreement with the Blasius equation, equation (17).

Data were obtained in the transition region for the flow of both fluids. It is apparent from Figure 23 that the lower critical Reynolds number was 2300 for both fluids and that the transition to turbulent flow was complete at a Reynolds number of 3500. These values compare with 2000 and 3800 found by Cornish(17) for the flow of water in a rectangular conduit having an aspect ratio of 2.92, and with 2700 and 3300 obtained by Walker et al(92) for the flow of water in a conduit having an aspect ratio of 20.

B. TWO-PHASE FLOW

1. Flow regimes and interfacial structure

The flow regimes, i.e. the ranges of input conditions for which the phases were in laminar or turbulent flow, were determined by injecting dye into each phase through very fine hypodermic needles. The interfacial structure was observed visually by directing a flood lamp obliquely at the interface. In this way the slightest interfacial disturbances were readily visible.

In order to delineate the regimes and indicate the different forms of interfacial structure Figure 24 was prepared in which the superficial oil Reynolds number is the ordinate and the superficial water Reynolds number is the abscissa. The Reynolds numbers are superficial in the sense that they are based on the average velocities the phases would have if they flowed in the absence of the second phase, and on the equivalent diameter of the conduit. Since the physical properties of the fluids were constant the Reynolds numbers were simply proportional to the flow rates of the phases. The Reynolds number approach is, however, useful because it allows a direct comparison to be made with the single-phase results.

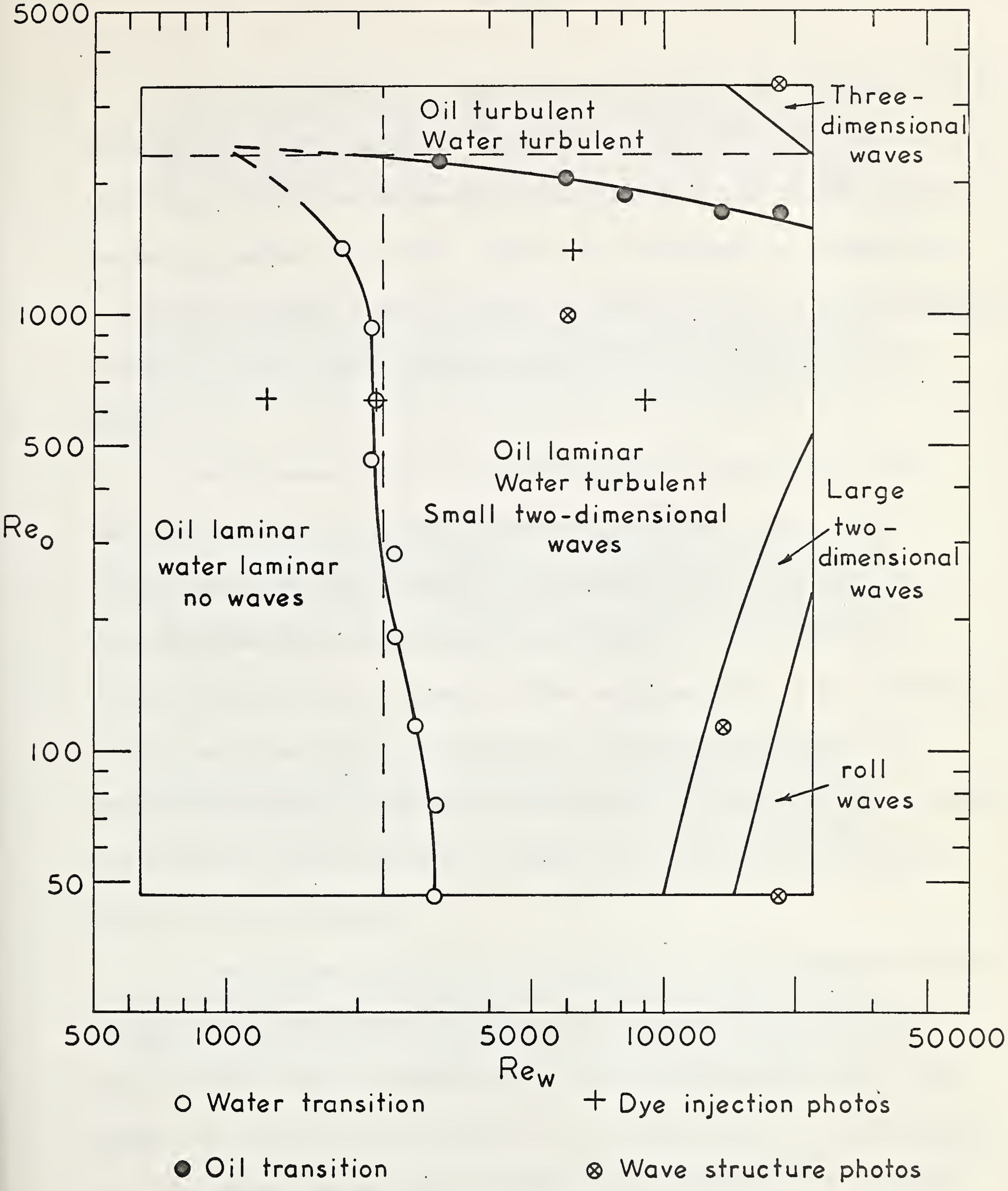

FIGURE 24 – FLOW REGIMES AND INTERFACIAL STRUCTURE

In the two-phase experiments oil Reynolds numbers ranged from 46 to 3,330 and water Reynolds numbers from 617 to 22,000. The single-phase experiments indicated that the lower critical Reynolds number was 2300. Hence, for purposes of comparison, a vertical broken line is drawn on Figure 24 at a water Reynolds number of 2300, and a similar horizontal line for the oil phase.

Both phases were in laminar flow at relatively low Reynolds numbers. Under these conditions no waves were perceptible at the interface, although slight interfacial disturbances were caused by the presence of the meniscus at the sides of the conduit. The meniscus was never perfectly smooth and the slight roughnesses caused disturbances to spread across the interface downstream of the roughness. These disturbances were, however, damped out within two or three feet of their source.

Conditions within the two phases in the laminar-laminar regime are illustrated in Figure 25 (i) for $Re_o = 649$ and $Re_W = 1225$. Dye filaments injected simultaneously into the upper oil phase, which shows as the darker band in the figure, and the water phase both retained their identity and showed the unidirectional nature of the motion.

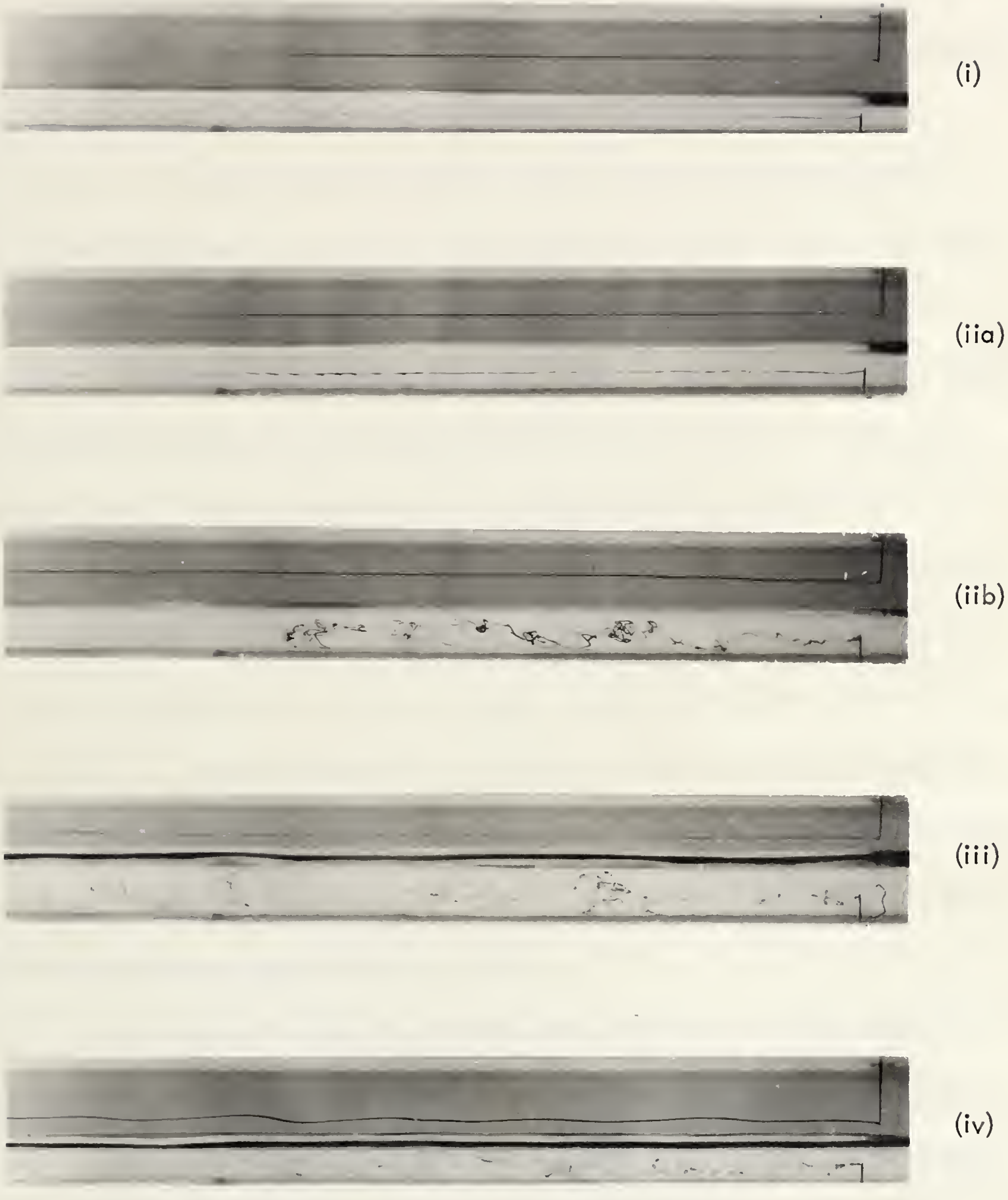

FIGURE 25 – DYE TRACES

Consider now a steady increase in the water flow rate at a constant oil flow rate with $Re_o = 649$. At a water Reynolds number of 2150 the water phase showed the first signs of turbulence, while the oil phase remained in laminar motion. Turbulent patches in the water phase travelled along the conduit and were separated by sections in which the flow was laminar. Slight increases in the water flow rate caused the turbulent patches to be generated more and more closely together until the transition to turbulence was complete. These observations of the initiation of turbulence are qualitatively very similar to those of Rotta(76) for the flow of a single phase in a circular pipe. No attempt was made in the present investigation to evaluate intermittency factors. It was also observed that the depth of the water phase momentarily increased slightly by 0.02-0.03 inches as a turbulent patch passed an observation point.

Coincident with the turbulent patches the interface was observed to be disturbed by two-dimensional waves, i.e. waves having crests several times longer than the wavelength. The wave crests were normal to the direction of flow. The waves had a relatively short wavelength of about 0.5 inches and a very small amplitude. There was absolutely no doubt

that the first interfacial waves were associated with the turbulent patches in the water phase. Between the turbulent patches the interface was free of waves and therefore the groups of waves travelled at the same velocity as the turbulent patches.

The groups of waves were first observed about 6-12 inches inside the calming section and it is, therefore, reasonable to conclude that the turbulent patches in the water phase originated there too. The turbulent patches, as evidenced by the interfacial waves, filled the entire width of the conduit soon after they were formed and increased in length as they travelled along the conduit - an observation also in accord with the observations of Rotta(76) on the initiation of turbulence in circular pipes.

The different conditions which existed in the two phases when the first signs of turbulence were observed are illustrated in Figure 25, (iia) and (iib). Both photographs were taken with $Re_o = 649$ and $Re_w = 2150$. In (iia) both phases were in laminar flow, the dye traces being similar to those shown in (i), and no waves were present at the interface. In (iib) a patch of turbulence existed in the water phase and associated with this turbulence were waves at the interface. It is also apparent that the oil was little

affected by the presence of the waves.

An increase of about 30 percent in the water flow rate caused the turbulence in the water phase to become continuous with an uninterrupted wave system at the interface.

The lower critical water Reynolds number was located at a number of oil Reynolds numbers and the data plotted in Figure 24. At all oil Reynolds numbers the transition was similar to that already described for an oil Reynolds number of 649. It is apparent that at low oil flow rates, i.e. small oil depths, the lower critical water Reynolds number was greater than that for the flow of water by itself. A similar effect was noted in Gazley's(36) data for the co-current flow of air and water in a circular pipe where the gas phase was stabilized by the presence of a moving water layer. Whether the increased stability was simply a result of the presence of a moving boundary, or whether it was due to the flexibility of the boundary, which has been shown to be important by Benjamin(5), is not clear. At $Re_o = 46$ the lower critical water Reynolds number was increased to 3000. As the oil Reynolds number was increased the critical water Reynolds number decreased until at $Re_o = 300$ the critical Reynolds number was again 2300.

On a further increase in the oil Reynolds number the trend of a decreasing critical water Reynolds number was temporarily arrested. For oil Reynolds numbers between 400 and 1000 the critical Reynolds number remained at approximately 2200. At an oil Reynolds number of 900 the relative interface position was approximately 0.7. Reference to the velocity profiles presented in Figure 4, which applies for the particular aspect and viscosity ratios of the experimental investigation, indicates that for such an interface position the maximum velocity occurred at or near the interface. It is suggested that this is the cause of the relative stability of the two-phase system. At lower oil Reynolds numbers the maximum velocity occurred within the water phase.

Further increase in the oil flow rate caused a sudden decrease in stability with the phases being mutually unstable in the region of $Re_o = 2300$ and $Re_w = 1000$. In this region the small water depth made dye injection studies of the conditions in the water phase difficult. Further, since the plastic conduit was preferentially wet by the oil, the oil tended to displace the water from the bottom of the conduit close to the sides. The depths of the phases were, therefore, not constant. In view of this a tentative continuation of the locus of the critical water Reynolds number is shown dotted

in this region.

The locus of the lower critical oil Reynolds number was determined in a similar way to that for water. Again, turbulent patches were observed first and their effect on the interfacial structure was to tend to destroy the two-dimensional nature of the waves. The presence of the turbulent water phase caused the critical oil Reynolds number to be less than that for single phase flow, the difference being more pronounced at high water flow rates. At a water Reynolds number of 22,000 the critical oil Reynolds number was 1600.

Consider again conditions for which $Re_o = 649$. The appearance of the two-dimensional waves remained much the same on increasing the water flow rate up to the capacity of the equipment, although the wavelength increased slightly to about 0.75 inches and the amplitude increased slightly too. Conditions within the phases at $Re_o = 649$ and $Re_w = 9060$ are illustrated in Figure 25 (iii). Under these conditions, although the water was highly turbulent and a continuous wave system present at the interface, the oil phase was still in basically unidirectional laminar motion. The general appearance of the two-dimensional waves is indicated in Figure 26 for $Re_o = 1000$ and $Re_w = 6000$.

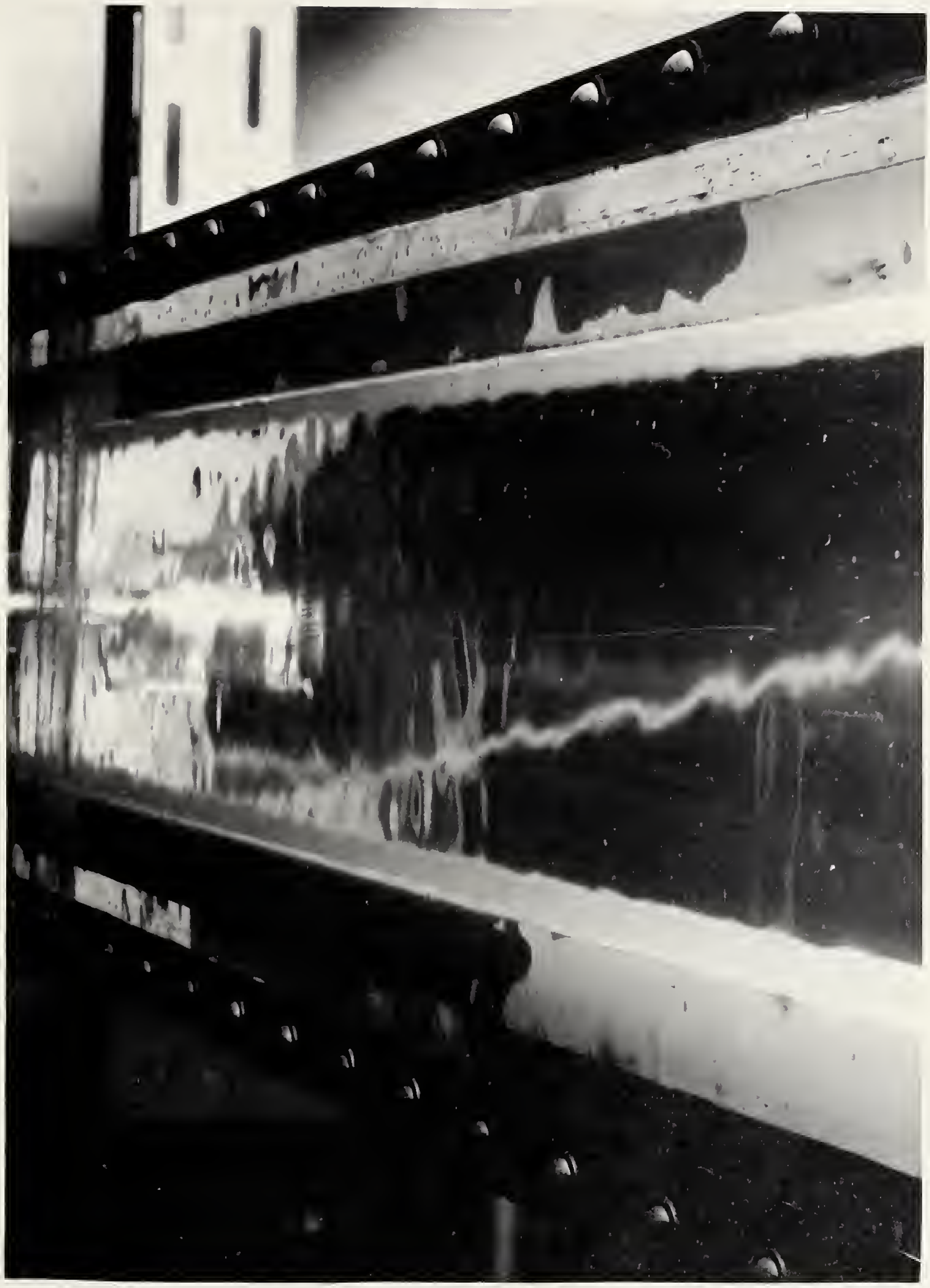

FIGURE 26 - SMALL TWO-DIMENSIONAL WAVES

22

At oil Reynolds numbers in the neighbourhood of 1500 and with the water phase in turbulent flow a definite oscillatory motion was observed in the oil phase. This is illustrated in Figure 25 (iv) in which the dye filament shows that the interfacial waves caused a more profound effect on the motion of the oil phase.

At oil Reynolds numbers below about 500 profound changes were noted in the nature of the two-dimensional waves as the water flow rate was increased. Large two-dimensional waves appeared with a wavelength of approximately 3 inches. The original small amplitude, short wavelength waves were superimposed upon the larger waves. These pronounced waves are shown in Figure 27 for $Re_o = 115.5$ and $Re_w = 13700$. The wave crests ran across the complete width of the conduit and the waves were very regular in appearance.

Further increase in the water flow rate, with a consequent thinning of the oil layer, caused roll waves to appear. Again the small amplitude waves were superimposed upon them. The roll waves moved relatively slowly, had sharp irregular crests, and a highly variable wavelength up to approximately 3 inches. The roll waves are shown in Figure 28 for $Re_o = 46.5$ and $Re_w = 18130$. While the term "roll waves" appears to most

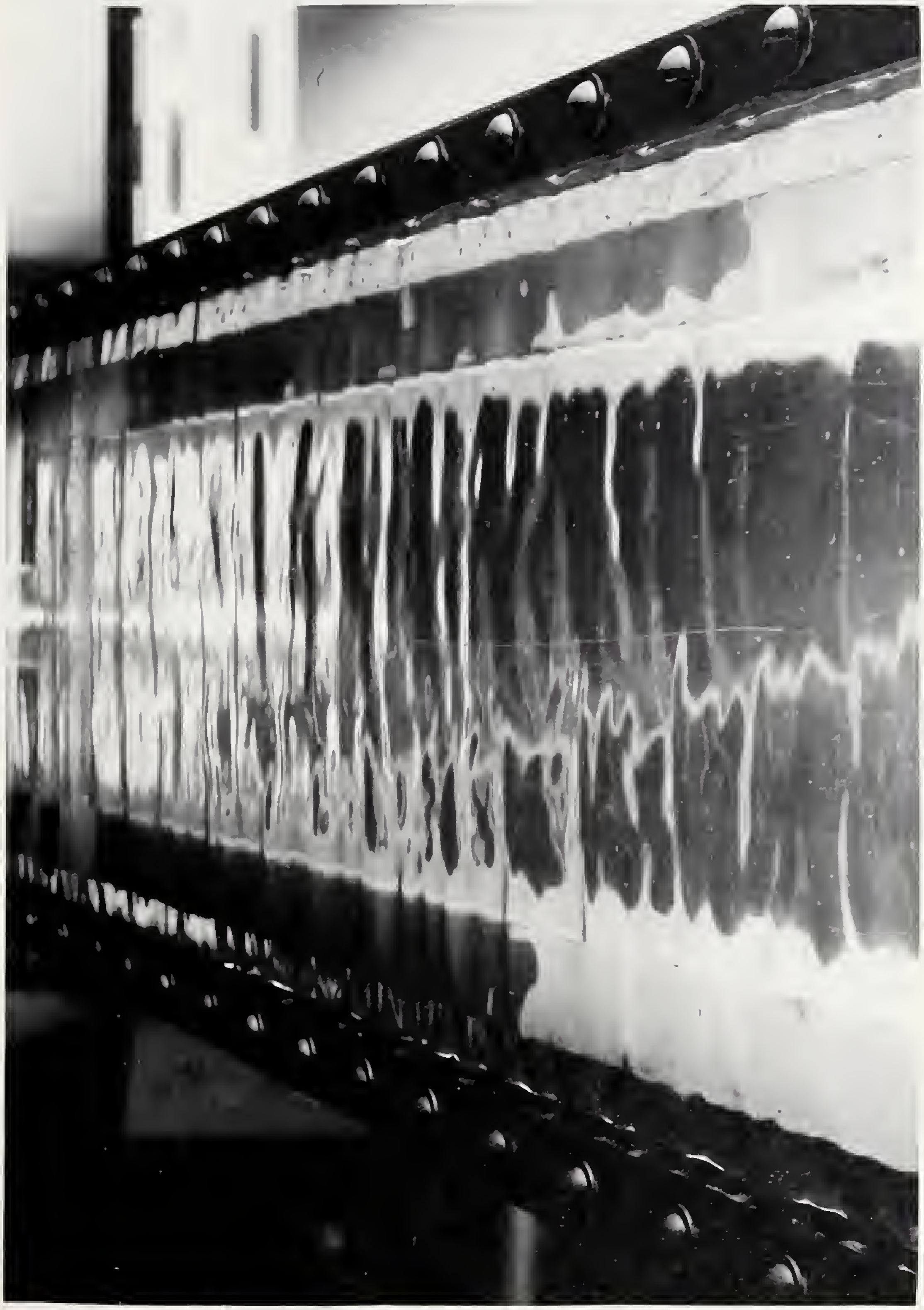

FIGURE 27 - LARGE TWO-DIMENSIONAL WAVES

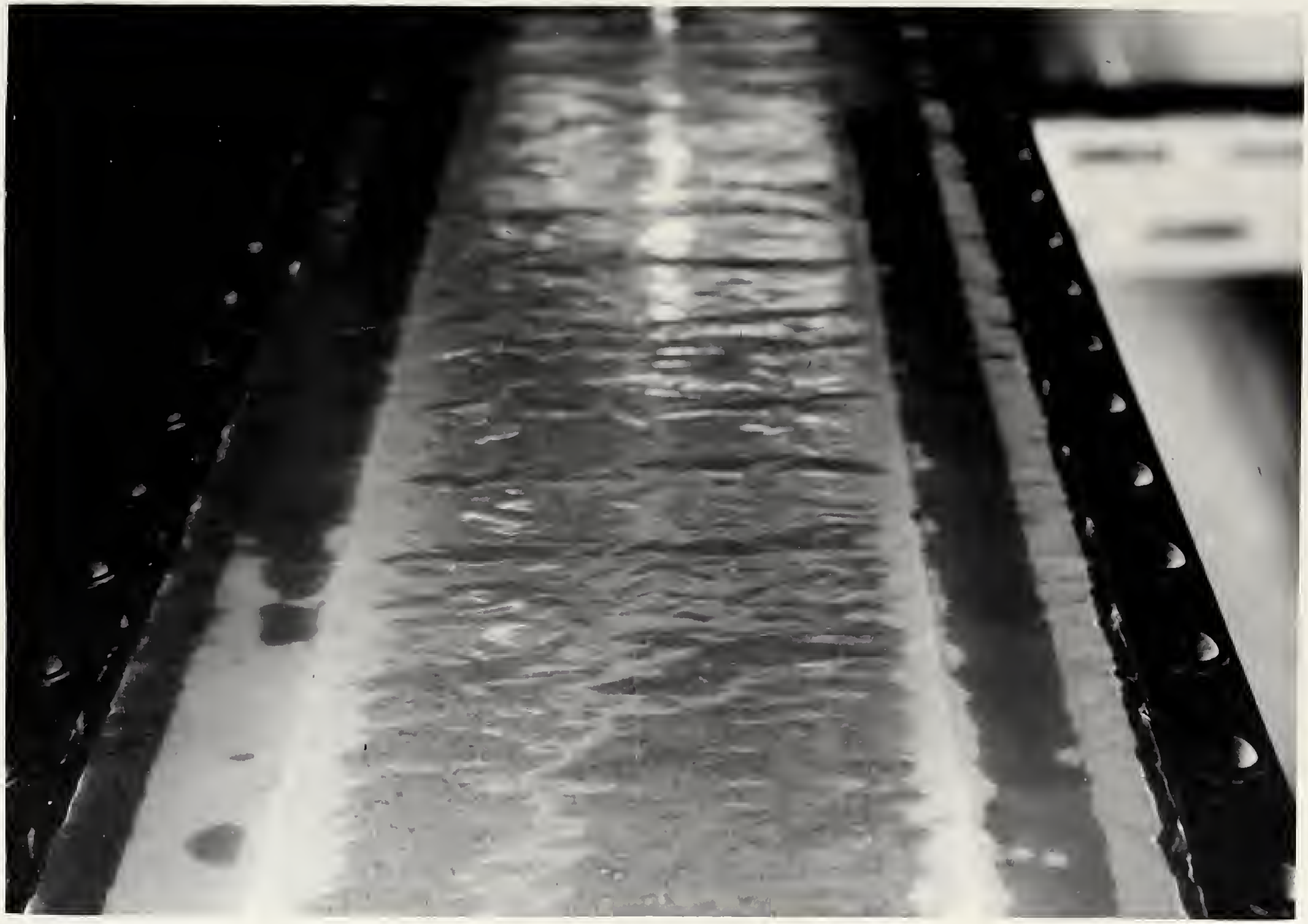

FIGURE 28 - ROLL WAVES

aptly describe the waves observed they did differ from the roll waves observed by Hanratty and Engen(40) for the air-water system. In the present investigation none of the more viscous phase was actually picked up and carried forward by the less viscous phase as in the air-water system.

It has already been remarked that the transition to turbulent flow in the oil phase tended to destroy the two-dimensional nature of the interfacial waves. As the Reynolds numbers of both phases were increased in the turbulent-turbulent regime the waves became more and more three-dimensional in character. Thus, three-dimensional waves, with the crest length approximately equal to the wavelength, were observed when the flow rates of both phases were close to the capacities of the respective pumps. The three-dimensional waves are illustrated in Figure 29 for $Re_o = 3030$ and $Re_w = 18{,}130$.

In order to clarify the transitional phenomena further, pressure gradient traverses are shown in Figures 30 and 31. In Figure 30 pressure gradient is shown as a function of water Reynolds number for $Re_o = 282$. For water Reynolds numbers less than about 2200 both phases were in laminar flow and the pressure gradient showed a gradual increase with increasing water Reynolds number. At water Reynolds numbers greater than 2200 the water was in turbulent flow with two-dimensional

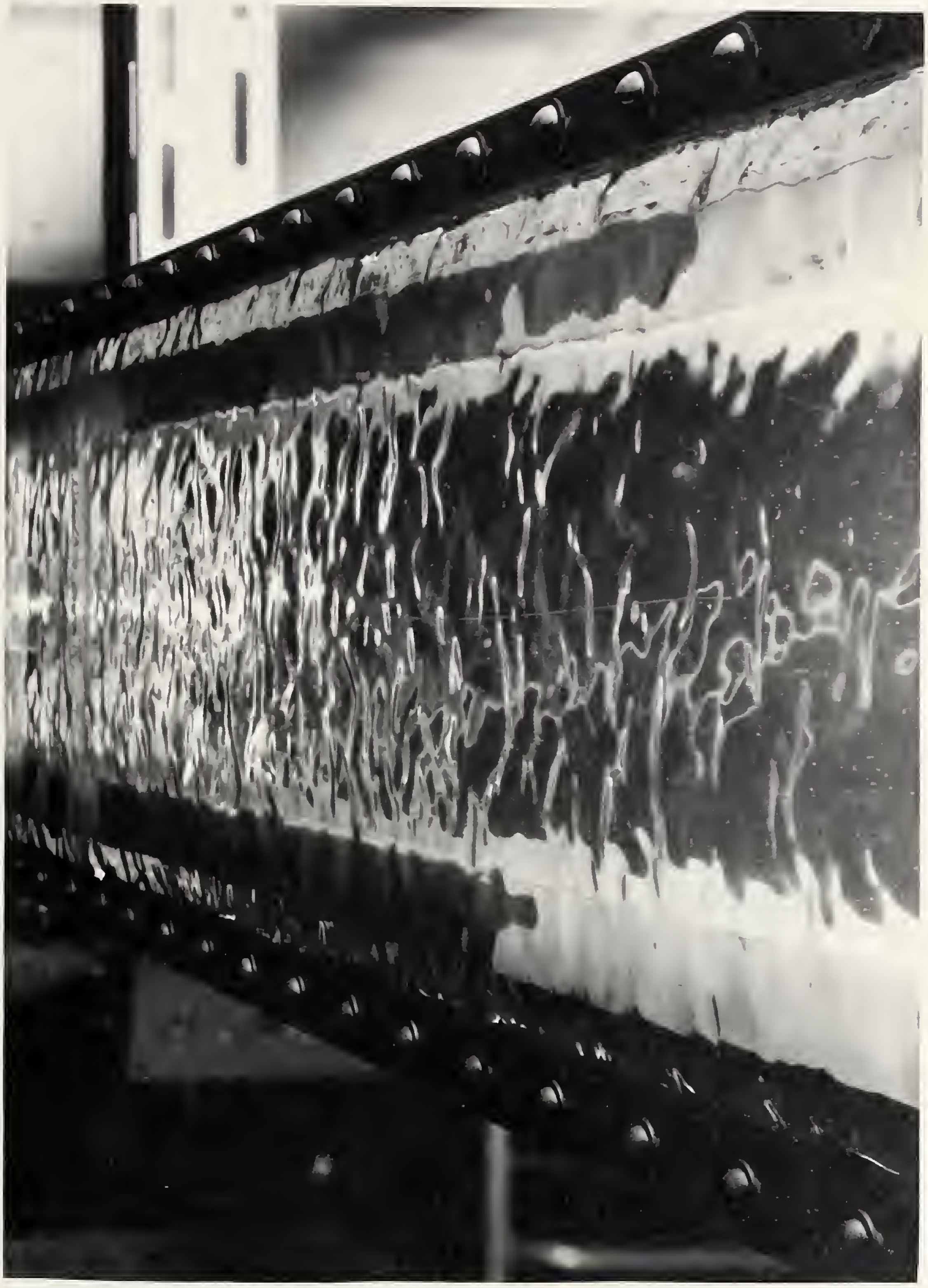

FIGURE 29 - THREE-DIMENSIONAL WAVES

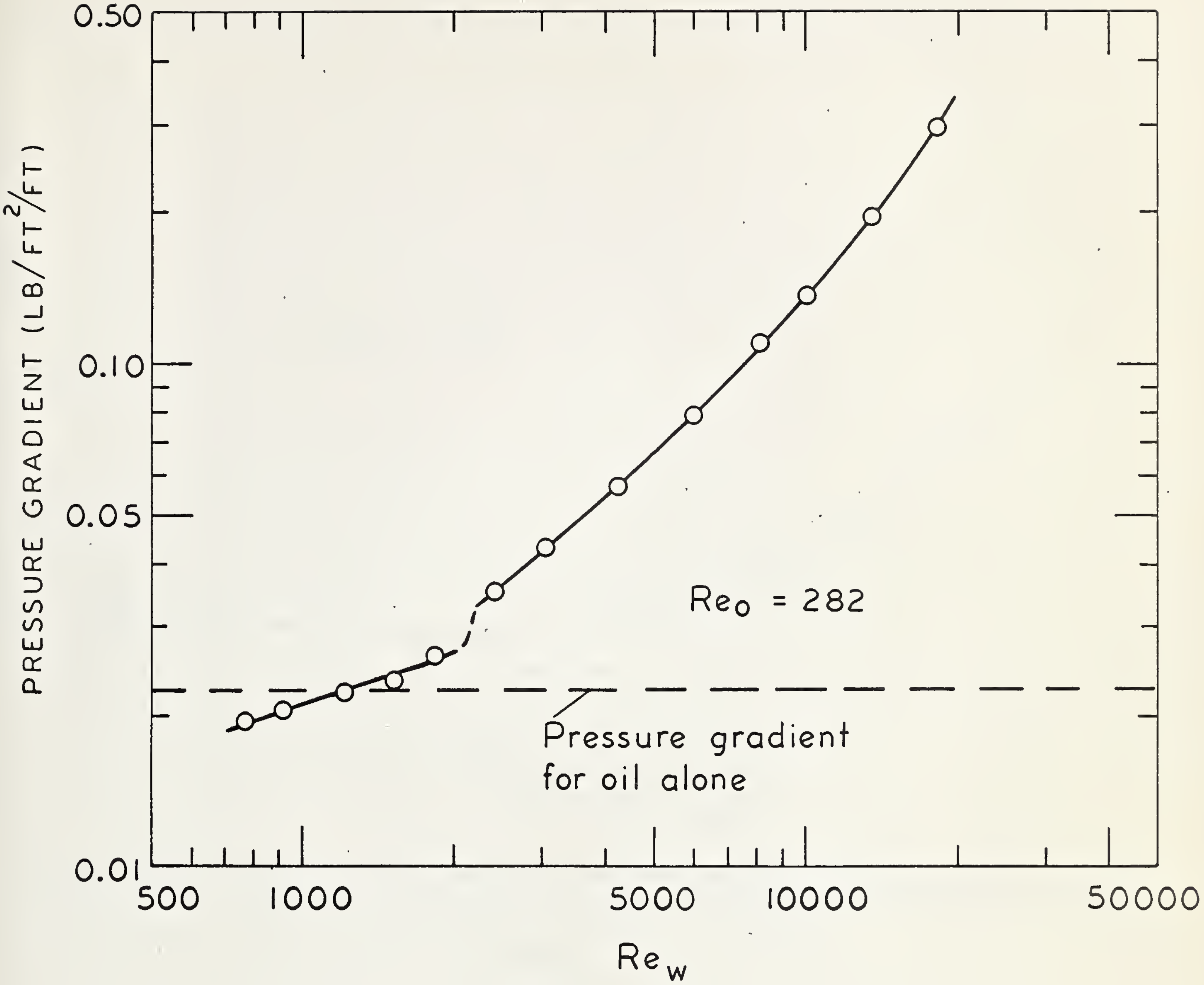

FIGURE 30 - PRESSURE GRADIENTS AT A CONSTANT OIL REYNOLDS NUMBER

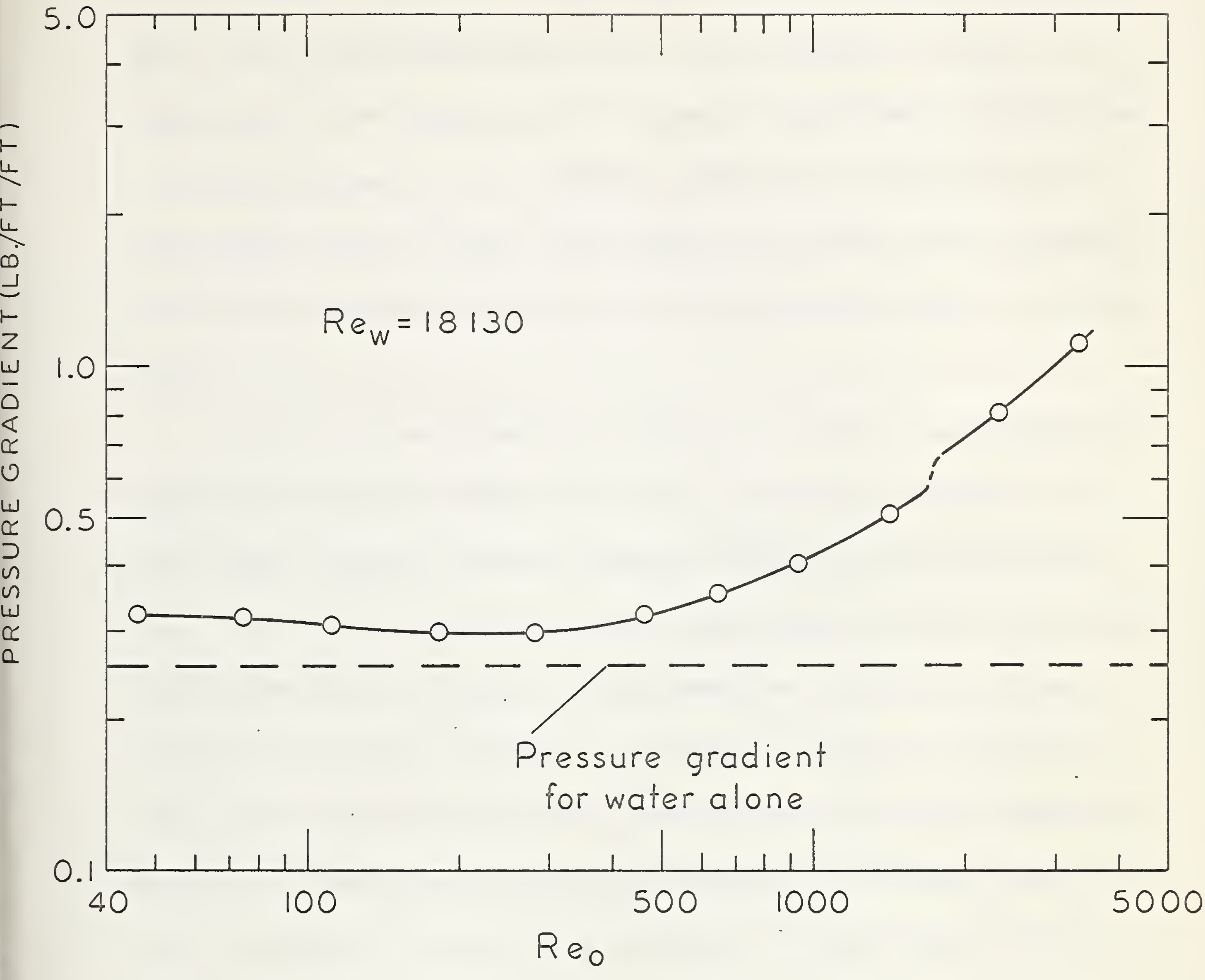

FIGURE 31 - PRESSURE GRADIENTS AT A CONSTANT WATER REYNOLDS NUMBER

waves at the interface and the pressure gradient increased more and more rapidly as the conditions were approached for which large two-dimensional waves were present. Also indicated in the figure is the pressure gradient for the flow of the oil alone. It is apparent that for relatively low water flow rates in the region where the water was in laminar flow the pressure gradient was reduced by the addition of the water.

The traverse shown in Figure 31 is for a constant water Reynolds number of 18130. At low oil Reynolds numbers roll waves were present and the pressure gradient was relatively high. As the oil Reynolds number was increased and the interface became less violently disturbed the pressure gradient actually decreased slightly. Further increase in the oil flow rate caused the pressure gradient to increase relatively sharply at the transition from laminar to turbulent flow in the oil phase. The pressure gradient for the flow of the water alone is also indicated for purposes of comparison and it is apparent that the two-phase pressure gradient always exceeded the single-phase pressure gradient.

The general nature of the observed interfacial structure agrees qualitatively with the observations of Scott Russell(77) and Benjamin(4) for the flow of air over liquids in that the

first waves observed appeared to be caused by the pressure fluctuations in the turbulent phase and the large two-dimensional waves appeared to be caused by an instability of the mean flow. However, for the liquid-liquid system, the waves generated by the pressure fluctuations in the less viscous phase had a definite two-dimensional character not observed for the air-water system.

In addition to the general agreement with the observations of Scott Russell and Benjamin, the transitional phenomena in the present investigation are in accord with the observations of Hanratty and Engen(40) for the flow of air and water in a rectangular conduit. The observations of Hanratty and Engen were made predominantly in the turbulent-turbulent regime and waves similar to the two-dimensional and three-dimensional waves which they observed were observed in the present study. Presumably if the water flow rate could have been increased further in the present investigation roll waves, similar to those observed by Hanratty and Engen, would have developed. It is also interesting to note a further point of agreement between the two systems; at the transition from two-dimensional to three-dimensional waves thinner layers of the more viscous phases were more stable than thicker ones.

The different regimes and interfacial structures will now be considered in more detail.

2. Laminar-laminar regime

In the laminar-laminar regime no waves were present at the interface and the experimental situation did, therefore, closely approximate the idealized model assumed in the foregoing theory for stratified flow. In the laminar-laminar regime experimental measurements of the interfacial velocity, the insitu ratio, and the pressure gradient reduction factor were made for oil Reynolds numbers from 111.5 to 1413, i.e. over more than a tenfold range, and water Reynolds numbers from approximately 700 up to the critical Reynolds number. The theoretical expressions were evaluated for the experimental aspect ratio, 7.95, and viscosity ratio, 5.326, which was the average value during the experiments. The theoretical quantities are tabulated in Table A3, Appendix A and the experimental data in Table F3, Appendix F.

The comparison of the theoretical and experimental quantities are shown in Figures 32, 33 and 34; the interface velocities are compared in Figure 32, the insitu ratios in Figure 33, and the pressure gradient reduction factors in Figure 34. Both the theoretical and experimental interface velocities are plotted as the dimensionless ratio of w_i, the interface velocity, to V_{rc}, the average velocity for the flow of the more viscous oil phase alone in the rectangular conduit

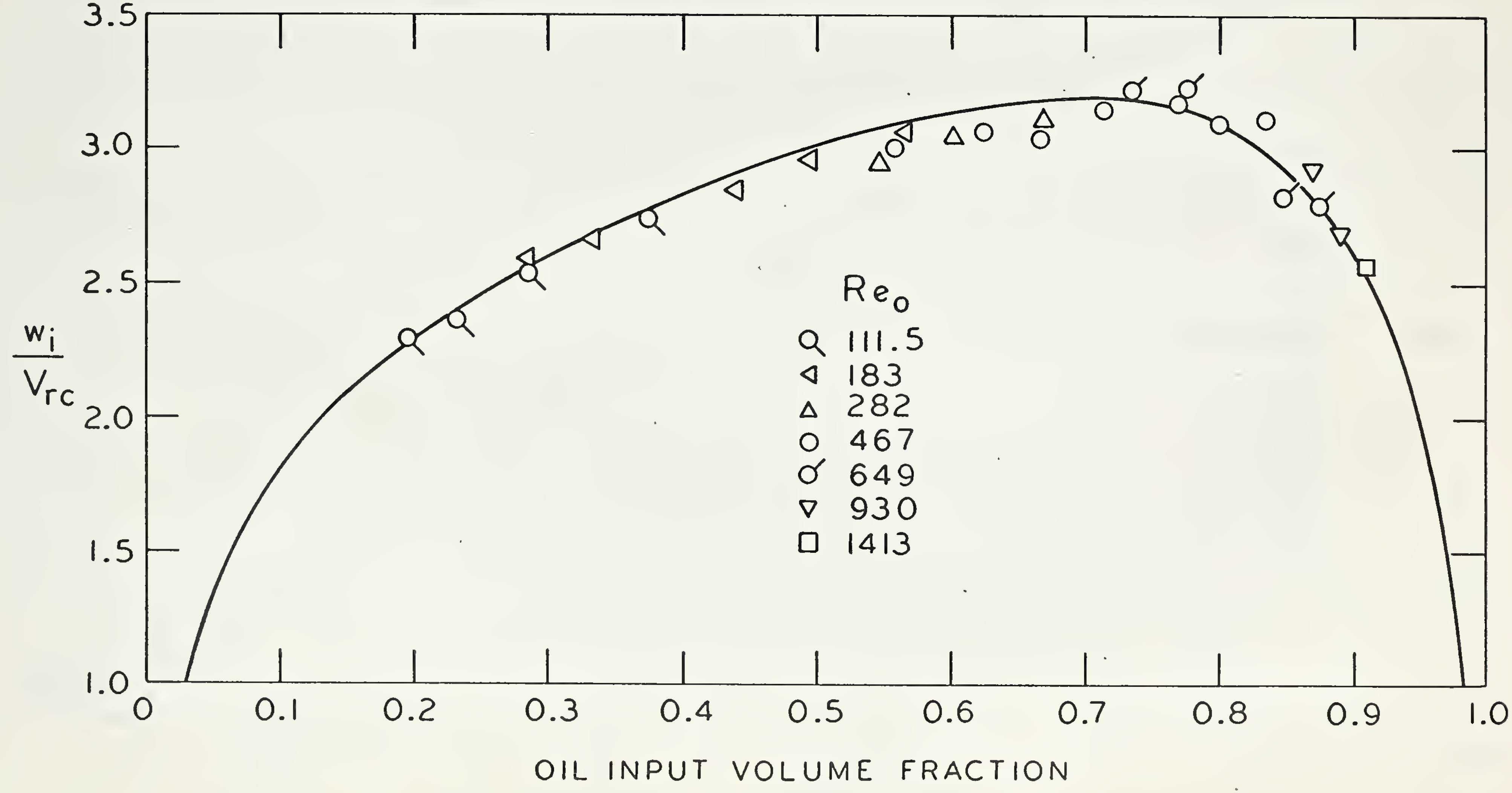

FIGURE 32 - COMPARISON OF EXPERIMENTAL AND THEORETICAL LAMINAR-LAMINAR INTERFACE VELOCITIES

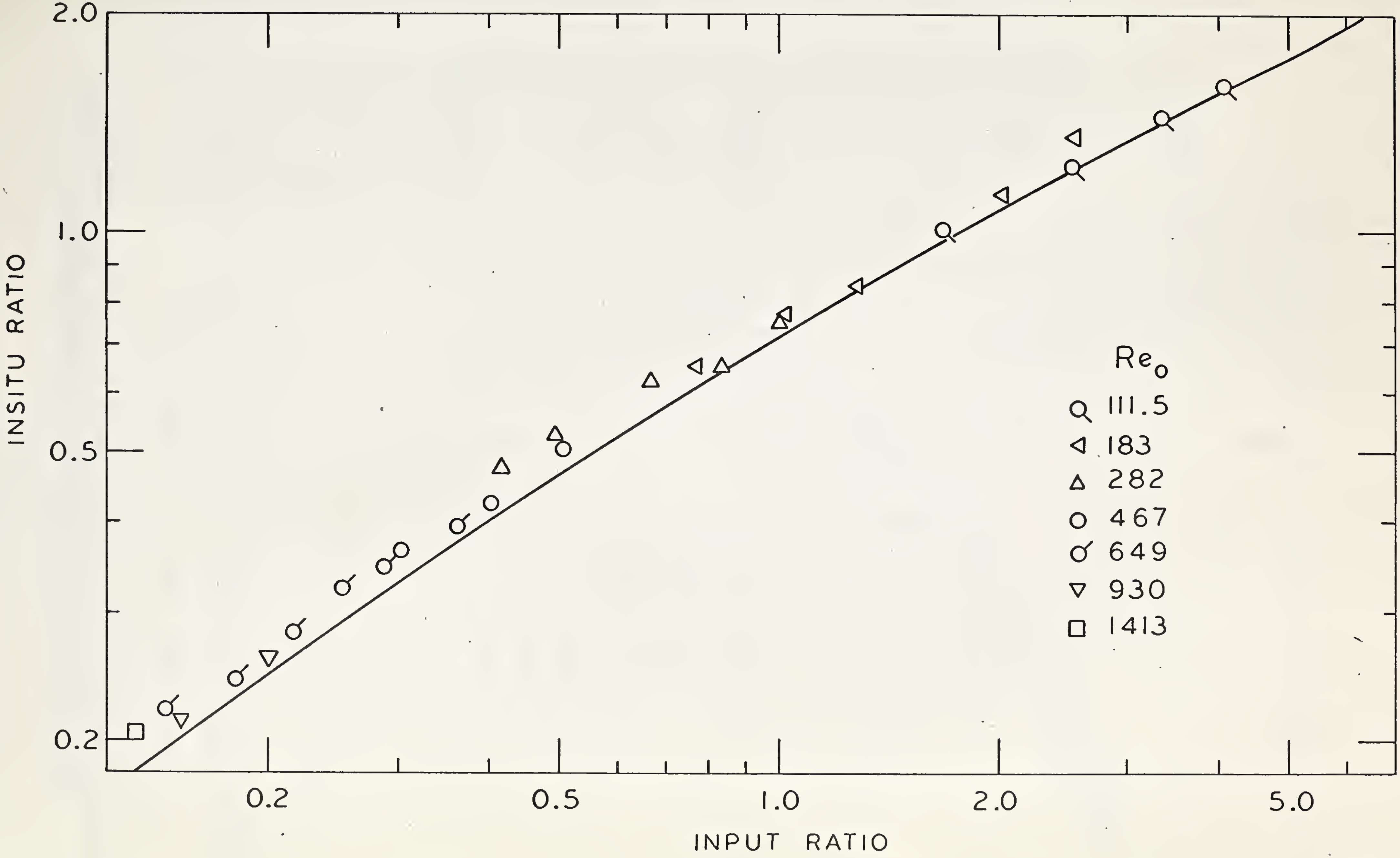

FIGURE 33 - COMPARISON OF EXPERIMENTAL AND THEORETICAL LAMINAR-LAMINAR INSITU RATIOS

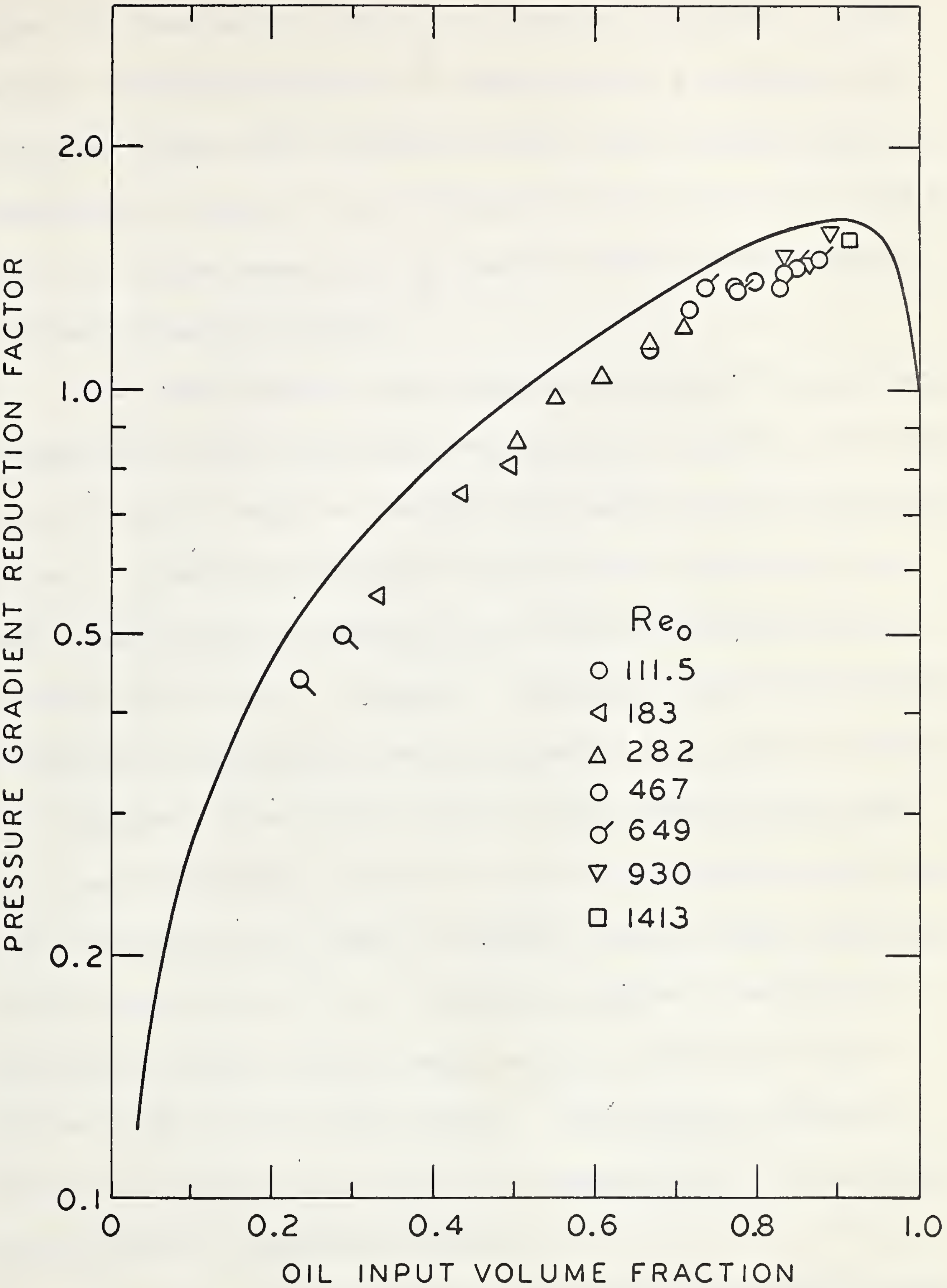

FIGURE 34 - COMPARISON OF EXPERIMENTAL AND THEORETICAL LAMINAR-LAMINAR PRESSURE GRADIENT REDUCTION FACTORS

under the theoretical two-phase pressure gradient. In this way the pressure gradient is eliminated as a variable and, for given aspect and viscosity ratios, the velocity ratio is predicted by theory to be a function of the input oil fraction only, as is the case with the insitu ratio and the pressure gradient reduction factor.

The experimental data confirm the unique relationship between the three ratios and the input oil fraction, or input ratio, and, in addition, verify the trends of the theoretical curves. It will be recalled that this was not so for the experimental data of Russell et al for stratified flow in a circular pipe shown in Figure 1. However, small differences between the theoretical and experimental quantities do exist. The experimental velocity ratios, while agreeing very well with the theoretical values at both relatively high and low input fractions, are about 4 percent low for input fractions in the range 0.4 to 0.7. The insitu ratios agree well at high input ratios but the experimental values are about 5 percent high at low input ratios. The pressure gradient reduction factors are consistently approximately 10 percent lower than the theoretical values.

While experimental errors and slight variation in the viscosity ratio no doubt account for the slight scatter of

the experimental data, it is unlikely that they account for the deviations noted above. The following departures from the theoretical model could possibly have contributed to these deviations:

(1) the presence of a large interfacial viscosity,

(2) not fully developed velocity distribution and

(3) the presence of a meniscus

Very high interfacial viscosities have been observed in some fluid-fluid systems(20). The effect of a high interfacial viscosity would tend to reduce the interface velocity at the centre line of the conduit, especially in conduits of small aspect ratio where the velocity distribution is not two-dimensional in the central region. This effect would, however, not be limited to certain interface positions and would not be expected to affect the interface velocity in the central region of a conduit with the relatively large aspect ratio of 7.95:1. It is, therefore, unlikely that high interfacial viscosity effects account for the deviations.

Despite the provision of a long calming section, the length of which was determined from the experimental data of Eckert and Irvine(26) for single phase flow in a rectangular conduit, it is possible that the velocity distribution was not in fact fully developed. In general, if this were so,

experimental velocity measurements in high velocity regions would tend to be lower than, and experimental pressure gradients higher than the theoretical values. These two effects are, in fact, apparent in the data. However, the deviation of the insitu ratio data from the theory is contradictory. At low water to oil input ratios the maximum velocity occurred in the oil phase. Under these conditions, if the velocity distribution was not fully developed the tendency would be for the depth of the water phase to be less than the theoretical value and thus the experimental insitu ratios to be less than the theoretical values rather than the converse.

The presence of a meniscus at the sides of the conduit was a definite departure from the theoretical model. Although the plastic walls of the conduit were preferentially oil wet the direction of the curvature depended on the previous history of the flow rates. If, for example, the water flow rate was increased to a new value the interface curved down to the sides of the conduit. Data were obtained with the meniscus curved both upwards and downwards and while, no doubt, the curvature contributed to the scatter of the data, it could not account for the overall deviations. However, the disturbances caused by the roughnesses in the meniscus resulted

in energy losses which certainly caused the pressure gradient to exceed the theoretical value, although they would probably have little or no effect on the interfacial velocity and insitu ratio. The lower pressure gradient reduction factors are, therefore, at least partially accounted for by these disturbances.

It would appear, therefore, that no single explanation can be advanced to explain all the small deviations observed. Despite these deviations, the experimental data verify the theory reasonably well and the numerical data evaluated from the theoretical expressions can be used with confidence. Further, the numerical results obtained by Charles and Redberger(13) and Gemmell and Epstein(37) for laminar, stratified flow in a circular pipe should also represent the practical situation well, provided the velocity distribution is fully developed and the pipe diameter is sufficiently large for meniscus effects at the pipe wall to be insignificant.

Lockhart and Martinelli(62) correlated pressure gradient data for the flow of gas-liquid mixtures through horizontal circular pipes by the four flow regimes and the parameters defined by equations (3) and (4) in the introduction. As was pointed out in the introduction subsequent experimentally

measured pressure gradients for stratified flow in the laminar-laminar and laminar-turbulent regimes have been less than those calculated from the relevant Lockhart-Martinelli curves. Nevertheless, it is interesting to explore what use could be made of the basic Lockhart-Martinelli parameters in correlating pressure gradient data for stratified flow.

When the two phases in stratified flow are considered as the more viscous and less viscous phases, then the Lockhart-Martinelli parameter ϕ_1^2, defined by equation (3) is simply the reciprocal of the pressure gradient reduction factor defined in the present study. Further, the Lockhart-Martinelli X^2, defined by equation (4), is equivalent to the reciprocal of the ratio $\left(\frac{\partial p}{\partial z}\right)_w \Big/ \left(\frac{\partial p}{\partial z}\right)_o$ where $\left(\frac{\partial p}{\partial z}\right)_w$ is the pressure gradient for the flow of the water alone and $\left(\frac{\partial p}{\partial z}\right)_o$ is the pressure gradient for the flow of the oil alone.

For laminar flow of both phases, it is readily shown by the use of equations (12), (13) and (14) that

$$\left(\frac{\partial p}{\partial z}\right)_w \Big/ \left(\frac{\partial p}{\partial z}\right)_o = \begin{pmatrix}\text{input}\\ \text{ratio}\end{pmatrix} \left(\frac{\mu_o}{\mu_w}\right)^{-1} \qquad (78)$$

Obviously, therefore, the pressure gradient reduction factor and the ratio of the single phase pressure gradients could not correlate data for different aspect ratios. Further, the complexity of the curves presented in Figures 6, 7, 8, and 9

in which the pressure gradient reduction factor is plotted against the interface position for different aspect ratios indicates that, even for a given aspect ratio, a Lockhart-Martinelli type correlation would be inadequate over the complete range of input conditions. However, it is evident from these figures that the pressure gradient reduction factor tends to become independent of the viscosity ratio at low relative interface positions. Under such conditions an analysis of the numerical data indicates that the input ratio is approximately proportional to the viscosity ratio and, therefore, a Lockhart-Martinelli type correlation would represent the data well. Low relative interface positions correspond to large input fractions of the less viscous phase.

Equation (78) would be unchanged for laminar-laminar flow in a circular pipe. The numerical results obtained by Charles and Redberger(13) and Gemmell and Epstein(37) for this flow situation also show that at high input fractions of the less viscous phase the input fraction is again approximately proportional to the viscosity ratio. Further, the numerical results were independent of the pipe diameter. There does, therefore, appear to be definite theoretical justification for the Lockhart-Martinelli correlation in the stratified laminar-laminar regime provided the input fraction

of the less viscous phase is relatively high.

3. Laminar-turbulent regime

When the oil was in laminar, and the water in turbulent flow, waves were always present at the interface, the three wave types observed in this regime being small two-dimensional waves, large two-dimensional waves, and roll waves. Turbulence in the water phase established a more uniform velocity distribution and increased the rate of dissipation of energy in the water phase compared with the corresponding laminar flow. The effect which these two factors had on the experimental insitu ratios, velocity ratios, and pressure gradient reduction factors will be illustrated by plotting representative data on the same basic co-ordinates as were used to represent the laminar-laminar data.

(i) Insitu ratios

It has been remarked that, on the transition to turbulence in the water phase, the level of the interface in a turbulent patch was higher than the level for the corresponding laminar-laminar flow, i.e. the insitu water to oil ratio was greater for laminar-turbulent flow than for the corresponding laminar-laminar flow. This effect, which was a consequence of the increased rate of energy dissipation in the water phase,

was apparent throughout the laminar-turbulent regime. To illustrate this, representative data are plotted in Figure 35. The data for Re_o = 649 are typical of the results obtained for conditions when small two-dimensional waves were present at the interface. The insitu ratios scattered slightly about a curve parallel to, and about 20-25 percent above, the theoretical laminar-laminar curve and showed no definite trend with oil Reynolds number.

At oil Reynolds numbers for which the large two-dimensional and roll waves were observed, the insitu ratios showed a further increase at the transition to large two-dimensional waves, reflecting the increased shear force at the interface caused by the presence of the larger waves. For oil Reynolds numbers in the range 46.5 to 183 a definite effect of oil Reynolds number existed. At a particular oil Reynolds number the insitu ratio increased rapidly with increase in the input ratio throughout the region for which large two-dimensional waves were present. At oil Reynolds numbers of 46.5 and 73.8 insitu ratios obtained with roll waves at the interface increased less rapidly with increasing input ratio.

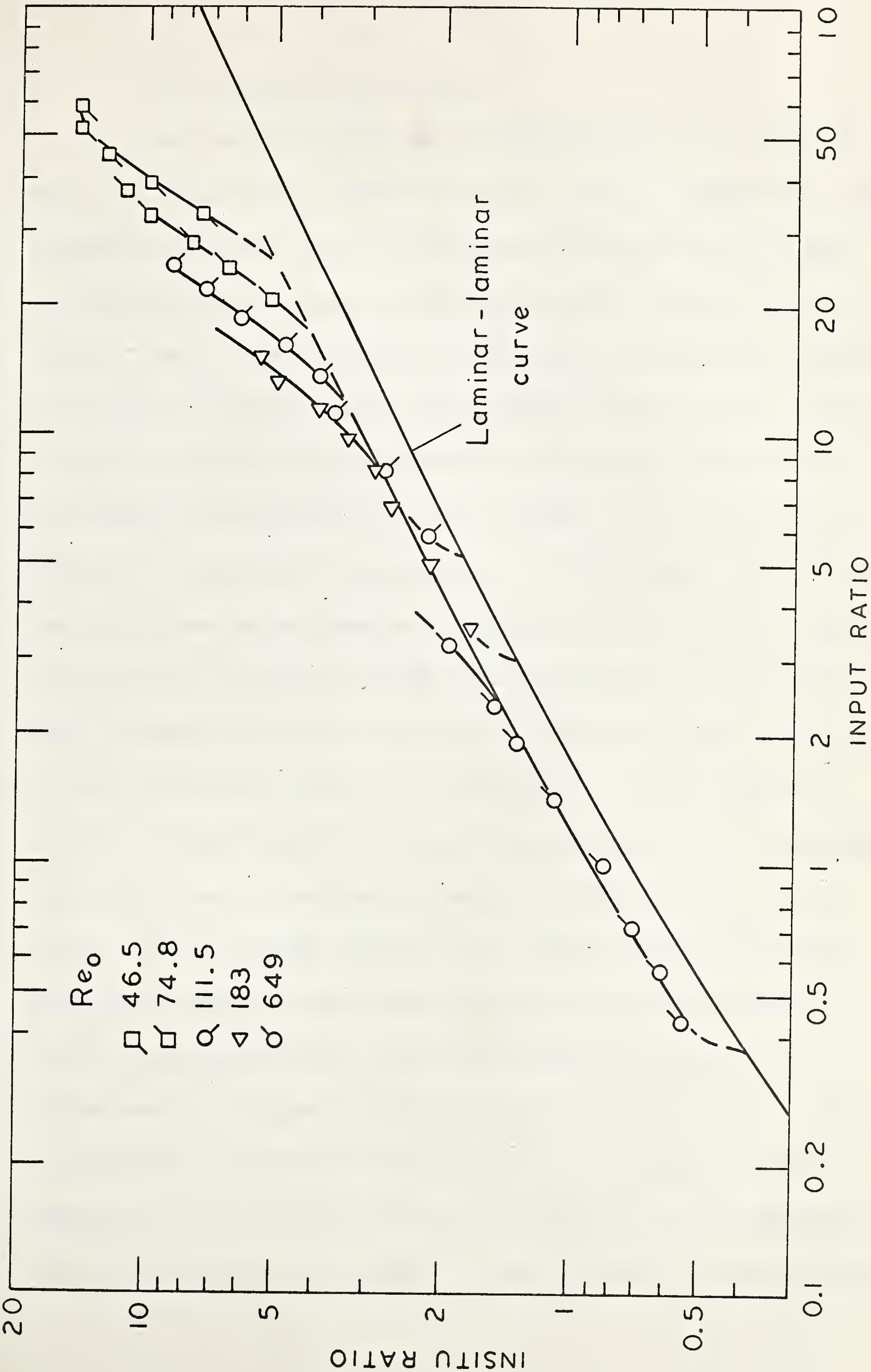

FIGURE 35 - LAMINAR-TURBULENT INSITU RATIOS

(ii) Interface velocities

Some laminar-turbulent velocity ratios are compared with the theoretical laminar-laminar curve in Figure 36. The pressure gradient used to calculate the denominator of the velocity ratio was again computed from the laminar-laminar theory. While the velocity ratio is now a fictitious quantity as far as the experimental data are concerned it does allow a valid and interesting comparison to be made with the data previously presented for laminar-laminar flow. Two definite effects are apparent in the data. At low input volume fractions the interface velocities were higher than the laminar-laminar values and at relatively high input fractions the converse was true. These deviations are readily explained with reference to the insitu ratio data just presented. At oil Reynolds numbers of 46.5 and 111.5 the oil was present as a relatively thin layer and the maximum velocity occurred in the water phase. The increased insitu ratio under laminar-turbulent conditions necessitated that the actual average velocity of the oil phase be greater than the laminar-laminar value. Consequently a higher interface velocity was observed. At oil Reynolds numbers of 649 and 930 the maximum velocity occurred in the oil phase when the transition to turbulence took place in the water phase. The increase in insitu ratio

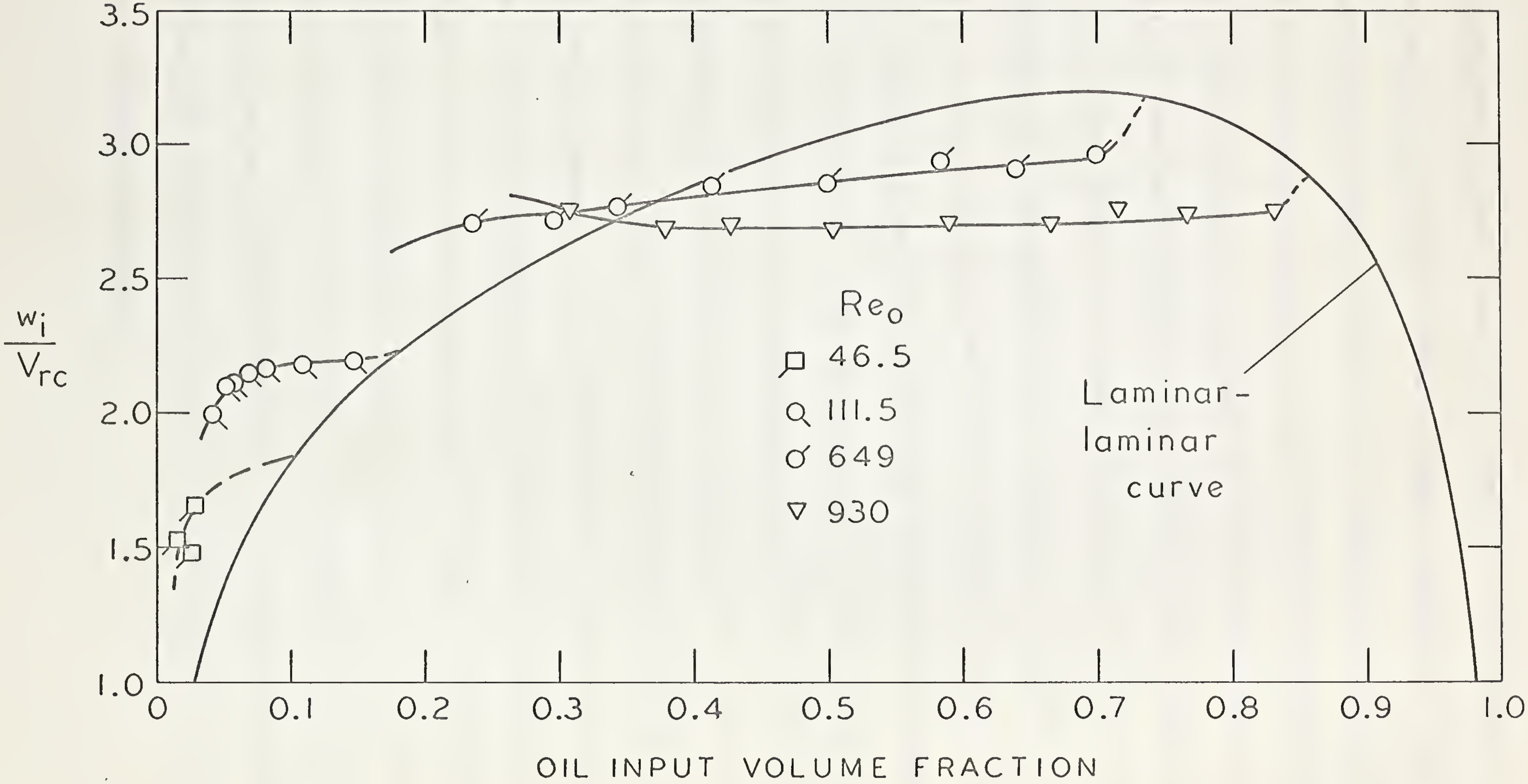

FIGURE 36 - LAMINAR-TURBULENT INTERFACE VELOCITIES

which accompanied the transition lowered the actual average water velocity and thus caused a lower interface velocity. With increasing water fraction at a constant oil Reynolds numbers of 649 and 930 the oil layer became progressively thinner and eventually interface velocities greater than the theoretical laminar-laminar values were again observed.

It would appear from the data that, at the transition to turbulence in the water phase, either an increase or a decrease in the interface velocity relative to the laminar-laminar value is possible, depending upon which phase contained the maximum velocity. The deviations of the interface velocities from the laminar-laminar curve were a direct consequence of the increased interfacial shear force and the more uniform nature of the velocity distribution under turbulent conditions in the water phase. It is important to note that for laminar-laminar flow the maximum in the curve of velocity ratio versus oil input fraction indicates the oil input fraction for which the interface velocity is a maximum for a given pressure gradient but this is not so for the experimental data in the laminar-turbulent regime because, for a given interface position, the flow rates are no longer directly proportional to the pressure gradient.

(iii) Pressure gradients

Representative laminar-turbulent pressure gradient data are plotted in Figure 37 in terms of the pressure gradient reduction factor and the oil input volume fraction. The laminar-laminar theoretical curve and the position of the laminar-laminar experimental data are included for comparison. The onset of turbulence in the water phase caused a sharp increase in the two-phase pressure gradient with a consequent decrease in the pressure gradient reduction factor. In the laminar-turbulent regime, for given aspect and viscosity ratios, the pressure gradient reduction factor is no longer a function of the input fraction only, but of the oil Reynolds number as well.

As the oil input fraction decreased the data deviated further and further from the theoretical laminar-laminar curve. At an oil Reynolds number of 74.8 and at an oil Reynolds number of 183 with input fractions less than about 0.10 large two-dimensional waves or roll waves were present at the interface. This is reflected in the increased steepness of the curves relative to the other curves for which the small two-dimensional waves were present at the interface.

The increase in pressure gradient accompanying the transition to turbulence in the water phase limits the fractional

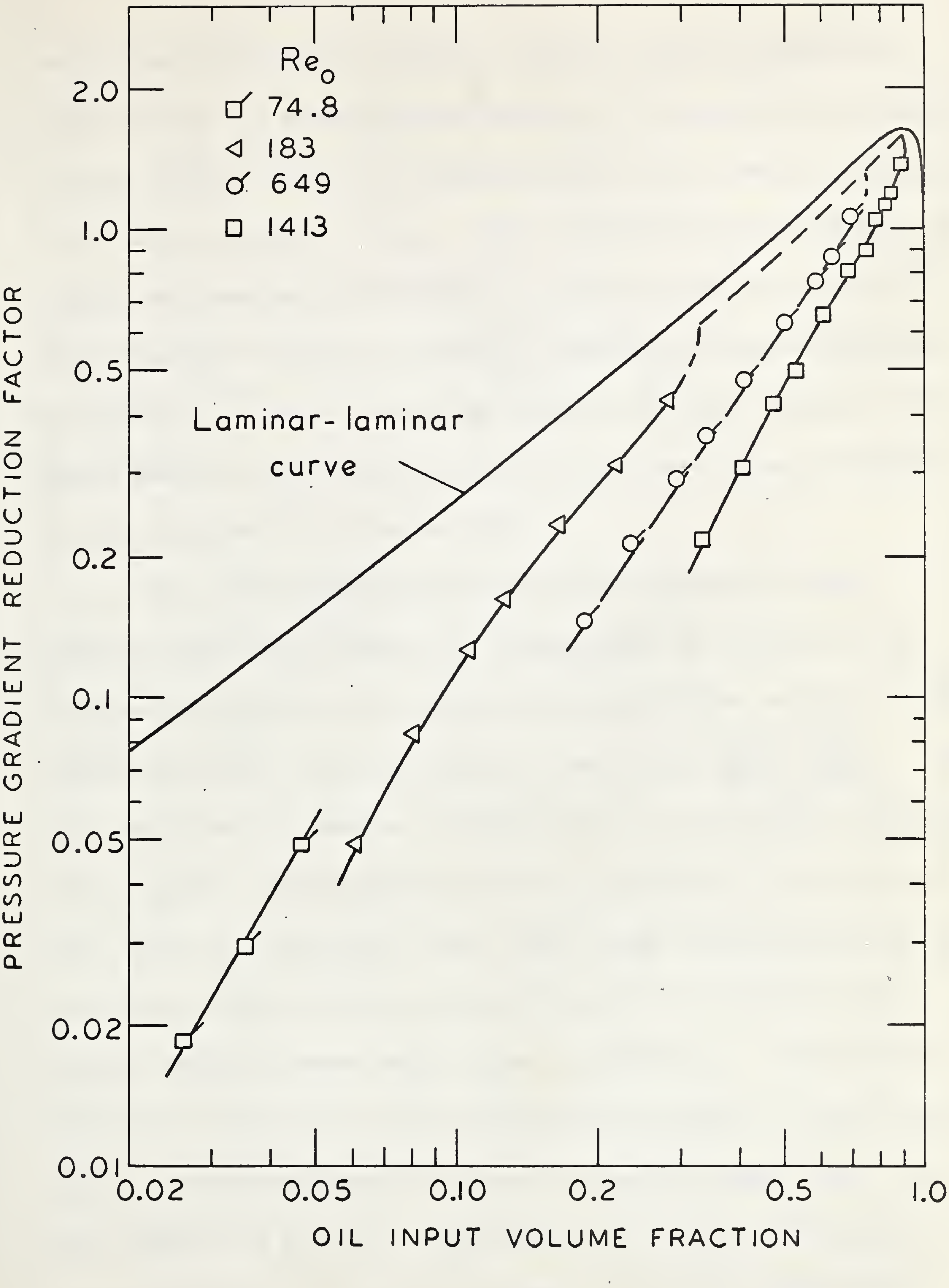

FIGURE 37 - LAMINAR-TURBULENT PRESSURE GRADIENT REDUCTION FACTORS

reduction in pressure gradient, which can be achieved for the flow of the more viscous phase at a given rate by adding a less viscous phase in turbulent flow, to a value less than the laminar-laminar value. This observation invalidates the tentative conclusion advanced by Charles and Redberger(13) that the high pressure gradient reduction factors obtained by Charles(11) were caused by much of the more viscous oil phase being transported in fast moving wave crests adjacent to the high velocity water layer.

All the pressure gradient data obtained in the laminar-turbulent regime are represented in Figure 38 by a Lockhart-Martinelli type correlation with the pressure gradient reduction factor plotted against the ratio $\left(\frac{\partial p}{\partial z}\right)_w \Big/ \left(\frac{\partial p}{\partial z}\right)_o$. The data fall very close to a single curve, the maximum deviation of any point being approximately 15 percent. The slope of the curve is relatively steep when large two-dimensional and roll waves were present at the interface, reflecting the higher energy losses under these conditions. The Lockhart-Martinelli curve for the corresponding regime of gas-liquid flow in circular pipes is also plotted for comparison. On this type of a plot the experimental data for stratified gas-liquid flow in circular pipes reported by Gazley(36),

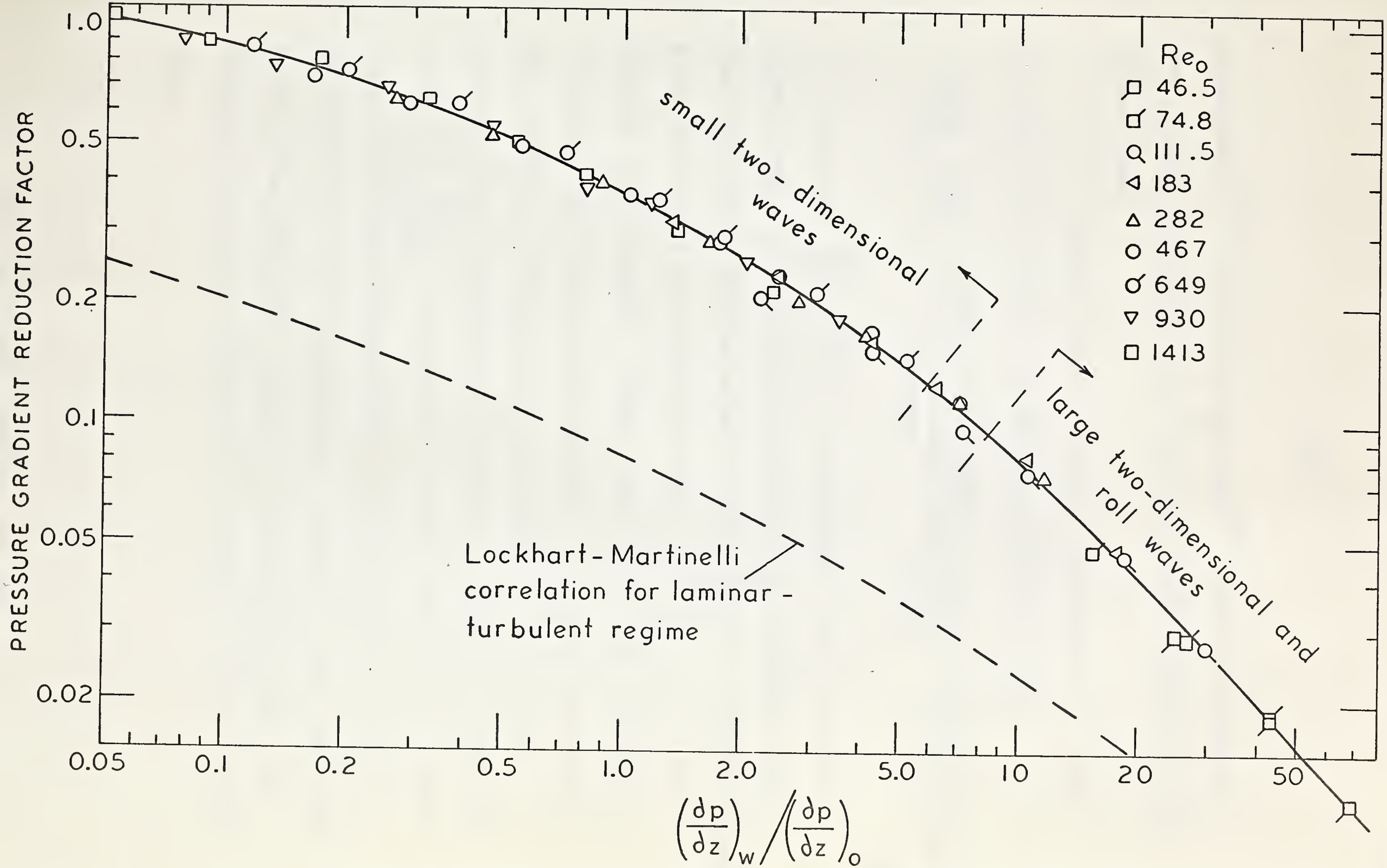

FIGURE 38 - CORRELATION OF LAMINAR-TURBULENT PRESSURE GRADIENT DATA

Hoogendoorn(44) and Govier and Omer(38) would fall between the Lockhart-Martinelli curve and the curve representing the present data.

It is readily shown, by using equations (12), (13), (14) and (17) that for the laminar-turbulent regime

$$\left(\frac{\partial p}{\partial z}\right)_w \Big/ \left(\frac{\partial p}{\partial z}\right)_o = \left(\begin{matrix}\text{function of aspect}\\ \text{ratio and equivalent}\\ \text{diameter}\end{matrix}\right)\left(\frac{\mu_o}{\mu_w}\right)^{-0.25}\left(\begin{matrix}\text{input}\\ \text{ratio}\end{matrix}\right)\left(Re_w\right)^{0.75} \tag{79}$$

i.e. the ratio $\left(\frac{\partial p}{\partial z}\right)_w \Big/ \left(\frac{\partial p}{\partial z}\right)_o$ is actually a function of the aspect ratio, the equivalent diameter, the viscosity ratio, the input ratio, and the water Reynolds number. In the present study the aspect and viscosity ratios, and the equivalent diameter were constant. Under these conditions, therefore, it appears that the pressure gradient reduction factor and the product of the input ratio and $(Re_w)^{0.75}$ should be reasonably good correlating parameters. Whether or not the ratio $\left(\frac{\partial p}{\partial z}\right)_w \Big/ \left(\frac{\partial p}{\partial z}\right)_o$ includes the correct functions of aspect ratio, equivalent diameter and viscosity ratio can only be determined by further experiments. However, other variables which may be important, notably the density ratio and the interfacial tension, would not be included in such a correlation.

(iv) Wave properties

Wave velocities were recorded for the three different wave types - the small two-dimensional waves, the large two-dimensional waves and the roll waves. The coincidence between the onset of turbulence in the water phase and the initiation of small two-dimensional waves suggested that these waves were generated and sustained by the turbulent pressure fluctuations in the water phase. It would be expected that the velocity of these waves would be a function of the linear velocity of the pressure fluctuations and, therefore, of the actual average velocity of the water phase. The wave velocities were, therefore, plotted against the average water velocity, as in Figure 39 which includes data for all wave types. Superimposed on the data is a line of unit slope. The data for the small two-dimensional waves fall very close to this line, indicating that the wave velocity was essentially the same as the actual water velocity. This provides further evidence that the small two-dimensional waves were directly related to the pressure fluctuations in the water phase. The theoretical approach of Phillips(73) should, therefore, be

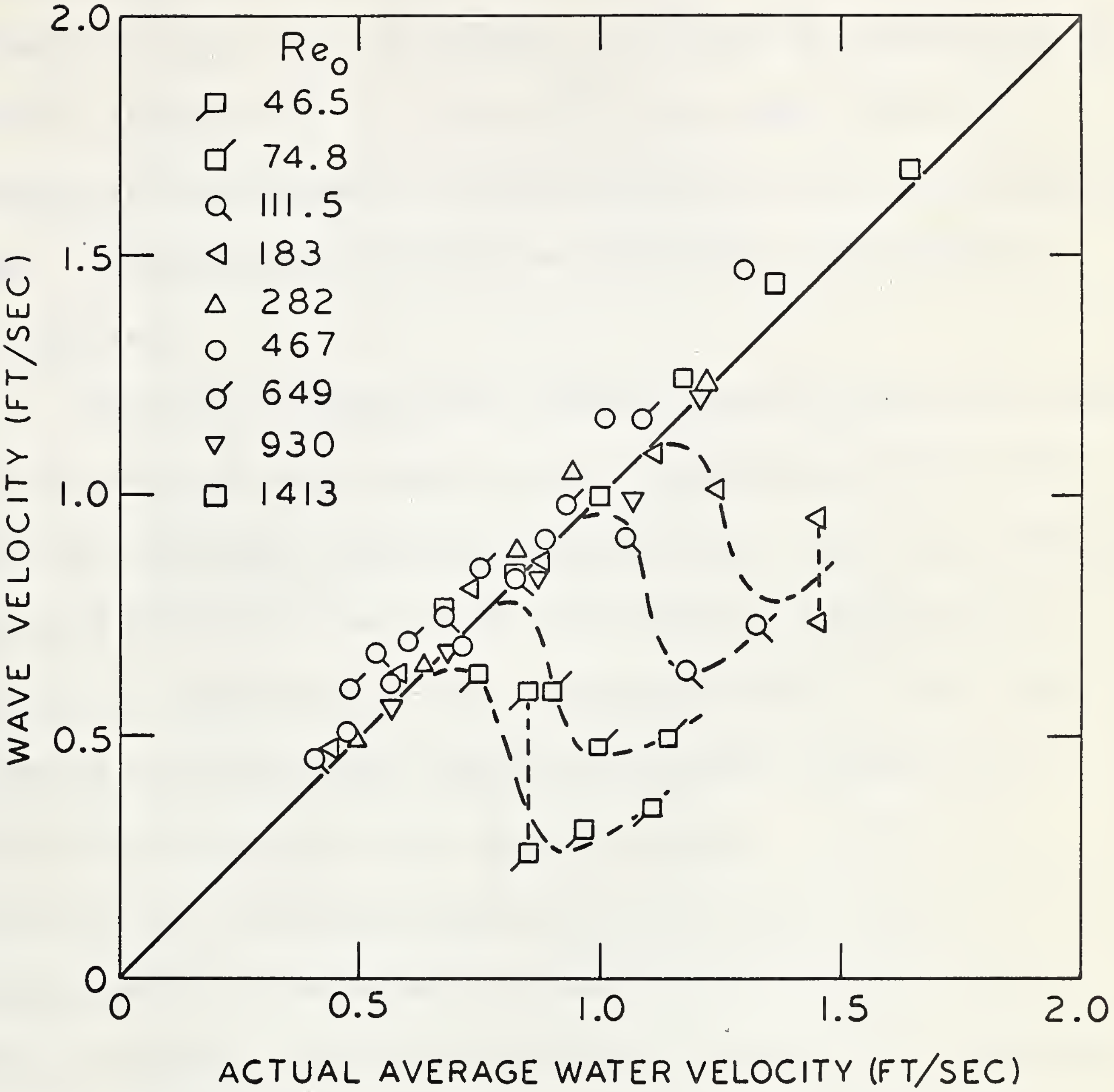

FIGURE 39 - LAMINAR-TURBULENT WAVE VELOCITIES

useful in characterizing these waves. That the waves observed were two-dimensional in character, and not three-dimensional as might be expected, is probably explained by the theoretical work of Jeffreys(48) and Squire(84) who showed that two-dimensional disturbances are more unstable than three-dimensional ones. Two-dimensional waves are, therefore, more likely to be observed.

Only the velocity data obtained for the large two-dimensional waves and roll waves deviate significantly from the line of unit slope. The velocities of the large two-dimensional and roll waves were very much less than the average water velocity. There is definite evidence in the data that the velocity of these waves increased with the average water velocity at a constant oil Reynolds number. It will be recalled that the small two-dimensional waves remained superimposed on the large two-dimensional waves and roll waves, although their two-dimensional character was then not so obvious. In one instance, at $Re_o = 46.5$ and an average water velocity of 0.854 ft./sec. it was possible to measure the velocity of both two-dimensional wave types. In Figure 39 the upper point at 0.596 ft./sec. represents the velocity of the small waves, and the lower one at 0.249 ft./sec. the velocity of the large waves.

The large two-dimensional waves appeared to be generated by a fundamental instability of the mean flow. If such is the case then theoretical approaches of the types offered by Lock(61) and Miles(68) for the air-water system should be useful in predicting the initiation of these waves. For liquid-liquid systems Keulegans's criterion, equation (2), is available for predicting interfacial instability. Large two-dimensional waves were first observed when the actual average water velocity was approximately 1 ft./sec. and this value compares with 0.4 ft./sec. calculated from Keulegan's criterion. The large discrepancy is, presumably, a consequence of the larger density ratio of the present study which would tend to stabilize the flow, for in other respects the experimental arrangements were similar.

The wavelength and amplitude of the large two-dimensional and roll waves were determined by the use of stereophotogrammetry, the theory and calibration procedure for which are described in Appendix E. Two representative stereo pairs of photographs are reproduced as positives in Figures 40 and 41. When viewing the negatives of these, and of the other, stereo pairs under the stereoscope a magnification of eight times was used.

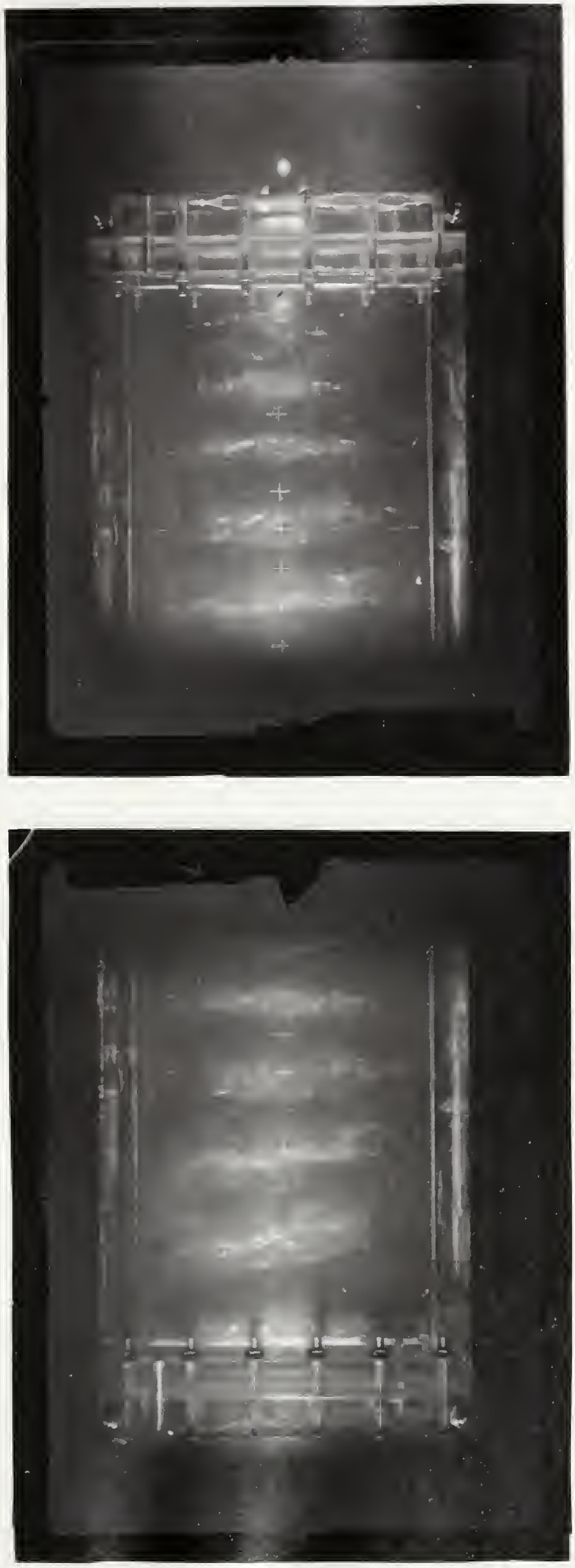

FIGURE 40 – STEREOPHOTOGRAPHS OF LARGE TWO-DIMENSIONAL WAVES

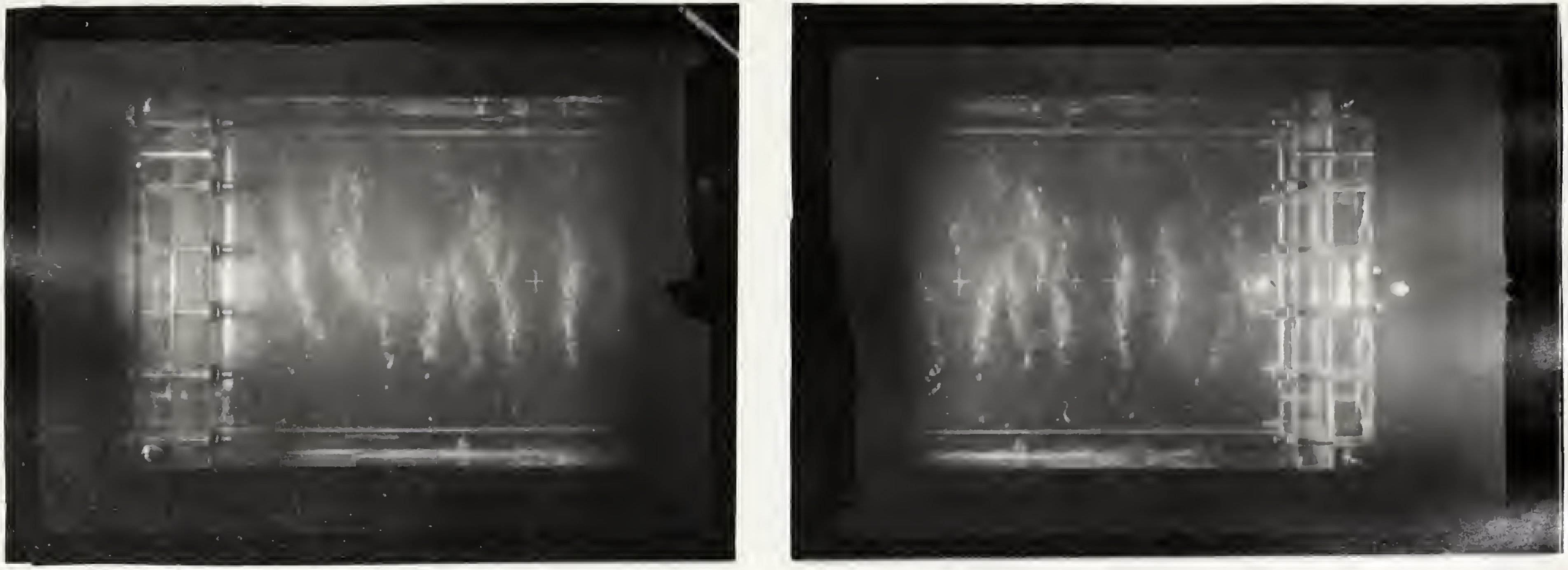

FIGURE 41 - STEREOPHOTOGRAPHS OF ROLL WAVES

The lighter bands in the photographs are caused by the preferential reflection of light from the aluminium powder at the interface when it coincided with the wave slopes facing the electronic flash. The flash was situated to the left of the photographs.

The regular, equally spaced nature of the large two-dimensional waves is evident in Figure 40 for which $Re_o = 74.8$ and $Re_w = 13700$, and, in comparison, the irregular nature of the roll waves is apparent in Figure 41 for which $Re_o = 74.8$ and $Re_w = 18130$.

The wavelengths and amplitudes for the different wave types are tabulated in Table III. At a given oil Reynolds number the wavelength tended to decrease from about three inches to two inches as the water Reynolds number increased, although the wavelength was highly variable for the roll waves. The decreasing wavelength is compatible with the increasing wave velocity previously noted in Figure 39. The amplitude of the waves also decreased slightly as the water Reynolds number increased, i.e. as the thickness of the oil layer decreased.

Table III

Data for Large Two-Dimensional and Roll Waves

Superficial Oil Reynolds Number	Superficial Water Reynolds Number	Wave Type	Wavelength (inches)	Wave Amplitude (mm)
183	18130	large 2-d	1.8	-
183	15800	large 2-d	2.0	0.21
183	13700	large 2-d	2.4	0.36
111.5	18130	roll	1.2-1.6	-
111.5	15800	large 2-d	1.8	-
111.5	13700	large 2-d	2.0	1.13
74.8	18130	roll	0.4-2.6	0.70
74.8	15800	large 2-d	1.96	0.60
74.8	13700	large 2-d	2.2	0.53
74.8	11800	large 2-d	3.0	1.11
46.5	18130	roll	1.4-3.0	-
46.5	15800	roll	2.6	0.58
46.5	13700	large 2-d	1.8	0.61
46.5	11800	large 2-d	2.0	0.85
46.5	10000	large 2-d	2.7	-

average amplitude for large two-dimensional waves = 0.70 mm

average amplitude for roll waves = 0.64 mm

4. Turbulent-turbulent regime

With the water in turbulent flow the transition to turbulence in the oil phase caused a further sharp increase in the pressure gradient and tended to destroy the two-dimensional character of the interfacial waves. At the highest flow rates attainable with the equipment the wave pattern was essentially three-dimensional, the amplitude of the waves being considerably greater than that of the small two-dimensional waves. The transition to a three-dimensional wave structure was gradual and appeared to be caused by the interaction of the pressure fluctuations in the two phases. No quantitative measurements of the three-dimensional wave properties were obtained.

Pressure gradient data for oil Reynolds numbers of 2330 and 3330 are plotted, along with the theoretical laminar-laminar curve, in Figure 42 which is directly comparable with Figure 37. At the lower of the oil Reynolds numbers the oil was in laminar flow when flowing alone and consequently the pressure gradient reduction factors were relatively low. On the other hand, at the higher Reynolds number the oil was in turbulent flow when flowing alone and the pressure gradient reduction factors were more favorable. The curves are relatively steep compared with those in the laminar-turbulent regime, and

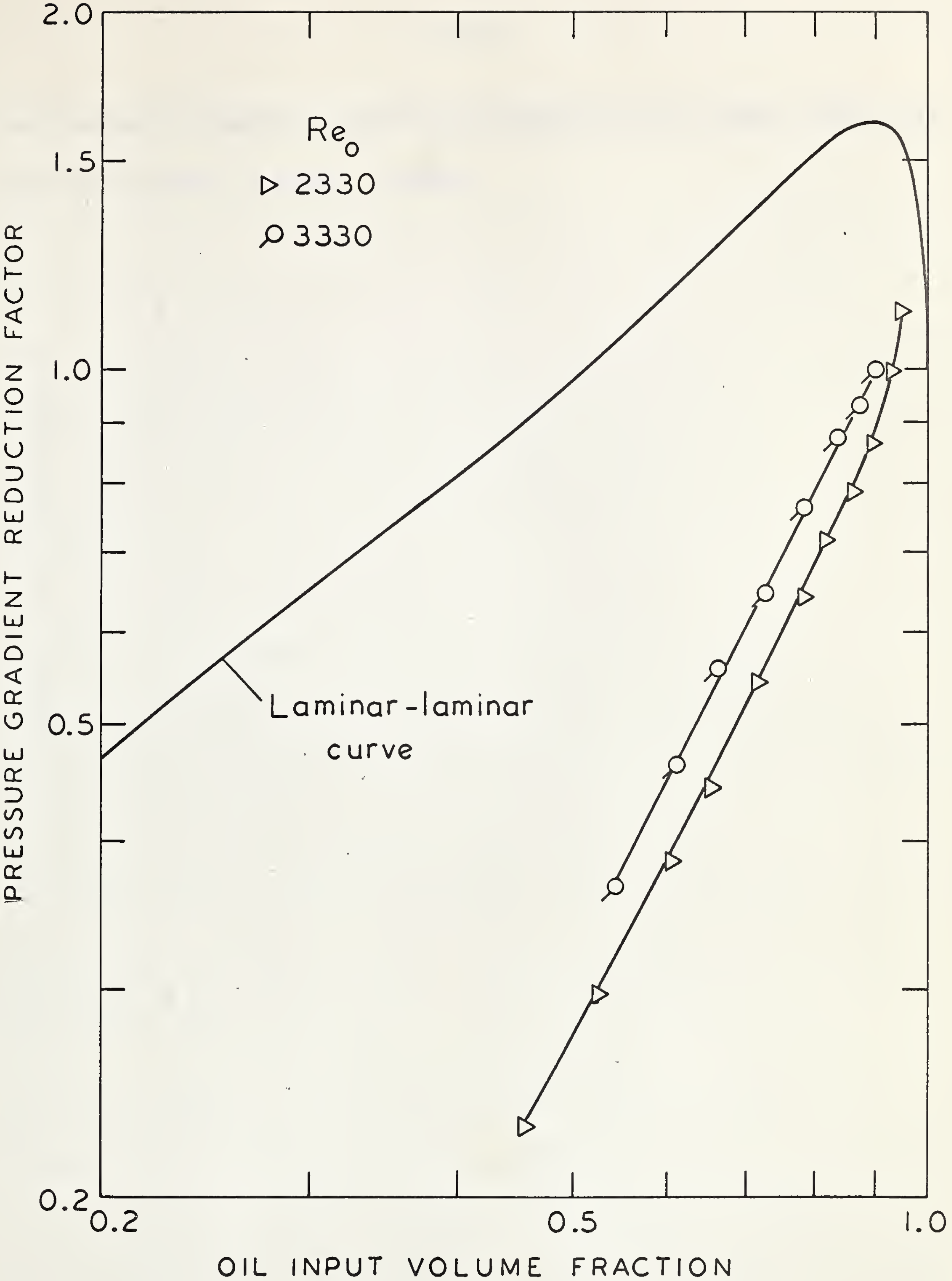

FIGURE 42 - TURBULENT-TURBULENT PRESSURE GRADIENT REDUCTION FACTORS

the pressure gradient reduction factors were always much less than the laminar-laminar values.

VI CONCLUSIONS

1. The theoretical expressions obtained for the velocity distributions and volumetric flow rates for the laminar, stratified flow of two immiscible liquids in a rectangular conduit were reasonably well verified for arbitrary viscosity and aspect ratios of 5.326 and 7.95:1 respectively. The computed theoretical results which cover viscosity ratios from 1 to 1000 and aspect ratios from 8:1 to 1:3 can therefore be used with confidence. Theory predicted that substantial reductions in pressure gradient can be achieved for the flow of a viscous liquid at a given rate in a rectangular conduit by the addition of a second less viscous liquid. For a viscosity ratio of 1000 the maximum pressure gradient reduction factor was 3.38 for an aspect ratio of 7.896:1 and 1.13 for an aspect ratio 1:3.

2. The critical Reynolds number for single-phase flow in the rectangular conduit was 2300. With the two-phase system the transition to turbulence in the water phase occurred at a higher Reynolds number in the presence of a laminar oil layer provided the input water to oil ratio was relatively high, while the transition in the oil phase took place at a lower

Reynolds number in the presence of a turbulent water layer.

3. Small two-dimensional waves appeared at the oil-water interface upon the transition to turbulence in the water phase and the velocity of these waves was essentially the same as the actual average water velocity. It appeared therefore that these small two-dimensional waves were generated and sustained by the pressure fluctuations in the turbulent less viscous phase.

4. At relatively low oil flow rates and relatively high water flow rates large two-dimensional and roll waves were observed. The velocity of these waves was considerably less than the actual average water velocity and they appeared to be the result of a basic instability of the mean flow.

5. In the laminar-turbulent regime the experimentally determined interface velocities, insitu ratios, and pressure gradient reduction factors deviated considerably from the laminar-laminar values. In particular, the pressure gradient reduction factors were always much lower than the laminar-laminar values. Lockhart-Martinelli type parameters were found to correlate the laminar-turbulent pressure gradient data very well.

6. The stereophotogrammetric technique yielded good estimates of the amplitudes of the large two-dimensional and roll waves. The accuracy of the method could be greatly improved by the use of cameras having wider fields of view. The cameras could then be positioned closer to the interface and farther apart so that parallaxes would be increased.

7. It would be interesting to extend the present investigation to cover higher water flow rates so that the transition to dispersed flow could be located, to obtain data for different viscosity and aspect ratios, and to predict theoretically the onset of the large two-dimensional waves from small disturbance principles.

VII NOMENCLATURE

a_i = coefficients in equation (104)

2a = width of rectangular conduit

actual average water velocity = $\dfrac{\text{water flow rate}}{\text{(depth of water) (width of conduit)}}$

A = quantity defined by equation (85)

$A_1(n)$ = coefficient defined by equation (50)

$A_2(n)$ = coefficient defined by equation (51)

$A_1'(n)$ = coefficient defined by equation (59)

$A_2'(n)$ = coefficient defined by equation (59)

2b = depth of rectangular conduit

b_1 = depth of lower less viscous phase in stratified flow

b_2 = depth of upper more viscous phase in stratified flow

B = quantity defined by equation (86)

$B_1(n)$ = coefficient defined by equation (52)

$B_2(n)$ = coefficient defined by equation (53)

$B_1'(n)$ = coefficient defined by equation (60)

$B_2'(n)$ = coefficient defined by equation (61)

c_i = coefficients in equation (103)

C = quantity defined by equation (87)

d = diameter of particle

D = diameter of circular pipe

D_e = equivalent diameter of non-circular conduit defined as four times the cross-sectional area divided by the wetted perimeter

E = difference between fluid and particle velocities

f = Fanning friction factor defined by equation (13)

g = gravitational acceleration

g_c = dimension conversion factor

h = elevation of point above datum plane

Δh_a = actual elevation difference

Δh_b = basic elevation adjustment

Δh_c = calculated crude elevation difference

Δh_r = refraction elevation adjustment

H = height of datum plane above camera lenses

holdup ratio = input ratio divided by insitu ratio

i = integer

input ratio = $\frac{Q_1}{Q_2}$

insitu ratio = $\frac{b_1}{b_2}$

k = $\frac{g_c}{\mu}\frac{\partial p}{\partial z}$ except in equation (76) where k = thermal conductivity

m = viscosity ratio $\frac{\mu_2}{\mu_1}$ and actual mass of particle

m* = virtual mass of particle

m' = induced mass of particle

M = number of sets of data in equation (109)

n = $\frac{(2i+1)\pi}{2a}$ except in equations (10), (11) and (12) where $n = 1,3,5....$

N = number of sets of data in equation (108)

p = pressure

P = parallax defined by equations (96) and (97)

pressure gradient reduction factor = $\left(\frac{\partial p}{\partial z}\right)_2 \Big/ \left(\frac{\partial p}{\partial z}\right)_{tp}$

q = heat generated/unit volume/unit time

Q = flow rate

Q_1 = flow rate of less viscous phase

Q_2 = flow rate of more viscous phase

R = density ratio (air/water)

Re = Reynolds number for flow in a circular pipe = $\frac{\rho VD}{\mu}$

Re' = Reynolds number for flow in a non-circular conduit = $\frac{\rho VD_e}{\mu}$

Re'_o = superficial oil Reynolds number in two-phase flow = $\frac{\rho_o V_o D_e}{\mu_o}$

Re'_w = superficial water Reynolds number in two-phase flow = $\frac{\rho_w V_w D_e}{\mu_w}$

relative interface position = $\frac{b_2}{b_1 + b_2}$

S = sheltering coefficient and transformed variable

t = time

T = temperature

V = average velocity for single-phase flow in a circular pipe or rectangular conduit defined by flow rate divided by cross-sectional area of conduit

V_p = vertical velocity of particle

V' = actual average fluid velocity in two-phase flow defined by flow rate divided by cross-sectional area occupied by fluid

V_o = superficial oil velocity in two-phase flow defined by oil flow rate divided by cross-sectional area of conduit

V_w = superficial water velocity in two-phase flow defined by water flow rate divided by cross-sectional area of conduit

V_{pp} = average velocity for the flow of the more viscous phase between parallel plates under the theoretical two-phase pressure gradient

V_{rc} = average velocity for flow of more viscous phase in a rectangular conduit under the theoretical two-phase pressure gradient

w = local fluid velocity in z-direction

w_1 = local velocity of less viscous fluid

w_2 = local velocity of more viscous fluid

w_i = local interface velocity

w_m = maximum velocity in parabolic profile

w_f = local fluid velocity in z-direction

w_p = particle velocity in z-direction

W = variable defined by equation (27)

x = Cartesian co-ordinate

X = Lockhart-Martinelli parameter defined by equation (4)

y = Cartesian co-ordinate

y_m = value of y for which E is a maximum

Y = variable defined by equation (35)

z = Cartesian co-ordinate

z_1 and z_2 = distances on stereo-negatives defined in Figure 49

γ = intermittency factor

θ = constant defined by equation (2)

μ = dynamic viscosity

μ' = dynamic viscosity of fluid particle

ν = kinematic viscosity

ρ = density

Γ_g = gas phase velocity profile factor in equation (5)

ϕ = Lockhart-Martinelli parameter defined by equation (3)

Subscripts

1 = fluid 1 or object 1

2 = fluid 2 or object 2

a = air

f = fluid

g = gas

o = oil

p = particle

w = water

j = 1 or 2

VIII BIBLIOGRAPHY

1. Anon, "Physical characteristics of Kodak glass base plates", Kodak Pamphlet Q-35, Eastman Kodak Co., Rochester, New York.

2. Baker, W.H., "Elements of photogrammetry", Ronald Press, New York (1960).

3. Bartell, F.E., and Miller, F.L., "A method for the measurement of interfacial tension of liquid-liquid systems", Jour. Amer. Chem. Soc., 50, 1961 (1928).

4. Benjamin, T.B., "Shearing flow over a wavy boundary", Jour. Fluid Mech., 6, 161 (1959).

5. Benjamin, T.B., "Effects of a flexible boundary on hydrodynamic stability", Jour. Fluid Mech., 9, 513 (1960).

6. Bentwich, M., "Two-phase flow in a circular pipe", Private communication, Aeronautics Department, Imperial College of Science and Technology, London, (1962).

7. Birkhoff, G., "Hydrodynamics - A study in logic, fact and similitude", Princeton Univ. Press, Princeton, N.J., (1960).

8. Brobikov, I.S., "The derivation of a generalised function for the propagation of the heights of waves on the surface of a heavy liquid" (in Russian), Trudi Gos. Okeanogr. ln-ta, 42, 105, (1958).

9. Bunt, B.P., "Measurement of thickness of thin transparent films using fluorescence", Brit. Jour. Appl. Phys., 12, 175, (1961).

10. Charles, M.E., "Horizontal pipeline flow of equal density oil and water mixtures", M.Sc. Thesis, Department of Chemical and Petroleum Engineering, University of Alberta, (1960).

11. Charles, M.E., "The reduction of pressure gradients in oil pipelines: experimental results for the stratified flow of a heavy crude oil and water", Can. Inst. Min. Met., Trans., 63, 305, 1960.

12. Charles, M.E., Govier, G.W., and Hodgson, G.W., "Horizontal pipeline flow of equal density oil-water mixtures", Can. Jour. Chem. Eng., 39, 27, (1961).

13. Charles, M.E. and Redberger, P.J., "The reduction of pressure gradients in oil pipelines by the addition of water: numerical analysis of stratified flow", Can. Jour. Chem. Eng., 40, 70, (1962).

14. Chilton, E.G., and Handley, L.R., "Method and apparatus for lubricating pipelines", U.S. Patent, 2, 821, 205 (1958).

15. Claibourne, H.C., "A critical review of the literature on pressure drop in non-circular ducts and annuli", Oak Ridge National Laboratory ORNL-1248.

16. Clark, A.F., and Shapiro, A., "Method of pumping viscous petroleum", U.S. Patent 2, 533, 878 (1950).

17. Cornish, R.J., "Flow in a pipe of rectangular cross-section", Proc. Roy. Soc. A120, 691, (1928).

18. Craya, A., "Theoretical research on the flow of non-homogeneous fluids", La Houille Blanche 4, 44, (1949).

19. Davies, J.T., "Some effects of surface-active agents on waves and ripples", Chemistry and Industry, p. 906, May 26, 1962.

20. Davies, J.T. and Rideal, E.K., "Interfacial Phenomena", Academic Press, New York (1961).

21. Deardorff, J.W., "On the stability of viscous plane Couette flow", Jour. Fluid Mech., 15, 623, (1963).

22. Drazin, P.G., and Howard, L.N., "Stability in a continuously stratified fluid", Jour. Eng. Mech. Div., Proc. Amer. Soc. Civ. Engrs., 87, EM6, 101 (1961).

23. Dukler, A.E. and Bergelin, O.P., "Wave forms for liquids flowing down polished flat plates measured with a capacitometer and oscillograph", Chem. Eng. Progress, 48, 557, (1952).

24. Dumitrescu, L. and Staniscu, C., "A boundary problem and its application to the flow of two viscous fluids in contact, and to the torsion of a non-homogeneous bar", Acad. Rep. Populare Romine, Rev. Mecan. Appl., 2, 2, (1957).

25. Eckart, C., "The generation of wind waves over a water surface", Jour. Appl. Phys. 24, 1485, (1953).

26. Eckert, E.R.G. and Irvine, T.F., "Incompressible friction factor, transition, and hydrodynamic entrance length studies of ducts with triangular and rectangular cross-sections", Proc. Fifth Midwestern Conf. on Fluid Mech., Univ. of Michigan Press, p. 122, (1957).

27. Ekman, V.W., "On the change from laminar to turbulent motion of liquids", Archiv fur Math. Astr. och Fys., 6, No. 12, (1910).

28. Eliassen, A., Høiland, E. and Riis, E., "Two-dimensional perturbations of a flow with constant shear of a stratified fluid", Inst. for Weather and Climate Research, Norwegian Academy of Science and Letters, Publication No. 1, (1953).

29. Ellis, S.R. and Gay, B., "The parallel flow of two fluid streams: interfacial shear and fluid-fluid interaction", Trans. Inst. Chem. Engrs., London, 37, 206, (1959).

30. Esch, R.E., "Stability of the parallel flow of a fluid over a slightly heavier fluid", Jour. Fluid Mech., 12, 192, 1962.

31. Esch, R.E., "The instability of a shear layer between two parallel streams", Jour. Fluid Mech., 3, 289, (1957).

32. Feldman, S., "On the hydrodynamic stability of two viscous incompressible fluids in parallel uniform shearing motion", Jour. Fluid Mech., 2, 343, (1957).

33. Gaffyn, J.E. and Underwood, R.M., "An improved method for the measurement of the velocity profiles in liquids", Nature, 169, 239, (1952).

34. Gallagher, A.P. and Mercer, A. McD., "On the behaviour of small disturbances in plane Couette flow", Jour. Fluid Mech., 13, 91, (1962).

35. Gariel, P., "Experimental research on the flow of non-homogeneous fluids", La Houille Blanche, 4, 56, (1949).

36. Gazley, C., "Interfacial shear and stability in two-phase flow", Ph.D. Thesis, Department of Chemical Engineering, University of Delaware, (1948).

37. Gemmell, A.R., and Epstein, N., "Numerical analysis of stratified laminar flow of two immiscible Newtonian liquids in a circular pipe", Can. Jour. Chem. Eng., 40, 215, (1962).

38. Govier, G.W., and Omer, M.M., "The horizontal pipeline flow of air-water mixtures", Can. Jour. Chem. Eng., 40, 93, (1962).

39. Graebel, W.P., "The stability of a stratified flow", Jour. Fluid Mech., 8, 321, (1960).

40. Hanratty, T.J., and Engen, J.M., "Interaction between a turbulent air stream and a moving water surface", A.I.Ch.E. Jour., 3, 299, (1957).

41. Hanratty, T.J., and Hershman, A., "Initiation of roll waves", A.I.Ch.E. Jour., 7, 488, (1961).

42. Hinze, J.O., "Turbulence - An introduction to its mechanism and theory", McGraw-Hill Book Co., Inc., New York, (1959).

43. Hodgman, C.D., "Handbook of Chemistry and Physics", Chemical Rubber Publishing Co., Ohio, (1949).

44. Hoogendoorn, C.J., "Gas-liquid flow in horizontal pipes", Chem. Eng. Sci., 9, 205, (1959).

45. Hyzer, W.G., "Engineering and Scientific High Speed Photography", The MacMillan Company, New York (1962).

46. Ippen, A.T. and Harleman, D.R.F., "Steady-state characteristics of sub-surface flow", Proc. Semicentennial Symposium on gravity waves, U.S. Nat. Bur. Stds., Circular 521, (1952).

47. Isaacs, J.D., and Speed, J.B., U.S. Patent 759, 374 (1904).

48. Jeffreys, H., "On the formation of water waves by wind", Proc. Roy. Soc., A107, 189, (1925).

49. Johnson, J.W., and Rice, E.K., "A laboratory investigation of wind generated waves", Trans. Amer. Geophys. Union, 33, 845, (1952).

50. Keeping, E.S., "Introduction to statistical inference", D. Van Nostrand Co., Inc., New York, (1962).

51. Keulegan, G.H., "Interfacial instability and mixing in stratified flows", Jour. of Research, U.S. Nat. Bur. Stds., 43, 487, (1949).

52. Keulegan, G.H., "Wind tides in small closed channels", Jour. of Research, U.S. Nat. Bur. Stds., 46, 358, (1951).

53. Knudsen, J.G. and Katz, D.L., "Fluid dynamics and heat transfer", McGraw-Hill Book Co., Inc., New York, (1958).

54. Knuth, E.L., "The mechanics of film cooling", Jet Propulsion, 24, 359, (1954).

55. Lamb, H., "Hydrodynamics", 6th edition, Cambridge Univ. Press, p. 630, (1959).

56. Ibid., p. 461.

57. Leite, R.J., "An experimental investigation of the stability of Poiseuille flow", Jour. Fluid Mech., 5, 81, (1959).

58. Lilleleht, L.U., and Hanratty, T.J., "Measurement of interfacial structure for co-current air-water flow", Jour. Fluid Mech., 11, 65, (1961).

59. Lilleleht, L.U., and Hanratty, T.J., "Relation of interfacial shear stress to the wave height for co-current air-water flow", A.I.Ch.E. Jour., 7, 548, (1961).

60. Lin, C.C., "The theory of hydrodynamic stability", Cambridge Univ. Press, (1955).

61. Lock, R.C., "Hydrodynamic stability of the flow in the laminar boundary layer between parallel streams", Proc. Camb. Phil. Soc., 50, 105, (1954).

62. Lockhart, R.W., and Martinelli, R.C., "Proposed correlation of data for isothermal two-phase, two-component flow in pipes", Chem. Eng. Progress, 45, 39, (1949).

63. Lofquist, K., "Flow and stress near an interface between stratified liquids", Physics of Fluids, 3, 158. (1960).

64. Long, R.R., "Some aspects of the flow of stratified fluids. III Continuous density gradients", Tellus, 7, 341 (1955).

65. Long, R.R., "Some aspects of the flow of stratified fluids. I A theoretical investigation", Tellus, 5, 42, (1953).

66. Long, R.R., "Some aspects of the flow of stratified fluids. II Experiments with a two-fluid system", Tellus, 6, 97, (1954).

67. Macagno, E.O., and Rouse, H., "Interfacial mixing in stratified flow", Jour. Eng. Mech. Div., Proc. Amer. Soc. Civ. Engrs., 87, EM5, 55, (1961).

68. Miles, J.W., "On the generation of surface waves by shear flows", Jour. Fluid Mech., 3, 185, (1957).

69. Mittendorf, G.H., "The instability of stratified flow", M.Sc. thesis, State Univ. of Iowa, Iowa, (1961).

70. Mologin, M.S., "Wave motion on the surface of separated flow in horizontal pipes" (in Russian), Zh. Tekh. Fiz., 26, 1768, (1956).

71. Nedderman, R.M., "The use of stereoscopic photography for the measurement of velocities in liquids", Chem. Eng. Sci., 16, 113, (1961).

72. Nikuradse, J., "Investigations of turbulent flows in non-circular ducts", Ing.-Arch., 1, 306, (1930).

73. Phillips, O.M., "On the generation of waves by turbulent wind", Jour. Fluid Mech., 2, 417, (1957).

74. Reynolds, O., "An experimental investigation of the circumstances which determine whether the motion of water shall be direct or sinuous, and the laws of resistance in parallel channels", Phil. Trans. Roy. Soc. (London), 174A, 935, (1883).

75. Robertson, J.M., "On turbulent plane-Couette flow", Proc. 6th Midwestern Conf. on Fluid Mech., Univ. of Texas, p. 169, (1959).

76. Rotta, J., "An experimental investigations of the origin of turbulent flow in a pipe", Ing-Arch 24, 258 (1956).

77. Russell, Scott, "Report on waves", Brit. Assoc. Report (1844).

78. Russell, T.W.F. and Charles, M.E., "The effect of the less viscous liquid in the laminar flow of two immiscible liquids", Can. Jour. Chem. Eng., 37, 18, (1959).

79. Russell, T.W.F., Hodgson, G.W., and Govier, G.W., "Horizontal pipeline flow of mixtures of oil and water", Can. Jour. Chem. Eng., 37, 9, (1959).

80. Sawistowski, H., and Goltz, G.E., "The effect of interface phenomena on mass transfer rates in liquid-liquid extraction", Trans. Inst. Chem. Engrs. (London), 41, 174, (1963).

81. Schlichting, H., "Boundary layer theory", McGraw-Hill Book Co., Inc., New York, (1960).

82. Schumacher, A., "Results of Exact wave measurements (by stereophotogrammetry) with special reference to the more recent theoretical investigation", U.S. Nat. Bur. Stds., Circ 521, p. 69, (1952).

83. Sparrow, E.M., "Laminar flow in isosceles triangular ducts", A.I.Ch.E. Jour., 8, 599, (1962).

84. Squire, H.B., "On the stability of three-dimensional disturbances of viscous flow between parallel walls", Proc. Royal Soc., A142, 621, (1933).

85. Sternling, C.V. and Scriven, L.E., "Interfacial turbulence: Hydrodynamic instability and the Marangoni effect", A.I.Ch.E. Jour., 5, 514, (1959).

86. Taylor, G.I., "Effect of variation in density on the stability of superposed streams of fluid", Proc. Roy. Soc., A 132, 499, (1931).

87. Taylor, G.I., "An experiment on the stability of superposed streams of fluid", Proc. Camb. Phil. Soc., 23, 730, (1927).

88. Thompson, E.H., "Heights from parallax measurements", The Photogrammetric Record, 1, No. 4, 38, (1954).

89. Ursell, F., "Wave generation by wind" in "Surveys in Mechanics", Ed. G.K. Barchelor and R.M. Davies, Cambridge Univ. Press, p. 216, (1956).

90. Van Driest, E.R., "Experimental investigation of turbulence diffusion - a factor in transportation of sediment in open-channel flow", Jour. Appl. Mech., 12, A91, (1945).

91. Van Rossum, J.J., "Experimental investigation into wave formation, atomization and film thickness in horizontal liquid films", Chem. Eng. Sci., 11, 35, (1959).

92. Walker, J.E., Whan, G.A. and Rothfus, R.R., "Fluid friction in non-circular ducts", A.I.Ch.E. Jour., 3, 484, (1957).

93. Wasow, W., "On small disturbances of plane Couette flow", Jour. of Res. U.S. Nat. Bur. of Stds., 51, 195, (1953).

94. Wuest, W., "Theory of the origin of wind generated water waves", Z. angew. Math. Mech., 29, 239, (1949).

95. Yih, C.S., "On the flow of stratified fluid", Proc., Third U.S. Natl. Congress of Applied Mech., p. 857, (1958).

96. Yih, C.S., "On stratified flows in a gravitational field", Tellus 9, 220, (1957).

97. Zondek, B. and Thomas, L.H., "Stability of a limiting case of plane Couette flow", Physical Rev., 90, 738, (1953).

IX APPENDICES

APPENDIX A

NUMERICAL DATA EVALUATED FROM LAMINAR STRATIFIED FLOW THEORY

Table A1 contains the velocity data used to prepare Figures 4 and 5. The data for the vertical velocity profiles, i.e. at x = 0 appear in Table A1(a) and the data for the interfacial velocity profiles, i.e. at y = 0, appear in Table A1(b).

Table A2 contains the numerical data used to prepare Figures 6-15. The table is subdivided according to aspect ratio and viscosity ratio.

Table A3 gives the numerical data for an aspect ratio of 7.95:1 and a viscosity ratio of 5.326. These data were used to plot the theoretical laminar-laminar curves in Figures 32-37 and 42.

TABLE A1

THEORETICAL VELOCITY DATA

Table A1(a) Velocity ratios, $\frac{W_j}{V_{pp}}$ for vertical velocity profiles at $x = 0$

aspect ratio = 7.95:1 viscosity ratio = 5.326

Distance from bottom of conduit divided by depth of conduit	Relative Interface Position				
	0.1	0.3	0.5	0.7	0.9
0.1	0.522	0.633	0.720	0.766	0.706
0.2	3.048	1.196	1.350	1.427	1.290
0.3	4.967	1.626	1.858	1.960	1.751
0.4	6.204	3.327	2.247	2.386	2.091
0.5	6.787	4.425	2.503	2.683	2.316
0.6	6.753	4.847	3.289	2.866	2.422
0.7	6.103	4.636	3.448	2.920	2.405
0.8	4.796	3.760	2.960	2.616	2.264
0.9	2.840	2.293	1.863	1.657	2.008

Table A1(b) Velocity ratios, $\frac{W_i}{V_{pp}}$ for interfacial velocity profiles at y = 0

viscosity ratio = 5.326 relative interface position = 0.9

	Aspect Ratio			
$\frac{x}{a}$	7.95:1	3:1	1:1	1:3
0	2.010	1.907	0.9420	0.1888
0.1	2.008	1.897	0.9338	0.1873
0.3	2.005	1.845	0.8702	0.1732
0.4	2.008	1.778	0.8121	0.1609
0.5	1.991	1.686	0.7364	0.1448
0.7	1.892	1.346	0.5236	0.1006
0.8	1.736	1.070	0.3828	0.0721
0.9	1.279	0.629	0.2090	0.0385

TABLE A2

Theoretical pressure gradient reduction factors and holdup ratios for viscosity ratios from 1 to 1000 and aspect ratios from 7.896:1 to 1:3.

Table A2(a)

Aspect Ratio = 7.896:1

(i) Viscosity Ratio = 1

Relative Interface Position	Insitu Ratio	Input Ratio	Pressure Gradient Reduction Factor	Holdup Ratio
1.000	0	0	1.000	-
0.900	0.1111	0.02943	0.970	0.2649
0.800	0.2500	0.1172	0.893	0.4686
0.700	0.4286	0.2777	0.782	0.6480
0.600	0.6667	0.5451	0.646	0.8177
0.500	1.000	1.000	0.499	1.000
0.400	1.500	1.834	0.353	1.223
0.300	2.333	3.601	0.217	1.543
0.200	4.000	8.536	0.1047	2.134
0.100	9.000	33.98	0.0287	3.776

(ii) Viscosity Ratio = 5.259

Relative Interface Position	Insitu Ratio	Input Ratio	Pressure Gradient Reduction Factor	Holdup Ratio
1.000	0	0	1.000	-
0.950	0.05263	0.02297	1.418	0.4364
0.900	0.1111	0.06661	1.582	0.5995
0.850	0.1765	0.1253	1.607	0.7100
0.800	0.2500	0.2019	1.554	0.8078
0.750	0.3333	0.3028	1.453	0.9084
0.700	0.4286	0.4376	1.326	1.021
0.650	0.5385	0.6207	1.185	1.153
0.600	0.6667	0.8740	1.038	1.311

Relative Interface Position	Insitu Ratio	Input Ratio	Pressure Gradient Reduction Factor	Holdup Ratio
0.550	0.8182	1.232	0.891	1.505
0.500	1.000	1.748	0.750	1.748
0.450	1.222	2.512	0.615	2.055
0.400	1.500	3.682	0.491	2.455
0.350	1.857	5.567	0.379	2.998
0.300	2.333	8.698	0.280	3.728
0.250	3.000	14.33	0.1951	4.778
0.200	4.000	25.54	0.1252	6.384
0.150	5.667	51.88	0.0702	9.155
0.100	9.000	132.3	0.0312	14.70
0.050	19.000	590.6	0.00790	31.09

(iii) Viscosity Ratio = 10

1.000	0	0	1.000	
0.975	0.02564	0.01112	1.480	0.4338
0.950	0.05263	0.02989	1.735	0.5679
0.925	0.08108	0.05269	1.870	0.6498
0.900	0.1111	0.07920	1.925	0.7128
0.875	0.1429	0.1097	1.933	0.7682
0.850	0.1765	0.1452	1.920	0.8227
0.800	0.2500	0.2345	1.810	0.9381
0.700	0.4286	0.5327	1.485	1.243
0.600	0.6667	1.145	1.132	1.718
0.500	1.000	2.481	0.799	2.481
0.400	1.500	5.643	0.515	3.762
0.300	2.333	14.28	0.289	6.121
0.200	4.000	44.44	0.1278	11.11
0.100	9.000	241.6	0.0315	26.84

(iv) Viscosity Ratio = 50

1.000	0	0	1.000	--
0.975	0.02564	0.02009	2.39	0.7833
0.950	0.05263	0.04490	2.64	0.8532
0.925	0.08108	0.07542	2.66	0.9302
0.900	0.1111	0.1140	2.61	1.026

Relative Interface Position	Insitu Ratio	Input Ratio	Pressure Gradient Reduction Factor	Holdup Ratio
0.875	0.1429	0.1630	2.52	1.141
0.850	0.1765	0.2267	2.41	1.285
0.800	0.2500	0.4150	2.17	1.660
0.700	0.4286	1.234	1.68	2.880
0.600	0.6667	3.332	1.232	4.997
0.500	1.000	8.570	0.852	8.570
0.400	1.500	22.10	0.537	14.73
0.300	2.333	61.00	0.300	26.14
0.200	4.000	203.9	0.131	50.96
0.100	9.000	1164	0.0327	129.3

(v) Viscosity Ratio = 100

1.000	0	0	1.000	-
0.975	0.02564	0.02434	2.78	0.9491
0.950	0.05263	0.05344	2.91	1.015
0.925	0.08108	0.09194	2.86	1.134
0.900	0.1111	0.1445	2.76	1.300
0.875	0.1429	0.2161	2.63	1.513
0.850	0.1765	0.3147	2.50	1.783
0.800	0.2500	0.6263	2.229	2.505
0.700	0.4286	2.096	1.710	4.891
0.600	0.6667	6.050	1.249	9.075
0.500	1.0000	16.17	0.8591	16.17
0.400	1.500	42.66	0.5426	28.44
0.300	2.333	119.5	0.3001	51.20
0.200	4.000	403.1	0.1308	100.8
0.100	9.000	2317	0.03188	257.4

(vi) Viscosity Ratio = 500

1.000	0	0	1.000	-
0.9875	0.01266	0.02252	3.216	1.779
0.9750	0.02564	0.04633	3.285	1.807
0.9625	0.03896	0.07484	3.251	1.921
0.9500	0.05263	0.1095	3.191	2.080
0.9375	0.06667	0.1560	3.121	2.340

Relative Interface Position	Insitu Ratio	Input Ratio	Pressure Gradient Reduction Factor	Holdup Ratio
0.9250	0.08108	0.2126	3.046	2.623
0.9000	0.1111	0.3762	2.891	3.386
0.8000	0.2500	2.304	2.281	9.216
0.7000	0.4286	8.981	1.734	20.96
0.6000	0.6667	27.79	1.261	41.68
0.5000	1.000	76.95	0.8651	76.95
0.4000	1.500	207.1	0.5452	138.1
0.3000	2.333	587.2	0.3011	251.7
0.2000	4.000	1997	0.1311	499.3
0.1000	9.000	11540	0.0319	1282

(vii) Viscosity Ratio = 1000

1.000	0	0	1.000	-
0.9875	0.01266	0.03493	3.370	2.759
0.9750	0.02564	0.07265	3.366	2.833
0.9625	0.03896	0.1194	3.306	3.064
0.9500	0.05263	0.1780	3.232	3.383
0.9375	0.06667	0.2601	3.153	3.901
0.9250	0.08108	0.3617	3.072	4.461
0.9000	0.1111	0.6644	2.909	5.980
0.8000	0.2500	4.399	2.288	17.60
0.7000	0.4286	17.59	1.737	41.03
0.6000	0.6667	54.96	1.263	82.44
0.5000	1.000	152.9	0.8656	152.9
0.4000	1.500	412.7	0.5455	275.1
0.3000	2.333	1172	0.3012	502.2
0.2000	4.000	3989	0.1311	997.4
0.1000	9.000	23070	0.03192	2563

(viii)

Viscosity Ratio	Maximum Pressure Gradient Reduction Factor
1	1
5.259	1.61
10	1.93
50	2.66
100	2.91
500	3.28
1000	3.38

Table A2(b)

Aspect Ratio = 3:1

(i) Viscosity Ratio = 1

Relative Interface Position	Insitu Ratio	Input Ratio	Pressure Gradient Reduction Factor	Holdup Ratio
1.000	0	0	1.000	-
0.900	0.1111	0.02962	0.9716	0.2666
0.800	0.2500	0.1181	0.8952	0.4725
0.700	0.4286	0.2784	0.7827	0.6500
0.600	0.6666	0.5460	0.6470	0.8190
0.500	1.000	1.000	0.5002	1.000
0.400	1.500	1.831	0.3533	1.221
0.300	2.333	3.591	0.2179	1.539
0.200	4.000	8.466	0.1057	2.117
0.100	9.000	33.76	0.02878	3.751

(ii) Viscosity Ratio = 3

1.000	0	0	1.000	-
0.900	0.1111	0.05383	1.280	0.4845
0.800	0.2500	0.1773	1.262	0.7093
0.700	0.4286	0.3871	1.113	0.9032

Relative Interface Position	Insitu Ratio	Input Ratio	Pressure Gradient Reduction Factor	Holdup Ratio
0.600	0.6666	0.7495	0.9051	1.124
0.500	1.000	1.418	0.6800	1.418
0.400	1.500	2.781	0.4617	1.854
0.300	2.333	6.048	0.2715	2.592
0.200	4.000	16.42	0.1243	4.106
0.100	9.000	79.01	0.03153	8.779

(iii) Viscosity Ratio = 10

1.000	0	0	1.000	-
0.9875	0.01266	0.003382	1.254	0.2672
0.9750	0.02564	0.01024	1.429	0.3993
0.9625	0.03896	0.01883	1.553	0.4832
0.950	0.05263	0.02862	1.640	0.5438
0.3975	0.06667	0.03944	1.701	0.5916
0.9250	0.08108	0.05124	1.742	0.6320
0.9125	0.09589	0.06404	1.769	0.6679
0.9000	0.1111	0.07792	1.783	0.7013
0.8000	0.2500	0.2402	1.674	0.9607
0.7000	0.4286	0.5607	1.402	1.308
0.6000	0.6667	1.214	1.095	1.821
0.5000	1.000	2.609	0.7935	2.609
0.4000	1.500	5.832	0.5226	3.888
0.3000	2.333	14.39	0.2984	6.167
0.2000	4.000	44.06	0.1328	11.01
0.1000	9.000	237.2	0.03263	26.35

(iv) Viscosity Ratio = 30

1.000	0	0	1.000	-
0.9875	0.01265	0.006034	1.630	0.4767
0.9750	0.02564	0.01526	1.912	0.5953
0.9625	0.03896	0.02570	2.057	0.6597
0.950	0.05263	0.03724	2.133	0.7076
0.9375	0.06667	0.05000	2.171	0.7500
0.9250	0.08108	0.06417	2.185	0.7914
0.9125	0.09589	0.07997	2.183	0.8340

Relative Interface Position	Insitu Ratio	Input Ratio	Pressure Gradient Reduction Factor	Holdup Ratio
0.9000	0.1111	0.09767	2.170	0.8790
0.8875	0.1268	0.1175	2.149	0.9272
0.8000	0.2500	0.3468	1.896	1.387
0.7000	0.4286	0.9721	1.534	2.268
0.6000	0.6666	2.452	1.171	3.678
0.5000	1.000	5.926	0.8354	5.926
0.4000	1.500	14.46	0.5436	9.643
0.3000	2.333	38.15	0.3074	16.35
0.2000	4.000	122.9	0.1354	30.739
0.1000	9.000	689.0	0.03300	76.56

(v) Viscosity Ratio = 100

1.000	0	0	1.000	-
0.9875	0.01265	0.008572	2.197	0.6772
0.9750	0.02564	0.01929	2.422	0.7523
0.9625	0.03896	0.03157	2.490	0.8104
0.950	0.05263	0.04597	2.501	0.8734
0.9375	0.06667	0.06313	2.488	0.9469
0.9250	0.08108	0.08375	2.460	1.033
0.9125	0.09589	0.1086	2.426	1.133
0.9000	0.1111	0.1385	2.386	1.247
0.8875	0.1268	0.1744	2.342	1.376
0.8000	0.2500	0.6871	1.996	2.748
0.7000	0.4286	2.378	1.587	5.548
0.6000	0.6666	6.750	1.201	10.13
0.5000	1.0000	17.50	0.8514	17.50
0.4000	1.500	44.65	0.5516	29.77
0.3000	2.333	121.3	0.3107	51.99
0.2000	4.000	399.1	0.1364	99.77
0.1000	9.000	2270	0.03308	252.3

(vi) Viscosity Ratio = 300

1.000	0	0	1.000	-
0.9875	0.01265	0.01060	2.596	0.8375
0.9750	0.02564	0.02356	2.684	0.9188
0.9625	0.03896	0.04015	2.680	1.031

Relative Interface Position	Insitu Ratio	Input Ratio	Pressure Gradient Reduction Factor	Holdup Ratio
0.9500	0.05263	0.06216	2.650	1.181
0.9375	0.06667	0.09153	2.608	1.373
0.9250	0.08108	0.1303	2.561	1.608
0.9125	0.09589	0.1809	2.511	1.886
0.9000	0.1111	0.2456	2.459	2.210
0.8875	0.1268	0.3272	2.406	2.581
0.8000	0.2500	1.650	2.027	6.598
0.7000	0.4286	6.384	1.603	14.90
0.6000	0.6666	19.02	1.210	28.53
0.5000	1.000	50.56	0.8569	50.56
0.4000	1.500	130.9	0.5538	87.25
0.3000	2.333	358.9	0.3116	153.8
0.2000	4.000	1188	0.1367	296.9
0.1000	9.000	6789	0.03313	754.3

(vii) Viscosity Ratio = 1000

1.000	0	0	1.000	-
0.9875	0.01265	0.01477	2.807	1.167
0.9750	0.02564	0.03529	2.799	1.373
0.9625	0.03896	0.06675	2.759	1.713
0.9500	0.05263	0.1153	2.708	2.191
0.9375	0.06667	0.1874	2.655	2.811
0.9250	0.08108	0.2899	2.600	3.575
0.9125	0.09589	0.4303	2.543	4.487
0.9000	0.1111	0.6168	2.488	5.551
0.8875	0.1268	0.8583	2.431	6.771
0.8000	0.2500	5.014	2.038	20.06
0.7000	0.4286	20.40	1.609	47.61
0.6000	0.6666	61.97	1.213	92.95
0.5000	1.000	166.3	0.8579	166.3
0.4000	1.500	432.7	0.5546	288.4
0.3000	2.333	1190	0.3120	510.1
0.2000	4.000	3940	0.1368	987.3
0.1000	9.000	22600	0.03312	2511

(viii)

Viscosity Ratio	Maximum Pressure Gradient Reduction Factor
1	1.0
3	1.29
10	1.79
30	2.185
100	2.50
300	2.685
1000	2.81

Table A2(c)

Aspect Ratio = 1:1

(i) Viscosity Ratio = 1

Relative Interface Position	Insitu Ratio	Input Ratio	Pressure Gradient Reduction Factor	Holdup Ratio
1.000	0	0	1.000	-
0.950	0.05263	0.008419	0.9919	0.1599
0.900	0.1111	0.03242	0.9689	0.2918
0.850	0.1765	0.07135	0.9336	0.4043
0.800	0.2500	0.1258	0.8884	0.5033
0.750	0.3333	0.1976	0.8352	0.5929
0.700	0.4286	0.2899	0.7754	0.6763
0.650	0.5385	0.4072	0.7108	0.7562
0.600	0.6667	0.5567	0.6426	0.8351
0.550	0.8182	0.7490	0.5719	0.9154
0.500	1.000	1.000	0.5001	1.000
0.450	1.222	1.335	0.4283	1.092
0.400	1.500	1.796	0.3577	1.198
0.350	1.857	2.456	0.2895	1.322
0.300	2.333	3.450	0.2248	1.479
0.250	3.000	5.060	0.1651	1.687

Relative Interface Position	Insitu Ratio	Input Ratio	Pressure Gradient Reduction Factor	Holdup Ratio
0.200	4.000	7.947	0.1118	1.987
0.150	5.667	14.02	0.06661	2.473
0.100	9.000	30.85	0.03141	3.427
0.050	19.000	118.8	0.008351	6.252
(ii) Viscosity Ratio = 3				
1.000	0	0	1.000	-
0.950	0.05263	0.01769	1.114	0.3361
0.900	0.1111	0.05789	1.138	0.5211
0.850	0.1765	0.1173	1.121	0.6649
0.800	0.2500	0.1987	1.083	0.7949
0.750	0.3333	0.3070	1.030	0.9210
0.700	0.4286	0.4491	0.9670	1.048
0.650	0.5385	0.6348	0.8953	1.179
0.600	0.6667	0.8777	0.8179	1.317
0.550	0.8182	1.198	0.7351	1.465
0.500	1.000	1.628	0.6484	1.628
0.450	1.222	2.216	0.5594	1.813
0.400	1.500	3.048	0.4696	2.032
0.350	1.857	4.278	0.3807	2.303
0.300	2.333	6.203	0.2945	2.658
0.250	3.000	9.461	0.2141	3.154
0.200	4.000	15.62	0.1422	3.906
0.150	5.667	29.41	0.08225	5.189
(iii) Viscosity Ratio = 10				
1.000	0	0	1.000	-
0.950	0.05263	0.02956	1.305	0.5616
0.900	0.1111	0.08668	1.327	0.7801
0.850	0.1765	0.1768	1.296	1.002
0.800	0.2500	0.3130	1.243	1.252
0.750	0.3333	0.5112	1.178	1.534
0.700	0.4286	0.7912	1.104	1.846
0.650	0.5385	1.179	1.023	2.191
0.600	0.6667	1.713	0.9348	2.570

Relative Interface Position	Insitu Ratio	Input Ratio	Pressure Gradient Reduction Factor	Holdup Ratio
0.550	0.8182	2.447	0.8412	2.991
0.500	1.000	3.465	0.7429	3.465
0.450	1.222	4.905	0.6411	4.013
0.400	1.500	7.005	0.5376	4.670
0.350	1.857	10.20	0.4344	5.493
0.300	2.333	15.36	0.3345	6.583
0.250	3.000	24.38	0.2411	8.126
0.200	4.000	42.01	0.1582	10.50
0.150	5.667	82.81	0.08989	14.61
0.100	9.000	208.9	0.03959	23.21
0.050	19.000	953.7	0.009563	50.19

(iv) Viscosity Ratio = 30

1.000	0	0	1.000	-
0.9875	0.01265	0.005873	1.321	0.4639
0.9750	0.02564	0.01500	1.404	0.5851
0.9625	0.03896	0.02602	1.436	0.6678
0.9500	0.05263	0.03924	1.447	0.7456
0.9375	0.06667	0.05514	1.449	0.8271
0.9250	0.08108	0.07425	1.446	0.9157
0.9125	0.09589	0.09710	1.438	1.013
0.9000	0.1111	0.1244	1.429	1.120
0.8875	0.1268	0.1565	1.417	1.234
0.850	0.1765	0.2877	1.377	1.630
0.800	0.2500	0.5686	1.312	2.274
0.750	0.3333	1.0129	1.239	3.039
0.700	0.4286	1.677	1.158	3.913
0.650	0.5385	2.635	1.072	4.894
0.600	0.6667	3.990	0.9790	5.985
0.550	0.8182	5.896	0.8808	7.206
0.500	1.000	8.587	0.7778	8.587
0.450	1.222	12.45	0.6709	10.19
0.400	1.500	18.17	0.5622	12.11
0.350	1.857	26.98	0.4535	14.53
0.300	2.333	41.38	0.3483	17.73
0.250	3.000	66.85	0.2503	22.28
0.200	4.000	117.3	0.1636	29.31
0.150	5.667	235.2	0.09238	41.51
0.100	9.000	603.6	0.04038	67.07

Relative Interface Position	Insitu Ratio	Input Ratio	Pressure Gradient Reduction Factor	Holdup Ratio
(v) Viscosity Ratio = 100				
1.000	0	0	1.000	-
0.9875	0.01265	0.007936	1.483	0.6270
0.9750	0.02564	0.01911	1.523	0.7451
0.9625	0.03896	0.03427	1.528	0.8797
0.9500	0.05263	0.05516	1.523	1.048
0.9375	0.06667	0.08355	1.514	1.253
0.9250	0.08108	0.1212	1.503	1.495
0.9125	0.09589	0.1700	1.489	1.773
0.9000	0.1111	0.2324	1.475	2.091
0.8875	0.1268	0.3090	1.459	2.438
0.850	0.1765	0.6478	1.411	3.671
0.800	0.2500	1.432	1.340	5.728
0.750	0.3333	2.735	1.263	8.203
0.700	0.4286	4.740	1.179	11.06
0.650	0.5385	7.689	1.091	14.28
0.600	0.6667	11.92	0.9961	17.88
0.550	0.8182	17.92	0.8959	21.90
0.500	1.000	26.46	0.7910	26.46
0.450	1.222	38.82	0.6822	31.76
0.400	1.500	57.19	0.5713	38.12
0.350	1.857	85.65	0.4607	46.12
0.300	2.333	132.4	0.3536	56.73
0.250	3.000	215.4	0.2538	71.81
0.200	4.000	380.5	0.1655	95.12
0.150	5.667	768.7	0.0933	135.6
0.100	9.000	1987	0.0407	220.8
0.050	19.000	9299	0.009709	489.4
(vi) Viscosity Ratio = 300				
1.000	0	0	1.000	-
0.9875	0.01265	0.009553	1.562	0.7547
0.9750	0.02564	0.02508	1.569	0.9781
0.9625	0.03896	0.05138	1.561	1.319
0.9500	0.05263	0.09371	1.549	1.780

Relative Interface Position	Insitu Ratio	Input Ratio	Pressure Gradient Reduction Factor	Holdup Ratio
0.9375	0.06667	0.1574	1.535	2.361
0.9250	0.08108	0.2479	1.520	3.057
0.9125	0.09589	0.3705	1.505	3.864
0.9000	0.1111	0.5327	1.489	4.795
0.8875	0.1268	0.7367	1.472	5.812
0.850	0.1765	1.668	1.421	9.452
0.800	0.2500	3.887	1.348	15.56
0.750	0.3333	7.643	1.270	22.93
0.700	0.4286	13.48	1.186	31.45
0.650	0.5385	22.12	1.096	41.07
0.600	0.6667	34.55	1.001	51.83
0.550	0.8182	52.26	0.9003	63.88
0.500	1.000	77.53	0.7950	77.53
0.450	1.222	114.1	0.6854	93.38
0.400	1.500	168.7	0.5739	112.4
0.350	1.857	253.3	0.4628	136.4
0.300	2.333	392.4	0.3551	168.2
0.250	3.000	639.9	0.2547	213.3
0.200	4.000	1132	0.1661	283.2
0.150	5.667	2292	0.09355	404.4
0.100	9.000	5938	0.04075	659.8

(vii) Viscosity Ratio = 1000

1.000	0	0	1.000	-
0.9875	0.01265	0.01299	1.595	1.026
0.9750	0.02564	0.04349	1.587	1.696
0.9625	0.03896	0.1086	1.574	2.788
0.9500	0.05263	0.2259	1.558	4.292
0.9375	0.06666	0.4131	1.543	6.197
0.9250	0.08108	0.6882	1.527	8.488
0.9125	0.09589	1.069	1.511	11.15
0.9000	0.1111	1.581	1.494	14.23
0.8875	0.1268	2.231	1.477	17.59

(viii)

Viscosity Ratio	Maximum Pressure Gradient Reduction Factor
1	1
3	1.138
10	1.329
30	1.449
100	1.528
300	1.569
1000	1.595

Table A2(d)

Aspect Ratio = 1:3

Relative Interface Position	Insitu Ratio	Input Ratio	Pressure Gradient Reduction Factor	Holdup Ratio
(i) Viscosity Ratio = 1				
1.00	0	0	1.000	-
0.900	0.1111	0.04736	0.9549	0.4263
0.800	0.2500	0.1631	0.8599	0.6526
0.700	0.4286	0.3413	0.7456	0.7964
0.600	0.6667	0.6026	0.6240	0.9038
0.500	1.000	1.000	0.5001	1.000
0.400	1.500	1.660	0.3761	1.106
0.300	2.333	2.930	0.2545	1.256
0.200	4.000	6.130	0.1403	1.532
0.100	9.000	21.11	0.04523	2.346
(ii) Viscosity Ratio = 3				
1.000	0	0	1.00	-
0.900	0.1111	0.08561	1.006	0.7705
0.800	0.2500	0.3240	0.9181	1.296
0.600	0.6667	1.372	0.6872	2.058
0.500	1.000	2.318	0.5641	2.318

Relative Interface Position	Insitu Ratio	Input Ratio	Pressure Gradient Reduction Factor	Holdup Ratio
0.400	1.500	3.836	0.4378	2.557
0.200	4.000	13.35	0.1805	3.337
0.100	9.000	45.98	0.05946	5.109

(iii) Viscosity Ratio = 10

Relative Interface Position	Insitu Ratio	Input Ratio	Pressure Gradient Reduction Factor	Holdup Ratio
1.000	0	0	1.000	-
0.9875	0.01265	0.004504	1.060	0.3558
0.975	0.02564	0.01312	1.072	0.5115
0.9625	0.03896	0.02516	1.074	0.6457
0.9500	0.05263	0.04127	1.070	0.7840
0.9375	0.06667	0.06217	1.065	0.9325
0.925	0.08108	0.1092	1.058	1.092
0.9125	0.09589	0.1211	1.051	1.262
0.900	0.1111	0.1602	1.042	1.442
0.800	0.2500	0.7581	0.9560	3.033
0.700	0.4286	1.930	0.8482	4.503
0.600	0.6667	3.769	0.7294	5.653
0.500	1.000	6.530	0.6050	6.530
0.400	1.500	10.88	0.4772	7.250
0.300	2.333	18.67	0.3448	7.999
0.200	4.000	37.32	0.2056	9.331
0.100	9.000	131.3	0.0675	14.59

(iv) Viscosity Ratio = 30

Relative Interface Position	Insitu Ratio	Input Ratio	Pressure Gradient Reduction Factor	Holdup Ratio
1.000	0	0	1.000	-
0.800	0.2500	1.934	0.9699	7.737
0.700	0.4286	5.236	0.8630	12.22
0.600	0.6667	10.49	0.7445	15.74
0.500	1.000	18.39	0.6201	18.39
0.400	1.500	30.74	0.4914	20.49
0.300	2.333	-	0.3577	-
0.200	4.000	-	0.2147	-

Relative Interface Position	Insitu Ratio	Input Ratio	Pressure Gradient Reduction Factor	Holdup Ratio
(v) Viscosity Ratio = 100				
1.000	0	0	1.000	-
0.9875	0.01265	0.008913	1.114	0.7041
0.9750	0.02564	0.03052	1.111	1.190
0.9625	0.03896	0.07492	1.105	1.923
0.9500	0.05263	0.1518	1.097	2.883
0.9375	0.06667	0.2699	1.089	4.049
0.925	0.08108	0.4374	1.081	5.395
0.9125	0.09589	0.6614	1.072	5.898
0.900	0.111	0.9483	1.063	8.535
0.800	0.2500	6.012	0.9770	24.05
0.600	0.6667	33.97	0.7502	50.95
0.500	1.000	59.81	0.6259	59.81
0.400	1.500	100.2	0.4971	66.79
0.300	2.333	171.9	0.3627	73.68
0.200	4.000	343.4	0.2183	85.85
0.100	9.000	1225	0.07140	136.2
(vi) Viscosity Ratio = 1000				
1.000	0	0	1.000	-
0.900	0.1111	8.760	1.065	78.84
0.800	0.2500	58.54	0.9776	234.2
0.700	0.4286	164.9	0.8709	384.9
0.600	0.6667	335.7	0.7525	503.6
0.500	1.000	592.3	0.6280	592.3
0.400	1.500	992.9	0.4994	661.9
0.300	2.333	1704	0.3645	730.3
0.200	4.000	3403	0.2197	850.9
0.100	9.000	12170	0.7181	1352

(vii)

Viscosity Ratio	Maximum Pressure Gradient Reduction Factor
1.0	1.0
3.0	(1.025)
10.0	1.072
100.0	1.113
1000	(1.128)

TABLE A3

Theoretical data for a viscosity ratio of 5.326 and an aspect ratio of 7.95:1.

(a) Holdup ratios and pressure gradient reduction factors

Insitu Ratio	Input Ratio	Volume Percent Oil in Total Flow	Holdup Ratio	Pressure Gradient Reduction Factor
0.1111	0.06688	93.8	0.6019	1.596
0.2500	0.2025	83.2	0.8101	1.567
0.4286	0.4391	69.6	1.024	1.336
0.6666	0.8779	53.4	1.317	1.045
1.0000	1.758	36.4	1.758	0.7540
1.500	3.709	21.4	2.473	0.4940
2.333	8.778	10.32	3.762	0.2815
4.000	25.81	3.77	6.452	0.1258
9.000	133.8	0.751	14.87	0.03137

(b) Interface velocities

Insitu Ratio	Input Ratio	$\frac{w_i}{V_{rc}}$	Volume Percent Oil in Total Flow
0.1111	0.06688	2.19	93.8
0.251	0.203	3.00	83.0
0.432	0.445	3.20	69.2
0.675	0.890	3.06	52.9
1.014	1.80	2.74	35.7
1.532	3.90	2.31	20.4
2.41	9.40	1.78	9.62
4.18	27.0	1.208	3.57

APPENDIX B

PHYSICAL PROPERTIES OF THE OIL AND WATER

The density and viscosity of the oil were determined as a function of temperature by two independent laboratories - the Instruments Laboratory, Department of Chemical and Petroleum Engineering, University of Alberta and the Gasoline and Oil Laboratory, Research Council of Alberta. Measurements of both quantities agreed to within 0.5 percent at any temperature. The density had a low temperature coefficient and was essentially constant at 0.819 gm/cc during the experiments. The viscosity is shown as a function of temperature over a range of 72 to 82°F in Figure 43. At 76.5°F, the average temperature of the oil during the two-phase experiments, the viscosity was 4.82 centipoise.

The density and viscosity of water were obtained from the Handbook of Chemistry and Physics (43). The density of the water was approximately constant at 0.997 gm/cc and at 76°F, the average temperature of the water during the two-phase experiments the viscosity was 0.905 centipoise.

The viscosity ratio is shown as a function of temperature in Figure 43, for which both liquids are assumed to be

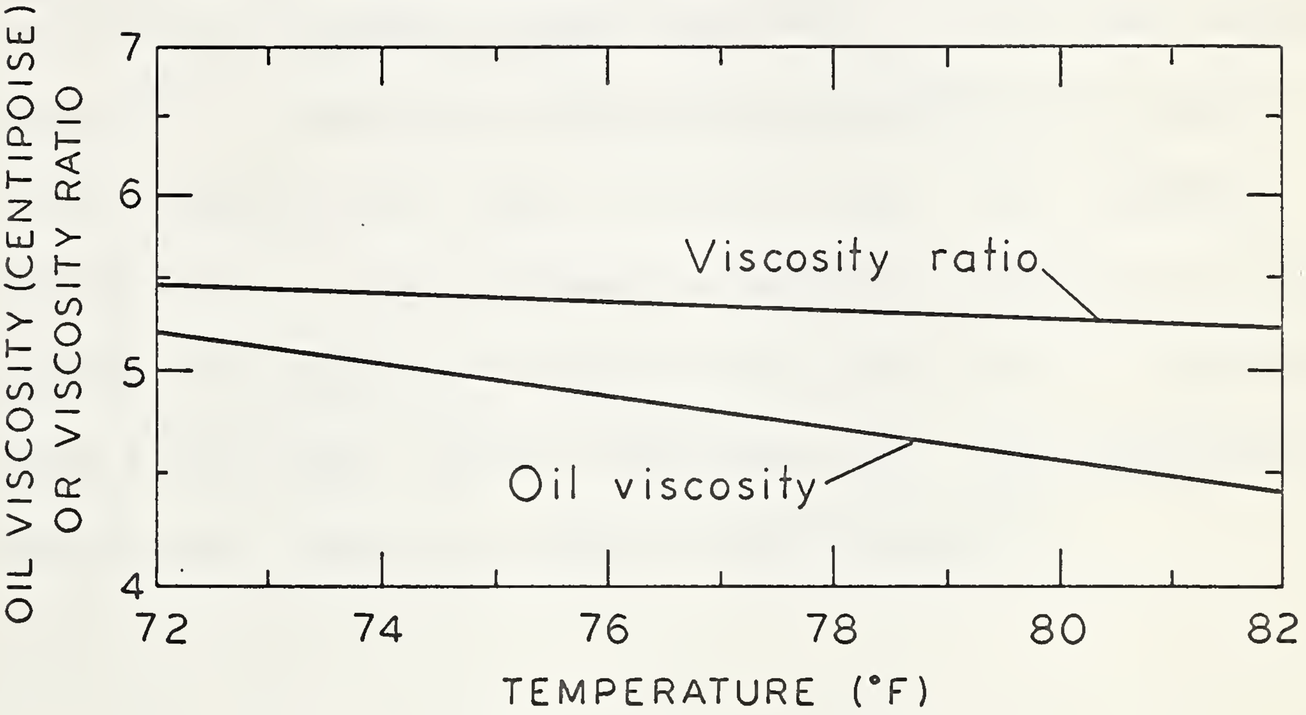

FIGURE 43 - OIL VISCOSITY AND VISCOSITY RATIO AS A FUNCTION OF TEMPERATURE

at the same temperature. Using the average viscosities given above the viscosity ratio was 5.326.

The oil-water interfacial tension was determined by the capillary rise method developed by Bartell and Miller(3), the application of which in the determination of oil-water interfacial tensions has been described in a previous investigation(10). Using pure water and pure benzene the diameter of the capillary was found to be 0.861 mm. The subsequent determination of the oil-water interfacial tension at 76.5°F yielded 42.2 dynes/cm using distilled water and 41.9 dynes/cm using water taken from the separator tank. The interfacial tension was, therefore, taken to be 42 dynes/cm.

APPENDIX C

CALIBRATION OF ROTAMETERS

The rotameter type flow meters were calibrated by weighing the amount of fluid discharged in a known time for different rotameter settings. For this purpose a special temporary copper line was installed which carried the flow directly from the rotameters to the separator without the need for it to pass through the conduit. The outlet of a side arm to this copper line was positioned over an open barrel on a weigh scale. Quick action gate valves enabled the flow to be diverted instantaneously from the separator to the barrel and vice versa.

The weigh scale itself was calibrated with known weights and was found to be accurate to within 0.2 lbs up to 250 lbs. In general, a sufficient time was allowed to elapse so that at least 100 lbs. of fluid were collected. Two weight measurements were made for each rotameter setting and were found to agree very closely, usually to within about 0.2 percent.

Flow rate, in U.S. gallons per minute, was plotted against scale reading for each rotameter and the resulting curves used to determine the rotameter setting necessary to

[illegible]

[illegible]

[illegible]

[illegible]

provide a given flow rate. Flow rates obtained in this way were accurate to within 1 percent. In order to present the calibrations as concisely as possible, flow rate in U.S. gallons per minute divided by scale reading, which should be a constant for a well designed rotameter, is plotted against scale reading in Figure 44 for the three water rotameters, and in Figure 45 for the three oil rotameters. The manufacturer, tube number and float number are given for each rotameter. Also included in the figure for the water rotameters are the manufacturer's curves.

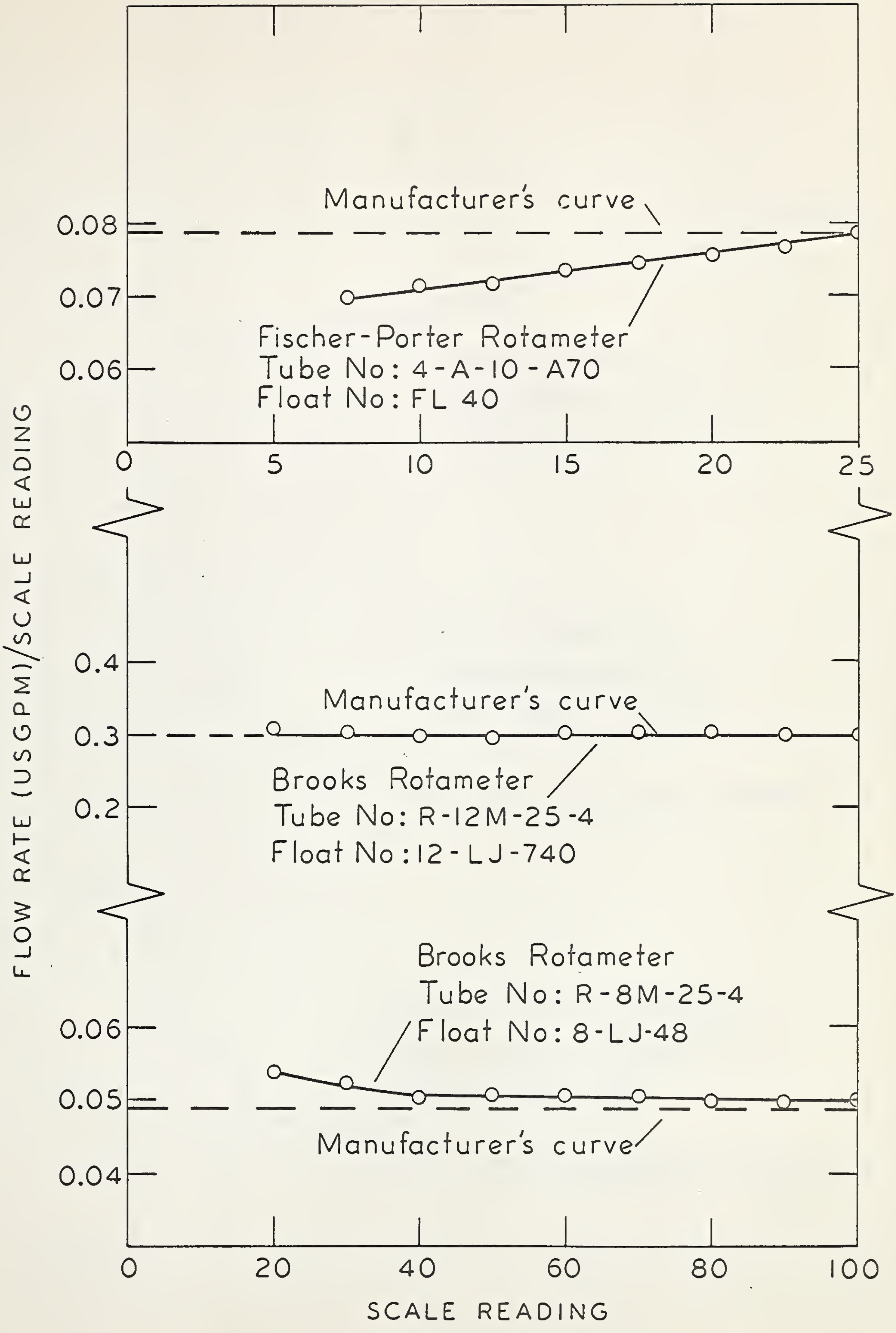

FIGURE 44 - CALIBRATION CURVES FOR WATER ROTAMETERS

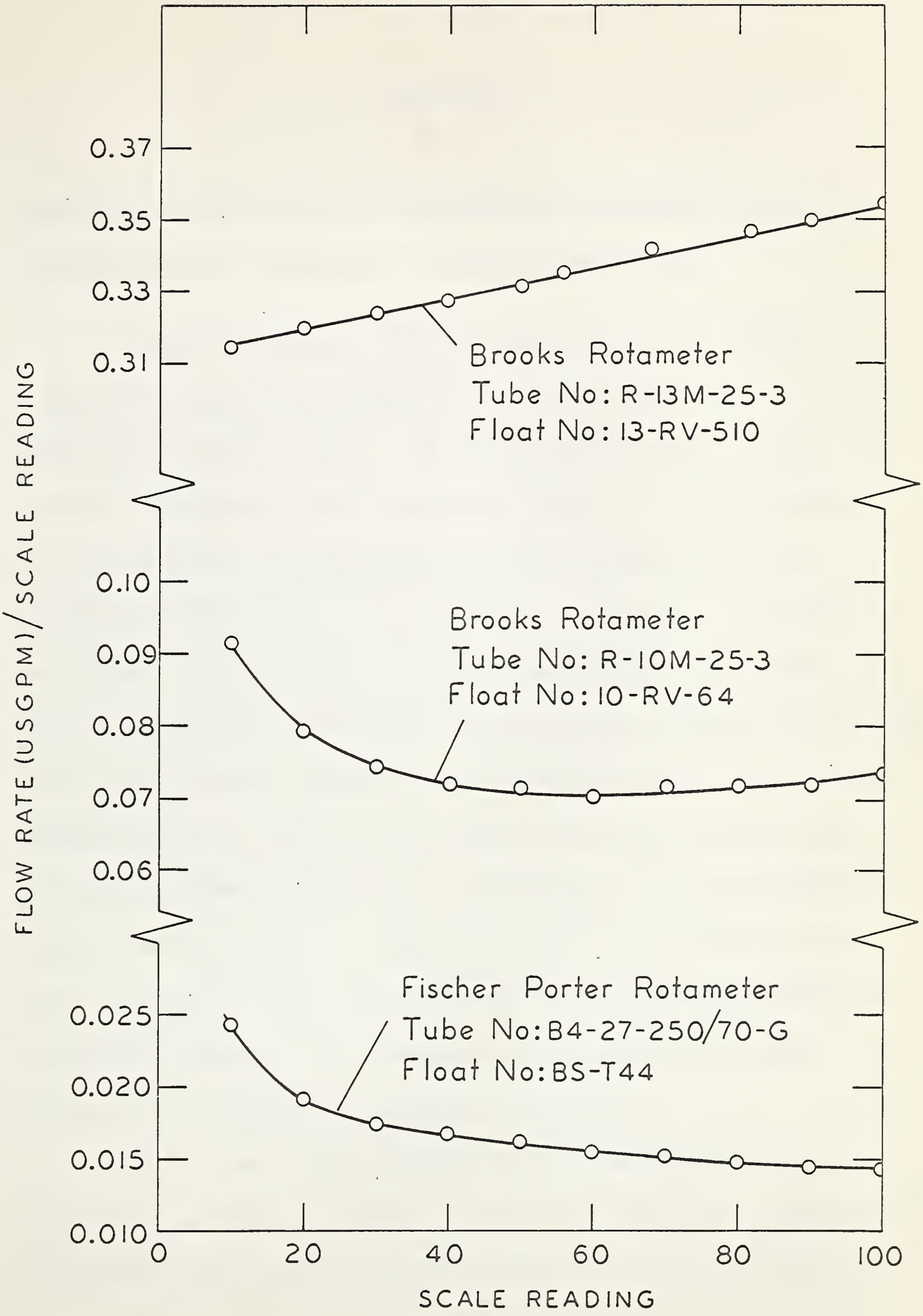

FIGURE 45 - CALIBRATION CURVES FOR OIL ROTAMETERS

APPENDIX D

THEORETICAL ANALYSIS OF THE MOTION OF A SPHERICAL PARTICLE RISING THROUGH A PARABOLIC VELOCITY DISTRIBUTION

Consider a small particle, such as an air bubble, injected through the bottom of a conduit containing a laminar, parabolic velocity field. As the particle rises, it will be carried horizontally by the moving fluid. For the purposes of the present investigation it will be assumed that the vertical velocity V_p of the particle is constant. Actually, of course, if the particle were injected with essentially zero vertical velocity there would be an initial acceleration period until the particle reached its terminal velocity. For certain combinations of particle and fluid this acceleration period would be extremely short and in any event could be completely eliminated by having an injection system which would allow the particle to attain its terminal velocity before entering the conduit itself. The assumption of constant vertical velocity is, therefore, entirely reasonable.

If at time t the co-ordinates of the position of particle are y and z with the y-axis vertical, the z-direction coincident with the direction of flow of the fluid, and the

particle moving in the plane $x = 0$, and at time $t + \Delta t$ the co-ordinates are $y + \Delta y$ and $z + \Delta z$ then the horizontal velocity of the particle at $(y + \frac{\Delta y}{2})$ is given approximately by $\frac{\Delta z}{\Delta t}$, provided Δt, Δy and Δz are small quantities. Using stroboscopic or intermittent illumination, Δz could be determined with the aid of photography at various points on the particle trajectory and the velocity of the particle established. If the particle assumed the fluid velocity instantaneously for all values of y then the particle velocity will be representative of the fluid velocity. Obviously the particle has inertia and this will not be so. The object of the following theory is to estimate, by making suitable assumptions, the magnitude of the difference of the particle and fluid velocities as a function of y.

It will be assumed that

(1) the particle has a spherical shape,

(2) the virtual mass of the particle should be used in Newton's law of motion instead of the real mass of the particle,

(3) the drag force exerted in the horizontal direction on the particle by the fluid is given by $3\pi\mu d(w_f - w_p)$ where μ is the fluid viscosity, d is the particle diameter, w_f is the fluid velocity and w_p is the particle velocity and

(4) any effects due to the rotation of the particle under the velocity gradient are negligible.

The inertia of a submerged particle is increased by the fluid around it and hence

$$m^* = m + m' \tag{80}$$

where m^* = virtual mass

m = real mass

m' = induced mass

It may be shown(7) that in the movement of a spherical particle through an incompressible, nonviscous fluid the kinetic energy of the fluid is equal to that which would be possessed by a particle moving with the same velocity as the particle and whose mass m' is equal to half the mass of the fluid displaced. It will be assumed that the virtual mass of a submerged particle can be evaluated in the same way for a viscous fluid.

The value of the drag force is that given by Stokes's law which is strictly true only for solid particles moving under steady-state conditions at particle Reynolds numbers less than 0.5 in an infinite expanse of fluid. For a particle consisting of a second immiscible fluid circulation within the particle has to be taken into account and the corresponding

theoretical drag force is given(7) by $3\pi\mu d(w_f - w_p)\left(\frac{2\mu + 3\mu'}{3\mu + 3\mu'}\right)$ where μ' is the viscosity of the fluid composing the particle. If μ is very much greater than μ', as in the case of an air bubble moving relative to a liquid, the theoretical drag force becomes $2\pi\mu d(w_f - w_p)$. However Birkhoff(7) reports that the experimental evidence suggests that even for a fluid particle the drag is given by $3\pi\mu d(w_f - w_p)$, i.e. a fluid particle behaves much like a solid particle, and this value will be used in the present analysis.

Consider now a particle of virtual mass m* moving with horizontal velocity w_p in a fluid having a velocity w_f, then application of Newton's law of motion to the z-direction gives

$$m^* \dot{w}_p = 3\pi\mu d(w_f - w_p) \tag{81}$$

where the dot over w_p represents a derivative with respect to time.

If the origin of co-ordinates is coincident with the point where the particle enters the conduit, then the parabolic velocity distribution can be described as

$$w_f = w_m \frac{y}{b}\left(2 - \frac{y}{b}\right) \tag{82}$$

where 2b is the distance between the top and bottom of the conduit and w_m is the maximum fluid velocity at $y = b$. Since

$$y = V_p t \tag{83}$$

where V_p is the vertical velocity of the particle and t is time, equation (81) becomes

$$\dot{w}_p + A\, w_p = Bt - Ct^2 \tag{84}$$

in which

$$A = \frac{3\pi \mu d}{m^*} = \frac{18\mu}{d^2(\rho_p + \frac{\rho_f}{2})} \tag{85}$$

$$B = \frac{6\pi \mu d\ W_m V_p}{m^*\ b} = \frac{36\ W_m\ V_p \mu}{b\ d^2(\rho_p + \frac{\rho_f}{2})} \tag{86}$$

$$C = \frac{3\pi \mu d\ W_m V_p^2}{m^*\ b^2} = \frac{18\ W_m\ V_p^2 \mu}{b^2 d^2(\rho_p + \frac{\rho_f}{2})} \tag{87}$$

where ρ_p and ρ_f are the particle and fluid densities respectively.

The Laplace transform of equation (84) is

$$s\, w_p(s) - w_p(o) + A\, w_p(s) = \frac{B}{s^2} - \frac{2C}{s^3} \tag{88}$$

If the particle has zero horizontal velocity at $t = 0$ then $w_p(o) = 0$ and

$$w_p(s) = \frac{B}{s^2(s + A)} - \frac{2C}{s^3(s + A)} \tag{89}$$

[illegible]

$$[illegible]$$

[illegible]

$$[illegible]$$

$$[illegible]$$

$$[illegible]$$

$$[illegible]$$

[illegible]

$$[illegible]$$

[illegible]

$$[illegible]$$

i.e. $$w_p(s) = \left[\frac{B}{A^2} + \frac{2C}{A^3}\right]\frac{1}{s + A} - \frac{2C}{As^3} + \left[\frac{B}{A} + \frac{2C}{A^2}\right]\frac{1}{s^2} - \left[\frac{B}{A^2} + \frac{2C}{A^3}\right]\frac{1}{s} \quad (90)$$

from which, by taking the inverse transform

$$w_p(t) = \frac{1}{A^2}\left[B + \frac{2C}{A}\right]e^{-At} - \frac{C}{A}t^2 + \frac{1}{A}\left[B + \frac{2C}{A}\right]t - \frac{1}{A^2}\left[B + \frac{2C}{A}\right] \quad (91)$$

a solution which satisfies the original differential equation and boundary condition.

Alternatively, using equation (83)

$$w_p(y) = \frac{1}{A^2}\left[B + \frac{2C}{A}\right]e^{-\frac{A}{V_p}y} - \frac{C}{AV_p^2}y^2 + \frac{1}{AV_p}\left[B + \frac{2C}{A}\right]y - \frac{1}{A^2}\left[B + \frac{2C}{A}\right] \quad (92)$$

Let

$$E = w_f - w_p, \quad (93)$$

substitute for w_f and w_p, and equate the derivative of E with respect to y to zero, then

$$e^{-\frac{A}{V_p}y_m} = 1 - \frac{AB}{AB + 2C} \quad (94)$$

i.e. the value of y for which the difference between the fluid and particle velocities is a maximum is given by

$$y_m = \frac{V_p}{A}\ln\left(\frac{AB + 2C}{2C}\right) \quad (95)$$

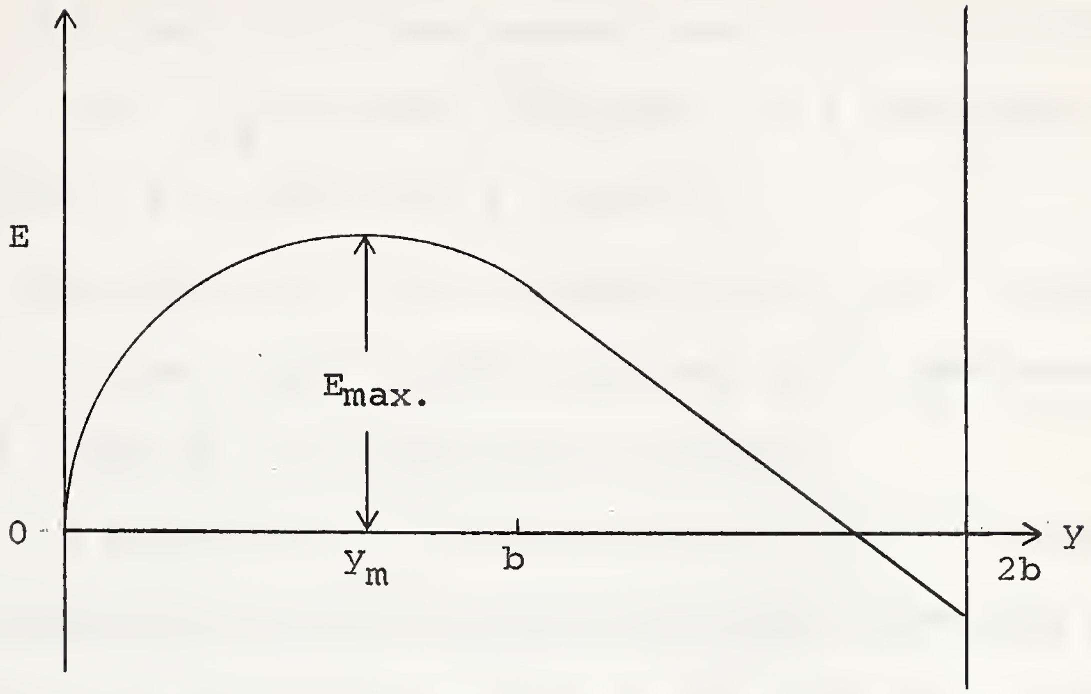

FIGURE 46 - DIFFERENCE BETWEEN FLUID AND PARTICLE VELOCITIES AS A FUNCTION OF y

The general way in which the difference between the fluid and particle velocities varies with y is shown in Figure 46. E is initially positive, passes through a maximum and then becomes negative as the particle approaches the top surface of the conduit.

The particle velocity was evaluated as a function of y from equation (92) for two particular cases of interest.

(1) the movement of an air bubble of diameter 0.5 mm in water flowing with w_m = 1ft/sec and 2b = 1 inch and

(2) the movement of an air bubble of diameter 0.5 mm in oil of viscosity 5 centipoise flowing with w_m = 1 ft/sec and 2b = 1 inch.

[illegible]

[illegible]

[illegible]

For case (1) it was assumed that $V_p = 0.2$ ft/sec, $\rho_f = 1$ g/cc, $\rho_p = 0.00121$ g/cc and $\mu = 1$ centipoise. Thus A = 140.97, B = 1353.3 and C = 3247.9.

For case (2) it was assumed that $V_p = 0.07$ ft/sec, $\rho_f = 0.8$ g/cc, $\rho_p = 0.00121$ g/cc and $\mu = 5$ centipoise. Thus A = 898.51, B = 3018.9 and C = 2535.9.

In both cases the vertical velocities of the particles were estimated using the standard procedure involving drag coefficient and particle Reynolds number. For case (1) the particle Reynolds number for the vertical motion was approximately 30 and for case (2) it was approximately 1.8.

A comparison of the fluid and bubble velocities is presented in Figure 47. It is apparent that the relatively low vertical velocity of the bubble rising in oil, combined with the relatively high drag exerted by the oil render the inertial effect of the bubble and its associated fluid completely negligible. By comparison the inertial effect for the bubble rising in water is by no means negligible and the result is a distorted velocity profile.

For the air-water system the value of y for which E is a maximum as calculated from equation (95) is 0.116b, while for the air-oil system it is only 0.0117b.

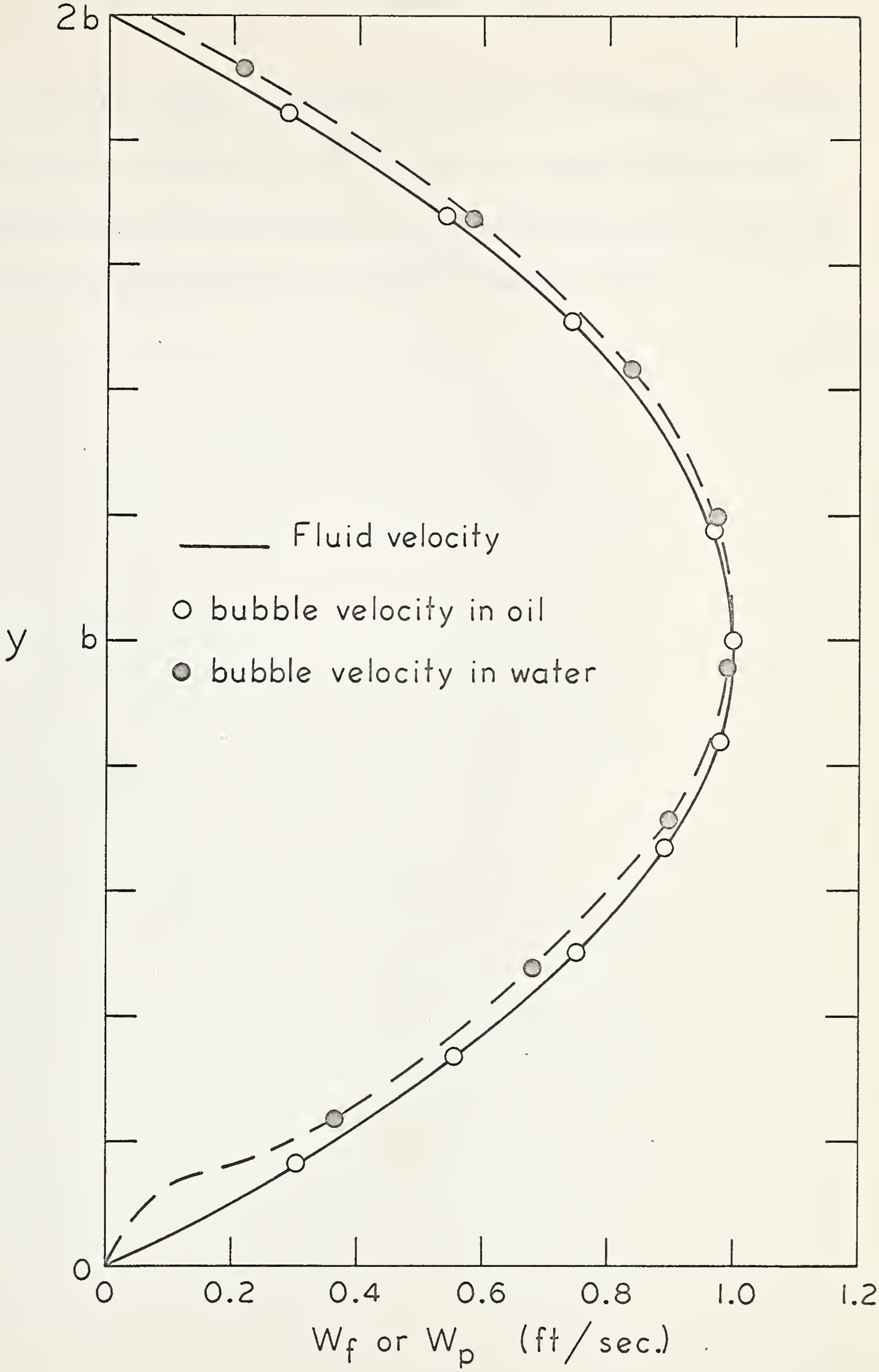

FIGURE 47 - COMPARISON OF FLUID AND BUBBLE VELOCITIES

It would appear, therefore, that the proposed technique would be quite adequate for relatively viscous liquids with viscosities greater than about five centipoise but should be used with caution when water is the flowing fluid.

APPENDIX E

APPLICATION OF STEREOPHOTOGRAMMETRY TO THE MEASUREMENT OF WAVELENGTH AND AMPLITUDE

Stereophotogrammetry was used to estimate the wavelength and amplitude of interfacial waves. When the stereo pairs of photographs obtained with the equipment described under experimental procedure were viewed under the stereoscope the three-dimensional character of the interfacial structure was readily apparent. In this appendix the theory and calibration procedure used in the determination of wavelength and amplitude are discussed.

1. Determination of wavelength

The determination of wavelength was relatively simple and entailed the measurement of the wavelength as it appeared on one of the negatives. This wavelength was then converted into an actual wavelength by the use of a previously determined scale factor. Measurements were made on the left hand, i.e. the downstream, negative with a transparent scale having 0.2 mm divisions.

With the cameras in a fixed position the scale factor was a function of water depth only, i.e. the scale factor was not a function of position on the negative. The functional relationship was determined by the use of a flat plate marked with half-inch squares immersed at various known depths in water inside the conduit. As may be seen from Figure 48 the scale factor was essentially a linear function of water depth. When used to calculate the actual wavelength the scale factor was evaluated at the mean water depth, obtained by taking the difference of the conduit depth and the mean oil depth.

2. Determination of wave amplitude

(i) Theory

The determination of amplitude required the use of a considerably more complex procedure than that necessary for the determination of wavelength. Consider the idealized arrangement depicted in Figure 49. Two cameras, with lenses L and L' have photoplanes AB and A'B' perfectly parallel to the datum plane. Rays of light from the objects 1 and 2 pass through the lens centres without refraction. The heights of the objects above the datum plane are h_1 and h_2 and the camera lenses are both distance H from the datum plane.

[illegible]

[illegible]

[illegible]

[illegible]

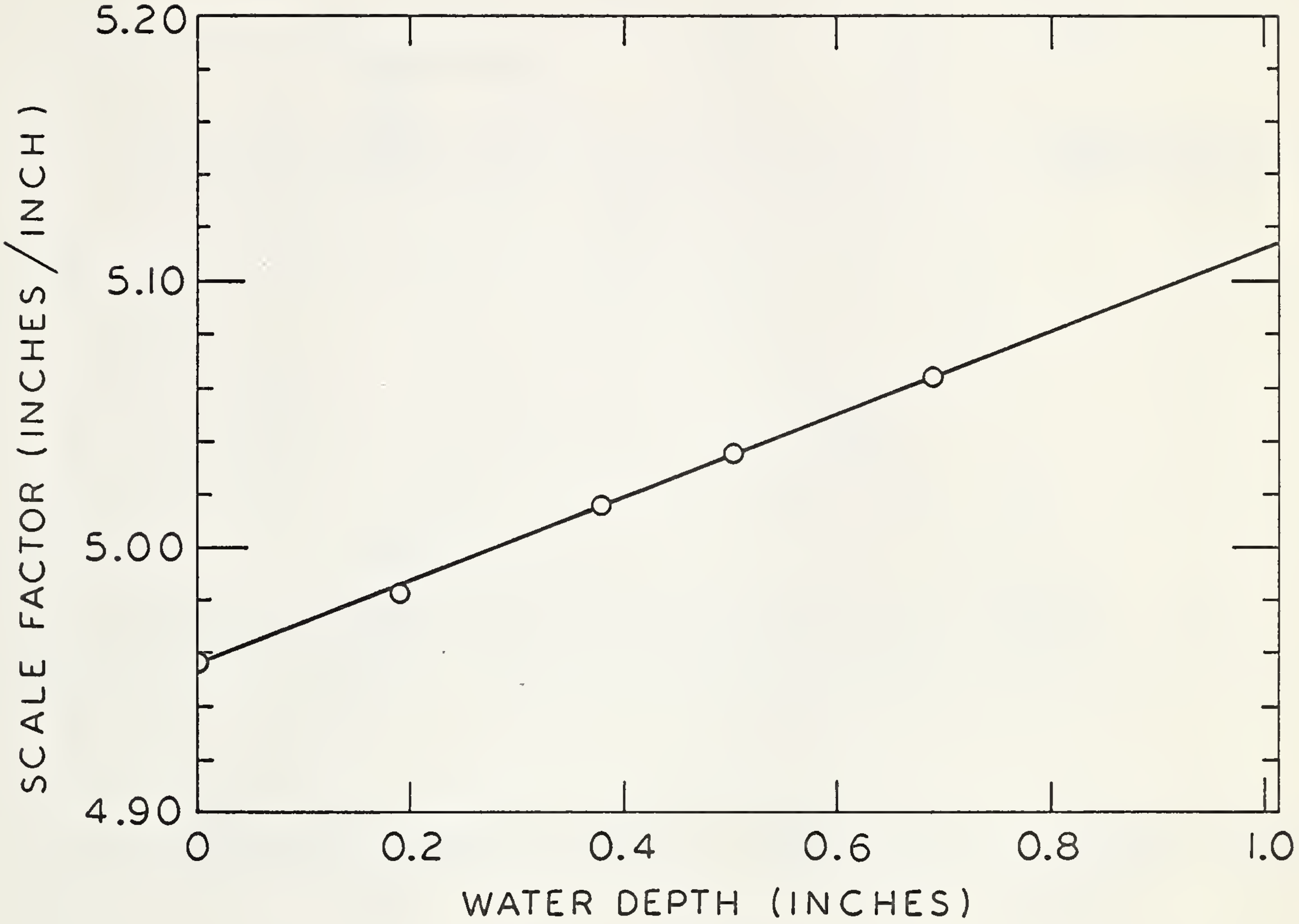

FIGURE 48 - HORIZONTAL SCALE FACTOR

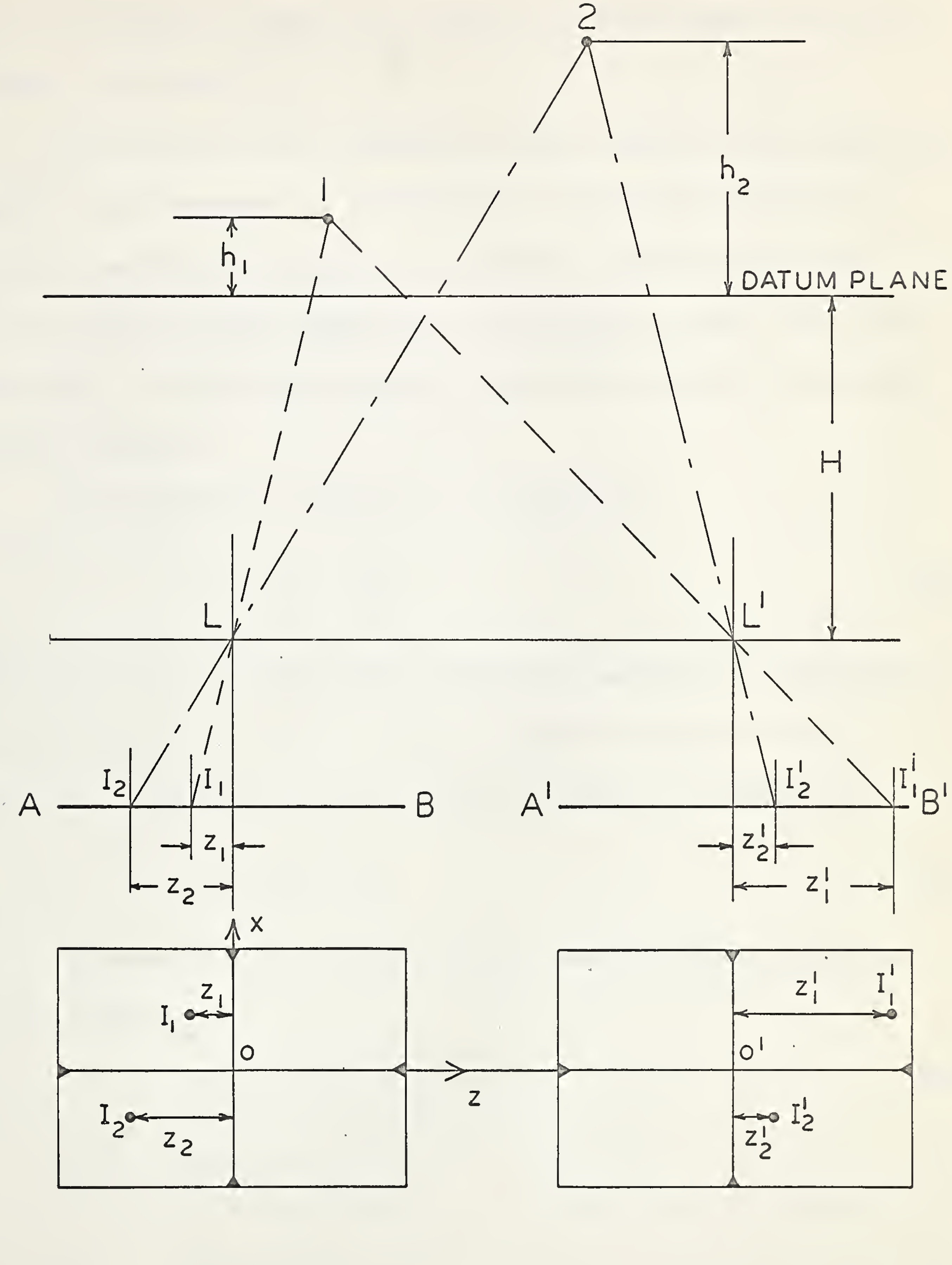

FIGURE 49 - IDEALIZED STEREO-MODEL

Images of object 1 occur at I_1 and I_1', while images of object 2 occur at I_2 and I_2'.

Also shown in the figure are plan views of the negatives showing the positions of the images. The lines joining the fiducial marks define an x-z co-ordinate system with origin at 0 on the left hand negative. The points 0 and 0' are also the points at which the optical axes of the cameras intersect the photo planes.

The parallax of object 1 is given by

$$P_1 = Z_1 - Z_1' \tag{96}$$

where Z_1 and Z_1' are distances from the centres of projection to the images of object 1. Z_1' is assumed positive and Z_1 negative. Similarly the parallax of object 2 is given by

$$P_2 = Z_2 - Z_2' \tag{97}$$

Thomson(88) has shown that for the situation depicted in the figure

$$\Delta h_{12} = (H - h_1) \frac{\Delta P_{12}}{P_2} \tag{98}$$

where $$\Delta h_{12} = h_1 - h_2 \tag{99}$$

and $$\Delta P_{12} = P_1 - P_2 \tag{100}$$

Hence, by knowing the parallaxes of objects 1 and 2 and the height of one of them, it is possible to calculate the height of the other. If object 1 is a point in the datum plane then $h_1 = 0$ and equation (98) becomes

$$h_2 = H \frac{\Delta P_{12}}{P_2} \tag{101}$$

or

$$h_2 = \frac{H \quad \Delta P_{12}}{P_1 - \Delta P_{12}} \tag{102}$$

Now, equation (102) has been derived assuming that the photoplanes of the cameras are both perfectly parallel to the datum, that no distortion is caused by the camera lenses, and that no medium other than air lies between the objects and the camera lenses. In addition, in order to apply the equation to parallaxes measured under the stereoscope the negatives must be positioned in exactly the same relative positions with respect to each other as they were in the cameras. Slight rotation of one of the negatives with respect to the other, while not destroying the three-dimensional effect, causes erroneous parallax measurements to be obtained. While equation (102) could no doubt be modified to take into account the effects of tilt of the photoplanes, the presence of dense media and relative orientation of the negatives, this would necessarily be a very complex procedure. An empirical approach was,

therefore, used to develop adjustments to be applied to the crude elevations calculated from equation (102).

The possible effects resulting from the departures from the idealized situation for which equation (102) applies will now be considered. In doing so reference will be made to Figure 50 where the object, the oil-water interface, is horizontal and parallel to the datum plane which is the outside surface of the bottom of the conduit. Elevations of points (2) in the interface with respect to a point (1) in the datum plane are assumed calculated from equation (102). The effect of relative rotation of the negatives is a linear deformation of the parallaxes and hence of the computed elevations. The interface, therefore, appears tilted. The effect of tilt of the photoplanes is to add to the tilt of the interface and, in addition, to introduce a second degree distortion so that the interface acquires curvature. The exact effect of lens distortion is not known and it can either be assumed to be negligible or included in the other effects. The presence of a water layer, with a refractive index of 1.33 and a 1-inch thick plastic layer with a refractive index of 1.48, between the interface and the cameras is primarily to reduce the elevations considerably and make the interface appear nearer to the datum level than it actually is. In addition,

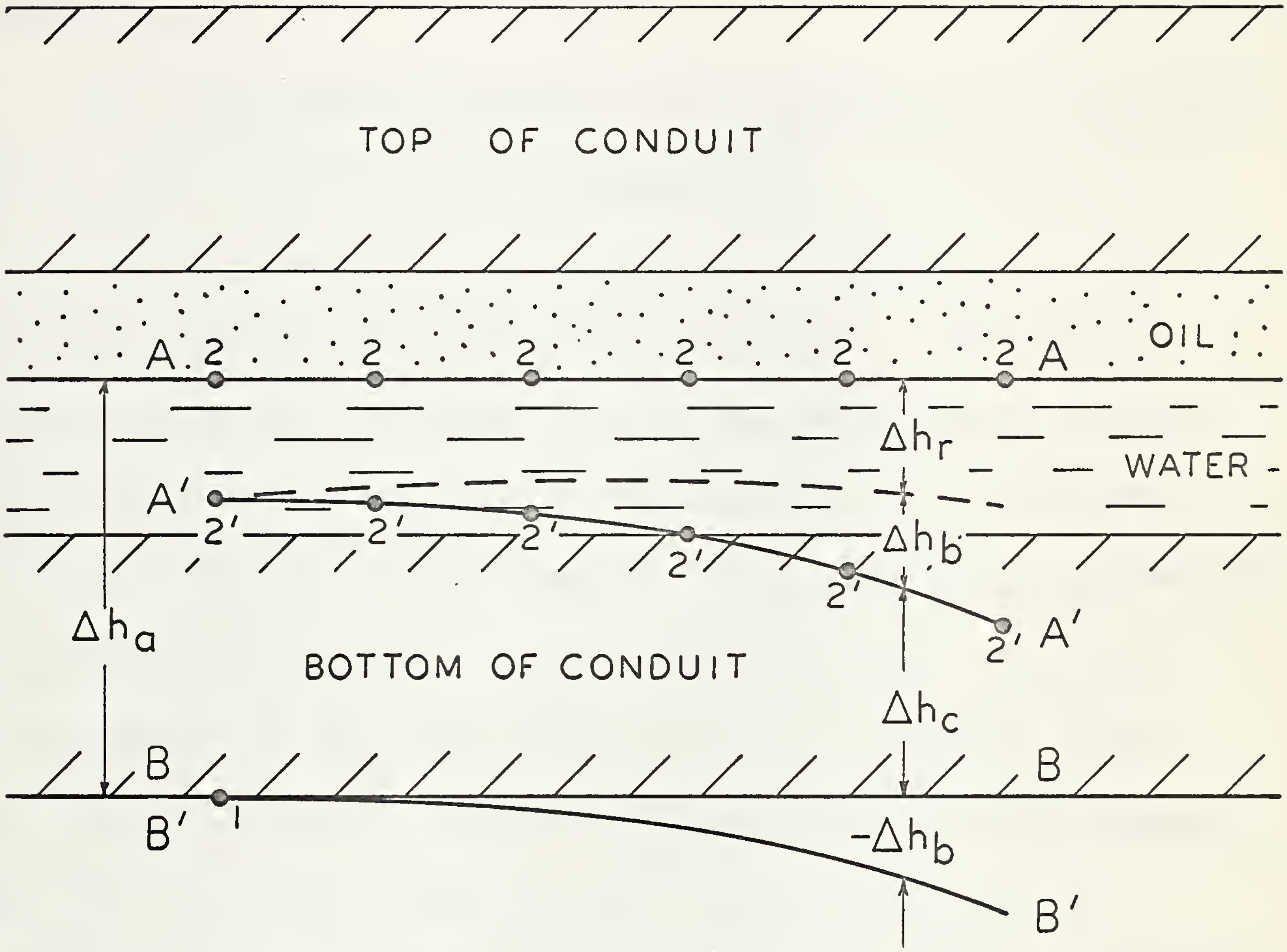

FIGURE 50 - ELEVATION ADJUSTMENTS FOR ACTUAL SYSTEM

the refraction effects may also introduce a second degree distortion of the interface. The sum of the individual effects may well, therefore, cause the points 2 to appear to be at 2' and a section of the interface AA to appear in the position A'A'.

For fixed camera positions the adjustments to be applied for the effects of tilt of the photoplanes, relative rotation of the negatives and lens distortion will be functious only of the position of the point on the negative. Adjustments for the effect of refraction through the dense media besides being a function of position on the negative are, of course, also functions of the water depth. It is, therefore, convenient to define two adjustments - the basic adjustment, Δh_b which is independent of the water depth and the refraction adjustment, Δh_r which is a function of the water depth. The adjustments Δh_b and Δh_r are shown in the figure as well as the crude elevation, Δh_c calculated from equation (102). Obviously the datum plane is also distorted, by an amount $-\Delta h_b$, relative to point 1. The true datum plane BB appears, therefore, to be at B'B'. With the assumption that the deformations of a flat interface can be represented by terms of second degree in x and z, the basic adjustment can then be defined by

$$\Delta h_b = c_o + c_1 x + c_2 z + c_3 x^2 + c_4 xz + c_5 z^2 \tag{103}$$

where the coefficients c_i are constant only for each viewing of each stereo pair and Δh_r by

$$\Delta h_r = a_o + a_1 x + a_2 z + a_3 x^2 + a_4 xz + a_5 z^2 \tag{104}$$

where the coefficients a_i are functions of the water depth only provided the cameras remain in a fixed position, and where x and z are the co-ordinates shown on the left hand negative in Figure 49. The z-direction coincided with the direction of fluid flow and the x-direction was, therefore, normal to it.

In an investigation of the variation of wave amplitude across the width of the conduit the general forms of equation (103) and (104) would be necessary. However, in order to reduce considerably the amount of photographic interpretation and computation required for the present project, the determination of the wave amplitude was limited to the centre line of the conduit, i.e. to the z-axis of the co-ordinate system. With x = 0 equations (103) and (104) reduce to

$$\Delta h_b = c_o + c_2 z + c_5 z^2 \tag{105}$$

and

$$\Delta h_r = a_o + a_2 z + a_5 z^2 \tag{106}$$

The actual elevation Δh_a was, therefore, calculated from the expression

$$\Delta h_a = \Delta h_c + \Delta h_b + \Delta h_r \tag{107}$$

It is apparent that in order to determine the coefficients in equations (105) and (106) at least three values of Δh_b and Δh_r must be evaluated at different values of z. Since the values of Δh_b, Δh_r and z are subject to experimental error it is better to use more than the minimum number and a least squares approach to determine the "best" values of the coefficients. Thus if N sets of corresponding values of Δh_b and z are available then c_o, c_2 and c_5 are given by the solution of the matrix equation

$$\begin{Bmatrix} N & \sum z_i & \sum z_i^2 \\ \sum z_i & \sum z_i^2 & \sum z_i^3 \\ \sum z_i^2 & \sum z_i^3 & \sum z_i^4 \end{Bmatrix} \begin{Bmatrix} c_o \\ c_2 \\ c_5 \end{Bmatrix} = \begin{Bmatrix} \sum \Delta h_{bi} \\ \sum z_i \Delta h_{bi} \\ \sum z_i^2 \Delta h_{bi} \end{Bmatrix} \tag{108}$$

where $i = 1,2,3 \ldots N \qquad N > 3$

Similarly if M sets of corresponding values of Δh_r and z are available then a_o, a_2 and a_5 are given by the solution of

$$\begin{Bmatrix} M & \sum z_i & \sum z_i^2 \\ \sum z_i & \sum z_i^2 & \sum z_i^3 \\ \sum z_i^2 & \sum z_i^3 & \sum z_i^4 \end{Bmatrix} \begin{Bmatrix} a_o \\ a_2 \\ a_5 \end{Bmatrix} = \begin{Bmatrix} \sum \Delta h_{ri} \\ \sum z_i \Delta h_{ri} \\ \sum z_i^2 \Delta h_{ri} \end{Bmatrix} \tag{109}$$

where $i = 1,2,3 \ldots M \qquad M \geqslant 3$

(ii) Calibration procedure

The calibration procedure consisted of the determination of the coefficients c_o, c_2 and c_5, and a_o, a_2 and a_5. The coefficients c_i must be determined for each viewing of each stereo pair of negatives while the coefficients a_i are a function of the water depth only.

In order to determine the coefficients c_i, seven crosses were scribed on the outside surface of the bottom of the photographic section which was levelled to within 0.002 inches. These crosses were positioned such that they appeared more or less coincident with the z-axis of the negatives as is apparent in the positive stereo pairs reporduced in Figures 40 and 41. The fiducial marks are also visible in these figures. The left hand cross was selected as the reference point for all elevation calculations. The elevations of the other six points were calculated from equation (102) and since these elevations were not subject to the refraction adjustment they were a direct measure of the basic adjustment Δh_b, only with the sign changed.

In using equation (102) to calculate elevations of points (2) relative to the reference point (1) it was necessary to know the distance of the lens centres from the datum plane,

H, the parallax of the reference point P_1, and the differences in parallax ΔP_{12}. Since the cameras were always in the same positions H and P_1 were constants and equal to 677 mm. and 34.5 mm. respectively. The differences in parallax were obtained by the use of the parallax bar, the use of which has been described by Baker(2). The stereoscope was fitted with eyepieces having a magnification of eight times. With the negative plates firmly attached to the light table readings were recorded to 1 micron, although they were reproducible only to within 10 microns. The expected error in the elevations calculated from equation (102) was, therefore, approximately 0.2 mm.

Equation (108) was solved by using Jordon's method for matrix inversion(50) and the University of Alberta IBM 1620 computer. The matrix inversion sub-routine was available as a library program from the computing centre. The program was written in Forgo. As a check on the calculations, the computer calculated the sum of the errors, error being defined as the difference between a particular Δh_b and the value calculated from equation (105) using the computed values of c_o, c_2 and c_5. In all cases the error sum was essentially zero, as it should have been. The errors were also used to calculate a standard deviation which varied between 0.1 and

0.3 mm. Since the cameras were rigidly fixed in position and because parallax measurements were confined to the z-axis where the effect of relative rotation of the negatives is a minimum the values of c_o, c_2 and c_5 were approximately the same for each stereo pair.

The coefficients a_o, a_2 and a_5 in the equation (106) were determined in the following way. A glass plate, painted white and ruled with lines half an inch apart was submerged at various known water depths in the conduit. Parallax readings were obtained for the seven crosses on the bottom of the conduit and for fifteen points on the grid plate. For each stereo pair the basic adjustment was calculated in the manner outlined above. This adjustment was used, together with the crude elevations calculated from equation (102) for points on the plate, to determine the refraction adjustment from equation (107). The coefficients a_o, a_2 and a_5 were then obtained by again using Jordon's method and the IBM 1620 computer to solve the matrix equation (109).

The coefficients a_o, a_2 and a_5 are shown as functions of the water depth in Figure 51. The coefficient a_o was a linear function of water depth, the slope being 0.295 mm/mm. The coefficients a_2 and a_5 scattered somewhat, probably due to errors in the parallaxes. However, the coefficients were

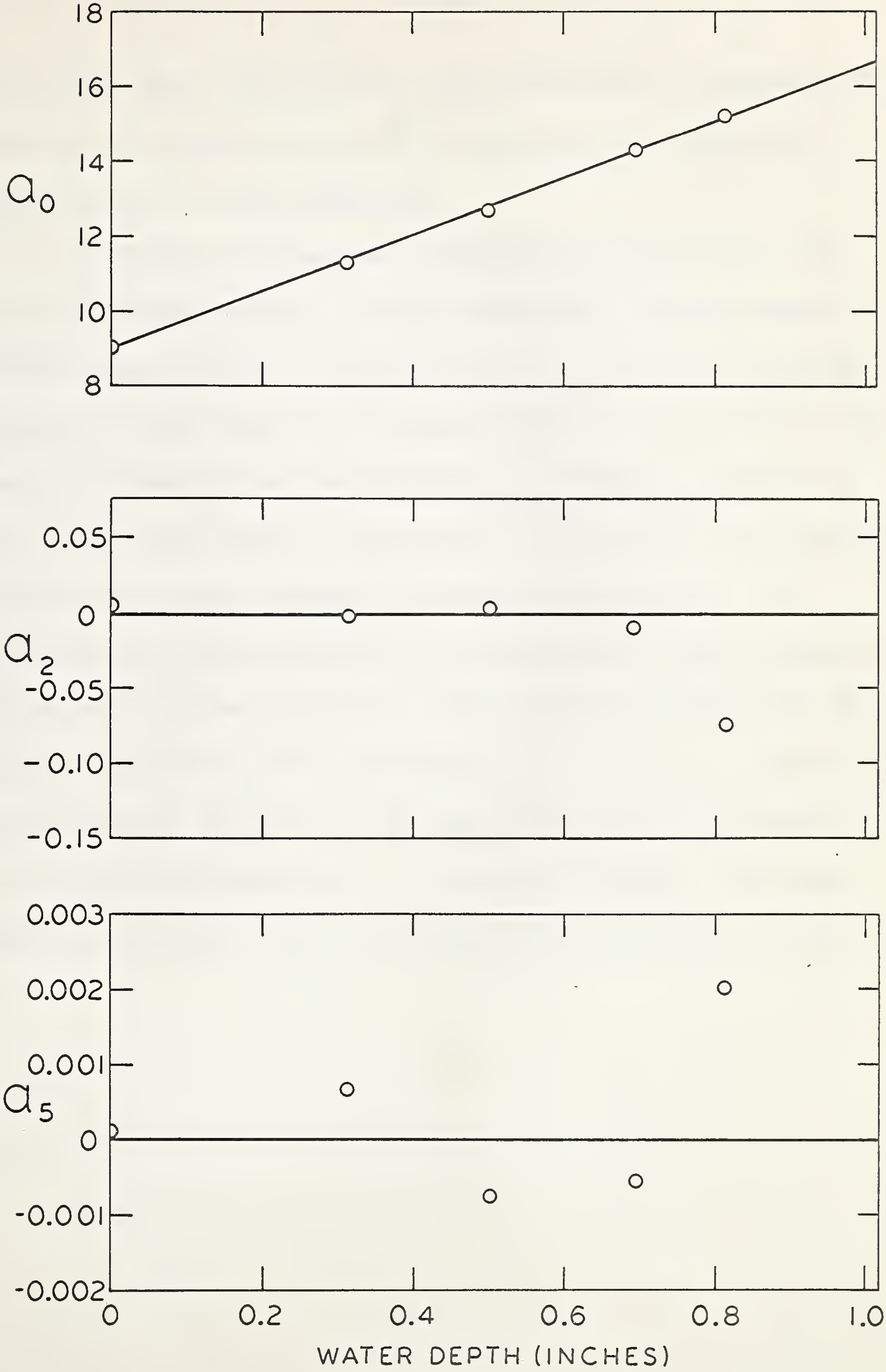

FIGURE 51 - REFRACTION ADJUSTMENT COEFFICIENTS

relatively small and differed little from zero. Consequently both a_2 and a_5 were assumed to be zero for the subsequent calculations of wave amplitude.

In order to check the calibration procedure and its use in the determination of wave amplitude a plastic model of a square wave having a wavelength of one inch and an average trough to crest height of 2 mm was submerged in water in the conduit. Parallax bar readings were obtained for points on the crests and troughs of the model. The actual and computed elevations or water depths are shown in Figure 52. The agreement is very reasonable, considering the error involved in the parallax bar readings. The standard deviation of the computed from the actual elevations is 0.35 mm. In computing the refraction adjustment the water depth used to evaluate a_o was the actual water depth. In general, however, the water depth is not known and a trial and error procedure is necessary.

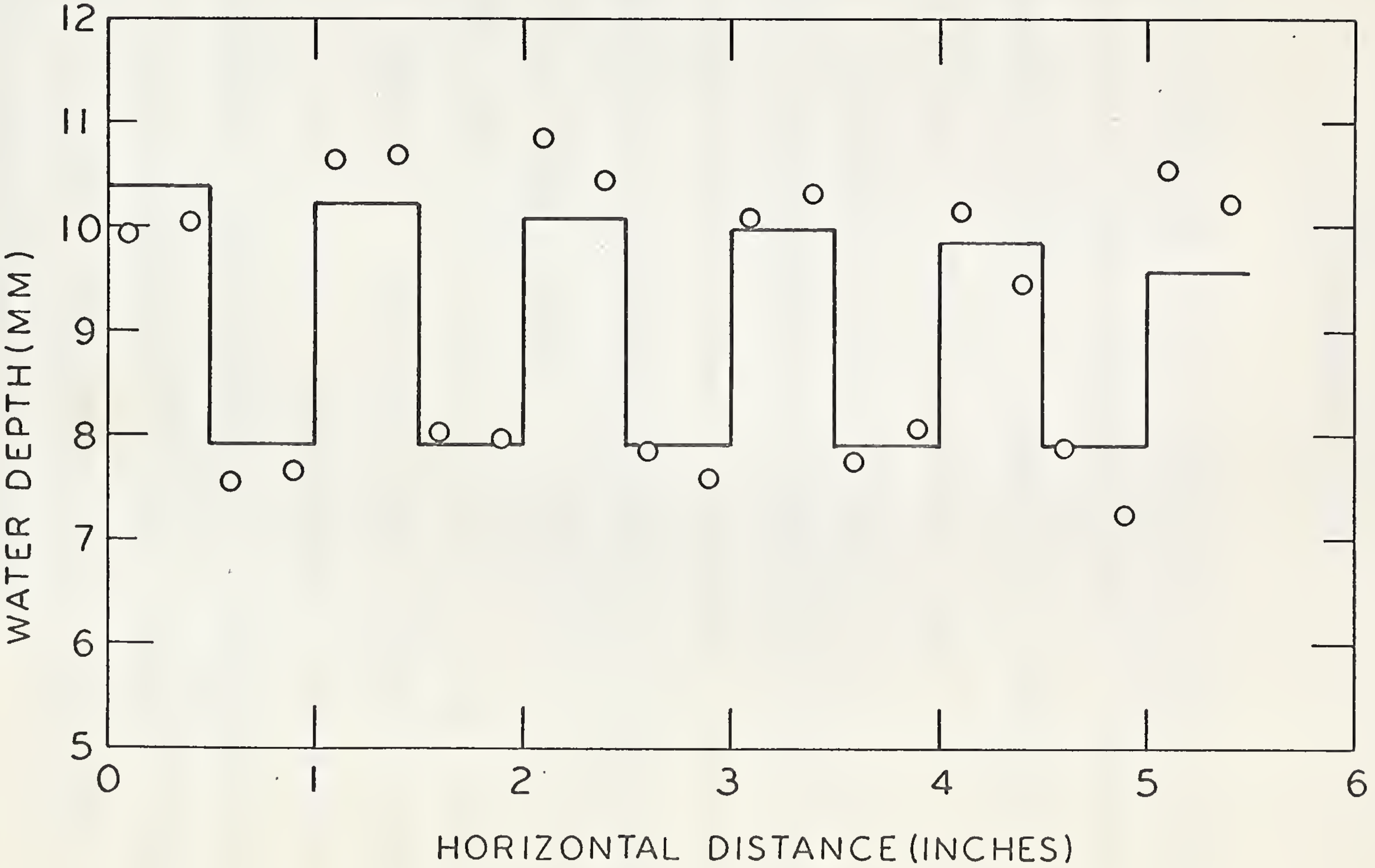

FIGURE 52 - COMPARISON OF COMPUTED AND ACTUAL ELEVATIONS

APPENDIX F

EXPERIMENTAL DATA

Data for the flow of oil alone are given in Table F1, data for the flow of water alone in Table F2, and data for the two-phase system in Table F3. Table F3 is subdivided according to the superficial oil Reynolds number, Re_o, which was calculated using a viscosity of 4.82 centipoise, i.e. the viscosity corresponding to the average oil temperature of 76.5°F. All other quantities involving the oil viscosity were calculated using the actual oil viscosity prevailing in each experiment. The oil depth readings reported are based on the average conduit depth of 1.007 inches and were used in the computation of the actual water velocity. Since the water viscosity varied only slightly during the two-phase experiments the average value of 0.905 centipoise, corresponding to a temperature of 76°F, was used in the calculation of the water Reynolds number.

A set of sample calculations follow each table to illustrate how each quantity was computed.

TABLE F1

DATA FOR THE FLOW OF OIL ALONE

Oil viscosity = 4.95 centipoise. Oil specific gravity = 0.819

Conduit depth = 1.007 inches. Conduit width = 8.01 inches.

Equivalent diameter of conduit = 1.786 inches.

Experiment Number	Oil Flow Rate (USGPM)	Average Velocity (ft/sec)	Pressure Gradient $lb/ft^2/ft$	Reynolds Number	Fanning Friction Factor
101	13.8	0.548	0.104	1250	0.0162
102	17.0	0.675	0.128	1540	0.01315
103	19.9	0.790	0.150	1800	0.0113
104	22.8	0.905	0.174	2060	0.00997
105	25.8	1.025	0.196	2340	0.00875
106	30.0	1.19	0.255	2710	0.00844
107	35.8	1.42	0.411	3240	0.00957
108	13.8	0.548	0.1038	1250	0.01618
109	17.0	0.675	0.1275	1540	0.01315
110	19.9	0.790	0.1505	1800	0.0113
111	22.8	0.905	0.173	2060	0.00992
112	25.8	1.025	0.196	2340	0.00875
113	30.0	1.19	0.254	2710	0.00842
114	35.8	1.42	0.420	3240	0.00981

Sample calculations for Table Fl

For experiment number 101 oil flow rate - 13.8 USGPM

$$\text{Average velocity} = \frac{\text{flow rate}}{\text{conduit cross-sectional area}}$$

$$= \frac{(13.8)(0.1336)(144)}{(60)(8.01)(1.007)} = 0.548 \text{ ft/sec}$$

From equation (14) $\text{Reynolds number} = \dfrac{\rho V\, D_e}{\mu}$

$$= \frac{(0.819)(62.4)(0.548)(1.786)(3600)}{(4.95)(2.42)(12)}$$

$$= 1250$$

From equation (13) $\text{Fanning fraction factor} = -\dfrac{1}{2}\dfrac{\partial p}{\partial z}\dfrac{g_c\, D_e}{\rho V^2}$

$$= -\frac{(-0.104)(32.2)(1.786)}{(2)(0.819)(62.4)(12)(0.548)^2}$$

$$= 0.0162$$

TABLE F2

DATA FOR THE FLOW OF WATER ALONE

water specific gravity = 0.997

conduit depth = 1.007 inches   conduit width = 8.01 inches

Equivalent diameter of conduit = 1.786 inches

Experiment Number	Water Flow Rate USGPM	Average Velocity ft/sec	Viscosity cp	Pressure Gradient $lb/ft^2/ft$	Reynolds Number	Fanning Friction Factor
115	3.99	0.1585	0.953	0.00605	2300	0.00923
116	4.47	0.1775	0.953	0.00769	2580	0.00933
117	5.02	0.199	0.979	0.0104	2810	0.01002
118	5.02	0.199	0.958	0.00940	2880	0.00908
119	6.19	0.246	0.979	0.0158	3470	0.00998
120	6.19	0.246	0.958	0.0165	3530	0.01045
121	9.11	0.362	0.965	0.0344	5200	0.01006
122	11.94	0.475	0.979	0.0521	6700	0.00888
*123	11.94	0.475	0.979	0.0540	6700	0.00915
124	11.94	0.475	0.965	0.0527	6820	0.00894
125	14.88	0.591	0.965	0.0798	8480	0.00874
126	18.16	0.721	0.979	0.111	10190	0.00813
127	18.16	0.721	0.965	0.111	10330	0.00813
*128	18.16	0.721	0.979	0.111	10190	0.00813
129	21.18	0.841	0.974	0.144	11950	0.00778
130	21.18	0.841	0.974	0.1383	11950	0.00738
*131	21.18	0.841	0.979	0.149	11950	0.00808
132	24.03	0.956	0.974	0.176	13600	0.00738

TABLE F2 (Continued)

Experiment Number	Water Flow Rate USGPM	Average Velocity ft/sec	Viscosity cp	Pressure Gradient $lb/ft^2/ft$	Reynolds Number	Fanning Friction Factor
*133	24.03	0.956	0.979	0.181	13500	0.00755
134	26.95	1.070	0.974	0.221	15200	0.00738
135	29.92	1.19	0.974	0.258	16900	0.00684
136	36.91	1.465	0.953	0.383	21300	0.00682

* pressure drop measured over downstream half of test section

Sample calculations for Table F2

For experiment number 115 water flow rate = 3.99 USGPM

$$\text{Average velocity} = \frac{\text{flow rate}}{\text{conduit cross-sectional area}}$$

$$= \frac{(3.99)\,(0.1336)\,(144)}{(60)\,(8.01)\,(1.007)} = 0.1585 \text{ ft/sec}$$

From equation (14) Reynolds number $= \dfrac{\rho V\, D_e}{\mu}$

$$= \frac{(0.997)\,(62.4)\,(0.1585)\,(1.786)\,(3600)}{(0.953)\,(2.42)\,(12)}$$

$$= 2300$$

From equation (13) Fanning friction factor $= -\dfrac{1}{2}\dfrac{\partial p}{\partial z}\dfrac{g_c\; D_e}{\rho V^2}$

$$= -\frac{(-0.00605)\,(32.2)\,(1.786)}{(2)\,(0.997)\,(62.4)\,(12)\,(0.1585)^2}$$

$$= 0.00923$$

TABLE F3

TWO-PHASE DATA

Conduit depth = 1.007 inches   Conduit width = 8.01 inches

Equivalent diameter of conduit = 1.786 inches

Water viscosity = 0.905 centipoise

(a) Oil Flow Rate = 0.500 USGPM, Re_o = 46.5

Experiment Number	Water Flow Rate (USGPM)	Superficial Water Reynolds Number	Input Water-to-oil Volume Ratio	Input Oil Volume Fraction	Oil Depth (ins)	Insitu Water-to-oil Ratio
201	16.5	10000	33.0	0.0294	0.119	7.46
202	19.5	11800	39.0	0.0250	0.092	9.93
203	22.6	13700	45.2	0.0222	0.0754	12.35
204	26.1	15800	52.3	0.0188	0.065	14.4
205	29.9	18130	59.8	0.0165	0.065	14.4

Experiment Number	Pressure Gradient ($lb/ft^2/ft$)	Oil Viscosity (cp)	Flow Regime	Pressure Gradient for flow of oil alone	Pressure Gradient Reduction Factor	Interface Velocity (ft/sec)
201	0.124	4.82	L-T	0.00372	0.0300	0.321
202	-	4.82	L-T	-	-	0.332
203	0.1955	4.82	L-T	0.00372	0.0190	0.373
204	-	4.82	L-T	-	-	0.418
205	0.322	4.82	L-T	0.00372	0.0115	0.490

TABLE F3 (Continued)

Experiment Number	Velocity Ratio w_i/V_{rc}	Wave Velocity (ft/sec)	Actual Average Water Velocity*	$\left(\frac{\partial p}{\partial z}\right)_w \Big/ \left(\frac{\partial p}{\partial z}\right)_o$
201	1.655	0.625	0.743	25.0
202	1.480	0.249-0.596	0.854	-
203	1.486	0.304	0.970	42.9
204	1.46	0.343	1.11	-
205	1.52	0.395	1.27	69.2

* (ft/sec)

(b) Oil Flow Rate = 0.805 USGPM, $Re_o = 74.8$

Experiment Number	Water Flow Rate (USGPM)	Superficial Water Reynolds Number	Input Water-to-oil Volume Ratio	Input Oil Volume Fraction	Oil Depth (ins)	Insitu Water-to-oil Ratio
206	16.5	10000	20.5	0.0466	0.1645	5.12
207	19.5	11800	24.2	0.0397	0.136	6.42
208	22.6	13700	28.1	0.0356	0.114	7.82
209	26.1	15800	32.5	0.0299	0.092	9.93
210	29.9	18130	37.2	0.0262	0.082	11.22

TABLE F3 (Continued)

Experiment Number	Pressure Gradient $(lb/ft^2/ft)$	Oil Viscosity (cp)	Flow Regime	Pressure Gradient for flow of oil alone	Pressure Gradient Reduction Factor	Interface Velocity (ft/sec)
206	0.124	4.82	L-T	0.00600	0.0483	0.412
207	-	4.82	L-T	-	-	0.422
208	0.201	4.82	L-T	0.00600	0.0298	0.481
209	-	4.82	L-T	-	-	0.540
210	0.320	4.82	L-T	0.00600	0.01875	0.583

Experiment Number	Velocity Ratio w_i/V_{rc}	Wave Velocity (ft/sec)	Actual Average Water Velocity*	$\left(\frac{\partial p}{\partial z}\right)_w \Big/ \left(\frac{\partial p}{\partial z}\right)_o$
206	1.935	0.728	0.786	15.5
207	1.715	0.591	0.895	-
208	1.78	0.472	1.01	26.6
209	1.76	0.494	1.14	-
210	1.68	0.558	1.295	43.0

* (ft/sec)

TABLE F3 (Continued)

(c) Oil Flow Rate = 1.20 USGPM, Re_o = 111.5

Experiment Number	Water Flow Rate (USGPM)	Superficial Water Reynolds Number	Input Water-to-oil Volume Ratio	Input Oil Volume Fraction	Oil Depth (ins)	Insitu Water-to-oil Ratio
211	2.01	1218	1.675	0.374	0.501	1.01
212	3.03	1840	2.52	0.284	0.452	1.23
213	3.98	2420	3.32	0.232	0.413	1.44
214	5.00	3030	4.17	0.1935	0.388	1.595
215	7.00	4240	5.84	0.1465	0.320	2.15
216	9.90	6000	8.24	0.1083	0.265	2.80
217	13.40	8130	11.17	0.0822	0.216	3.66
218	16.50	10000	13.75	0.0678	0.203	3.97
219	19.5	11800	16.25	0.0580	0.1745	4.77
220	22.60	13700	18.8	0.0504	0.144	6.00
221	26.1	15800	21.8	0.0439	0.122	7.25
222	29.9	18130	24.9	0.0386	0.103	8.77

Experiment Number	Pressure Gradient ($lb/ft^2/ft$)	Oil Viscosity (cp)	Flow Regime	Pressure Gradient for flow of oil alone	Pressure Gradient Reduction Factor	Interface Velocity (ft/sec)
211			L-L			0.171
212	0.01795	4.83	L-L	0.00890	0.497	0.196
213	0.0203	4.83	L-L	0.00890	0.438	0.216
214	0.0302	4.85	L-L	0.00894	0.296	0.241
215	0.0429	4.85	L-T	0.00894	0.208	0.285

TABLE F3 (Continued)

Experiment Number	Pressure Gradient $(lb/ft^2/ft)$	Oil Viscosity (cp)	Flow Regime	Pressure Gradient for flow of oil alone	Pressure Gradient Reduction Factor	Interface Velocity (ft/sec)
216	0.0575	4.75	L-T	0.00872	0.152	0.355
217	0.0895	4.75	L-T	0.00872	0.0975	0.418
218	0.1161	4.75	L-T	0.00872	0.0750	0.512
219	-	4.83	L-T	-	-	0.564
220	0.184	4.70	L-T	0.00864	0.0470	0.606
221	-	4.83	L-T	-	-	0.666
222	0.307	4.70	L-T	0.00864	0.0281	0.691

Experiment Number	Velocity Ratio w_i/V_{rc}	Wave Velocity*	Actual Average Water Velocity*	$\left(\frac{\partial p}{\partial z}\right)_w \Big/ \left(\frac{\partial p}{\partial z}\right)_o$
211	2.74			
212	2.53			
213	2.37			
214	2.28			
215	2.19	0.449	0.407	2.24
216	2.18	0.676	0.533	4.28
217	2.16	0.746	0.677	7.24
218	2.15	0.824	0.822	10.65
219	2.11	0.745	0.938	
220	2.10	0.913	1.047	18.55
221	1.99	0.639	1.18	29.9
222		0.723	1.325	29.9

* (ft/sec)

TABLE F3 (Continued)

(d) Oil Flow Rate = 1.97 USGPM, Re_o = 183

Experiment Number	Water Flow Rate (USGPM)	Superficial Water Reynolds Number	Input Water-to-oil Volume Ratio	Input Oil Volume Fraction	Oil Depth (ins)	Insitu Water-to-oil Ratio
223	1.512	918	0.768	0.566	0.609	0.653
224	2.01	1218	1.02	0.493	0.570	0.768
225	2.52	1530	1.28	0.438	0.545	0.847
226	3.98	2420	2.02	0.332	0.472	1.135
227	5.00	3030	2.54	0.283	0.428	1.355
228	7.00	4240	3.53	0.221	0.373	1.70
229	9.90	6000	5.02	0.166	0.324	2.11
230	13.40	8130	6.81	0.128	0.275	2.66
231	16.50	10000	8.38	0.1065	0.258	2.90
232	19.50	11800	9.90	0.0917	0.229	3.39
233	22.60	13700	11.46	0.0803	0.202	3.98
234	26.1	15800	13.25	0.0703	0.169	4.97
235	29.90	18130	15.2	0.0617	0.156	5.47

Experiment Number	Pressure Gradient ($lb/ft^2/ft$)	Oil Viscosity (cp)	Flow Regime	Pressure Gradient flr flow of oil alone	Pressure Gradient Reduction Factor	Interface Velocity (ft/sec)
223	-	4.75	L-L	0.0144	-	0.218
224	0.01795	4.75	L-L	0.0144	0.803	0.236
225	0.01925	4.77	L-L	0.0144	0.749	0.253
226	0.0260	4.77	L-L	0.0144	0.555	0.298
227	0.0336	4.77	L-L	0.0144	0.428	0.325
228	0.0470	4.95	L-T	0.01495	0.318	0.374
229	0.0640	4.95	L-T	0.01495	0.234	0.453

TABLE F3 (Continued)

Experiment Number	Pressure Gradient ($lb/ft^2/ft$)	Oil Viscosity (cp)	Flow Regime	Pressure Gradient for flow of oil alone	Pressure Gradient Reduction Factor	Interface Velocity (ft/sec)
230	0.0920	4.90	L-T	0.01480	0.161	0.533
231	0.1178	4.90	L-T	0.01480	0.1256	0.598
232	-	4.82	L-T	-	-	0.717
233	0.1790	4.90	L-T	0.01480	0.0826	0.777
234	-	4.82	L-T	-	-	0.843
235	0.299	4.77	L-T	0.0144	0.0482	-

Experiment Number	Velocity Ratio w_i/V_{rc}	Wave Velocity (ft/sec)	Actual Average Water Velocity (ft/sec)	$\left(\frac{\partial p}{\partial z}\right)_w \Big/ \left(\frac{\partial p}{\partial z}\right)_o$
223	3.07			
224	2.96			
225	2.84			
226	2.66			
227	2.58			
228	2.35	0.472	.442	1.34
229	2.28	0.627	.581	2.49
230	2.23	0.804	.732	4.26
231	2.14	0.853	.883	6.28
232	2.33	0.922	1.00	-
233	2.27	1.09	1.12	10.8
234	2.23	1.01	1.245	-
235	-	0.958 0.723	1.405	17.9

TABLE F3 (Continued)

(e) Oil Flow Rate = 3.03 USGPM, Re_o = 282

Experiment Number	Water Flow Rate (USGPM)	Superficial Water Reynolds Number	Input Water-to-oil Volume Ratio	Input Oil Volume Fraction	Oil Depth (ins)	Insitu Water-to-oil Ratio
236	1.261	766	0.417	0.707	0.683	0.474
237	1.512	918	0.499	0.668	0.657	0.530
238	2.01	1218	0.664	0.602	0.619	0.626
239	2.52	1530	0.832	0.546	0.608	0.653
240	3.03	1840	1.000	0.500	0.574	0.753
241	3.98	2420	1.315	0.432	0.526	0.914
242	5.00	3030	1.650	0.378	0.481	1.09
243	7.00	4240	2.31	0.302	0.447	1.25
244	9.90	6000	3.26	0.235	0.383	1.63
245	13.40	8130	4.42	0.185	0.353	1.85
246	16.50	10000	5.44	0.1555	0.304	2.31
247	22.6	13700	7.45	0.1185	0.270	2.73
248	29.9	18130	9.87	0.0920	-	-

Experiment Number	Pressure Gradient ($lb/ft^2/ft$)	Oil Viscosity (cp)	Flow Regime	Pressure Gradient for flow of oil alone	Pressure Gradient Reduction Factor	Interface Velocity (ft/sec)
236	0.0193	4.95	L-L	0.0230	1.19	-
237	0.0202	4.95	L-L	0.0230	1.14	0.300
238	0.0222	4.95	L-L	0.0230	1.035	0.322
239	0.0234	4.90	L-L	0.0228	0.974	0.340
240	0.0262	4.85	L-L	0.0225	0.859	-

TABLE F3 (Continued)

Experiment Number	Pressure Gradient (lb/ft^2/ft)	Oil Viscosity (cp)	Flow Regime	Pressure Gradient for flow of oil alone	Pressure Gradient Reduction Factor	Interface Velocity (ft/sec)
241	0.0351	4.85	L-T	0.0225	0.642	-
242	0.0432	4.82	L-T	0.0224	0.520	-
243	0.0566	4.82	L-T	0.0224	0.396	0.496
244	0.0786	4.82	L-T	0.0224	0.285	0.552
245	0.1100	4.82	L-T	0.0224	0.204	0.658
246	0.1364	4.85	L-T	0.0225	0.165	0.763
247	0.197	4.85	L-T	0.0225	0.114	0.974
248	0.299	4.77	L-T	0.02215	0.074	-

Experiment Number	Velocity Ratio w_i/V_{rc}	Wave Velocity (ft/sec)	Actual Average Water Velocity (ft/sec)	$\left(\frac{\partial p}{\partial z}\right)_w \Big/ \left(\frac{\partial p}{\partial z}\right)_o$
236				
237	3.11			
238	3.03			
239	2.94			
240	-			
241	-			0.269
242	-			0.469
243	2.67	0.489	0.500	0.889
244	2.41	0.648	0.635	1.66
245	2.38	0.894	0.823	2.80
246	2.42	1.052	0.942	4.14
247	2.25	1.231	1.225	7.12
248				11.66

TABLE F3 (Continued)

(f) Oil Flow Rate = 5.02 USGPM, Re_o = 467

Experiment Number	Water Flow Rate (USGPM)	Superficial Water Reynolds Number	Input Water-to-oil Volume Ratio	Input Oil Volume Fraction	Oil Depth (ins)	Insitu Water-to-oil Ratio
249	1.014	616	0.202	0.833		
250	1.261	766	0.252	0.798	.761	0.323
251	1.512	918	0.302	0.768	.737	0.367
252	2.01	1218	0.401	0.713	.707	0.423
253	2.52	1530	0.502	0.666	.668	0.507
254	3.03	1840	0.603	0.624	.628	0.602
255	3.98	2420	0.794	0.558	.590	0.707
256	5.00	3030	0.996	0.502	.560	0.798
257	7.00	4240	1.395	0.418	.510	0.972
258	9.90	6000	1.975	0.336	.452	1.23
259	13.40	8130	2.67	0.273	.403	1.50
260	16.50	10000	3.29	0.233	.358	1.81
261	22.6	13700	4.50	0.182	.310	2.25
262	29.9	18130	5.96	0.1435	-	-

TABLE F3 (Continued)

Experiment Number	Pressure Gradient ($lb/ft^2/ft$)	Oil Viscosity (cp)	Flow Regime	Pressure Gradient for flow of oil alone	Pressure Gradient Reduction Factor	Interface Velocity (ft/sec)
249	0.0267	4.78	L-L	0.0368	1.38	0.394
250	0.0271	4.78	L-L	0.0368	1.36	0.401
251	0.0275	4.78	L-L	0.0368	1.34	0.428
252	0.0293	4.78	L-L	0.0368	1.26	0.450
253	0.0326	4.75	L-L	0.0366	1.122	0.464
254	0.0409	4.75	trans	0.0366	0.891	0.496
255	0.0497	4.70	trans	0.0362	0.728	0.533
256	0.0583	4.70	L-T	0.0362	0.621	0.576
257	0.0728	4.70	L-T	0.0362	0.497	0.632
258	0.0970	4.70	L-T	0.0362	0.373	0.792
259	0.128	4.70	L-T	0.0362	0.283	0.922
260	0.160	4.90	L-T	0.0378	0.236	0.981
261	0.227	4.90	L-T	0.0378	0.1665	1.166
262	0.323	4.78	L-T	0.0368	0.114	-

TABLE F3 (Continued)

Experiment Number	Velocity Ratio w_i/V_{rc}	Wave Velocity (ft/sec)	Actual Average Water Velocity (ft/sec)	$\left(\frac{\partial p}{\partial z}\right)_w \Big/ \left(\frac{\partial p}{\partial z}\right)_o$
249	3.12			
250	3.09			
251	3.17			
252	3.14			
253	3.03			
254	3.06			
255	3.00			0.167
256	2.89	0.502	0.448	0.290
257	2.76	0.602	0.564	0.553
258	2.78	0.685	0.713	1.031
259	-	0.914	0.889	1.74
260	2.54	1.16	1.02	2.46
261	2.47	1.47	1.30	4.23
262	-	-	-	7.02

TABLE F3 (Continued)

(g) Oil Flow Rate = 6.98 USGPM, Re_o = 649

Experiment Number	Water Flow Rate (USGPM)	Superficial Water Reynolds Number	Input Water-to-oil Volume Ratio	Input Oil Volume Fraction	Oil Depth (ins)	Insitu Water-to-oil Ratio
263	1.014	616	0.145	0.873	0.826	0.220
264	1.261	766	0.181	0.846	0.809	0.243
265	1.512	918	0.217	0.823	0.785	0.282
266	2.01	1218	0.238	0.777	0.747	0.349
267	2.52	1530	0.361	0.734	0.722	0.395
268	3.03	1840	0.434	0.698	0.652	0.542
269	3.98	2420	0.570	0.638	0.628	0.602
270	5.00	3030	0.715	0.583	0.590	0.707
271	7.00	4240	1.002	0.500	0.550	0.830
272	9.90	6000	1.42	0.413	0.482	1.09
273	13.40	8130	1.92	0.343	0.432	1.33
274	16.50	10000	2.36	0.297	0.402	1.50
275	22.6	13700	3.24	0.236	0.344	1.93
276	29.9	18130	4.28	0.1895	-	-

TABLE F3 (Continued)

Experiment Number	Pressure Gradient ($lb/ft^2/ft$)	Oil Viscosity (cp)	Flow Regime	Pressure Gradient for flow of oil alone	Pressure Gradient Reduction Factor	Interface Velocity (ft/sec)
263	0.0349	4.70	L-L	0.0505	1.445	0.468
264	0.0359	4.70	L-L	0.0505	1.405	0.480
265	0.0375	4.70	L-L	0.0505	1.345	
266	0.0388	4.85	L-L	0.0521	1.345	0.608
267	0.0388	4.85	L-L	0.0521	1.345	0.642
268	0.0490	4.85	L-T	0.0521	1.065	0.617
269	0.0604	4.85	L-T	0.0521	0.864	0.669
270	0.0686	4.85	L-T	0.0521	0.760	0.728
271	0.0826	4.81	L-T	0.0517	0.631	0.808
272	0.108	4.81	L-T	0.0517	0.478	0.939
273	0.143	4.81	L-T	0.0517	0.361	1.073
274	0.176	4.81	L-T	0.0517	0.294	1.19
275	0.244	4.81	L-T	0.0517	0.212	1.426
276	0.353	4.78	L-T	0.0515	0.146	-

TABLE F3 (Continued)

Experiment Number	Velocity Ratio w_i/V_{rc}	Wave Velocity (ft/sec)	Actual Average Water Velocity (ft/sec)	$\left(\frac{\partial p}{\partial z}\right)_w \Big/ \left(\frac{\partial p}{\partial z}\right)_o$
263	2.79			
264	2.82			
265				
266	3.23			
267	3.22			
268	2.97			
269	2.91			0.116
270	2.93	0.598	.480	0.202
271	2.85	0.692	.601	0.387
272	2.83	0.848	.755	0.721
273	2.77	0.980	.932	1.22
274	2.72	1.16	1.09	1.80
275	2.70			3.10
276				5.20

TABLE F3 (Continued)

(h) Oil Flow Rate = 10.0 USGPM, Re_o = 930

Experiment Number	Water Flow Rate (USGPM)	Superficial Water Reynolds Number	Input Water-to-oil Volume Ratio	Input Oil Volume Fraction	Oil Depth (ins)	Insitu Water-to-oil Ratio
277	1.261	766	0.1261	0.888		
278	1.512	918	0.151	0.868	.829	0.213
279	2.01	1218	0.201	0.832	.799	0.258
280	3.03	1840	0.303	0.766	.746	0.349
281	3.98	2420	0.398	0.716	.663	0.518
282	5.00	3030	0.500	0.667	.652	0.542
283	7.00	4240	0.700	0.588	.598	0.682
284	9.90	6000	0.990	0.503	.554	0.814
285	13.40	8130	1.34	0.427	.510	0.972
286	16.50	10000	1.65	0.378	.462	1.18
287	22.6	13700	2.26	0.307	.422	1.38
288	29.9	18130	2.99	0.251	-	-

Experiment Number	Pressure Gradient ($lb/ft^2/ft$)	Oil Viscosity (cp)	Flow Regime	Pressure Gradient for flow of oil alone	Pressure Gradient Reduction Factor	Interface Velocity (ft/sec)
277	0.0457	4.67	L-L	0.0717	1.57	0.638
278	0.0546	5.08	L-L	0.0783	1.435	0.761
279	0.0535	5.08	trans	0.0783	1.465	0.739
280	0.0757	5.03	L-T	0.0774	1.022	0.776
281	0.0869	5.03	L-T	0.0774	0.892	0.833

TABLE F3 (Continued

Experiment Number	Pressure Gradient ($lb/ft^2/ft$)	Oil Viscosity (cp)	Flow Regime	Pressure Gradient for flow of oil alone	Pressure Gradient Reduction Factor	Interface Velocity (ft/sec)
282	0.1015	5.08	L-T	0.0783	0.771	0.885
283	0.1135	5.03	L-T	0.0774	0.682	0.987
284	0.142	5.08	L-T	0.0783	0.551	1.136
285	0.201	5.03	L-T	0.0774	0.385	1.305
286	0.218	5.08	L-T	0.0783	0.359	1.45
287	0.304	5.03	L-T	0.0774	0.255	1.72
288	0.402	4.78	L-T	0.0735	0.183	

Experiment Number	Velocity Ratio w_i/V_{rc}	Wave Velocity (ft/sec)	Actual Average Water Velocity (ft/sec)	$\left(\frac{\partial p}{\partial z}\right)_w \Big/ \left(\frac{\partial p}{\partial z}\right)_o$
277	2.69			
278	2.93			
279	2.75			
280	2.74			
281	2.76			0.0782
282	2.70	0.560	0.564	0.134
283	2.71	0.677	0.685	0.258
284	2.68	0.832	0.875	0.477
285	2.70	0.989	1.078	0.815
286	2.69	1.205	1.21	1.19
287	2.73			2.07
288				3.51

TABLE F3 (Continued)

(i) Oil Flow Rate = 15.2 USGPM, Re_o = 1413

Experiment Number	Water Flow Rate (USGPM)	Superficial Water Reynolds Number	Input Water-to-oil Volume Ratio	Input Oil Volume Fraction	Oil Depth (ins)	Insitu Water-to-oil Ratio
289	1.512	918	0.0995	0.910		
290	2.01	1218	0.132	0.883	.835	.206
291	2.52	1530	0.1655	0.857		
292	3.03	1840	0.199	0.835	.790	.273
293	3.98	2420	0.262	0.793	.748	.348
294	5.00	3030	0.329	0.753	.708	.423
295	7.00	4240	0.460	0.686	.668	.508
296	9.90	6000	0.651	0.606	.613	.640
297	13.40	8130	0.881	0.532	.550	.831
298	16.50	10000	1.084	0.480	.521	.934
299	22.60	13700	1.485	0.402	.457	1.205
300	29.9	18130	1.965	0.337	-	-

Experiment Number	Pressure Gradient ($lb/ft^2/ft$)	Oil Viscosity (cp)	Flow Regime	Pressure Gradient for flow of oil alone	Pressure Gradient Reduction Factor	Interface Velocity (ft/sec)
289	0.071	4.67	L-L	0.109	1.535	0.933
290	0.0847	5.00	L-T	0.1164	1.375	0.943
291	0.0978	5.00	L-T	0.1164	1.19	0.968
292	0.105	5.00	L-T	0.1164	1.11	1.01
293	0.1160	5.00	L-T	0.1164	1.03	1.102

TABLE F3 (Continued)

Experiment Number	Pressure Gradient ($lb/ft^2/ft$)	Oil Viscosity (cp)	Flow Regime	Pressure Gradient for flow of oil alone	Pressure Gradient Reduction Factor	Interface Velocity (ft/sec)
294	0.1285	4.95	L-T	0.1152	0.899	1.17
295	0.1430	4.95	L-T	0.1152	0.808	1.32
296	0.1795	4.95	L-T	0.1152	0.643	1.45
297	0.231	4.95	L-T	0.1152	0.499	1.645
298	0.275	4.95	L-T	0.1152	0.420	1.865
299	0.375	4.95	L-T	0.1152	0.308	-
300	0.512	4.78	L-T	0.1117	0.218	-

Experiment Number	Velocity Ratio w_i/V_{rc}	Wave Velocity (ft/sec)	Actual Average Water Velocity (ft/sec)	$\left(\frac{\partial p}{\partial z}\right)_w \Big/ \left(\frac{\partial p}{\partial z}\right)_o$
289	2.57			
290	2.43			
291	2.46			
292	2.54			
293	2.64	0.684	0.615	0.0520
294	2.70	0.764	0.670	0.0901
295	2.77	0.840	0.827	0.1725
296	2.72	1.00	1.004	0.322
297	2.72	1.25	1.172	0.544
298	2.83	1.44	1.36	0.802
299	-	1.68	1.64	1.380
300	-	-	-	2.40

TABLE F3 (Continued)

(j) Oil Flow Rate = 25.1 USGPM, Re_o = 2330

Experiment Number	Water Flow Rate (USGPM)	Superficial Water Reynolds Number	Input Water-to-oil Volume Ratio	Input Oil Volume Fraction	Oil Depth (ins)	Insitu Water-to-oil Ratio
301	1.512	918	0.0603	0.943		
302	2.01	1218	0.0800	0.926		
303	3.03	1840	0.1208	0.892		
304	3.98	2420	0.1588	0.864		
305	5.00	3030	0.1995	0.836	.754	0.331
306	7.00	4240	0.279	0.783	.713	0.414
307	9.90	6000	0.395	0.717	.668	0.508
308	13.40	8130	0.534	0.652	.643	0.565
309	16.5	10000	0.657	0.606	.580	0.737
310	22.6	13700	0.900	0.527	.540	0.863
311	29.9	18130	1.19	0.457		

Experiment Number	Pressure Gradient ($lb/ft^2/ft$)	Oil Viscosity (cp)	Flow Regime	Pressure Gradient for flow of oil alone	Pressure Gradient Reduction Factor	Interface Velocity (ft/sec)
301	0.1642	4.81	T-T	0.186	1.132	1.22
302	0.187	4.81	T-T	0.186	0.995	1.22
303	0.216	4.81	T-T	0.186	0.861	1.31
304	0.236	4.78	T-T	0.185	0.788	1.33
305	0.258	4.78	T-T	0.185	0.717	1.45
306	0.288	4.78	T-T	0.185	0.643	

TABLE F3 (Continued)

Experiment Number	Pressure Gradient $(lb/ft^2/ft)$	Oil Viscosity (cp)	Flow Regime	Pressure Gradient for flow of oil alone	Pressure Gradient Reduction Factor	Interface Velocity (ft/sec)
307	0.348	4.90	T-T	0.1895	0.544	1.74
308	0.428	4.90	T-T	0.1895	0.443	
309	0.493	4.90	T-T	0.1895	0.385	
310	0.634	4.90	T-T	0.1895	0.299	
311	0.804	4.78	T-T	0.185	0.230	

Experiment Number	Velocity Ratio w_i/V_{rc}	Wave Velocity (ft/sec)	Actual Average Water Velocity (ft/sec)
301	1.94		
302	1.98		
303	2.13	0.840	
304	2.14	0.922	
305	2.29	1.04	.790
306		1.117	.953
307	2.34	1.116	1.17
308			
309			
310			
311			

TABLE F3 (Continued)

(k) Oil Flow Rate = 35.8 USGPM, Re_o = 3330

Experiment Number	Water Flow Rate (USGPM)	Superficial Water Reynolds Number	Input Water-to-oil Volume Ratio	Input Oil Volume Fraction	Pressure Gradient ($lb/ft^2/ft$)	Oil Viscosity (cp)
312	3.98	2420	0.1112	0.902	0.422	4.78
313	5.00	3030	0.1396	0.879	0.450	4.78
314	7.00	4240	0.1955	0.837	0.480	4.78
315	9.90	6000	0.2760	0.784	0.551	4.78
316	13.40	8130	0.374	0.728	0.648	4.78
317	16.50	10000	0.461	0.684	0.754	4.78
318	22.6	13700	0.632	0.613	0.910	4.78
319	29.9	18130	0.835	0.546	1.114	4.78

Experiment Number	Flow Regime	Pressure Gradient for flow of oil alone	Pressure Gradient Reduction Factor
312	T-T	0.420	.995
313	T-T	0.420	.934
314	T-T	0.420	.875
315	T-T	0.420	.762
316	T-T	0.420	.648
317	T-T	0.420	.558
318	T-T	0.420	.462
319	T-T	0.420	.368

Sample calculations for Table F3

For experiment number 215

oil flow rate = 1.20 USGPM

Superficial average oil velocity, V_o =

$$= \frac{\text{oil flow rate}}{\text{conduit cross-sectional area}}$$

$$= \frac{(1.20)(0.1336)(144)}{(60)(8.01)(1.007)}$$

$$= 0.0476 \text{ ft/sec}$$

Superficial oil Reynolds number

$$= \frac{\rho_o V_o D_e}{\mu_o}$$

$$= \frac{(0.819)(62.4)(0.0476)(1.786)(3600)}{(4.82)(2.42)(12)}$$

$$= 111.5$$

Water flow rate = 7.00 USGPM

Superficial average water velocity, V_w

$$= \frac{(7.00)(0.1336)(144)}{(60)(8.01)(1.007)}$$

$$= 0.278 \text{ ft/sec}$$

Superficial water Reynolds number

$$= \frac{\rho_w V_w D_e}{\mu_w}$$

$$= \frac{(0.997)(62.4)(0.278)(1.786)(3600)}{(0.905)(2.42)(12)}$$

$$= 4240$$

Input ratio $= \frac{7.00}{1.20} = 5.84$

Input oil fraction $= \frac{1.20}{1.20 + 7.00} = 0.1465$

Insitu ratio $= \frac{\text{water depth}}{\text{oil depth}} = \frac{1.007 - 0.320}{0.320} = 2.15$

Equation (11) reduces to

$$\frac{\partial p}{\partial z} = 1026\,\mu\,Q$$

for the particular conduit used for the experiments. Hence the pressure gradient for the flow of oil alone, $\left(\frac{\partial p}{\partial z}\right)_o = 1026\,\mu_o Q_o$

$$= \frac{(1026)(4.85)(2.42)(1.20)(0.1336)}{(3600)(60)}$$

$$= 0.00894 \text{ lb/ft}^2\text{/ft}$$

Pressure gradient reduction factor

$$= \frac{0.00894}{0.0429} = 0.208$$

From a plot of the data presented in Table A3(a) the theoretical pressure gradient reduction factor for an input ratio of 5.84 is 0.365.

Hence the theoretical two-phase pressure gradient assuming laminar flow in both phases

$$= \frac{0.00894}{0.365} = 0.0245 \text{ lb/ft}^2\text{/ft}$$

$$V_{rc} = \frac{1}{4ab} \left(\frac{\partial p}{\partial z}\right)_o \frac{1}{1026\,\mu_o}$$

$$= \frac{(144)(0.0245)(3600)}{(4)(4.005)(0.5035)(1026)(4.85)(2.42)}$$

$$= 0.130 \text{ ft/sec}$$

Velocity ratio, $\frac{w_i}{V_{rc}} = \frac{0.285}{0.130} = 2.19$

Actual average water velocity

$$= \frac{(7.00)(0.1336)(144)}{(60)(8.001)(0.687)}$$

$$= 0.407 \text{ ft/sec}$$

B29814